Spatial flood extent modelling
A performance-based comparison

Micha Werner



Spatial flood extent modelling
A performance-based comparison

Cover: Flood extent map of the River Eden, just upstream of Carlisle. Reproduced by kind permission of the Environment Agency, UK. The flood extent map shown is based on synthetic data and has no bearing on real flood maps for the reach shown.

Spatial flood extent modelling
A performance-based comparison

PROEFSCHRIFT

ter verkrijging van de graad van doctor
aan de Technische Universiteit Delft,
op gezag van de Rector Magnificus prof.dr.ir. J.T. Fokkema,
voorzitter van het College van Promoties,
in het openbaar te verdedigen

op dinsdag 14 december 2004 te 13:00 uur

door Micha Guido Franciscus WERNER

civiel ingenieur

geboren te Nicosia (Cyprus)

Dit proefschrift is goedgekeurd door de promotoren:
Prof. dr. ir. H.H.G. Savenije
Prof. dr. ir. M.J.M. Bogaerts

Samenstelling promotiecommissie:

Rector Magnificus, voorzitter
Prof. dr. ir. H.H.G. Savenije, promotor
Prof. dr. ir. M.J.M. Bogaerts, promotor
Prof. dr. ir. G.S. Stelling, Technische Universiteit Delft
Prof. ir. E. van Beek, Technische Universiteit Delft
Prof. dr. K.J. Beven, University of Lancaster
Prof. dr. A. Bronstert, University of Potsdam
Dr. J.C.J. Kwadijk, Delft Hydraulics

Published and distributed by: DUP Science

DUP Science is an imprint of
Delft University Press
P.O. Box 98
2600 MG Delft
The Netherlands
Telephone: +31 15 27 85 678
Telefax: +31 15 27 85 706
E-mail: info@library.tudelft.nl

ISBN 90-407-2558-6

Keywords: Flood extent / GIS / Uncertainty analysis / numerical model

Copyright © 2004 by Micha Werner

All rights reserved. No part of the material protected by this copyright notice may be reproduced or utilised in any form or by any means, electronic or mechanical, including photocopying, recording or by any information storage and retrieval system, without written permission of the publisher: Delft University Press

Printed in the Netherlands

Contents

List of Figures **ix**

List of Tables **xi**

1 Introduction **1**
1.1 Background . . . 1
1.2 Objectives and approach . . . 2
1.3 Motivation . . . 3
1.4 Structure of this thesis . . . 4

2 GIS and hydrological modelling **7**
2.1 Introduction . . . 7
2.2 Modelling approaches and complexity . . . 8
2.3 Levels of integration . . . 10
2.3.1 Loosely coupling . . . 10
2.3.2 Tightly coupling - shared data model . . . 12
2.3.3 Tightly coupling - embedded process model . . . 12
2.3.4 Time and GIS . . . 13
2.3.5 3D GIS . . . 15
2.4 Discussion . . . 15
2.5 Conclusions . . . 16

3 Flood Extent Estimation **17**
3.1 Introduction . . . 17
3.2 One-dimensional hydrodynamic modelling . . . 20
3.2.1 Model concept . . . 20
3.2.2 Integration with GIS . . . 21
3.3 Two-dimensional hydrodynamic modelling . . . 24
3.3.1 Model concept . . . 24
3.3.2 Integration with GIS . . . 26
3.4 Hybrid one-two dimensional modelling . . . 27
3.4.1 Model concept . . . 27
3.4.2 Integration with GIS . . . 28
3.5 Simplified two-dimensional modelling . . . 29

3.5.1 Model concept . . . 29
3.5.2 Integration with GIS . . . 32
3.6 Roughness value parameterisation . . . 33
3.7 Discussion . . . 34
3.8 Conclusions . . . 35

4 Model performance: reliability, calibration and uncertainties 37
4.1 Introduction . . . 37
4.2 Model calibration . . . 39
4.3 Model uncertainty . . . 40
4.4 Methods in estimating parameter uncertainties . . . 41
4.4.1 Monte Carlo Simulation . . . 42
4.4.2 Boot-Strapping and Jack-Knifing . . . 44
4.4.3 Other uncertainty estimation methods . . . 45
4.5 Generalised Likelihood Uncertainty Estimation . . . 45
4.6 Discussion . . . 47
4.7 Conclusions . . . 48

5 Evaluation of flood extent models 49
5.1 Introduction . . . 50
5.2 Discharge prediction in compound channels . . . 51
5.3 Inundation Modelling Approaches . . . 56
5.4 Application . . . 56
5.5 Results . . . 58
5.5.1 Straight channel configurations . . . 58
5.5.2 Meandering channel configurations . . . 63
5.5.3 Influence of grid resolution . . . 64
5.6 Discussion . . . 64
5.7 Conclusions . . . 67

6 Predictive reliability 69
6.1 Introduction . . . 70
6.2 Study site and available data . . . 71
6.3 Approach . . . 72
6.3.1 Model parameterisation and calibration . . . 73
6.4 Application . . . 73
6.5 Results and discussion . . . 78
6.5.1 Impact of elevation model quality . . . 78
6.5.2 Effect of updating likelihood values using multiple data sets . . . 78
6.5.3 Comparison of predictive reliability of modelling concepts . . . 79
6.6 Conclusions . . . 82

7 Spatially distributed observations **85**
7.1 Introduction . . . 86
7.2 Study site and available data . . . 87
7.3 Approach . . . 89
7.3.1 SOBEK-1D model . . . 89
7.3.2 SOBEK-1D2D model . . . 89
7.3.3 GLUE methodology . . . 90
7.3.4 Effect of topographical uncertainty . . . 92
7.4 Application and results . . . 92
7.4.1 Model validation against flood extent and point observations 92
7.4.2 Assessments of impacts of uncertainty in digital elevation model 96
7.5 Discussion . . . 98
7.5.1 Comparison of model approach . . . 98
7.5.2 Utility of available data in constraining uncertainties . . . 99
7.5.3 Uncertainties in elevation model data . . . 101
7.6 Conclusions . . . 101

8 Distributed land use data **103**
8.1 Introduction . . . 104
8.2 Study site and available data . . . 107
8.3 Approach . . . 109
8.3.1 Model description . . . 109
8.3.2 Evaluating model performance . . . 110
8.3.3 Sensitivity analysis . . . 112
8.3.4 Uncertainty analysis . . . 112
8.4 Results . . . 113
8.4.1 Sensitivity Analysis . . . 113
8.4.2 GLUE Analysis . . . 114
8.5 Discussion . . . 119
8.5.1 Impact of floodplain roughness aggregation on model performance . . . 119
8.5.2 Identifiability of distributed floodplain roughness . . . 121
8.6 Conclusions . . . 123

9 Summary and Conclusions **125**
9.1 Introduction . . . 125
9.2 Summary of research results . . . 126
9.2.1 Hydraulic assessment of codes for predicting flood extent . . 126
9.2.2 Predictive uncertainties in flood extent models . . . 127
9.2.3 Utility of spatially distributed observations . . . 128
9.2.4 Utility of distributed roughness data . . . 129
9.3 Uncertainty in flood extent modelling . . . 130
9.4 Performance of the integrated GIS-model . . . 131

10 Samenvatting **133**
10.1 Inleiding . . . 133
10.2 Samenvatting van de onderzoeksresultaten . . . 134
10.2.1 Hydraulische evaluatie van overstromingsmodellen . . . 134
10.2.2 Betrouwbaarheid van modelvoorspellingen . . . 135
10.2.3 Waarde van ruimtelijke gegevens . . . 136
10.2.4 Waarde van gedistribueerde ruwheden . . . 137
10.3 Onzekerheden in overstromingsmodellering . . . 138
10.4 Prestaties van het geïntegreerde systeem . . . 139

References **141**

A Notation **157**

B Interpolation of 1D results **159**
B.1 Introduction . . . 159
B.2 Inverse distance weighted interpolation . . . 160
B.3 Estimating extent of flooding map . . . 161
B.4 Impact of grid size on accuracy . . . 162
B.5 Test case: Schwemlinger Wiesen . . . 163
B.6 Conclusions and discussion . . . 164

C Numerical methods **171**

Acknowledgements **175**

Curriculum Vitae **176**

List of Figures

2.1 Taxonomy of hydrological models 9
2.2 Levels of GIS-model integration 11
2.3 Flux in and out of a single cell in a cell inundation model 14

3.1 Integrating cross section data sampled from a DEM and surveyed cross section data 23
3.2 Impression of connection between 1D and 2D domains in the SOBEK-1D2D code 28

5.1 Division of compound channel in *vdcm* 52
5.2 Division of compound channel into sections in the *hdcm* method . . 52
5.3 Division of compound meandering channel into four zones. 54
5.4 Impression of channel configurations *s1* (left) and *m3*. 57
5.5 Comparison between the calculated discharge relationships from the *vdcm* and *tmlh* methods and experimental results from the SERC-Flood Channel Facility. 58
5.6 Comparison between calculated velocity distribution and experimental results from the SERC -Flood Channel Facility. 59
5.7 Depth averaged velocities at a discharge of $100m^3/s$ for straight channel with horizontal floodplains. 59
5.8 Predicted stage and discharge in a straight channel with smooth horizontal floodplains (*s1*) 61
5.9 Predicted stage and discharge in a straight channel with rough horizontal floodplains (*s2*) 62
5.10 Predicted staged for different discharges for meandering channel with horizontal floodplains (*m1* & *m2*). 63

6.1 River Saar between Fremersdorf and Mettlach. 71
6.2 Flood hydrographs at the Fremersdorf gauging station. 72
6.3 Comparisons of DEM levels along the line of a dyke. 74
6.4 Schematic overview of three model structures showing 1D and 2D domains. 75
6.5 Cumulative likelihood for peak level predictions at Fremersdorf. . . . 79

6.6 Cumulative likelihood distributions for (a) main channel and (b) floodplain roughness. 80
6.7 Quantiles for peak level predictions using different model concepts. . 80
6.8 Dotty plots for main channel roughness. 81

7.1 Aerial photo of the town of Usti nad Orlici showing the extent of flooding during the 1997 event. 88
7.2 Observed hydrographs of the 1997 event. 88
7.3 Contour lines for the $F^{<2>}$ performance measure. 93
7.4 Contour lines for the MSE performance measure. 94
7.5 Dotty plots for likelihoods derived using the *sbk1D* model. 95
7.6 Dotty plots for likelihoods derived using the *sbk1D2D* model. 95
7.7 Cumulative likelihood distributions for model prediction of flooded area. 97
7.8 Inundation likelihood map. 97
7.9 Variogram of sampled residuals between elevation models. 98
7.10 Impact of elevation model uncertainty on model performance. 99

8.1 Meuse river between Borgharen-Dorp and Grevenbricht. 106
8.2 Gauged levels and discharges at Borgharen-Dorp, Elsloo and Grevenbricht. 108
8.3 Sensitivity analysis for single floodplain roughness class. 114
8.4 Sensitivity analysis for two floodplain roughness classes. 115
8.5 Sensitivity analysis for five floodplain roughness classes 115
8.6 Dotty plots for single floodplain roughness class. 117
8.7 Dotty plots for two floodplain roughness classes. 117
8.8 Dotty plots for five floodplain roughness classes. 117
8.9 Posterior parameter distributions for single floodplain roughness class. 118
8.10 Posterior parameter distributions for two floodplain roughness classes. 118
8.11 Posterior parameter distributions for five floodplain roughness classes. 118
8.12 Constrained parameter ranges after applying threshold. 119

B.1 Example of a quadrant used to select known points. 162
B.2 Elevation model and layout of Schwemlinger Wiesen. 164
B.3 Initial flood depth for 1/50 year event. 165
B.4 Friction map for 1/50 year event. 165
B.5 Cost distance map for 1/50 year event. 166
B.6 Final flood depth map for 1/50 year event. 166
B.7 Flood Extent map for the 200 year event using $5 \times 5m^2$ grid. 167
B.8 Flood Extent map for the 200 year event using $25 \times 25m^2$ grid. . . . 167

List of Tables

3.1 Different approaches in inundation modelling 19
3.2 Categories of topographical data required for a 1D hydrodynamic model 22

5.1 Summary of channel configurations 57
5.2 Comparison of calculated stages for straight channel configuration with inclined floodplains (*s3*). 63

6.1 Peak discharge and level at Fremersdorf. 72
6.2 Prior parameter ranges for main channel and floodplain roughness . 76
6.3 Overview of runs and priors used in updating likelihoods. 78

7.1 Prior parameter ranges. 93
7.2 Shannon entropy values and 90% uncertainty bounds. 96

8.1 Land-use, roughness values and aggregated classes. 107
8.2 Summary of observed data sources. 109
8.3 Range of Mannings-n roughness values. 110
8.4 Shannon-Entropy measure. 120
8.5 Correlation between parameter values and likelihoods. 122

B.1 Flood Area and evaluation time for different grid sizes. 168

Truth is subjectivity and beware of the crowd

Kierkegaard(1813-1855)

1

Introduction

1.1 Background

Present day hydrological research and practice is unthinkable without the use of some form of Geographical Information System (GIS), as GIS has fast evolved to become the primary tool for disseminating spatial information in hydrological analysis. Geographical information has a pivotal role in hydrology (*Chow et al.* 1988; *Clark* 1998), and the definition of GIS by *Burrough and McDonnel* (1998) as a set of tools for storing, manipulating, analyzing and retrieving geographical information provides sufficient explanation of this natural integration of GIS and modelling.

The benefit of GIS may be no more than allowing for the automation of the traditional process of retrieving a map from the library, analyzing for instance catchment boundaries and stream networks, manipulate the data to derive hydrologically meaningful information, such as catchment area and stream length, and storing this in a table for later use in a hydrological analysis. A brief review of the wide array of publications in books and conference proceedings dedicated to the integration of GIS and models (e.g. *Singh and Fiorentino* 1996; *Kovar and Nachtnebel* 1996; *Gurnell and Montgomery* 1997), however, would confirm that even if this was the case, GIS has certainly revolutionised this process in hydrological modelling. Particularly in the case of distributed modelling, the manual process has become intractable, and the ability of GIS to provide this automation has meant that it is fast becoming indispensable.

There is no doubt of the importance of this facet of GIS within hydrology but this does limit GIS to the role of a tool that allows only for efficient analysis. *Goodchild* (1993) describes the role of GIS in hydrological modelling as being of three levels, (i) the use of GIS for pre-processing geographic data suitable for a hydrological process model as described above, (ii) the development of the hydrological process model within the GIS itself, and (iii) post-processing of data for analysis by the user. The first and last of these could relate again to GIS as an efficient way of analyzing the spatial data required, the second step suggests a much tighter integration by embedding the model within GIS. Traditionally, GIS has had limited functionality in dealing with time integration, a pre-requisite of embedding hydrological process models (*Burrough* 2000). General purpose GIS with intrinsic dynamic modelling functionality have, however, been developed in recent years (*Van Deursen* 1995; *Karssenberg* 2002), specifically enabling this embedding, as demonstrated by a wide number of applications (see for example *De Roo* (1998); *Bates and de Roo* (2000); *De Wit* (2001); *Huang and Jiang* (2002)).

While the embedding of process models in GIS has shown to be successful, concessions in the modelling approach may have been made that have impact on how the embedded model represents the system to be modelled (*Sui and Maggio* 1999). This holds particularly for the embedding of highly dynamic systems that require numerical schemes using implicit time integration, a facet of dynamic data handling as yet unavailable in GIS. Although a disadvantage, the best modelling solution may not require the solution of partial differential equations. The most parsimonious approach to follow depends on how well the process can be described within the constraints of the data available, and this has direct implications on the most applicable method of integration with GIS. Conversely, it is important to note that although the integration of the model with GIS may enhance the ease of handling the spatial data and support state of the art visualisation, it will not be able to make a conceptually bad approach successful. *Fedra* (1993) points out that "GIS is not a source of information, but only a way to manipulate information. Unless appropriate spatially distributed data exist, even a state of the art GIS coupled with a 3D model will not guarantee reasonable results".

If the available data support added complexity through including dynamic processes, which requires numerical solving techniques not readily available in GIS, then embedding the model may compromise model results. Likewise, embedding models with a native data structure disparate to that of GIS may compromise results by requiring significant changes in the model concept, typically making the model spatially distributed as opposed to lumped. *Karssenberg* (2002) notes also that although maintainability is improved, for most models embedded in GIS, computational performance is inferior to stand alone optimised codes. This is due to the embedding of the model being achieved through script languages typically available in dynamic GIS, which may not be as efficient as native code.

This discussion shows that there are more aspects to integration of models with GIS than the technical. While it is very apparent to anybody who has undertaken the task of integrating a model with GIS that this is not to be underestimated, it is not unsurmountable. As suggested by *Sui and Maggio* (1999), a broader view needs to be taken in assessing model integration, and this needs to be assessed on the basis of performance of the integrated model. In performance, though, more aspects than just the technical performance in terms of computational speed are relevant, considering the balance of accuracy, computational efficiency, simplicity, and flexibility as described by *Kisiel* (1971) as early as 1971.

1.2 Objectives and approach

The objective of this research is to assess the integration of models used in environmental modelling with GIS from the perspective of performance, where performance takes this broader view than just computational performance as described in the previous section. The central question posed in the research is:

- What are the concepts of integrating hydrological models with GIS, and given an available method of integration, what are the consequences this may have on the reliability of the integrated GIS and model.

To address this question, research is restricted to a sub-set of hydrological models, being hydraulic models for flood extent estimation at the river reach scale. This field is chosen as the available models cover a wide range in terms of complexity and integration, as well as a very apparent interest in coupling with GIS in integrated flood risk assessment studies. Application of these models has shown, however, that a general lack of observed spatial data may have implications on the most appropriate model concept. In addressing the main research question but focusing on the field of flood extent modelling, a number of secondary research questions are posed:

- What concepts are available in flood extent modelling at the river reach scale, and what potential is there for integration with GIS.
- Given possible integration with GIS, what assumptions on the hydraulic behaviour of reach scale inundation need to be made to allow integration, and how do these affect model reliability.
- What is the impact of limited data availability on reliability of the modelling concepts, and how does this influence selection of the appropriate model concept, and with that the associated method of GIS integration.
- What is the influence of the accuracy of spatial GIS data on model reliability.

These secondary research questions indicate the limitations posed. From the extremely wide range of different modelling problems in hydrology, only flood extent modelling is considered, and then only at the river reach scale. The type of inundation event is also restricted to floodplain inundation as opposed to inundation through shock events such as dam breaks. In the approach taken, integration with GIS is viewed very much as a requirement of the application of the different modelling concepts. Thus the technical aspect to performance in terms of computational speed and efficiency in integration is determined largely through model selection. The focus on assessing performance is primarily on the reliability of the integrated model, taken synonymously as the reciprocal to predictive uncertainty. Despite the limited field of modelling considered, the conclusions found can be easily projected on the use of other types of (distributed) modelling in hydrology.

1.3 Motivation

As it was originally conceived, this research project had the objective of investigating the integration of GIS and hydrological modelling, and to look at the performance issues in this integration. Originally, this considered performance in terms of, *how fast will it run, and can we make it faster* with some emphasis on the technological aspect of the integration. Computational efficiency, while being very relevant, is, however, somewhat of a transient problem. This is exemplified if literature from some 30 years previous is considered, with the then relative views on what slow and fast computing is, and how well things would improve once the great leap forward in terms of computing power was achieved. One such relative

view on performance is easily obtained from *Gelb* (1982), who describes a 1963 computer taking $1000\mu s$ to divide two floating point numbers as slow, while a 1982 computer taking only $4\mu s$ was considered fast. At the time of writing, computer speed was being measured in terms of Teraflops, or trillion floating point operations per second, thus showing the relativity of such figures. Who knows what this figure will be at the time of reading. In hydrological modelling *Nash and Sutcliffe* (1970) report that "even now with high speed electronic computers, some simplification of boundary conditions seems necessary". Although simplification where possible is a very good idea, "high speed" is probably not longer an appropriate adjective when compared to computers of today.

Assessing performance as covering only speed is therefore considered a little limiting. There are volumes of conference proceedings and books dedicated to the integration of models and GIS (e.g. *Singh and Fiorentino* 1996; *Kovar and Nachtnebel* 1996; *Gurnell and Montgomery* 1997). These make clear not only that just about every method of integration has been attempted, but also that there is not a singularly best practice. The variety of methods of doing some form of coupling hydrological modelling with GIS do add to the question on *how fast can it run*, the problem of *how fast can I get it to run*. This brings in the dimension of ease of integration and maintainability of the integrated system (*Karssenberg* 2002). The next step is perhaps more relevant than the first two, posing the question: *does it still make sense?* This relates to *what did I gain in integrating*, or to put it in a more negative perspective, *what did I lose in integrating*. For many existing models it is the definite modern step to integrate in some form with GIS, but this may result in having to make changes in the model concept or data structure to allow integration (*Miles and Ho* 1999; *Sui and Maggio* 1999).

In any case integration with GIS usually provides a more appealing interface to the model. The motivation behind emphasising reliability or uncertainty in integration comes from a sometimes sceptical view on the ever increasing usability of complex simulation models, together with the trust vested in these integrated systems in supporting decisions, even by experts. *Klemeš* (1999) summarises this as:

> There are too many models now with nice-looking user interfaces but no contents whatsoever. The planners believe that these will solve all their problems.

1.4 Structure of this thesis

The second chapter of this thesis explores the general context of integration of GIS and hydrological modelling. Different approaches and issues related to this integration are discussed, and how these influence usability of the integrated system. The third chapter concentrates on the field of flood extent modelling, describing the concepts available and the underlying assumptions made. For each approach the model complexity is considered, and the most apparent level of integration with GIS discussed. Particular issues relating to the complexity of GIS data manipulation to achieve this integration are described.

Chapter 4 is central to the thesis as the concept of performance is introduced. Performance is predominantly viewed from the point of view of model reliability. With reliability expressed as the reciprocal to predictive uncertainty, methods used in this thesis for the assessing of model uncertainties are discussed.

The models described in chapter 3 are revisited in chapter 5, and before applying these to field data, the underlying assumptions of the different methods are compared to theoretical analysis of hydraulic flow in two-stage channels. Predictive uncertainties in different model approaches are studied in chapter 6, where different sets of calibration data are used to establish models for a reach of the Saar River in Germany. The models are validated against the largest event on record, exploring the impact of the different datasets on reliability of extrapolation. Chapter 7 applies two of these concepts to field data from a flood event in the town of Usti nad Orlici in the Czech Republic. For this event, different types of spatial data are available, and the value of this data in constraining predictive uncertainties is explored. The implications of error in the underlying GIS data, and its influence on resulting uncertainties is also investigated. Chapter 8 finally explores the use of distributed GIS data in a reach of the Meuse River in the Netherlands, exploring how availability of these data influence predictive uncertainties.

The summary and conclusions in chapter 9, draw attention to both specific aspects of flood extent modelling discussed in the main research chapters, as well as to more general conclusions regarding performance on integration of hydrological models with GIS.

2

Geographic Information Systems and hydrological modelling

2.1 Introduction

In the previous chapter the most basic form in which a model can be coupled to GIS implies that GIS is in effect a tool for efficient processing and preparing of data for hydrological analysis. The number of applications of such analysis is almost limitless, with examples including the use of GIS to establish spatial characteristics of thunderstorms (*Tsanis and Gad* 2001; *Syed et al.* 2003), spatial correlation of rainfall (*Holawe and Dutter* 1999), establishing relations between land-forms and vegetation (*Hoersch et al.* 2002), and establishing vulnerability of catchments to flash flooding based on topological characteristics (*Carpenter et al.* 1999). Particularly in areas with high spatial variability, GIS is invaluable in establishing hydrological characteristics (*Marquínez et al.* 2003; *Hock* 2003; *Weingartner et al.* 2003). Global databases such as the GTOPO30 and even more detailed data sets currently becoming available, have enabled this type of analysis to be extended to cover even the more data scarce parts of the world (cf. *Chalise et al.* 2003; *Döll and Lehner* 2002). GIS also provides for spatial techniques such as classification and geo-statistical analysis required for processing of the vast amount of remote sensing data, and usefully integrating these data into hydrological analysis (*Brackendridge et al.* 1998; *Horritt* 1999; *Mason et al.* 2003; *Pauwels et al.* 2001; *Schmugge et al.* 2002)

In all these examples, however, there is no requirement of actual integration between the models and GIS, as a simple exchange of data between the two systems suffices. The potential of a more integrated approach in linking GIS and hydrological models is apparent, and has been widely established and demonstrated (*Karssenberg* 2002). Various classifications of the different methods of linking hydrological models and GIS can be adopted, but mostly the levels of integration are differentiated as (i) loosely coupled systems, and (ii) tightly coupled systems (*Van Deursen* 1995; *Clark* 1998; *Pullar and Springer* 2000; *Karssenberg* 2002; *Leavesley et al.* 2002). The first level considers the situation where the data structure of the modelling system is inherently different to that of the GIS, and data is passed between the two systems on an *ad-hoc* basis. The second level implies the GIS and hydrological modelling system effectively share the same data model. If this is the case, further distinction can be made between (i) sharing of the same data model but preserving the two as separate systems, and (ii) actually embedding the model within the GIS

as a series of spatial operators (*Huang and Jiang* 2002).

Each of these three levels of integration has advantages and disadvantages, and although often the integration approach is explored from the point of view of efficiency in programming and ease of use (*Karssenberg* 2002), more aspects must be considered. The complexity of the modelling approach may determine to a large extent the types of integration level that can be achieved. Even if for most hydrological problems a modelling approach can be found to suit a data model that allows tight coupling through embedding the model in GIS, this may have implications on the underlying assumptions that need to be made in the modelling approach (*Sui and Maggio* 1999). These assumptions may in turn have significant impact on the reliability of results, thus leaving the relevant question on the gain in integration with GIS only partly answered. This chapter begins with a brief overview of modelling approaches and model complexity. The different levels of integration are then discussed against the light of model complexity.

2.2 Modelling approaches and complexity

Models used in hydrology cover a wide spectrum of approaches. In order to attempt some sort of categorisation, *Chow et al.* (1988) classified these on the assumptions made with respect to three key parameters; randomness, space, and time. Depending on how a given model approaches each of these parameters, it can be classified in one of eight categories, although there will always be grey areas where models fall into more than one category. An alternative categorisation often referred to in model application can be found through the concepts applied in the model in describing the behaviour of the system to be modelled;

Black box models In black box, or data driven modelling a relation is established between the inputs and outputs of interest. Examples of these types of models include database mechanistic modelling (*Young et al.* 1997; *Lees* 2000) and Artificial Neural Networks (*Cameron et al.* 2002). To set up these models, a large amount of inputs and known outputs are required to establish a reliable relationship. This relationship usually does not reflect the physics between inputs and outputs, although there are recent attempts at incorporating some physical basis in data driven modelling techniques such as neural networks (*Aarts and van der Veer* 2001).

Physically based models Physically based models are the most complex family of models. The principle on which physically based models are founded is that these are derived from established physical principles, as given in appropriate assumptions and laws. The ideal of the physically based model, is that given sufficient physically measurable data, a model can be constructed that adequately describes the behaviour of the system without the need for calibration. In practice, it is generally found, however, that while the laws and assumptions made apply reasonably well to the laboratory scale or to the field point scale, they are less applicable to the scale of grids used in modelling a real-world system (*Beven* 2002). Some calibration is therefore

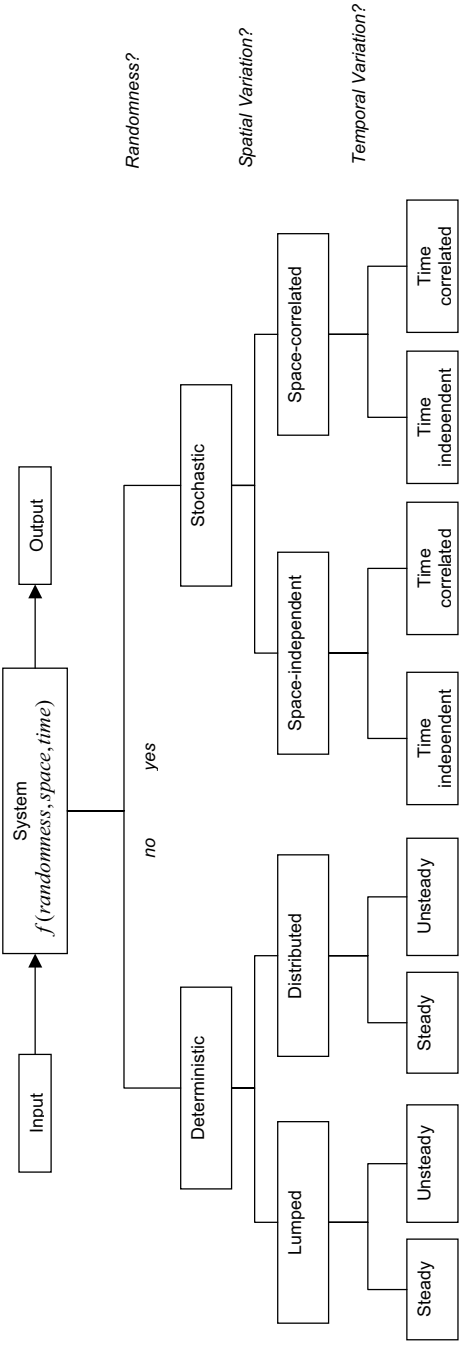


Figure 2.1: Taxonomy of hydrological models (after *Chow et al.* (1988); *Sui and Maggio* (1999)).

typically needed before the model can be reliably applied, and the parameters initially derived only through using observed attribute data need to be adjusted accordingly (*Madsen* 2003).

Conceptual models Conceptual models offer a practical compromise between physically based and black-box models (*Viney et al.* 2000). Rather than exact physical balance equations, conceptual models rely on empirical descriptions of the processes considered as dominant. Most conceptual hydrological rainfall runoff models will for example contain a combination of (non) linear stores, with different stores to describe fast responding overland flow, intermediate response from interflow and slow responding groundwater flow. Generally these models are applied either as lumped models (see figure 2.1) or semi-distributed. Vast amounts of distributed attribute data as in the physically based models are not necessary, but a drawback is that the models rely heavily on calibration with a suitable set of observed response data required.

Although different categorisations than those discussed are available, models in all categories of the taxonomy according to *Chow et al.* (1988), and in the black box, conceptual, and physically based categorisation, can potentially be integrated with GIS. For space independent stochastic models, as well as many black box type models, the need for integration would seem less apparent. For the remaining categories, the issues in integrating the models with GIS are closely related to how these deal with the three parameters of randomness, space, and time. The most simple form of modelling is described by *Chow et al.* (1988) as being deterministic, lumped and time invariant (steady state), but this may not necessarily be the category most easily integrated with GIS as the lumped concept will require some form of transformation to allow integration with the distributed GIS data. Besides the elementary issues in terms of the three parameters suggested, the question on *how* these models deal with in particular spatial and temporal variation is very relevant to possible integration with GIS. Many of the currently available GIS deal well with spatial resolution, sometimes equally supporting vector data, grid data, and triangulated irregular network TIN data. If this is the case, then the issue of temporal variation is the most critical point of consideration in integrating GIS and models (*Schultz* 1996). Traditionally, GIS have clearly lagged behind in supporting temporal variation, but the development of a number of dynamic modelling GIS (*Van Deursen and Wesseling* 1996; *Karssenberg* 2002) have resolved this problem to some extent for models dealing with temporal variation through explicit integration, but less so for models requiring implicit time integration.

2.3 Levels of integration

2.3.1 Loosely coupling

Figure 2.2 schematically shows three possible levels of integration of GIS and environmental models. The most commonly applied of the three approaches is that where the model is loosely coupled with GIS. Integration between GIS and the hydrological model is then provided through a (file based) exchange of data either as

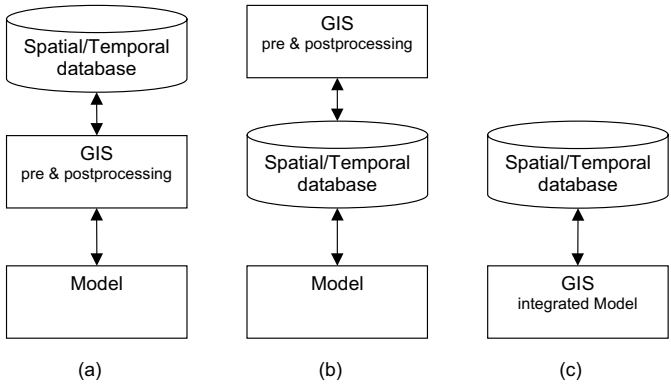


Figure 2.2: Levels of GIS-model integration (a) loosely coupled; (b) tightly coupled through shared database; (c) tightly coupled through embedded model).

a pre-processing or as a post-processing exercise. Of the categories of models described above, integration through loose coupling is most apparent for the lumped (conceptual) models. GIS offers invaluable support in deriving model parameters that can be related to topographical attributes such as area, elevation, slope vegetation types etc. Models integrated with GIS through loosely coupling are often existing models, and the approach minimises development or amendment of model code (*Sui and Maggio* 1999). Moreover, many standard GIS currently provide libraries of hydrological oriented spatial analysis functions (*Kopp* 1998), reducing the amount of development of GIS code. The number of examples of loosely coupled models is too large to mention, but include lumped or semi-distributed hydrological models (e.g. *Schumann et al.* 2000; *Leavesley et al.* 2002; *Lacroix et al.* 2002) and (one dimensional) hydraulic models (e.g. *Nickel* 1998; *Scholten* 2000; *Tate et al.* 2002). Examples of analysis of post-processed model outputs using the loosely coupled approach can be found in flood risk mapping (e.g. *Nickel* 1998; *Harris and Archer* 1999; *Tate et al.* 2002). The loosely coupled approach is also widely applied in spatial decision support systems where user interaction and dissemination of results is through GIS, while evaluation of proposed measures is through one or more loosely coupled models (e.g. *Brimicombe* 1992; *Goodchild* 1993; *Fedra* 1993; *Uran and Janssen* 2003). From the wide variety of applications of which only a very small selection is given, it is clear that the loosely coupled approach has shown to be attractive. The disadvantage is, however, that the coupling is somewhat *ad-hoc* and the spatial and model databases remain independent. The exchange of data between the two is error-prone, and implementing changes in the integrated system can be difficult as it requires extensive knowledge of both systems (*Karssenberg* 2002).

2.3.2 Tightly coupling - shared data model

The disadvantages of the *ad-hoc* interchange of data is resolved in the intermediate approach in coupling models shown in figure 2.2. Here the model and the GIS share a common spatially distributed data model, but are still independent entities with the evaluation of modelling functions within the model. This requires the GIS data structures to be sufficiently open (*Van Deursen* 1995), but does not pose any restrictions on how variation in time and space are dealt with. As GIS have limited abilities in resolving time integration in dynamic modelling, this may be an advantage for highly dynamic systems where some form of implicit numerical modelling is required. These models requiring implicit time integration often belong to the physically based category, and are generally deterministic, spatially distributed and unsteady (see figure 2.1).

Data represented in the models is mostly continuous in space and is represented using regular grid data structures (*Burrough and McDonnel* 1998). Examples include the physically based hydrological model SHE (*Abbott et al.* 1986), the modular modelling system (*Leavesley et al.* 2002) and a wide variety of grid based flood inundation model codes (e.g. *Stelling et al.* 1998; *Beffa and Connell* 2001). Other codes use Triangulated Irregular Network (TIN) to represent the continuous data (e.g *Hervouet* 2000). Particularly the availability of (pixel based) remote sensing and laser altimetry data has led to rapid expansion model applications using this approach (e.g. *Marks and Bates* 2000; *Brackendridge et al.* 1998; *Horritt* 1999; *Mason et al.* 2003; *Pauwels et al.* 2001; *Schmugge et al.* 2002).

Despite the problem of error-prone code development to exchange information between the model and the GIS being reduced, there are still dependencies on the openness of the GIS data structures, and consequences on maintainability as hydrologists involved will still need to be proficient in both GIS and the model code itself (*Karssenberg* 2002).

2.3.3 Tightly coupling - embedded process model

To avoid possible issues on the exchange of data between different systems as in the loosely coupled approach, or on openness and maintainability of shared databases, the third approach in Figure 2.2 in coupling hydrological models and GIS is through embedding the hydrological model within GIS. The advantage of this approach is that the full potential of GIS can be employed within the model for both data manipulation as well as the powerful visualisation associated with GIS, without the need for any overheads incurred due to transfer of data between systems (*Van Deursen* 1995). GIS has traditionally been relatively poor in supporting dynamic modelling (*Burrough and McDonnel* 1998), but recent developments allowing more complete support of dynamic continuous spatial data in both widely used desktop GIS (*ESRI* 1996) and specialist GIS (PCRASTER, see *Van Deursen and Wesseling* (1996); *Karssenberg* (2002)) have helped improve this deficiency. Particularly the availability of powerful, easy to understand, integrated script languages has empowered hydrologists with the ability to easily assemble spatially distributed models within the GIS itself (*Karssenberg* 2002). This has given development and research

in such integrated models a significant boost, and numerous examples of such fully integrated systems exist, including hydrological models of varying concepts and complexity (e.g. *Kwadijk* 1993; *Huang and Jiang* 2002; *Van der Linden and Woo* 2003), models for sediment or nutrients transport (*De Roo* 1998; *De Wit* 2001), and floodplain inundation models (*Bates and de Roo* 2000).

2.3.4 Time and GIS

Developments in GIS to allow embedded dynamic modelling have resolved some of the issues related to dealing with temporal variation, but while these developments have proven very useful in dynamic modelling, the actual technological advance in GIS are limited (*Peuquet* 2000). *Peuquet* (2001) identifies two fundamental concepts in spatio-temporal modelling. The first is the "discrete view", where distinct spatial entities are identified in GIS, each with attribute data that can relate to time, such as validity. This relates to the origin of GIS as primarily a means of storing spatial data, and although validity of data is not unimportant, it is rarely explicitly considered in environmental modelling (*Burrough* 2000). In other fields of application of GIS, such as cadastral databases (*Van Oosterom* 2000), the underlying data models deal explicitly with validity of data. To reduce storage, data models for such applications can follow the event driven approach, storing only a list of events and their sequence (*Chen and Jiang* 2000). The second concept is the "continuous view", where individual objects or properties are attributes to a given location and time. Current GIS, however, cannot dynamically maintain topological relationships between rapidly changing spatial entities (*Pang and Shi* 2002). For environmental modelling, where data follows the "continuous view", it can be either stored as a sequence of snapshots or layers in time, or in the form of an update model, where an initial data set is stored together with time and location of changes (*Zang and Hunter* 2000). Despite the redundancy in the first approach, this is the most viable option currently available in environmental modelling in GIS (*Burrough and McDonnel* 1998). This serves the purpose of environmental modelling well, but does pose limitations on the complexity of the model, as none of the currently available GIS can deal with implicit time integration. Dynamic environmental models typically describe the change in a system state due to changing boundary conditions:

$$\frac{\partial \hat{X}}{\partial t} = f(\hat{X}, t) + g(t) \tag{2.1}$$

where f is a function determining how the state X changes in time, depending on the state itself and the time varying boundary conditions g. Note that the state may be either in zero, one, two or three dimensions. The function f can be highly non-linear. Given the limited ability GIS has in handling time means there may be limitations on how such a relationship can be embedded. A good example to illustrate this, is the cell inundation model. Figure 2.3 gives a schematic representation of a single cell in such a model, where ζ is the water level (above absolute reference) and Q indicates a flux across a cell boundary. The relationship between the volume in the cell and the inflow per unit time step,

$$\frac{\Delta V_i}{\Delta t} = \sum_k Q_k \tag{2.2}$$

where V_i is the volume in cell and Q_k is the discharge into the cell from cell k, and $\sum_k$ is the sum of all discharges of cells k connected to cell i. The discharge between two cells is determined through the difference in surface level between two cells using Manning's equation (*Cunge et al.* 1980),

$$Q_k = Sign(\zeta_k - \zeta_i)\frac{h_{flow}^{5/3}}{n}\left(\frac{|\zeta_k - \zeta_i|}{\Delta x}\right)^{1/2}\Delta y \tag{2.3}$$

with Q_k the discharge from cell k to cell i and h_{flow} is the effective depth of flow at the cell interface, and ζ is the water level above a reference plane. Δx and Δy are the grid cell resolution in x and y. A common numerical approach to implement the non-linear relationship between stage in the two cells and discharge between them is (*Cunge et al.* 1980):

$$A_i\frac{h_i^{t+1} - h_i^t}{\Delta t} = \Theta\sum_k Q(h_i^{t+1}, h_k^{t+1}) + (1-\Theta)\sum_k Q(h_t^n, h_t^n) \tag{2.4}$$

To allow stable solution at an acceptable time step, the problem should be solved implicitly by taking $0 < \Theta \leq 1$ and , but implicit integration in time is not possible in standard GIS and as a result Θ must be taken equal to 1. To allow embedding of a model in GIS the explicit solution must be followed, and this will remain stable only if the time step is kept very small in rapidly changing conditions *Estrela and Quintas* (1994).

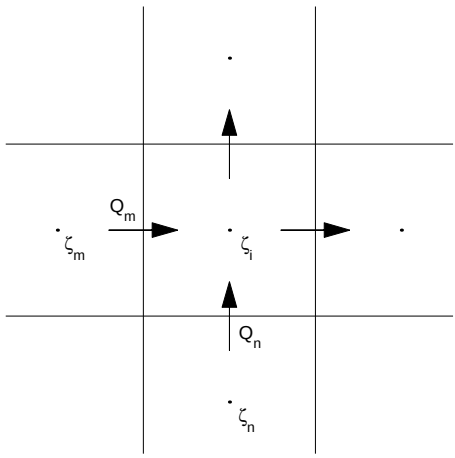


Figure 2.3: Flux in and out of a single cell in a cell inundation model. The total flux in and out of cell i is found through summing $k = m, n, ...$ components.

2.3.5 3D GIS

Generally the GIS used in hydrological modelling represent spatial data in two dimensions. Although some of the data used such as digital elevation models suggest three dimensions, these are essentially two dimensional with height a function of x and y, and should be referred to as at best $2.5D$ (*Bergougnoux* 2000). In true $3D$ a parameter is a function of three independent spatial coordinates x,y and z. Although there are hydrodynamic modelling problems where variation in the third dimension may need to be considered (e.g density flows), this complexity is not warranted in flood extent modelling and flow is resolved at most in two dimensions assuming hydrostatic pressure in the vertical. The concept of 3D GIS is therefore not further considered in this thesis.

2.4 Discussion

The increasing levels of integration discussed in the previous sections suggest an increasing level of significance in the contribution of GIS to hydrological modelling. *Clark* (1998) points out, however, that this may be misleading, as the value of GIS can not be determined by how much it is in control of the modelling process. Numerous examples are available where GIS have proven invaluable in establishing hydrological models with high resolution spatial data (e.g. *Marks and Bates* 2000; *Puech and Raclot* 2002; *Cobby et al.* 2003), but the role of GIS in improving model reliability itself should not be overplayed so as not to avoid disappointment or unfounded belief. First the scale at which (GIS) data is available may not be the same scale at which the data is used in the model, thus leaving the problem of parameterisation unresolved (*Schumann et al.* 2000). In both GIS and in the model, parameters such as soil characteristics will have a different scale than the point measurement. As it is impossible to measure every point in a catchment, these characteristics will be represented both in GIS and in the model as "effective" parameters at a scale appropriate to each respective system. These "effective" parameters may, however, be derived on an entirely different basis. For example in GIS the characteristic shown may be the area majority, whereas in the model the characteristic dominating the hydrological response is more suitable. Second a range of different data may be required for full parameterisation of the hydrological model. While some of these data may be available at high resolution, it may be impossible to know all details at all levels required, particularly not at the same resolution (*Beven* 2001b).

The result is that model reliability will not increase simply because high resolution data of for example surface topography (e.g. LiDAR data) or classified land use are available through GIS to an embedded process model. A finer balance needs to be established. The level of detail of the data provided through GIS to the model needs to be considered, as this should be such that it is of adequate resolution in view of all the other model data requirements, but should not be too high as this may lead to a false sense of belief in the model and its results. The level of integration of the model with the GIS that is used equally needs to be considered. While an embedded model may enhance the modelling process and allow the full

visual power of GIS to be employed, it may equally require important hydrological processes to be neglected. A less technically advanced level of integration may be then be more suitable.

2.5 Conclusions

In this chapter different methods of integration of hydrological models and GIS were explored. The numerous applications of such an integrated system, both as a modelling tool and in integrated spatial decision support systems, show the value of such integration. These also show that although the applications are varied, the integration can be categorised into three classes. In the first the model and GIS are loosely linked through file based exchange, including possible reformatting of data to fit differing concepts in dealing with the spatial dimension. In the second model and GIS share a common database, but the two systems are still separate, while in the third the model is actually embedded within the GIS. From the perspective of technological integration and good maintainability of the integrated system the last approach is clearly superior. Depending on how the model to be integrated deals with spatial and temporal variation, this approach may, however, not be feasible without changing the concepts and assumptions on which the model is founded. This may have implications on the reliability of the integrated system.

3

Flood Extent Estimation

3.1 Introduction

A natural integration between GIS and hydrological modelling can be found in flood risk assessment. This is described as the combination of the vulnerability of a given area with the hazard potential flooding poses to the area (*Penning-Rowsell and Tunstall* 1996; *Gilard and Givone* 1997). Vulnerability is established through the spatial acceptability of flooding, often expressed in terms of design return periods. Although the general public may take the point of view that all flooding is unacceptable, it is clear that this is impossible to achieve. An acceptable value in terms of return period of flooding needs to established. This acceptable return period may be established through cost-benefit evaluation comparing potential losses due to flooding against the costs of building defences, with stage-damage functions used to estimate losses (*Dutta et al.* 2003). The clear spatial dimension of properties at risk, as well as the availability of for example cadastral databases clarify the natural integration of flood risk assessment and GIS. Once the spatial vulnerability to flooding has been mapped, the problem is how to establish the hazard to flooding. This problem does not lie in the requirements as these are quite clear; what is needed is a map of the extent of flooding and perhaps flow velocities for one or more design floods of given return periods. Establishment of such flood zones is often even a legislative obligation (*Harris and Archer* 1999; *Penning-Rowsell and Tunstall* 1996) or may be required for pricing insurance policies (*Clark* 1998; *Hausmann and Weber* 1996). The problem does lie in how to derive a reliable map of the extent of flooding for a given return period.

Table 3.1 gives an overview of a variety of different methods in use for flood extent modelling. The most simple approach involves estimating a planar water level surface using observed water levels at gauges. This planar surface is then crossed with a digital elevation model of the reach and areas with a depth greater than zero retained (*Priestnall et al.* 2000). The approach takes no account of the hydraulics of floodplain and main channel flow, and the extreme simplicity of the approach is reflected in its bad performance (*Horritt and Bates* 2001a). Application to design floods moreover requires reliable extrapolation of rating curves at the gauges used, making the approach unviable in reliable flood extent estimation.

The storage inundation cell method was described first by *Cunge* (1975), and has since been applied widely (*Cunge et al.* 1980; *Jonge et al.* 1996; *Romanowicz and Beven* 1998). The floodplain is simply divided into large storage cells, with water flowing from main river into these cells, as well as between cells. The method

is particulary suited to inundation of extensive low-lying areas such as polder areas where dykes and embankments form natural cell boundaries. Water levels in each of the cells is constant, determined using a balance of inflows and outflows, with these fluxes described using uniform flow and/or weir equations. As a result of the discretisation, flooding is a binary process, with the flood extent being constrained by how the cells are defined.

Through dividing the floodplain in cells delineated by natural boundaries, the extent of inundation is not independent of the discretisation. This is resolved by taking smaller cells without natural boundaries between them (*Romanowicz et al.* 1994), and results finally in applying the storage cell approach where storage cells are based on the underlying DEM.

This thesis focuses on estimating flood extent using the three hydrodynamic modelling approaches described in table 3.1, as well as the simple storage cell approach using small inundation cells. The four methods selected do not cover all of the variations described in table 3.1, but represent the type of model used in practice in flood extent modelling. All four methods allow flood extent estimation independently of the model structure such as when applying large storage cells. Differences between the methods are found primarily in hydraulic complexity, and how these can be integrated with GIS. In this chapter the theoretical basis and assumptions of the selected methods are discussed, as well as to what degree these can be integrated with GIS.

Table 3.1: Different approaches in inundation modelling, in order of increasing (hydraulic) complexity (after *Bates and de Roo* (2000))

Method	Description	Codes (Examples)	Applications
Planar Water Surface	A planar flood surface is obtained using water levels established through rating curves at river gauges. This surface is then overlain on the DEM and all areas where the surface is above the DEM are considered as flooded	None	*Priestnall et al.* (2000)
Large storage cell	Main channel and floodplain are considered separately. Floodplain is discretised as inundation cells, often using natural divisions such as dykes and other embankments. Flow in main channel and between cells is described using uniform flow equations (e.g. Manning, Weir formula)		*Cunge* (1975); *Jonge et al.* (1996)
Small storage cell	Similar approach to the previous, but rather than discretisation of floodplain in designated cells, these are automatically derived from the DEM, either raster or TIN based. Main channel flow is resolved one-dimensionally using either kinematic or diffusive wave model	FLOODSIM, LISFLOOD-FP	*Bechteler et al.* (1994); *Bates and de Roo* (2000)
1D hydrodynamic models	Solution of the full 1D Saint Venant equations using a series of cross sections of main channel and floodplain perpendicular to the main channel. Resulting water levels at 1D computational grid points can be mapped to a 2D inundation extent map using spatial interpolation.	HEC-RAS, ISIS, MIKE11, SOBEK	*Tate and Maidment* (1999); *Penning-Rowsell and Tunstall* (1996); *Gourbesville* (1998); *Werner* (2001)
2D hydrodynamic models	Solution of the full 2D shallow water equations, possibly with turbulence closure. Discretisation of floodplain and main channel using structured or unstructured grid (regular, TIN, curvilinear)	TELEMEAC-2D, MIKE21, DELFT-FLS, DELFT3D	*Hervouet* (2000); *McCowan and Collins* (1999); *Beffa and Connell* (2001); *Stelling and Duinmeijer* (2003)
Integrated 1D-2D hydrodynamic models	Solution of the full 2D shallow water equations for floodplain flow. Main channel flow is solved using the 1D approach.	SOBEK OVERLAND FLOW, MIKE FLOOD	*Verwey* (2001); *Frank et al.* (2001)

3.2 One-dimensional hydrodynamic modelling

3.2.1 Model concept

One dimensional hydrodynamic codes are widely applied for studying flood levels and discharges in river systems, and have been applied successfully in modelling flood routing at river reach scales from tens to hundreds of kilometres (e.g. *Wijbenga et al.* 1994; *Lammersen et al.* 2002; *Yoshida and Dittrich* 2002). Although not as computationally efficient as simple hydrological routing methods, such as kinematic wave routing and Muskingum routing, 1D hydrodynamic models allow for rapid evaluation of distributed water levels and discharges in both dendritic and networked river system, considering effects such as backwater, advection and diffusion.

These codes are founded on the assumptions of one-dimensional flow, with the most relevant being that stage and discharge vary only in the longitudinal direction. Flow is also considered to vary only gradually thus allowing the pressure to be assumed as hydrostatic, and that it is fully turbulent. River topology is given as a number of one-dimensional branches interconnected at nodes, while the geometry is described as a series of cross sections perpendicular to the flow direction. Following the assumption of one-dimensional flow, water levels calculated for the cross section are considered constant across the cross-section.

A variety of commercial and non-commercial codes are available (see Table 3.1 for some examples). These vary somewhat in scope of application, schematisation approach and mathematical solution method, but are all founded on the common principle of the 1D equations for continuity and momentum (equations 3.1 and 3.2, *Chow* (1959)). Applying Mannings-n as the roughness formulation and ignoring wind friction these are given as:

$$\frac{\partial A}{\partial t} + \frac{\partial Q}{\partial x} = q_{lat} \tag{3.1}$$

$$\frac{1}{A}\frac{\partial Q}{\partial t} + \frac{1}{A}\frac{\partial}{\partial x}\left(\frac{Q^2}{A}\right) + g\frac{\partial \zeta}{\partial x} + \frac{n^2 Q|Q|}{A^2 R^{4/3}} = 0 \tag{3.2}$$

As a general analytical solution of these equations does not exist, the codes solve these numerically, mainly through the finite difference approach. Two types of spatial discretisation are in use, (i) the box-scheme, or Preissmen scheme, where water level and discharge variables are co-located on calculation grid points, or (ii) staggered schemes where water level and discharge variables are located on alternate grid points (*Cunge et al.* 1980).

In this thesis, the SOBEK 1D hydrodynamic code is applied (see table 3.1). This code allows a choice of numerical engine, using either the box-scheme or the staggered grid numerical scheme. In the (older) numerical engine applying the box scheme, cross sections are represented as one-dimensional level width tables, where at each increasing level in the cross section the corresponding flow and storage widths are given. This version was developed primarily for modelling rivers with floodplains, and the definition of cross section supports allocation of floodplain and

main channel sections, with different roughness values defined in each section. In solving dynamic water flow, cross section conveyance is solved as the sum of conveyance of the main channel and two floodplain sections, with water level continuity across the complete section. A zero shear stress assumption is made for the vertical division between the sections.

The (newer) numerical engine uses the staggered scheme, and allows different methods of cross section definition. These include cross sections as described above, but also a more flexible cross definition as a table of coordinates giving distance across the section and associated bed elevation. Roughness values may be defined for each section between coordinate pairs. Conveyance is again evaluated first for each section individually, and summed across all sections, assuming zero shear stress along the vertical division between sections.

3.2.2 Integration with GIS

The one-dimensional nature implies that these models can only reasonably be integrated with GIS using the loosely coupled approach. Some attempts have been made at defining 1D branches in GIS, through for example a raster representation of the main channel (*Bates and de Roo* 2000), but the numerical routines used in solving dynamic flow were limited to simple kinematic or diffusive wave modelling. For full simulation of hydrodynamic flow, such as in 1D codes as the SOBEK code, the numerical procedures required in solving the partial differential equations are complex, usually applying implicit time integration, making an integration with GIS through embedding the model impossible.

In the loosely coupled setup between GIS and the 1D hydrodynamic model code, the GIS is positioned on the one hand as a pre-processor to derive model data, and as a post-processor for dissemination of results. Table 3.2 gives an overview of the typical types of topological data required in setting up a 1D hydrodynamic model. Most of the data describing the structure of the river network can be obtained from map data, and GIS offer a useful toolkit for retrieving these data from spatial datasets. Simple GIS functionality can be applied in deriving for example lengths of branches between nodes etc. Other data, obtained typically from river surveys is often of a dimension incompatible to the 2D GIS representation, but may be stored as attribute data to a point location in the GIS. This approach was taken in the Integrated Catchment Model described by *Blongewicz* (2000).

To pass this data to the hydrodynamic model, appropriate interchange formats must be defined. Export functionality must be provided in GIS on the one hand, and import functionality for the model on the other, to allow exchange of data between the two systems. Although the role of GIS in preparing this data is somewhat modest, the power of GIS to aid in analysis of topographical data such as in digital elevation models can be used to complement data from river survey data such as for cross sections where this data is lacking or of insufficient extent.

This is particularly relevant to cross section data. These form an important part of setting up a one-dimensional flow model, but are often found to be sparse (*Hicks* 1996; *Nickel* 1998). In other cases, available cross sections may not be fully suitable, as the data may not cover the floodplain to the full extent required for

Table 3.2: Typical categories of topographical data required for a 1D hydrodynamic model of a river reach

Data	Description	Possible source
Branches	Layout of river network	GIS
Nodes	Locations of model boundaries as well as confluences etc.	GIS
Main channel	Delineation of main channel	GIS
Floodplain	Delineation of floodplain	GIS
Structure Locations	Location of structures (e.g. weirs, bridges)	GIS
Structure Description	Properties of structures (e.g. dimensions, operation)	Survey data
Cross Section locations	Locations of cross sections	Survey data
Cross Section topology	Cross section data	Survey data

modelling higher flood stages in flood extent modelling (*Nickel* 1998; *Harris and Archer* 1999; *Werner et al.* 2000).

With the increasing availability of high resolution elevation data of rivers and their floodplains (*Marks and Bates* 2000), surveyed cross sections can be enhanced where lacking using GIS procedures. A number of methods have been proposed to sample cross sections from a digital elevation of floodplain and/or main channel (*Harris and Archer* 1999; *Krahe et al.* 2000; *Scholten* 2000). The most simple is to define a line along which the cross section is to be extended along the floodplain and sample the digital elevation model along this line at regular intervals (for a full description see *Werner et al.* (2000)). To correctly represent floodplain flow, cross sections should also be more or less perpendicular to the direction of flow such that the assumption of constant water level across the cross section holds as well as possible (*Chow et al.* 1988). Even where surveyed data of sufficient extent is available, the delineation of these surveyed cross sections may not follow this ideal line, and sampling from the digital elevation model using a more appropriate cross section delineation may help establish more appropriate data. The division of the two data sources can be set at the intersection between main channel and floodplain. Typically, there will be some discrepancy between the two data sources (*Tate et al.* 2002), and these difference will need to be smoothed. This is clearly shown in Figure 3.1 where an example of integrating a cross section sampled from a digital elevation model of the floodplain with the surveyed data is given.

The different methods available in deriving cross sections from surveyed data and samples taken from digital elevation data, will have effect on the conveyance of the cross sections (*Werner et al.* 2000). This is a disadvantage of the loosely coupled approach, as ambiguity on how the data to be transformed is introduced.

In calibrating models with cross sections derived by any of the available methods, these differences in conveyance will typically be smoothed out, but differences will then reflect in the estimated roughness values.

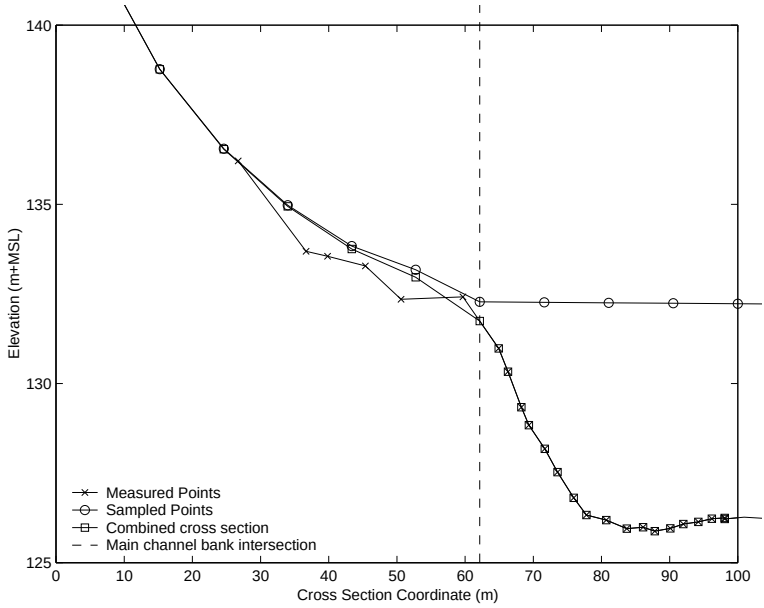


Figure 3.1: Integrating cross section data sampled from a DEM and surveyed cross section data (from *Werner et al.* (2000)).

The other role of GIS in one-dimensional modelling is as a post-processing tool. Most results from a 1D model are time series data such as water levels and discharges. These data are distributed both in time and space, and can again be stored in GIS using the point-attribute concept (*Blongewicz* 2000). To allow for visual interpretation of results, the data can also be thematically represented in GIS.

A powerful use of GIS in post-processing is in the projection of the water level results as a 2D water level surface. In combination with a digital elevation model of the reach, this can be used to estimate the extent of inundation. Traditionally flood zones based on levels in the river were hand-drawn on paper maps, an expensive and time consuming exercise (*Jones et al.* 1996). Post-processing the results of the 1D model using GIS can expedite this process (*Jones et al.* 1996; *Harris and Archer* 1999), and also provide additional information such as distributed flood depth. Distributed depth data may be useful in more detailed flood damage assessment through the use of stage-damage curves (*Dutta et al.* 2003). With the development of flood zone maps becoming a statutory obligation in many countries (e.g. the National Flood Insurance Programme (NFIP) undertaken by the U.S Federal Environmental Management Agency (FEMA) or the Section 105 modelling programme undertaken by the U.K. Environment Agency), the need for efficient tools

for developing flood inundation maps has risen. Of the tools officially accredited by FEMA to support this mapping (see http://www.fema.gov/ for details), most are one dimensional hydraulic models, with the results of these projected in GIS to obtain a 2D inundation map.

The basis for deriving a 2D representation of the 1D simulation results is the assumption made in 1D hydrodynamic modelling that water levels are constant along the cross section. Given that the cross section represents not only a single point in the 1D model but also a line on a map, this assumption can be exploited to project the calculated water levels along these geo-referenced cross sections. Following allocation of water levels along the cross section lines, spatial interpolation techniques available in GIS can be applied in determining a water level surface. Examples are triangulation used in HEC-GEORAS (*Tate and Maidment* 1999) and other systems (*Nickel* 1998), kriging (*Marche et al.* 1990), or inverse distance interpolation (*Werner* 2001). The latter technique is used throughout in this thesis for projecting 1D hydrodynamic model results in the 2D plane, and the method is described in detail in Appendix B.

Although these methods give powerful visual representation of the results of 1D hydrodynamic modelling, the results are no more than that, as there is no explicit representation of hydraulic detail between the cross sections (*Bates and de Roo* 2000).

3.3 Two-dimensional hydrodynamic modelling

3.3.1 Model concept

As application of 1D hydrodynamic modelling is founded on the assumption of horizontal water levels across the section, with a single dominant flow direction such as in typical valley flooding, it may be less suited to situations where floodplain flow is more complex. This may be the case where water flows out from a breach in a river dyke (*Hesselink et al.* 2003), or across a flat floodplain (*Aronica et al.* 1999). Although applying 1D models using a network of channels may go some way in to a solution (e.g. *Doull and Bright* 1996), direction of flow at any one point is still constrained by the delineation of the one-dimensional channels, thus giving unsatisfactory results where flow direction at a point may change significantly depending on condition (*Beffa and Connell* 2001), or velocities in different directions may be of the same order of magnitude (*Paquier and Farissier* 1996). In these conditions a two-dimensional depth averaged hydrodynamic code is required as a minimum.

Two-dimensional flow models using finite difference staggered grid solvers were first developed and applied in estuaries and for modelling coastal flows (*Li and Falconer* 1995). For modelling flood propagation on complex floodplain topography, with problems of wetting and drying and possibly rapidly varied flow these techniques have been found to be unsuitable, becoming unstable and non-conservative (*Beffa and Connell* 2001).

The importance of modelling floodplain inundation at a reach scale has, however, led to the requirement of robust numerical techniques that allow modelling

of complex floodplain flow. *Bates et al.* (1996) list a number of criteria such a hydraulic code should fulfil:

- The flow field must be represented in at least two dimensions in order to capture known process dynamics.
- An efficient numerical solution algorithm must be used to allow for a tractable computational problem.
- The model should adequately represent the complex floodplain topography as well as channels meandering in the floodplain.
- The numerical scheme must be able to deal with moving boundaries on the floodplain, resulting in wetting and drying of floodplain elements.
- The characteristics of the turbulence field relevant to the reach scale should be adequately considered.

A number of codes that fulfil some, or all of these criteria, have since been developed or adapted from two-dimensional models used in estuarine and coastal modelling (e.g. *Hervouet and Haren* 1996; *Stelling et al.* 1998; *Beffa and Connell* 2001). All of these apply the two-dimensional shallow water equations, which under the absence of wind friction are given as:

$$\frac{\partial \zeta}{\partial t} + \frac{\partial (uh)}{\partial x} + \frac{\partial (vh)}{\partial x} = 0 \tag{3.3}$$

$$\frac{\partial u}{\partial t} + u\frac{\partial u}{\partial x} + v\frac{\partial u}{\partial y} + g\frac{\partial \zeta}{\partial x} + \frac{n^2 u\sqrt{u^2+v^2}}{h^{4/3}} = 0 \tag{3.4}$$

$$\frac{\partial v}{\partial t} + v\frac{\partial v}{\partial x} + u\frac{\partial v}{\partial y} + g\frac{\partial \zeta}{\partial y} + \frac{n^2 v\sqrt{u^2+v^2}}{h^{4/3}} = 0 \tag{3.5}$$

The codes differ in the numerical approach used in solving these equations, as well as in the topographic discretisation used. There are three main principles, (i) structured, regular grids, (ii) curvilinear grids, and (iii) unstructured grids. Of these, the first and last are most common in floodplain inundation simulation. The advantage of the unstructured grid is that this allows for describing complex floodplain topography with a minimum of points, thus potentially resulting in a computationally efficient model (*Bates et al.* 1996; *Aronica et al.* 1999).

Discretising the floodplain using structured grids has the disadvantage of redundancy in flatter areas of the floodplain, but efficient numerical techniques applicable only to structured problems (*Stelling et al.* 1998) may be used. Models of both types have been applied in real world flood extent simulation (e.g. *Connell et al.* 2001; *Hesselink et al.* 2003; *Hervouet* 2000).

In applying these models at the reach scale, a balance between a tractable computational problem, and a model that adequately represents flow characteristics must be established. In most valley type flooding, main channel flow dominates the flow field, and even in more two dimensional inundation events, flow along channels

and ditches can significantly impact the flow field. To properly model flow in these one-dimensional elements, grid resolution in the channel elements needs to be carefully selected to minimise the impact grid resolution has on channel conveyance. This holds both for structured (*Beffa and Connell* 2001) and unstructured (*Bates et al.* 1996) grids.

In this thesis a code applying a structured grid is selected. This code, DELFT-FLS, is described in full by *Stelling et al.* (1998) and *Stelling and Duinmeijer* (2003), numerically solves the shallow water equations discretely using a finite volume approach with a central water level variable at each grid cell centre and a flux across cell boundaries (see figure 2.3). This is a staggered grid as in the 1D code above and is used also by other similar models (*Beffa and Faeh* 1994; *Beffa and Connell* 2001; *Molinaro et al.* 1994). The selected code applies a numerical scheme that ensures strictly positive water levels and uses an adaptive time-stepping strategy to ensure stability across the full range of possible flow conditions, including wetting and drying, sub- and supercritical conditions and transitions. The scheme is described in *Stelling and Duinmeijer* (2003), and is also given in Appendix C. Verification of the code against laboratory dam break simulations shows accurate results (*Stelling and Duinmeijer* 2003).

3.3.2 Integration with GIS

Most GIS follow the principle of two dimensional representation of spatial data, or perhaps 2.5 dimensional if elevation in a digital elevation model is considered. This representation is in good agreement with the data structures underlying two-dimensional hydrodynamic codes, and it therefore follows that integration with GIS is much more straightforward than for one-dimensional codes. Both unstructured and structured grids are data formats that can be handled by the more mature GIS (e.g. ArcInfo,ArcView), allowing all manipulation and analysis of spatial data required in setting up a model using these 2D codes to be done within GIS. The code can employ these data without the requirement of aggregation or disaggregation across disparate dimensions. The actual numerical solving techniques employed in these full hydrodynamic models are, however, quite complex. Implicit time integration is again required, such that embedding of the code is impossible, even in the currently available GIS specifically adapted to deal with dynamic data. The most apparent method of integration with GIS follows the tightly coupled shared data model principle described in chapter 2.

Unstructured grids (such as triangulated irregular networks, TIN) can be handled by many commercially available GIS. When using these for model development, particular attention must be given to making these suitable as constraints are posed on variations in grid from the hydraulic perspective (*Bates et al.* 1998). This makes the use of unstructured grids a little more complex than for structured grids, and often specialised mesh generators are used to set up the model on the basis of the available GIS data. For structured grids, again specific attention must be given to grid manipulation (see this thesis, chapter 6), but these are easily dealt with using standard GIS functionality. The added advantage of the structured grid format is that results are available in the same two-dimensional data structures as model

inputs and can therefore be readily integrated and displayed again in GIS.

The increasing availability of high resolution digital elevation data of high accuracy from, for example, aircraft borne laser altimetry (*Marks and Bates* 2000), has led to widespread practical application of two-dimensional hydrodynamic models at the reach scale. Unfortunately, less data is generally available on the bathymetry of the main channel, and mostly this needs to be interpolated from the available surveyed cross sections and integrated with the floodplain elevation data (e.g. *Bates et al.* 1996; *Marks and Bates* 2000; *Werner et al.* 2000). As the main channel is mostly dominant in conveying flow, this lack of main channel bathymetry will introduce uncertainty despite the accuracy of floodplain elevation data.

3.4 Hybrid one-two dimensional modelling

3.4.1 Model concept

The problem of balancing the requirement for high resolution representation of main channel flow, against minimising redundancy on the floodplain to reduce the computational problem, has led to a hybrid model approach, specifically developed for modelling inundation events at the reach scale. In this approach, the main channel, and any other predominantly one-dimensional flow conveyance elements, are modelled using a one-dimensional hydrodynamic approach. Overbank floodplain flow is modelled using the two-dimensional approach.

A number of such hybrid codes have been described, but most use simplified flow equations in describing the two-dimensional floodplain flow. These are described in the following section. The hybrid code applied here, SOBEK-1D2D, uses the full two-dimensional shallow water equations for describing floodplain flow, with main channel flow described using the full one-dimensional equations. The numerical procedure for the main channel is identical to that in the one-dimensional SOBEK code described previously, while overbank flows are modelled using the same structured grid and staggered discretisation as in the DELFT-FLS code described above. The two domains are coupled at grid cells overlying main channel computational points through mutual volumes of the connected cell and the adjoining channel section(s) as shown in equation 3.6.

$$\frac{d(\Delta x \Delta y h_{i,j})}{dt} + \Delta y\left((uh)_{i,j} - (uh)_{i-1,j}\right) + \Delta x\left((vh)_{i,j} - (vh)_{i,j-1}\right) + Q_k - Q_{k-1} = 0 \qquad (3.6)$$

$(uh)_{i-1,j}$ is the x unit discharge at the interface between cells $i-1$ and i and Q_{k-1} is the discharge in the between main channel reach segment $k-1$ and k. h is the depth in cell i, j.

Figure 3.2 gives an impression of the connection between the 1D and the 2D domains. The division between the two domains follows the principle of the horizontal divided channel method (see this thesis, chapter 5), but in contrast to that method the division between main channel and floodplain is not assumed as being

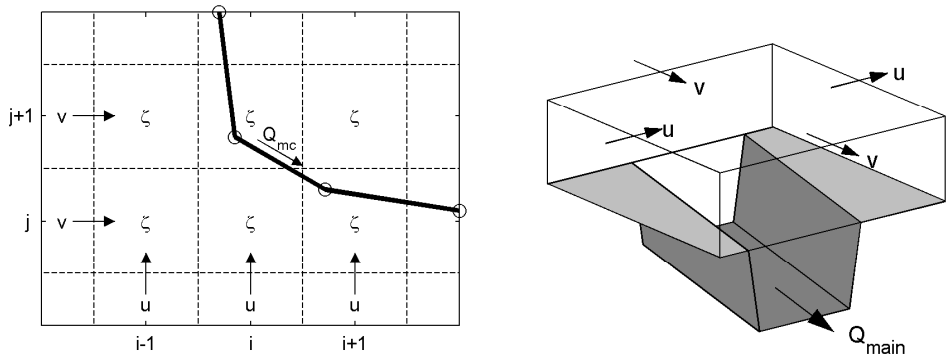


Figure 3.2: Impression of connection between 1D and 2D domains in the SOBEK-1D2D code (after *Frank et al.* (2001). Water level in grid cells i, j are indicated by ζ. u and v are fluxes across cell boundaries. The main channel is shown as a solid black line with circles indicating $1D$ calculation points. These share the water level ζ of the cells they fall in.

a zero-shear interface. A roughness value can be defined at the interface, and although momentum exchange between the two domains is not taken explicitly into account, this implicitly acts to dissipate momentum due to the complex turbulent interaction between main channel and floodplain flow. The code has been demonstrated several practical applications (e.g. *Frank et al.* 2001; *Dhondia and Stelling* 2002).

3.4.2 Integration with GIS

Integration with GIS is a combination of integration of one-dimensional and two-dimensional codes as described above. The one-dimensional channel elements are modelled relatively independent of the floodplain, and as in one-dimensional modelling require cross sections at regular intervals along the reach. These cross sections, however, do not need to extend across the floodplain as in the pure one-dimensional situation, with surveyed cross sections generally being sufficient. The two-dimensional floodplain is modelled using the same concepts as the pure two-dimensional code, although the hybrid code used here allows for mixing structured grids with different resolutions (*Dhondia and Stelling* 2002).

In combining the two domains, care must be taken as to the correct representation of the intersection. Cross sections used to describe the main channel are in effect cut at the bankfull level, and must be checked such that these points are correctly represented. Conversely, the elevation model representing the floodplain must be checked to ensure main channel is not represented in the elevation model as this would result in a double accounting of conveyance area. Standard GIS functionality can be used to "fill" the main channel at the bankfull level where required.

Integration with GIS can be seen to be as hybrid as the model itself, ranging between the loosely coupled and the tightly coupled with a shared data model.

Estimated flood extent follows the same format as in the full two-dimensional codes, and therefore follows the tightly coupled shared data model approach. As the integration with GIS does not required complicated procedures in migrating data across disparate dimensions, the hybrid code is considered in this thesis as following the tightly coupled shared data model principle.

3.5 Simplified two-dimensional modelling

3.5.1 Model concept

The hybrid code described allows robust application to flooding at the reach scale, even for events where hydraulic shocks may occur such as in dyke breaches. The nature of most flood events in valley river reaches being less dynamic than is the case of a breach, has led to the development of more simpler hydraulic models of two-dimensional flow. This can be achieved by neglecting the local and convective acceleration terms in the shallow water equations, an approximation admissible only for low Froude numbers (*Molinaro et al.* 1994). The first of these simple cell-inundation based codes was proposed by *Cunge* (1975), where the floodplain was modelled as a series of interconnected cells. These cells were found through identifying natural boundaries such as levees and dykes, with water levels within the cell being considered as horizontal. Under the assumption that flooding takes place slowly, inertial terms can be neglected and the exchange of flow between cells solely driven by the water level difference between cells. These flows are described using a suitable functional relationship such as the weir equation or Manning's equation (*Cunge* 1975).

Successive generations of these simplified two-dimensional codes applied the same cell inundation (or quasi-2D) approach, to a continuous calculation domain represented by the digital elevation model of the floodplain. A number of model codes that follow this principle have been recently described (e.g. *Estrela and Quintas* 1994; *Bechteler et al.* 1994; *Bladé et al.* 1994; *Molinaro et al.* 1994; *Bates and de Roo* 2000; *Sen* 2002). In contrast with the development of full 2D hydrodynamic codes, the starting point is now the digital elevation model, and a minimal representation of the dynamic flooding process is selected (*Bates and de Roo* 2000). This dynamic process is considered at the reach scale, and while neglecting acceleration terms may lead to inaccuracies for relatively small areas, the simplified equations give a good representation at that scale. It is reasoned that uncertainties in representation of topography and roughness will, moreover, influence results more than these inaccuracies in hydraulic representation (*Molinaro et al.* 1994).

As with the hybrid full hydrodynamic code, most codes of this type represent main channel flow using a one dimensional scheme connected to the floodplain. While some cell inundation codes use the same full hydrodynamic formulation as in the hybrid code (e.g. *Han et al.* 1998; *Sen* 2002), others use control volumes (*Giammarco et al.* 1994) or simplified representation of channel flow (e.g. *Bates and de Roo* 2000). The most simple representation of this one-dimensional flow is using the kinematic wave formulation. This simplification of the momentum equation (equation 3.2) is obtained through ignoring local and convective acceleration and

assuming that friction and gravity forces are in balance (*Chow et al.* 1988). The momentum equation is reduced to the friction slope S_f being equal to the channel bed slope S_o. Friction slope can be described using standard formulations such as Manning's equation:

$$Q = \frac{1}{n} A R^{2/3} \sqrt{S_o} \tag{3.7}$$

or with the hydraulic radius being the flow area A divided by the wetted perimeter P;

$$\frac{n^2 P^{4/3} Q^2}{A^{10/3}} = S_o \tag{3.8}$$

This scheme is suitable for describing the downstream propagation of the dynamic flood wave, and requires only the provision of an upstream flow boundary. It does not allow for the influence of backwater effects, and requires that the channel slope is monotonic in the downstream direction. Although successfully applied in describing inundation events (*Bates and de Roo* 2000), the interest in inundation modelling is on distributed water levels along the channel, and the restrictions posed may lead to large inaccuracies in these. By independently considering free surface and friction flow through expanding equation 3.7 to include the diffusion term, these restrictions are reduced;

$$\frac{n^2 P^{4/3} Q^2}{A^{10/3}} - \frac{\partial \zeta}{\partial x} = S_o \tag{3.9}$$

Using this formulation of the diffusion equation with the cross-sectional area A being the dependant variable, the explicit non-linear difference system can be solved using a Newton-Raphson technique, with the diffusion term included through modifying the bed slope (*Horritt and Bates* 2001a). To avoid instabilities in this explicit technique the model time step, Δt, must be kept sufficiently small (*Cunge et al.* 1980).

$$\Delta t \leq \frac{\Delta x}{\frac{Q}{A} \pm \sqrt{gh}} \tag{3.10}$$

Floodplain flow can be described using the same simplification of continuity and momentum equations, discretised across the floodplain topography. This is most commonly represented using a cartesian grid (*Estrela and Quintas* 1994; *Bechteler et al.* 1994; *Bladé et al.* 1994; *Bates and de Roo* 2000) or using triangulated irregular networks (*Sen* 2002), but in all cases each triangular or rectangular element having a constant elevation. In this inundation cell representation, the level is defined at the cell centre point and fluxes across the cell boundaries, with the relationship between the volume in the cell and the inflow can be given as

$$\frac{dV_i}{dt} = \sum_k Q_{i,k} \tag{3.11}$$

where V_i is the volume in cell i, and $Q_{i,k}$ is the discharge from cell k to cell i, and $\sum_k$ is the sum of all discharges of cells k connected to cell i. With the representation of the topography using a cartesian grid and assuming the change of inundated area with level is small when compared to the total area of the cell (*Cunge et al.* 1980), the continuity equation for a single cell can be discretely described as,

$$\frac{dh^{i,j}}{dt} = \Theta\frac{Q^{i-1,j}_{x,t} - Q^{i,j}_{x,t} + Q^{i,j-1}_{y,t} - Q^{i,j}_{y,t}}{A} + (1-\Theta)\frac{Q^{i-1,j}_{x,t+1} - Q^{i,j}_{x,t+1} + Q^{i,j-1}_{y,t+1} - Q^{i,j}_{y,t+1}}{A} \tag{3.12}$$

where $Q^{i,j}_{x,t}$ is the flow in the x direction between cells i and $i+1$ at time t, and $Q^{i,j}_{y}$ is the flow in the y direction between cells j and $j+1$. The term Θ is used to determine whether the equation is solved partially implicitly for $\Theta < 1$ or fully explicitly for $\Theta = 1$.

The diffusive equation given in 3.9 at time t can be discretised over the grid (see also *Horritt and Bates* (2001a) and *Aronica et al.* (2002));

$$Q^{i,j}_x = \frac{\frac{h^{5/3}_{flow}}{n}\left(\frac{h^{i-1,j}-h^{i,j}}{\Delta x}\right)\Delta y}{\left[\left(\frac{h^{i-1,j}-h^{i,j}}{\Delta x}\right)^{1/2} + \left(\frac{h^{i,j-1}-h^{j,j+1}}{2\Delta y}\right)^{1/2}\right]^{1/4}} \tag{3.13}$$

where the flow depth h_{flow} represents the depth over which water can flow between the two boundaries. *Bates and de Roo* (2000) define h_{flow} between cells i and $i-1$ as the difference between the maximum free surface and the maximum bed level $\texttt{max}(\zeta^i, z^i) - max(\zeta^{i-1}, z^{i-1})$, while *Cunge et al.* (1980) use the average of the free surface elevation minus the maximum bed level. Flow in the y direction can be similarly described. *Horritt and Bates* (2001a) found that using the diffusion wave approximation as in equation 3.13 did not improve results over the Manning's description of flow between two cells used originally by *Cunge* (1975), and therefore suggest using this formulation due to its simplicity. In contrast with the diffusion wave approximation, where flow in the x and y are linked, these are now considered independently,

$$Q^{i,j}_x = \frac{h^{5/3}_{flow}}{n}\left(\frac{h^{i-1,j} - h^{i,j}}{\Delta x}\right)^{1/2}\Delta y \tag{3.14}$$

$$Q^{i,j}_y = \frac{h^{5/3}_{flow}}{n}\left(\frac{h^{j-1,j} - h^{i,j}}{\Delta y}\right)^{1/2}\Delta x \tag{3.15}$$

While this fails to reproduce some of the features of floodplain flow, given a suitably fine resolution of the floodplain the differences are negligible in comparison to uncertainties in validation data (*Horritt and Bates* 2001a; *Aronica et al.* 2002). The cellular approach also has the advantage that it is more efficient, and that it allows easy adaptation to non-cartesian grids *Cunge* (1975) and unstructured grids *Sen* (2002). If these equations are written for every cell a system of linear algebraic

equations results with the water level change in each cell as unknowns. *Estrela and Quintas* (1994) applies a Gauss-Seidel numerical solution once the initial state and boundary conditions are known.

In this thesis, a simple two dimensional code is selected that describes floodplain flow using the cell-inundation method, while main channel flow is described using the diffusion wave approximation. The code, LISFLOOD-FP, is described in full by *Bates and de Roo* (2000). The numerical solution procedure is simplified by using the explicit formulation with $\Theta = 1$. The non-linearity of the flow equations clearly pose stability problems in using this explicit scheme (*Cunge et al.* 1980; *Beffa and Connell* 2001). Selection of a small time step partly solves the problem, but unless set to an extremely small value can not guarantee stability across all flow conditions. To limit stability problems at more reasonable time steps, a floodplain flow limiter was introduced in the original model,

$$Q_x^{i,j} = max\left(Q_x^{i,j}, \frac{1}{8}\frac{\Delta x \Delta y(h^{i,j} - h^{i-1,j})}{\Delta t}\right) \tag{3.16}$$

Although this indeed suppresses instabilities, it also significantly affects floodplain flow, and helps to explain insensitivity to variation in floodplain roughness shown in *Horritt and Bates* (2001a). In the version of the model used here, this is avoided by limiting the time step rather than the flow between the two cells. Stability was improved further by linearising the momentum equation if the water level difference is smaller than a given ϵ (*Cunge et al.* 1980). Main channel flow and floodplain flow are considered in sequence in the numerical solution procedure with an explicitly formulated volume exchange. In the explicit approach, negative depths may occur in the drying phase, and to avoid this, discharges from all k cells connected to cell i are reduced by a coefficient c should a negative depth occur,

$$c = \frac{V_t}{\Delta t \sum_k Q_{i,k}} \tag{3.17}$$

3.5.2 Integration with GIS

The simple numerical procedures used, make integration with GIS much more straightforward than in the preceding codes. Many of the codes using these simplified equations of flow were in fact developed specifically as GIS integrated codes. This holds for the LISFLOOD-FP code applied in this thesis, which was first developed embedded in a dynamic GIS environment (*Bates and de Roo* 2000), with the main channel being schematically represented in the grid. The dynamic GISused, PCRASTER (see *Van Deursen and Wesseling* (1996)), includes operators for solving kinematic flow along these main channel cells, and as such the level of integration with GIS can be considered as tightly coupled with an embedded process model. Since its initial development, the numerical code has again been separated from the dynamic GIS. This was done to allow easy implementation of the diffusion approach in solving main channel, as well as to increase computational efficiency. The concept of an explicit solution of the governing equations has, however, been maintained. Using the open interface provided by the PCRASTER package the potential for the

floodplain flow and diffusive main channel flow to be coded as embedded operators within the GIS remains. As a consequence this code remains to be considered here as being embedded within the GIS.

As with the hybrid code full hydrodynamic code, care must be taken in combining the one-dimensional and two-dimensional domains that the intersection is correctly represented. The conveyance in the main channel is given in the non conservative form (*Chow et al.* 1988) where the hydraulic radius R is taken to be equal to flow depth h, representation of the cross section geometry for the main channel is simply defined as the channel width, the bankfull depth, and the bed elevation level. These three variables are defined for each main channel cell. In keeping with the embedded principle, all model outputs representing flood extent are available within the GIS database.

3.6 Roughness value parameterisation

In all the codes described, the main calibration parameters are the floodplain and main channel roughness. Values for these are typically associated to the physical properties of the boundary, such as material (smooth concrete, pebbles, or boulders) and vegetation cover (*Chow* 1959), and various formulations are available in describing how these properties contribute to roughness factors to be applied in the model. These follow different relationships depending on whether the dimension of roughness elements is such that these are submerged within a laminar sub-layer close to the boundary (smooth turbulent flow), or if these elements protrude through the laminar sub-layer in fully turbulent flow (*French* 1986).

The dimensionless Darcy-Weisbach friction factor, first proposed for describing roughness in pipe flow, is suitable for both smooth and fully turbulent flow, and is perhaps the most applicable formulation for roughness parameterisation. Tables are available from experimental work to derive the Darcy-Weisbach friction factor as a function of the Reynolds number. Other formulations, such as that of Nikuradse, give a description of roughness as a characteristic length k_s (unit is m), from which the Darcy-Weisbach factor can be computed. This can be very suitable for application to describing roughness in the field, where a measure of roughness length can be estimated based on observations. Main channel and floodplain flow at the reach scale are, however, fully turbulent, and therefore independent of Reynolds number. The relationship between k_s and f has, moreover, been derived under scaled laboratory conditions, and the logarithmic formulation is not equally suitable for larger roughness lengths encountered in the field.

The widely used Manning's n and Chezy C roughness values are semi-empirical, and applicable to fully turbulent flow only. These are, however, appropriate for parameterising reach scale flood extent models (*French* 1986; *Sellin et al.* 2003). Although closely related to each other ($n = RC^{1/6}$), Manning's n is the most commonly applied, with various methods available in literature for estimation based on field observations. *Chow* (1959) provides the most thorough set of roughness values for various surface materials to date, including descriptions and photographs to help in estimation of suitable values. Similarly, *Acrement and Schneider* (1989)

provide a handbook for estimating roughness values, adding adjustment coefficients to allow for increased energy losses due to channel shape and planform. A complete overview of methods for establishing roughness values is given in *Sellin et al.* (2003).

In this thesis, Manning's n is applied throughout in describing roughness values. Through application of roughness value estimation methods, detailed GIS datasets of floodplain land use can potentially be valuable in estimating the value of Manning's n for floodplain flow. This is particularly the case in two-dimensional floodplain flow, with the parameterisation of roughness values using the same resolution as the definition of topography in the elevation model. In the $1D$ hydrodynamic approach the compound effect of the vegetation between cross sections will need to be estimated.

Most of the methods from literature for estimating roughness values can be useful in establishing the range of roughness values for a river reach. Calibrated roughness values are, however, effective at the reach scale (*Beven and Carling* 1992). These effective roughness values can, moreover, not be taken independent of model structure as will be shown later in this thesis. Boundary conditions and uncertainty in boundary conditions may also influence identification of model parameters. In this thesis the variability of due to boundary conditions is not explicitly considered. Although this will certainly play an important role in model application, a comparison is made here of different model concepts, with the same boundary conditions used for each.

3.7 Discussion

The four different codes described show the scope of approaches available in inundation modelling. Although the numerical procedures differ, as well as the levels of integration with GIS, outputs available for further analysis of flood risk or flood damage are very similar, with differences in GIS implementation being more a technical than a contextual challenge.

It is clear that the most complete representation of complex hydrodynamic flow on the floodplain is given by the two-dimensional hydrodynamic codes, and many authors argue that given this, other codes are inferior for simulating inundation events (*Paquier and Farissier* 1996; *Aronica et al.* 1998a; *McCowan and Collins* 1999; *Connell et al.* 2001). Correct representation of typically two dimensional flow, such as that resulting from a levee break requires a two-dimensional hydraulic representation that can also deal with hydraulic shocks (see e.g. *Hesselink et al.* (2003)), therefore requiring the use of two-dimensional codes. Parsimonious application of these to more typical valley flooding type events, where flow can be easily described as varying slowly in time, is not so apparent. The main difficulty in developing reach scale models with any code is the availability of a suitable description of complex floodplain topography on the one hand, and the lack of validation data with which to estimate suitable roughness values on the other. Few examples of field validation are found in literature, but where this is done (e.g. *Horritt and Bates* 2001a, 2002), differences in reliability against the validation data between 1D, full hydrodynamic 2D and simplified 2D codes are limited. Even at the labo-

ratory scale, depth averaged two-dimensional hydrodynamic codes with turbulence explicitly considered using appropriate turbulence closure modelling, may show significant differences in depth averaged velocities across the floodplain and channel when compared with experimental results (*Wilson et al.* 2002). As a result, reliable application in the field at the reach scale can never be without some form of calibration and validation.

The limited availability of field data on inundation events makes this calibration difficult, with precise values for roughness parameters being difficult to identify (*Horritt and Bates* 2001a, 2002; *Aronica et al.* 2002; *Romanowicz and Beven* 2003).

3.8 Conclusions

In this chapter, four approaches in modelling floodplain inundation have been described, with differences primarily in the complexity with which floodplain and main channel flow is hydraulically represented. In the commonly applied one dimensional hydrodynamic models, flow in both main channel and floodplain is described as varying only in the longitudinal direction, irrespective of flow depth. Despite the simple model structure, this restriction may preclude application to some problems as complexity of floodplain hydraulics is not well represented. The one-dimensional approach also makes integration with GIS difficult, with the loosely coupled level of integration being the only principle suitable. Although GIS techniques are available for both pre-processing and post processing model data, these may be *ad-hoc* or introduce ambiguity due to different, equally applicable, algorithms in transforming data across the disparate databases exist.

In the two dimensional, depth averaged hydrodynamic codes, flow direction may vary with depth, and the dimension with which flow is resolved being the same as the typical dimension with which GIS data is held, integration with GIS is more natural. The complex numerical solving techniques required in resolving the full shallow water equations, make embedding the model within GIS impossible, and the tightly coupled principle with a shared data model remains the suitable form of GIS integration. Resolving main channel flow accurately may, however, require very fine resolutions for computational grids, leading to an intractable computational problem. A hybrid model resolving main channel flow in one dimension and floodplain flow in two is described. Integration with GIS for this hybrid code follows the same balance between loosely coupled and tightly coupled with a shared data model as the descriptions of flow. However, as little manipulation of GIS data is required, it is considered to also follow the tightly coupled shared data model principle.

A more simple hybrid code is described, where under the assumption that flow conditions vary only slowly, local and convective acceleration terms are ignored. These simplifications allow for much simpler numerical techniques to be employed in solving the equations of flow, and ensures the code can be fully embedded within a GIS, provided that the GIS supports some form of dynamic simulation.

From each of the four approaches described, a code is selected to be used in this thesis. These then consider not only a range of modelling complexity representative of codes used in practical application at the reach scale, but also represent the

range of principles available for integration with GIS. In the previous chapter, the GIS embedded model was suggested as being one of optimal integration, but it is seen from the description of the codes given here that to allow this using currently available GIS, a significant number of assumptions in describing hydraulic flow need to be made. Computationally, the one-dimensional approach is the most efficient, but only allows integration with GIS using the simple and inefficient loosely coupled principle, and with the development and use or various links between the model and GIS application can be laborious. The simple two-dimensional codes are easiest to apply, and allow full embedding, but the assumptions made may have an impact on reliability of results. The more complex two-dimension full hydrodynamic codes (including the hybrid code) are a little less easy to apply, and are computationally most inefficient, but integration with GIS can still follow the tightly coupled principle, albeit with a shared data model rather than actually embedding the code. An optimal form of integrating inundation models and GIS can, as a consequence, not be universally established and will be very much case dependent. For all inundation models, some form of calibration of roughness factors is required, and the data available for model calibration and validation will very much determine how representation of hydraulic flow using either simple or complex concepts can be defended, thus implicitly determining the optimal form of integration with GIS.

4

Model performance: reliability, calibration and uncertainties

4.1 Introduction

Performance of the integrated GIS model is a central concept of this thesis. The concept of model performance follows *Kisiel* (1971), where the problem of model selection when given the choice between different concepts is described. Evaluation of one model against another is proposed to be done in the light of model performance, where model performance is described through four factors:

1. Accuracy.
2. Computational efficiency (speed).
3. Simplicity
4. Flexibility

In the discussion of the previous chapter the computational efficiency is considered to be a property of the different model concepts described as it is determined predominantly by the dimensionality and the selected numerical approach. For the one-dimensional concept computational efficiency is clearly superior to that of the other concepts, but at the same time the integrated GIS application of the one-dimensional concept is the least flexible due to the restriction of level of integration to the loosely coupled approach, with the requirement of communication between disparate data models. Conversely, the two dimensional approach is computationally inefficient, but allows more flexible application due to its more natural integration with GIS data formats. This shows that selection of a model structure implicitly deals largely with both flexibility and computational efficiency.

Model accuracy and simplicity are less tangible factors. At the start of the rapid development of computing power, some hope was expressed that this would increase the complexity with which underlying processes that add up to the behaviour of the complete system could be considered, thus creating more accurate models (*Nash and Sutcliffe* 1970). *Jakeman and Hornberger* (1993) comment that the complexity of hydrological models has indeed been increasing with computational resources, but found that the limited data available for calibrating the greater amount of parameters resulting from more complex process representation, made these parameters ever more difficult to identify. This danger of over-parameterisation has

been the subject of a wide range of research (e.g. *Sorooshian and Gupta* 1983; *Beven* 1989; *Gan et al.* 1997; *Perrin et al.* 2001)). *Van der Perk* (1997) show for a water quality modelling study, that increasing the complexity of the model used (and therefore the number of parameters to be estimated) may even be detrimental. Through validation it was shown that the uncertainty in identifying a larger number of parameters increased predictive uncertainty, thus reducing model accuracy. Accounting for correlation in parameters reduced this uncertainty, but this is synonymous to using less independent parameters.

Rather than assessing model accuracy, with its potential of leading to the misunderstanding that this describes the level of detail with which the underlying process is described, *Melching* (1995) introduces the concept of model output reliability in assessing model performance. In engineering, a general definition of reliability is the probability of that the load acting on a system, L, is less than or equal to the capacity of the system to resist the load, R (*Melching* 1992),

$$R_L = P_r(L \leq R) \tag{4.1}$$

where $P_r(X)$ is the probability of event X occurring. Resolving this for a known joint probability density functions of L and R can be easily calculated, particularly if these are statistically independent. This can be easily adopted in assessing the reliability of a model, R_{model}. The probability of the modelled value Q_{model} being within a given accuracy of the actual value Q_{actual} can be established as:

$$R_{model} = P_r(|Q_{model} \leq Q_{actual}|) \tag{4.2}$$

Sorooshian and Gupta (1998) note that any hydrological model can only be as reliable as the model assumptions, inputs and parameter estimates. This then results in two difficulties, the first is the selection of the model structure or concept, and the second is to estimate the associated parameters such that the model resembles the behaviour of the actual system (*Sorooshian and Gupta* 1995). The process whereby suitable parameter values are selected, and the model is tested against independent data to demonstrate its ability to reliably reproduce the behaviour of the actual system at the required spatial and temporal scale, is referred to as calibration and validation.

Recent research has shown, however, that despite the promise of improvement due to increasing computer resources, calibration of the type of models commonly used in hydrology and water resources is not without its problems (*Sorooshian and Gupta* 1983). Most models, and notably those of the conceptual and physically based types, contain some description of what are considered to be the most important dynamic fluxes of the process being modelled, either through the use of physically based equations, such as energy or mass balances, or through conceptual relationships between inputs and outputs. On the premise that if each known process is explicitly included, the model will be more capable of representing the response of the real system, most models will contain numerous such relationships. In each of these relationships some parameters will be included that need identifying in the calibration process, and the problem is that typically little or no independent data is available to identify suitable parameter values for each of the individual

processes. A good example is given in *Jakeman and Hornberger* (1993), who show that for modelling the hydrological response of many catchments a two component model with only two parameters in each component is as much complexity in model structure as can be identified, given the available data. Similar conclusions of limited identifiability of parameters due to the lack of information in available data were found by *Sorooshian et al.* (1983), *Freer et al.* (1996), *Van der Perk* (1997) and *Andréassian et al.* (2001), leading to uncertainty in appropriate values of these parameters (*Spear et al.* 1994). Subsequent extrapolation of model results while considering uncertain parameters shows that model predictions become more and more uncertain due to extrapolation, and are therefore detrimental to model reliability (*Uhlenbrook et al.* 1999). In this chapter the concept of calibration is discussed, before a closer look at the model uncertainty is taken. Methods used in establishing model parameter uncertainties are then briefly described. The technique adopted in this thesis for estimating parameter uncertainties in the models is described.

4.2 Model calibration

Unfortunately, the utopian ideal of a model structure that allows reliable model application without any form of calibration has hitherto not materialised. It is generally accepted that the reliability of application of any conceptual, and even physically based, model depends much on the success of the calibration process used to identify values for the free model parameters (*Seibert* 1997). Model parameters can largely be divided into two categories (*Melching* 1995); (i) parameters that can be directly inferred from observation, such as area, volume etc., and (ii) parameters that cannot be directly observed at the model scale and will need to be estimated. The last category includes parameters such as hydraulic conductivity, surface roughness, characteristic lag times. Some of these parameters, such as surface roughness, have some bearing on physically realistic properties, and may be observable at the laboratory and point scale. Application at the model scale, however, typically implies these are more effective parameters, and may include lumped effects of sub-grid variability (*Ackers* 1992).

Parameter calibration can either be done manually on a trail and error basis, or with the help of some form of automatic procedure (*Sorooshian and Gupta* 1983). In both, historical input and output records are used to evaluate how well the behaviour of the real system is represented using the selected parameters and model structure. If this behaviour is found to be significantly different, then the parameter values and sometimes model structure are changed until the differences are deemed acceptable, within the modelling objective. To establish the validity of the resulting model, the final model structure and calibrated parameters are faced with a second set of known inputs and outputs, and differences between calculated and known outputs assessed. Comparison of model outputs to expected outputs is either visual or encapsulated in an objective function, with widely known examples of the latter being the root mean square of residuals, and the Nash—Sutcliffe model efficiency parameter. The choice of objective function will clearly influence the resulting set of

calibrated parameters, as the different functions lay differing emphasis on different types of model residuals. For an overview of various forms of objective functions and how these respond to different types of residuals, see *Green and Stephenson* (1986) and *Gupta et al.* (1998).

Whether calibration is manual or automatic, the objective is to find a single parameter set that minimises the differences between modelled and expected outcomes as expressed in terms of the objective function. This optimum is, however, difficult to identify due to the objective function response surface often being multimodal (*Sorooshian et al.* 1993; *Bates and Campbell* 2001) and strong interaction between parameters (*Spear et al.* 1994).

Increasingly powerful mathematical techniques are becoming available to identify global optima in hydrological models, including gradient based methods, methods based on evolutionary computing (*Liong et al.* 2001; *Madsen* 2003; *Vrugt et al.* 2003a; *Sorooshian and Gupta* 1998), and even more exotic methods inspired by the behaviour of ant colonies (*Abbaspour et al.* 2001). Despite the value of these techniques in helping overcome the identification problem (*Sorooshian et al.* 1993), the underlying assumption is that there is indeed an unique optimal parameter set. The uniqueness of such a parameter set depends on how deterministic the behaviour of the system is. Even if a perfect model was available, differences between modelled and observed variables would still prevail due to the inherent uncertainty of nature. At the hydrological hillslope scale, *Bronstert* (1999) notes that it is unlikely that improvement of model process description will increase model accuracy beyond a certain limit. This is because of the effect of small scale spatial and temporal variations in catchment conditions, which introduce a stochastic component in the hydrological response. Although this small spatial and temporal scale variability will tend to be evened out as modelling scales increase to for example the reach scale, a number of studies show that global parameter optima may lie in different parts of the parameter space depending on the data sets used in calibration (*Sorooshian et al.* 1983). At the same time, many parameter sets may exhibit equal or near-equal performance to the optimal parameter set, referred to as equifinality by *Beven* (1993), leaving considerable uncertainty as to the correct value of the single optimal parameter set to be used in model prediction.

4.3 Model uncertainty

From the discussion above, it follows that uncertainty in identifying calibration parameters have an important part in determining the model reliability. *Van Gelder* (2000) describes uncertainties as being divided into two main categories; uncertainties due to the variability of samples from a population, therefore representing the randomness in samples, or inherent uncertainties; and, uncertainties that are due to a basic lack of knowledge, or epistemic uncertainties.

The lack of knowledge in epistemic uncertainties may be due to an incomplete understanding of the processes influencing the behaviour of the system, an incomplete set of data explaining the behaviour, or in applying models to simulate the behaviour, uncertainty in the model structure, underlying assumptions and model

parameters. The inherent uncertainty will, as described in the previous section, result in an inherent non-uniqueness of optimal parameter sets in calibration.

The different sources of uncertainty are closely related. Particularly uncertainties due to assumptions made in the model structure in omitting processes not considered as contributing to the reliability of the known result, and uncertainties due to incomplete knowledge of behaviour could be considered as model structural uncertainties. Uncertainty in the model structure is, however, closely related to parameter identifiability. Once it is accepted that for any model structure some form of calibration is required to estimate values of free parameters, the error compensation properties of the calibration process (*Melching* 1995) will make it difficult to distinguish between model structural errors and parameter identifiability problems. Problems with parameter identifiability, however, often due to over-parameterisation, reflect inadequate model structure given the calibration data available. This is clearly shown by *Van der Perk* (1997) where unless complex parameter interaction is considered (thus reducing the number of free parameters), the number of parameters to identify increase with expanding model complexity, leading to deterioration of model reliability. Identifiability is also a problem of modelling scale. *Savenije* (2001) compares the problem of distributed hydrological modelling with physical laws such as Boyle's gas law. These only become apparent above a given scale of integration, and will not hold from the point of view of the individual molecule. The same allegory can be used in distributed modelling by looking at bulk system behaviour from the point of view of the individual model element (*Beven* 1995). *Reggiani and Schellekens* (2003) similarly argue that application of physical fluxes in hydrological modelling can only be done appropriately from a representative scale at which these can be properly identified.

The difficulty in *a-priori* identification of the additional parameters as a result of the increase in complexity (*Romanowicz et al.* 1996; *Gan et al.* 1997; *Perrin et al.* 2001), will result in simpler model structures proving equally reliable to more complex structures. *Romanowicz et al.* (1996) argue that in inundation modelling the resulting uncertainty in calibration parameters is a dominant factor in the model reliability, as opposed to loss of hydraulic detail when using relatively simple model structures. This is corroborated by *Bates et al.* (1998), who find model bulk predictions more sensitive to calibration of boundary friction parameters than to error in representation of floodplain topography and resolution of numerical mesh. Predictive model uncertainty caused by uncertain parameters can therefore be considered a good indication of the model reliability. If in validation observations remain within the range of predictive uncertainties, then this can also be seen as an indication of the suitability of a selected model structure and parameters (*Beven and Binley* 1992).

4.4 Methods in estimating parameter uncertainties

For all but the simplest hydrological and hydraulic models, analytical assessment of the uncertainty in the model output due to the joint probability functions of the inputs is not possible (*Melching* 1995; *Boogaard et al.* 2000), and alternative

methods for estimating uncertainties are required. Some of the main methods used in determining parameter uncertainties are described in this section.

4.4.1 Monte Carlo Simulation

Monte Carlo simulation (MCS) is a straightforward and robust technique for estimating the posterior probability distribution of a complex non-linear model output. MCS is based on establishing the prior probability density distributions for each uncertain model input, and then generating random samples from these distributions (where a sample is defined as a value selected randomly from a given distribution, rather than a collection of realisations - see also *Mackay* (1997)). For each combination of sampled inputs, the model is run deterministically and the model output determined. Through running sufficient realisations of sampled inputs and calculating outputs, an estimate of the posterior distribution of model outputs due to uncertain inputs can be obtained.

The disadvantage of the method is that although it is conceptually simple to understand, it is essentially a brute force method. In order to reliably estimate posterior distributions, particularly for lower probabilities in the tails of distributions, the number of required simulations may be excessive. This number may run into the tens of thousands, and there is no reliable method of establishing a prior estimate of the number of runs required without making assumptions on the form of the posterior distribution function as in *Klis* (2003). *Mackay* (1997) notes that the number of runs required to visit every possible point in a 1000 dimensional problem with 50 increments in each dimension is in the order of the fourth power of the number of particles in the universe - something he quotes as a "horribly huge number". Even for 10 divisions in a 4 dimensional problem, the number of points to be visited is still in the order of 10000, which clearly forms a problem for simulation models with substantial run-times. To reduce the number of simulations compared to visiting every point in the parameter space, more efficient sampling strategies can be used.

Importance sampling

The concept of importance sampling (*Gelman et al.* 1995; *Mackay* 1997), is to select a distribution which approximates the (unknown) posterior parameter distribution from which random samples can be easily drawn. For each sampled parameter set, the relative weight, or importance weight in determining the posterior distribution is established, and once weights for all samples have been established, each importance weight is re-normalised such that the posterior distribution integrates to 1. This is the most commonly applied sampling strategy, and although the concept is simple, importance sampling may yield unreliable results when weights in a small part of the parameter hyperspace dominate the posterior distribution, in which case a very large number of samples may be required to obtain a reliable estimate (*Gelman et al.* 1995; *Mackay* 1997). If the number of samples is too small, these high density areas in the posterior distribution (see for example the posterior density function in *Spear et al.* (1994)) may be missed, or the samples may contain clusters or gaps

in the hyperspace, thus potentially missing relevant areas (*Owen* 1998).

Latin hypercube sampling

Latin hypercube sampling (LHS) (*McKay et al.* 1979; *Owen* 1998) ensures the samples are well represented over the parameter space, but the number of required samples are reduced when compared to random sampling as above. To generate a sample of size N, the prior parameter distributions are divided into N strata of equal probability $1/N$, and a sample is randomly drawn from each. The ensemble of parameter sets is constructed by matching samples from each parameter set at random. Posterior parameter distribution derived using LHS are shown to reliably compare to those found using random sampling by *Melching* (1995) and *Yu et al.* (2001), while significantly reducing the number of simulation runs to derive a stable estimate.

Klis (2003) comments that the disadvantage of LHS is the difficulty in determining the appropriate number of runs, as well as that it may be no more efficient than random sampling for non-monotonic problems. However, unless assumptions are made on the posterior distribution the problem of establishing the number of runs will need to be done on a trail and error basis. In all cases LHS will be either more efficient or as inefficient as random sampling, and as a consequence LHS is used throughout in this thesis. Despite that the parameter sets generated by LHS are ensured to represent a better spread in the parameter space, the concept is the same as in importance sampling, and the potential error due to dominant weights will prevail.

Markov Chain Monte Carlo

Markov Chain Monte Carlo (MCMC) (*Gelman et al.* 1995; *Mackay* 1997) sampling is a technique particularly suited to high dimensional Monte Carlo problems. It avoids the problems of unreliable results in highly complex posterior parameter distributions, and has been used widely in estimating parameter uncertainties in environmental models (*Kuczera and Parent* 1998; *Bates and Campbell* 2001; *Campbell et al.* 1999).

The most general and widely applied MCMC scheme uses the Metropolis-Hastings algorithm in determining the target joint posterior parameter distribution $p(\theta|y)$, where θ is the parameter set and y the available calibration data. The algorithm is described by *Gelman et al.* (1995) and *Kuczera* (1997) as an iteration of the following steps:

1. Draw an initial parameter set θ_i from a starting distribution $p_i(\theta)$. This distribution must be symmetric (see *Gelman et al.* (1995) for details).

2. Sample a candidate parameter set from a symmetric jump distribution, where the jump distribution is given as $j_i(\theta|\theta_{i-1})$.

3. Evaluate for the ratio $\psi = p(\theta_i|y)/p(\theta_{i-1}|y)$.

4. Randomly sample a value Z from a uniform distribution in the interval 0 to 1. If $Z > \psi$ then the jump distribution is selected as the starting distribution in the next step, otherwise the original distribution is retained.

The algorithm forms a Markov chain random walk of a sequence of iterations $\{\theta_0, ..., \theta_N\}$ that can be shown to converge on the stationary posterior distribution $p(\theta|y)$ (*Gelman et al.* 1995). Although efficient for high dimensional parameter spaces, the algorithm must be initiated a number of times to derive reliable estimates of the posterior distribution. Other factors are also important in determining the convergence on the stable distribution, including the choice of the jump distribution, although this convergence can be optimised (*Kuczera and Parent* 1998; *Vrugt et al.* 2003a). For a more complete description see *Kuczera and Parent* (1998).

4.4.2 Boot-Strapping and Jack-Knifing

Boogaard et al. (2000) describes the use of re-sampling techniques in estimating calibration parameter uncertainties. The advantage of re-sampling is that these are insensitive to the statistical properties of the data used, and these properties are rarely completely known. The essential characteristic of the techniques is that an ensemble of data sets is constructed through re-sampling the original data set, and then for each data set in the ensemble determining model parameter values using an optimisation technique. The statistics of the posterior parameter distributions can then be found using the ensemble of calibrated parameter sets.

Two re-sampling techniques are commonly applied (*Boogaard et al.* 2000), Jack-Knife re-sampling and Bootstrap re-sampling. These differ essentially in the method applied to generate the multiple data sets from the original data set.

- Jack-knifing: In this technique, with some similarity to split-sample testing, a fixed number of say j elements are randomly removed from the original data set of N elements. Each of the generated data sets thus has $N - j$ elements, with the total number of different subsets that can be generated as $N!/j!(N - j)!$. Obviously for large data sets this could give a very large number of possible combinations for large and the ensemble size is normally limited. An estimate of the mean and variance of model parameters can be given as a function of the total number of elements in the data set, the number of elements removed, and the size of the ensemble.

- Bootstrapping: Boot-strapping is a similar technique, but now elements are not only randomly removed, but also randomly replaced. As a consequence the number of elements in the calibration set will remain constant, but some of those in the original set will have been omitted, while others are represented twice or more. Again estimates of the mean and variance of model parameters can be given as a function of the total number of elements in the data set, the number of elements removed and subsequently replaced, and the size of the ensemble.

The elegance of these re-sampling techniques is that these explicitly explore the variance of parameter estimates on the basis that the available calibration data is

only a subset of realisations of all possible realisations (*Beven* 2001c). The techniques do, however, rely on the availability of large calibration sets of independent events. Particularly for calibration of flood inundation models this is a problem, making re-sampling techniques difficult to apply. With these techniques no correlation between the effective parameter sets and the magnitude of the events can be taken into account. There is some evidence that this may be the case for flood inundation models, as seen both in this thesis and other research (e.g. *Romanowicz and Beven* 2003). These techniques are not considered further in this thesis. For a more complete description see *Boogaard et al.* (2000).

4.4.3 Other uncertainty estimation methods

Several other methods of estimating parameter uncertainties have been described in literature. These include the Mean-Value First Order Second Moment Method, Advanced First Order Second Moment Method, Rosenbluth's point estimation method, and Harr's point estimation method *Melching* (1992, 1995); *Yu et al.* (2001). When comparing the estimated mean and variances of posterior parameter distributions to estimates derived through Monte Carlo Simulation, both *Melching* (1995) and *Yu et al.* (2001) find results to be unreliable. These methods are reliably applicable only for the case of linear models (*Vrugt et al.* 2003b), giving poor approximations of parameter statistics for non-linear models (*Kuczera and Parent* 1998), and are not considered further.

4.5 Generalised Likelihood Uncertainty Estimation

In this thesis the generalised likelihood uncertainty estimation (GLUE) methodology (*Beven and Binley* 1992) is used in estimating parameter and model predictive uncertainties. This accepts the concept that multiple parameter sets and multiple model structures are potentially feasible simulators of the system to be modelled. In the case of the single model structure the GLUE method is applied to most often (*Romanowicz and Beven* 2003), these acceptable parameter sets may be located in different parts of the parameter hyperspace, and the concept of multiple sets being equal or near-equal simulators of the system is referred to as equifinality (*Beven* 1993). When multiple model structures are considered, different structures may equally be considered equifinal. Posterior statistics of the ensemble of feasible sets can be seen as a measure of parameter uncertainty, with parameter interaction implicitly considered. As the approach is set within a Bayesian framework, uncertainties in model predictions can be established using all likely parameter sets in predictive mode, with model results weighted by the relative likelihood of the individual parameter set (*Romanowicz et al.* 1996).

The principle of GLUE is based on Monte Carlo simulation to sample prior parameter distributions, with the sampling strategy used in GLUE is similar to importance sampling where a uniform prior is used. The difference is however, that where importance sampling uses the density of the sampling with equal weights of samples to represent the shape of the posterior probability surface, GLUE uses a

uniform sampling strategy with weights of samples to represent the surface. The approach can be summarised in a number of steps (*Freer et al.* 1996):

1. For the free parameters to be considered, prior parameter ranges must be defined. Under normal application, these can be set to realistic ranges based on literature or experience. These should also be selected such that the high density region of resulting posterior parameter distributions falls well within these bounds. To allow practical use of the method, the prior distributions within each parameter range are typically selected as being uniform *Kuczera and Parent* (1998), an acceptable choice given the limited prior knowledge on parameter distributions typically available. Where additional knowledge on parameter prior distributions are available, such as statistical interaction between parameters, or where certain combinations of parameters lead to physically unrealistic parameter sets then these could be considered in sampling.

2. The next step is to sample an ensemble of parameter sets from the prior distributions, and the selection of uniform prior distributions makes the sampling relatively simple to implement. After sampling parameter sets from the initial distribution, these are retained as complete parameter sets in all further evaluation. The advantage of assessing parameter sets rather than individual parameter distributions is that the performance of the set as a whole implicitly reflects parameter interaction and insensitivity. This avoids the need to sample from multivariate distributions when using the posterior distributions in the next step (*Freer et al.* 1996).

3. The final step is to define a formal measure of likelihood to be used in comparing how well models using the sampled parameter sets can be considered true simulators of the real world system. In most applications, this is done through subjective selection of one or more objective functions. Besides objective functions widely selected in hydrological modelling, (see *Green and Stephenson* (1986) for an overview of commonly used objective functions), multiple objective functions can be used, as well as expert judgement on validity of model results or fuzzy measures (*Aronica et al.* 1998a). This step is crucial to the philosophy of the GLUE method, as it proposes to make the relative belief in the model explicit (*Beven* 1993), with relative belief expressed as a likelihood measure. Optionally, a behavioural threshold can be used in terms of this measure of belief, with models performing better than the threshold considered behavioural and retained, while those below the threshold being discarded. Parameter sets discarded are then assigned a zero likelihood and the remaining likelihood values re-scaled.

Likelihood measures derived using different objective functions can be easily combined (*Lamb et al.* 1998; *Franks et al.* 1998; *Beven* 2001a), or updated if new data becomes available (*Freer et al.* 1996). This is through application of Bayes theorem,

$$L(\theta_i \mid Y) = \frac{L_1(Y \mid \theta_i) L_0(\theta_i)}{\sum_{j=1}^{N} L_1(Y \mid \theta_j) L_0(\theta_j)} \tag{4.3}$$

where $L_0(\theta_i)$ is the prior likelihood measure for parameter set θ_i, $L_1(Y \mid \theta_i)$ is the likelihood measure derived by comparing model output using parameter set θ_i to observations Y using a selected objective function, $L_1(\theta_i \mid Y)$ is the posterior likelihood of parameter set θ_i given observations Y, and N is the number of parameter sets. In predictive mode, the likelihood values thus derived can be used to weight model predictions, thus obtaining statistics on model predictive uncertainties.

The GLUE procedure has been applied in a very wide range of environmental modelling, including runoff hydrology (*Beven and Binley* 1992; *Uhlenbrook et al.* 1999; *Blazkova et al.* 2002a), Inundation modelling (*Romanowicz et al.* 1996; *Aronica et al.* 2002; *Romanowicz and Beven* 2003), flood frequency analysis (*Cameron et al.* 1999; *Blazkova and Beven* 2002), groundwater modelling (*Feyen et al.* 2001), and hydrograph separation using geochemical mixing models (*Joerin et al.* 2002).

The procedure can be applied to assessing likelihoods for the parameters of a single model structure, but may equally be applied in simultaneously assessing different model structures as well as different parameters for each model structure (*Crosetto and Tarantola* 2001).

4.6 Discussion

Both the GLUE and the MCMC methods would seem to be suitable for establishing parameter uncertainties for selected model structures, thus giving an indication of the reliability of the modelling approach taken. Despite the methods being relatively similar, there are some marked differences in the philosophy behind development of the approaches. The MCMC method is well founded in statistical theory, respecting the rules of Bayesian theory as described in *Bates and Campbell* (2001). In most applications of the MCMC method (see e.g. *Kuczera and Parent* (1998)), likelihood measures are obtained through application of the maximum likelihood function, and while this is formally more correct from the Bayesian point of view (*Thiemann et al.* 2001), *Beven and Freer* (2001) point out that the maximum likelihood function is very discriminate, with the solution converging on a single parameter set (*Beven and Young* 2003) or being very peaked (*Freer et al.* 1996). The result is equally an estimate of posterior parameter uncertainties, conditioned on the available data, but the focus on optimisation is more akin to traditional model calibration. In GLUE the contrasting view is taken, with all possible model structures and parameters sets considered equally likely before conditioning using the available data, and of differentiated likelihood or even invalid after conditioning. This invalidation is expressed through the selection of how likelihood measures are derived through the choice of objective function and if applicable, behavioural threshold. *Freer et al.* (1996) note that the term likelihood in GLUE is used in a wider context than in the classical likelihood functions. *Romanowicz et al.* (1996) show that these classical likelihood functions can be used within the GLUE procedure, but require a number of assumptions to be made as to the nature of model errors. While the subjective selection of this likelihood measure in GLUE is the main criticism from the point of view of formal statistics, this is equally the attractive aspect of the method. In formulating the likelihood measure, explicit thought must

be given to how model performance is assessed in the light of model application. A behavioural threshold to distinguish acceptable from non-acceptable models also provides a concept much easier to grasp in for example engineering practice than the statistically more rigourous MCMC method. The added versatility of including various different types of criteria into the likelihood measure, including binary classification in comparing spatial data as described in *Aronica et al.* (2002) makes the concept attractive for evaluating reliability in flood extent modelling, as demonstrated in several examples (*Aronica et al.* 1998a; *Romanowicz and Beven* 1998; *Horritt and Bates* 2001a; *Romanowicz and Beven* 2003).

4.7 Conclusions

In this chapter the concept of model performance has been introduced, with model performance being described not only in terms of computational efficiency, but also in terms of application efficiency and model reliability. While computational efficiency is clearly determined by selection of the model structure and underlying assumptions, and application efficiency is closely related through for example integration with GIS, model reliability is less clearly defined for a particular code or family of codes. Model reliability and model uncertainty are closely related concepts, particularly if model uncertainty is taken from the point of view of how well a chosen model concept and parameterisation can be expected to simulate the real behaviour of the system being modelled.

The problem in application of almost all models is that a number of free parameters must be estimated by comparing model output variables to observed variables. These parameters must then be optimised through a process of calibration. Although some of these parameters are related to physically observable properties, these observations can only be made at the field (often point) scale, while the parameters in the models effectively act at the model scale. As a result, model parameters may serve as a form of closure, to cover not only the physical property they were introduced for, but also other effects not explicitly accounted for due to assumptions made, or through lack of knowledge. Together with inherent variability of nature, and a typical lack of comprehensive calibration data sets, the result may be considerable parameter uncertainty, which will influence predictive uncertainties and therefore model reliability.

To evaluate uncertainties in models using the various flood extent codes described in the previous chapter, the generalised likelihood uncertainty estimation (GLUE) method is applied throughout in this thesis. This method accepts all possible model structures and associated parameters as possible simulators of the system (where all possible approaches should obviously be taken within reason), and explicitly uses available calibration data to validate or invalidate the selected model structure and parameters. Each of the selected codes discussed in chapter 3 can in principle be used to create very comparable results of flood extent integrated with GIS. On the basis of the calibration data, however, the different approaches may be found to be more or less reliable. Together with the computational efficiency and ease of application, this then allows comparable assessment of performance.

5

Evaluation of reach scale flood extent models

Abstract

Discharge predictions using the four codes described in chapter 3 are compared to predictions derived using theoretical and empirical methods. The model codes vary in complexity but represent the types of code used in practical application due to their easy integration with available GIS data formats. Common to the codes is that turbulent momentum interaction between main channel and over-bank floodplain flow is not explicitly taken into account. It is shown for different configurations of a hypothetical channel that most codes significantly overestimate discharge capacity as a result. Applying these codes to flood extent modelling therefore requires calibration of roughness values to account for this additional momentum transfer, resulting in roughness factors derived no longer representing physical friction values only, but combined friction and momentum correction factors.

based on M.Werner and M. Lambert, "Evaluation of modelling approaches for river reach scale inundation modelling", Submitted for publication in *Journal of Hydraulic Research*

5.1 Introduction

Derivation of flood extent maps can be through a variety of approaches, ranging from the extremely simple where a planar representation of the water level surface is crossed with the digital elevation model (DEM) of the area of interest, through to application of complex 2D and 3D modelling codes. An overview of the variety of approaches is given in *Bates and de Roo* (2000). Most applications considering flood extent prediction at the reach scale, however, apply either a 1D hydrodynamic modelling code and subsequent GIS interpolation to derive a 2D map representation (*Werner* 2001; *Tate et al.* 2002) or a (quasi) 2D approach. Early examples of the latter include the cell inundation based technique (*Cunge* 1975; *Cunge et al.* 1980). Since these early attempts various codes for 2D modelling of floodplain flow have been presented (*Bladé et al.* 1994; *Bates et al.* 1996; *Bates and de Roo* 2000; *Beffa and Connell* 2001; *Stelling et al.* 1998).

A problem commonly noted in application of these in inundation modelling is the lack of data available for model calibration and verification. Typically the only data available is from river gauging stations at intervals of between 10 and $30km$ (*Bates and de Roo* 2000). This is very limited information when considering verification of a model that attempts to estimate the spatial extent of flooding. Typically these codes are based on the shallow water equations, with roughness and perhaps turbulence formulations to account for momentum loss. It is argued that by using this inherently sound physical formulation, the model has a sound physical basis, and is thus able to reliably reproduce behaviour of the system without the need of extensive calibration and verification. In calibrating the models to the limited available data, however, roughness values are used to crudely explain the net effect of momentum loss due to the complex flow patterns such as secondary currents and crossing flows, where flow passes from the floodplain to the main channel to the opposing floodplain (*Knight and Shiono* 1996).

Given this lack of calibration and verification data and the utilisation of roughness values to explain not only bed friction, but also many other phenomena either poorly understood or poorly described in the model, the use of complex model codes may not be warranted. Indeed comparisons of simple and complex model codes against observed data in relatively data rich cases show that the complex codes do not necessarily outperform simpler codes at the reach scale (*Bates and de Roo* 2000; *Horritt and Bates* 2002).

River flood inundation for most rivers can be described as flow in a two-stage or compound channel. Much experimental and theoretical work has been dedicated at discharge prediction in compound channels, including research into secondary currents and crossing flows in straight and meandering channels (*Sellin* 1964; *Ackers* 1992; *James and Wark* 1992; *Greenhill and Sellin* 1993; *Lambert and Sellin* 1996b; *Ervine et al.* 2000). Although this work provides useful practical relationships for estimating discharges in compound channels, these have found little application in inundation modelling codes. Generally these codes faithfully reproduce hydraulic flow and resulting stage-discharge relationships, given the assumptions made in developing the code. Typically these assumptions include ignoring secondary currents and crossing flows (*Ervine et al.* 2000). The experimental work has shown

that these assumptions may result in significant differences between stage-discharge relationships derived from model results and the observed stage-discharge relationships.

In this chapter stage discharge relationships derived using four different modelling codes used in flood extent modelling are compared to experimentally derived relationships. A similar comparison is presented by *Wilson et al.* (2002), who compare a 2D finite element model to experimental results, finding that stage discharge curves compare reasonably when using either a $\kappa - \epsilon$ or Elder turbulence closure models. They do note, however, that depth averaged velocities across the sections are poorly represented. Although hydraulically superior, verification of finite element models against field data show that these do not necessarily yield superior results to simple raster based finite difference models at the reach scale (*Horritt and Bates* 2002), with the latter being much easier to apply, particularly due to much simpler integration with available topographical data formats. The four modelling approaches selected here reflect this ease of application, and represent the type of model more likely to be applied in practical applications of reach scale inundation mapping. Impacts of variations in channel delineation, resolution and roughness on predicted stage-discharge curves are investigated and compared to discharge prediction relationships derived from experimental work.

5.2 Discharge prediction in compound channels

Research dedicated to describing flow in compound channels has been motivated by the requirement of providing engineers design guidelines for estimating discharge capacity for compound channels (*Sellin et al.* 1993). The most simple arrangement is to consider an average velocity across both channel and floodplain and apply for example Manning's equation in estimating this velocity. Differences in floodplain and main channel velocities, however, result in serious errors in discharge prediction if this single channel method is followed. One of the earliest estimation methods that recognised the need to consider the flow in main channel and floodplain separately in a compound channel was proposed by *Chow* (1959). The discharge for each section of the channel is estimated independently, with the total discharge found through summation of each individual section, under the assumption of zero shear between the sections (see figure 5.1);

$$\begin{aligned} Q = \quad & \tfrac{1}{n_{mc}} A_{mc} R_{mc}^{2/3} S^{1/2} + \\ & \tfrac{1}{n_{fp}} A_{fp-left} R_{fp-left}^{2/3} S^{1/2} + \\ & \tfrac{1}{n_{fp}} A_{fp-right} R_{fp-right}^{2/3} S^{1/2} \end{aligned} \tag{5.1}$$

This method is referred to as the vertical divided channel method (*vdcm*). Although attractive in its simplicity, it ignores secondary effects due to the interaction between fast velocities in the main channel and slow velocities on the floodplain, and as a consequence systematically overestimates discharge capacity (*Sellin* 1964; *Ackers* 1992). Even for simple channels the assumption of uniform flow across the cross section is a gross simplification with the actual flow structure being much

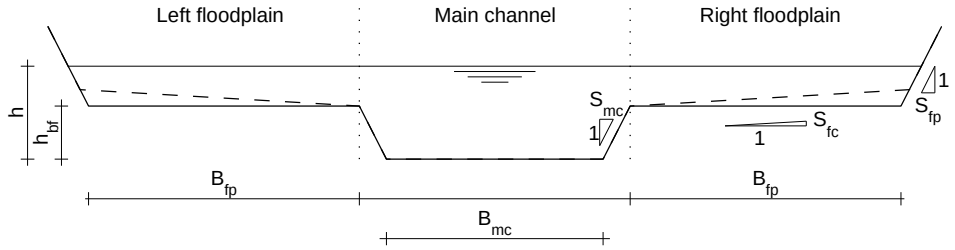


Figure 5.1: Division of compound channel in *vdcm*. Vertical dotted lines between main channel and floodplain

more complicated (*Sellin* 1964; *Bhowmik* 1982).

To account for the error in discharge prediction, *Ackers* (1992) introduces a stage dependent correction factor *disadf* to be applied to the discharge estimate using the *vdcm* method. Although good comparison is shown to experimental data, extrapolation to other types of geometry than those tested against is difficult (*Lambert and Myers* 1998).

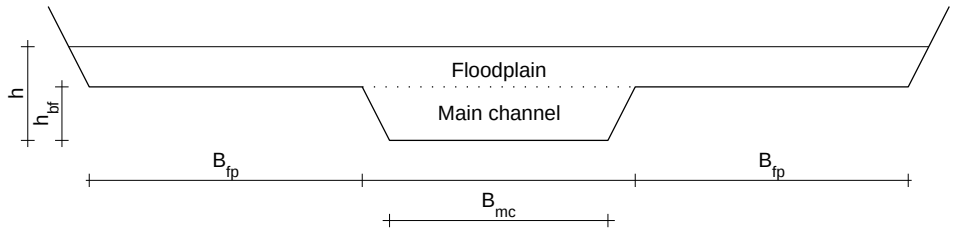


Figure 5.2: Division of compound channel into sections in the *hdcm* method. The horizontal dotted lines indicates the division between main channel and floodplain.

An alternative to the vertical division between main channel and floodplain is that of the horizontal divided channel method (*hdcm*). The main channel is now divided at the bankfull depth, with a uniform velocity assumed for the main channel underneath the division and another uniform velocity for the main channel and floodplain above the division (*Wormleaton et al.* 1982) as indicated in figure 5.2. Again the method is elegantly simple, but for small overbank flow depths the velocity gradient across the intersection overlying the main channel is physically unrealistic as is the case for very narrow floodplains (*Lambert and Myers* 1998). The *hdcm* is shown to systematically under-estimate discharges. Other approaches introduced to take account of the influence in floodplain flow on main channel flow is to use an inclined division (*Wormleaton et al.* 1982), but these are not explored further here.

In a critical review of these approaches *Lambert and Myers* (1998) note that turbulent momentum interchange between the main channel and the floodplain is essentially ignored. This turbulent interaction results in a reduction in discharge

capacity and thus underestimation of stages relating to a given (design) discharge. In keeping with the premise of establishing discharge in separate sections before summation, but without the requirement of fixing a division *a-priori*, they introduce a method of weighting the average velocity in the main channel and floodplain found through both the *vdcm* and *hdcm* methods;

$$V_{mc-\mathrm{AVE}} = \xi V_{mc-vdcm} + (1-\xi) V_{mc-hdcm} \tag{5.2}$$

where $V_{mc-vdcm}$ is the average velocity in the main channel zone derived using the *vdcm*, $V_{mc-hdcm}$ is the average velocity in the main channel zone derived using the *hdcm*, and $V_{mc-\mathrm{AVE}}$ is the weighted main channel velocity. ξ is a weighting factor between 0 and 1. The average main channel velocity determined is then applied to the main channel area between the vertical division line in figure 5.1. A similar expression can be established for the average floodplain velocity, and the total discharge derived by adding main channel and floodplain discharge.

For straight channels with a floodplain roughness equal to the main channel ξ is empirically derived as being in the order of 0.5, while for channels with rough floodplains a value of 0.2 is found more appropriate. While showing a better comparison to stage-discharge curves observed in the Flood Channel Facility at HR Wallingford (*Ackers* 1992), the method is still somewhat empirical with the factor ξ needing to be estimated as a function of the ratio of main channel and floodplain roughness. This method is referred to in this chapter as the weighted divided channel method (*wdcm*).

A conceptually more elegant method is introduced by *Lambert and Sellin* (1996a) based on the turbulent mixing length concept to take into account the turbulent momentum interchange between main channel and floodplain. The channel cross section is divided into a large number of small vertical elements. Prandtl's mixing length hypothesis is adapted to determine the apparent shear stress on the sides of each of the elements, and a resulting correction factor due to the momentum interchange is calculated for the discharge in each element. The total discharge is again found through summation of discharge in individual elements. Stage discharge curves determined show good comparison with experimental results for straight channels with horizontal floodplains, although some underestimation of discharge is shown for low over-bank depths. Depth averaged velocity distribution across the cross section is equally well represented, underwriting the physical basis on which the method is founded (*Lambert and Sellin* 1996a). This method is referred to in this chapter as the turbulent mixing length hypothesis method (*tmlh*).

The methods described above were derived for application to straight compound channels only. In more natural rivers the main channel often meanders across the floodplain, which in turn may be meandering through the landscape. Velocity distribution in the cross section for meandering rivers is much more complex (*Lambert and Sellin* 1996b; *Babaeyan-Koopaei et al.* 2002), partly due to crossing flows. Errors made by simply applying traditional divided channel methods as in the straight case may increase significantly to the order of 30% (*Greenhill and Sellin* 1993).

Most practical methods for estimating stage-discharge relationships for meandering channels become much more empirical than for example the *tmlh* method.

The traditional way to account for the meandering channel is to again apply the vertical divided channel method, but increase the main channel roughness by a ratio dependent on the sinuosity of the channel (*Chow* 1959; *French* 1986). This can lead to corrections of main channel roughness by up to 30% which is applied only when flow is in-bank. No corrections are applied for overbank flows, and again no account is taken of the complex momentum interchange and crossing flows and it is clear from comparison with experimental results that this results in significant over-prediction of discharges.

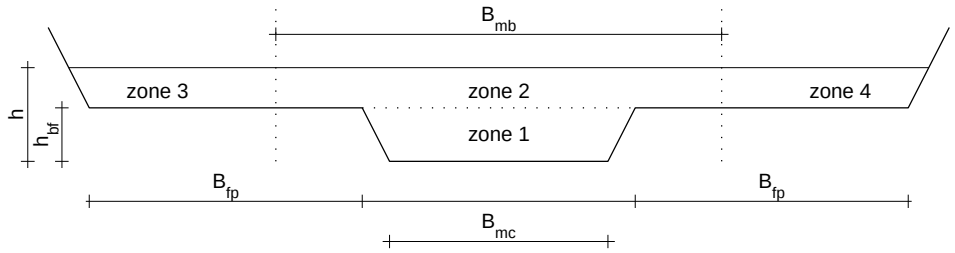


Figure 5.3: Division of compound meandering channel into four zones. The horizontal dotted lines indicate the division between the main channel zone and the meander zone. Left and right floodplain outside the meander belt are represented by zones 3 & 4

In an attempt to provide a more reliable estimate of discharge in meandering channels, yet maintain a simple analytical relationship, *Greenhill and Sellin* (1993) report an empirical method that takes into account channel sinuosity for overbank flows. The method divides the compound channel into four zones; (i) the main channel under the horizontal bankfull line (as in *hdcm*), ii) the floodplain and overbank main channel in the meander belt, and the (iii & iv) floodplain outside the meander belt (see figure 5.3). The discharge is the sum of discharges in each zone as given in equation 5.3. For the second zone, the main channel longitudinal slope is applied rather than the floodplain longitudinal slope. For more details, see *Greenhill and Sellin* (1993), where the method is applied to meandering channel with horizontal floodplains. It is also important that the interface between the zones is used in the calculation of hydraulic radius, and therefore not considered as having zero-shear. Reference is made to this method as *ghm5* (method 5 described in *Greenhill and Sellin* (1993)). The method is reported to give more accurate estimation of discharges in meandering channels, with an error in the order of between 5% (*Greenhill and Sellin* 1993) and 8% (*James and Wark* 1992).

$$\begin{aligned} Q = \quad & \tfrac{1}{n_{mc}} A_1 R_1^{2/3} S_{mc}^{1/2} + \\ & \tfrac{1}{n_{fp}} A_2 R_2^{2/3} S_{mc}^{1/2} + \\ & \tfrac{1}{n_{fp}} A_3 R_3^{2/3} S_{fp}^{1/2} + \\ & \tfrac{1}{n_{fp}} A_4 R_4^{2/3} S_{fp}^{1/2} \end{aligned} \tag{5.3}$$

James and Wark (1992) describe an alternative empirical method for estimating discharges in meandering compound channels. They divide the channel in four zones

similar to the division of *Greenhill and Sellin* (1993), but using vertical divisions between the floodplain inside and outside the meander belt (as given in figure 5.3). The method has been derived from extensive analysis of results from laboratory flumes, using many empirically derived coefficients.

Discharge in the main channel zone, Q_1, is derived by calculating the bankfull discharge Q_{bf} using the standard method of estimation, and applying a reduction factor Q'_1,

$$Q_1 = Q_{bf} Q'_1 \tag{5.4}$$

with the reduction factor Q'_1 given as,

$$Q'_1 = \mathtt{max}(1.0 - 1.69y', my' + Kc) \tag{5.5}$$

with

$$\begin{aligned} m &= 0.0147 B_{mc}^2/A + 0.032(f_2/f_1) + 0.169 \\ c &= 0.0132 B_{mc}^2/A - 0.302s + 0.851 \\ K &= 1.14 - 0.136(f_2/f_1) \\ y' &= (h - h_{bf})/(A/B_{mc}) \end{aligned} \tag{5.6}$$

Discharge in meander belt zone, Q_2 is given as,

$$Q_2 = A_2 V_2 \tag{5.7}$$

where the average velocity in zone 2 is given as,

$$V_2 = \left(\frac{2gSL}{(f_2 L)/(4R_2) + F_1 F_2 K_e} \right)^{1/2} \tag{5.8}$$

and

$$\begin{aligned} F_1 &= \mathtt{min}(0.1B^2/A, 1.0) \\ F_2 &= \mathtt{Sinuoisity}/1.4 \\ K_e &= C_{sl} C_{wd} (C_{sse}(1 - (h - h_{bf})/h)^2 + C_{sse} K_c) \\ C_{sl} &= 2(B_{mb} - B_{bf})/B_{mb} \\ C_{wd} &= 0.02(B_{bf}^2/A) + 0.69 \\ C_{sse} &= \mathtt{min}(1.0 - s_{mc}/5.7, 0.1) \\ C_{ssc} &= \mathtt{min}(1.0 - s_{mc}/2.5, 0.1) \end{aligned} \tag{5.9}$$

Discharge in zone 3 and 4, the floodplain outside the meander belt, are derived using the standard discharge estimation methods. The total flow is found through summing the discharge in the four zones. Although the method would seem to be highly empirical, different contributions to the total conveyance were analysed by *James and Wark* (1992), and when compared to experimental results the method was found to underestimate discharge by on average $\sim 2\%$, with a standard deviation of $\sim 10\%$, therefore an improvement over the results of *Greenhill and Sellin* (1993). Reference is made to this method in this chapter as *jwrk*.

Despite errors in predicted discharge for meandering channels using the method applied by *James and Wark* (1992) when compared to experimental results, the

method relies largely on empirical relationships. *Ervine et al.* (2000) describe a more physically based approach for addressing the problem of conveyance estimation. The approach is generically applicable to straight, skewed, as well as meandering channels. It uses an analytical solution of the depth-integrated turbulent form of the Reynolds averaged Navier-Stokes equations of flow, considering lateral shear, secondary and crossing flows as well as bed friction. The approach is extensively described in *Ervine et al.* (2000), and has been encapsulated in a software tool to allow easy estimation of conveyance in channels of all cross sections and planforms (*DEFRA* 2004). The method is referred to as *rans*.

5.3 Inundation Modelling Approaches

The four modelling codes discussed in chapter 3 are applied here to a hypothetical channel to establish stage-discharge relationships. The codes are discussed fully in that chapter, but for easy reference in the figures used in this chapter, the one-dimensional SOBEK code using the preismann box scheme is referred to as *sbk-riv*, the one-dimensional SOBEK code using the staggered scheme as *sbk-yz*, the full two dimensional DELFT-FLS code as *fls*, the hybrid SOBEK-1D2D code as *sbk1d2d*, and finally the GIS embedded LISFLOOD-FP code as *lfp*.

5.4 Application

The four model codes described are applied in exploring stage discharge relationships in a hypothetical compound channel. The cross section of the channel is comparable in form to cross sections applied in the Flood Channel Facility (*Ackers* 1992), although dimensions that allow easy variation in grid size definition and are more comparable to real rivers than the scale model are adopted. The cross section of the channel is depicted in figure 5.1.

- Main channel invert width (B_{mc}): $16m$
- Main channel depth (h_{bf}): $2m$
- Main channel and floodplain side slope s_{mc}, s_{fp}: $1:1$
- Longitudinal slope S: 0.04%
- Reach length L: $1600m$ (Sinuosity in meandering channel = 1.298)

Four variations of the reach are explored. First a simple straight channel with symmetrical horizontal floodplains is used. In a second series the same channel is used, but the floodplain is inclined. In a third series the main channel is allowed to meander with a sinuosity of 1.3 with a cross-over angle of 60^o, again with horizontal floodplains. In the fourth configuration the floodplains of the meandering channel are inclined. Table 5.1 gives an overview of the different configurations considered, and an impression of a small section for the first and last configurations is given in figure 5.4.

Table 5.1: Summary of channel configurations

Reach	floodplain		alignment	roughness	
	width [a]	inclination [b]		main channel	floodplain
	(B_{fp})	(S_{fc})	(-)	(n_{mc})	(n_{fp})
	(m)	(-)	(-)	($m^{-1/3}s$)	($m^{-1/3}s$)
S1	40	0	Straight	0.02	0.02
S2	40	0	Straight	0.02	0.05
S3	40	0.03	Straight	0.02	0.02
S4	40	0.03	Straight	0.02	0.05
M1	40	0	Meandering	0.02	0.02
M2	40	0	Meandering	0.02	0.05
M3	40	0.03	Meandering	0.02	0.02
M4	40	0.03	Meandering	0.02	0.05

[a] average floodplain width for meandering alignment
[b] average floodplain inclination for meandering alignment

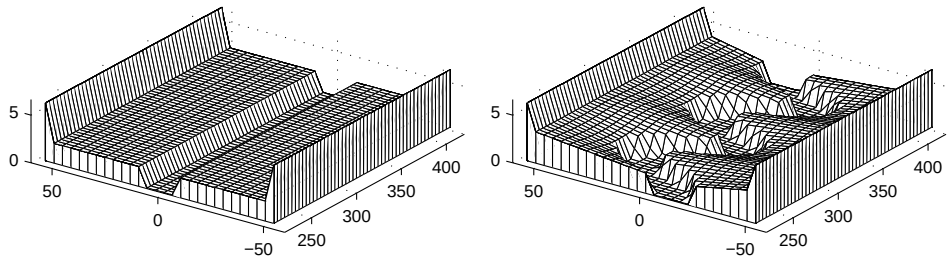


Figure 5.4: Impression of channel configurations *s1* (left) and *m3* (right) for a small section of the reach. The variation of floodplain inclination with meanders is clearly seen

With the exception of the 1D codes, the floodplain topography of the reach is described using a grid based digital elevation model (DEM) of suitable resolution. In theory a finer resolution grid should lead to a better representation of floodplain flow (*Beffa and Connell* 2001), but as selection of too fine a resolution would lead to an intractable computational problem, a balance between run-times and resolution was required. Elevation models were generated at grid cell resolutions of 2m, 4m and 8m, where the first two were applied in models using the *fls* code and the last two in those using the *sbk1d2d* and *lisflood-fp* codes.

In the first series of model runs, the four codes were applied to the straight channel configurations (*S1* through *S4*). For this channel, as in all the straight configurations, the bankfull discharge established using a single channel approach is in the order of $52m^3/s$. Nine discharge conditions representing two in-bank flows seven over-bank flows were selected; 40, 50, 60, 70, 85, 100, 125, 150 and $200m^3/s$. These were applied as upstream boundary to models of the reach, while the downstream boundary was given as a discharge related stage. This stage was initially estimated using the *vdcm*, samples of calculated stage in the main channel

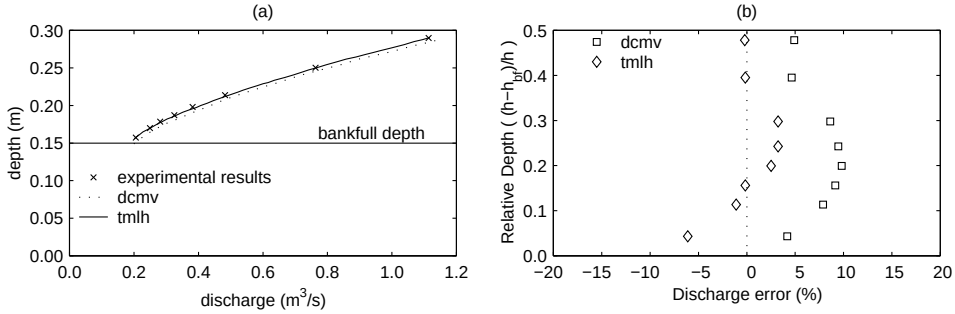


Figure 5.5: Comparison between the calculated discharge relationships from the *vdcm* and *tmlh* methods and experimental results from the SERC-Flood Channel Facility. (a) shows the absolute depths and discharges, (b) shows the error in calculated discharge against relative depth (after *Lambert and Sellin* (1996a))

were taken at 400 m and 800 m, and where differences were found in these the downstream boundary was adjusted until stable flow conditions prevailed. At the upstream flow boundaries, the imposed flow was divided across the 1D and 2D domains where applicable to allow a constant flow field to be established as soon as possible.

A similar approach was taken in the second series of runs considering the meandering channel configurations (*M1* through *M4*). The bankfull discharge for the meandering main channel is estimated at $40m^3/s$, and for discharges above this momentum exchange between the main channel is not only due to secondary currents, but also crossing flows from floodplain to main channel and main channel to floodplain. As the bankfull discharge is now lower than for the straight channel, two additional in-bank discharges of $20m^3/s$ and $30m^3/s$ were investigated.

In all runs using both the straight and meandering configurations, two selections of roughness for the non-zero shear interface between the inbank domain and the overbank domain in *sbk1d2d* were used. This was set either at a very low value such that the discharge found for the main channel zone (see figure 5.3) approaches that found for this zone using the *vdcm* method, or to the same value as the main channel bed roughness. Runs using the former roughness specification are denoted as *sbk1d2d**, while those using the second are denoted as *sbk1d2d***.

5.5 Results

5.5.1 Straight channel configurations

Figure 5.5 shows a comparison of the stage discharge curve found for both the *vdcm* and *tmlh* methods to experimental results (from *Lambert and Sellin* (1996a)). Although the difference between the stages would seem modest in absolute terms, when plotted as discharge error against relative depth (defined as $(h - h_{bf})/h_{bf}$), it is clear that the discharge prediction error can be quite significant for the *vdcm*

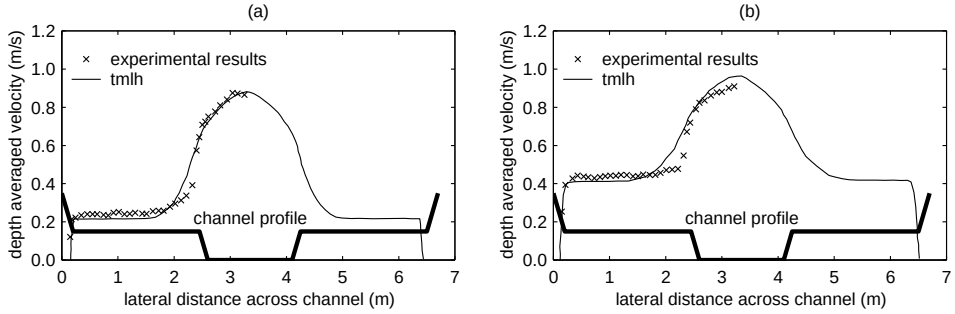


Figure 5.6: Comparison between calculated velocity distribution and experimental results from the SERC -Flood Channel Facility at relative depths of (a) 0.117 and (b) 0.197 (after *Lambert and Sellin* (1996a))

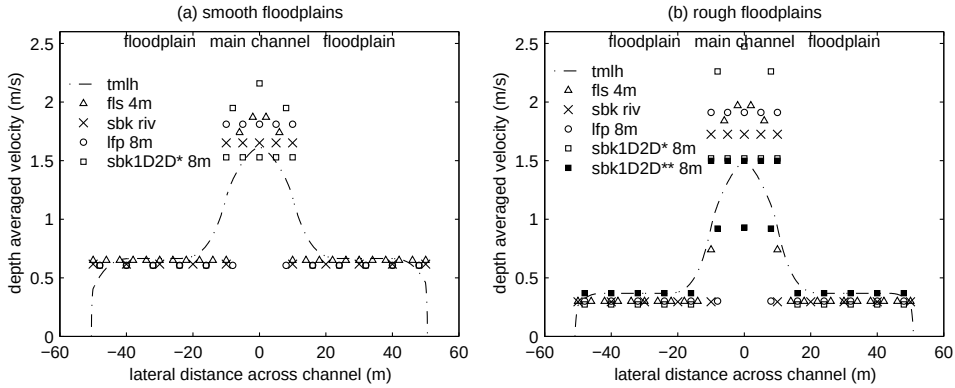


Figure 5.7: Depth averaged velocities at a discharge of $100^m/s$ for straight channel with horizontal floodplains (*s1* & *s2*).

method, reflecting overestimation of discharges using *vdcm* found by many authors (*Sellin* 1964; *Lambert and Myers* 1998). The error is smaller for the *tmlh* method, although best results are found for higher relative depths, with underestimation of discharges for low overbank flows. Figure 5.6 shows the depth averaged velocity profile across the channel for two relative depths calculated using the *tmlh* compared to experimental results, indicating that the velocity profile across the interface between the main channel and floodplain is well represented.

Figure 5.7 shows depth averaged velocities across the channel for both the smooth and rough channel configurations at a discharge of $100m^3/s$ compared against results found for the different model codes. Where flow is resolved using 1D, markers across the domain are plotted along a horizontal line. For the *sbk1d2d* codes, where inbank main channel flow is resolved in the 1D domain, while overbank flow is resolved in the 2D domain, two lines are given. These depth averaged velocities show that for all codes, velocities across the floodplain are constant,

without influence of the effect of the main channel / floodplain interaction as seen in the *tmlh* velocity profile. The same holds for the profiles across the main channel, except for the *fls* where some evidence of this interaction is seen.

Velocities on the floodplain do, however, agree reasonably well in magnitude, while main channel velocity profiles vary more between codes due to the different approaches taken in resolving main channel flow. Profiles of the *sbk-riv* code follow the average main channel velocity given by the *vdcm* exactly (not shown), while the *lfp* and *fls* codes show slightly higher velocities due to the reduced main channel width in the non-conservative approach. Following the horizontal division between in-bank and over-bank floodplain flows, two sets of velocities for the *sbk1d2d* code are shown in the main channel. For the run with the very smooth roughness factor applied to cells overlying the main channel (*sbk1d2d**) it can be seen that although the in-bank velocities are realistic, velocities for the cells overlying the main channel are unrealistically high, particularly for the case of rough floodplains where flow is concentrated in the main channel area. Conversely in run *sbk1d2d*** where the main channel roughness factor is applied at the horizontal interface velocities for the overlying cells are low.

The effects of the differences in velocity profile can be clearly seen in the stages calculated for the different discharge conditions considered. Figure 5.8(a) shows stages predicted at the discharges conditions for the *s1* channel configuration (smooth floodplains). For comparison the four discharge estimation methods are also given, showing the *wdcm* and *tmlh* methods to lie between the *vdcm* and *dcmh* methods. Figure 5.8(b) shows the same results, but now plotted against relative depth (compare with figure 5.5). Discharges are expressed in terms of percentage difference to those calculated using the *tmlh* method. Figure 5.9 shows the similar plots of for the *s1* channel configuration (smooth floodplains)

For both configurations, results using the *sbk-riv* code show to conform exactly to predictions using the *vdcm*. This is not surprising as the cross section in the model is sub-divided exactly as in the *vdcm* with a zero-shear interface between the divisions. The *sbk-yz* code follows the same principle, but the cross section is divided into a number of segments for which conveyance is treated individually before summing to find the total channel conveyance. As there is no momentum transfer between sections, conveyance is overestimated beyond the overestimation present in the *vdcm* method. This reflects (*Garbrecht and Brown* 1991), who show the overestimation to be influenced by the number of independent sections used, and when compared to the *vdcm* additional overestimation may be as much as 5%.

In both the *fls* and *lfp* codes, in-bank discharges are predicted using the non-conservative formulation, which again underestimates the wetted perimeter, and thus overestimates main channel discharges. In setting up the simple *lfp* model, however, the main channel geometry is modelled at a more conceptual level, with the width selected such that the bankfull discharge approaches that had the full conservative formulation been used (*Bates and de Roo* 2000). In the channel used here, this width is set to $16m$, giving an estimate of in-bank stages close to those found with the *vdcm* method. At the $4m$ resolution the *fls* model equally has a main channel width of four grid cells, equalling $16m$, thus giving identical results. For overbank flows, the *fls* model continues to follow the *vdcm* method, while *lfp* tends

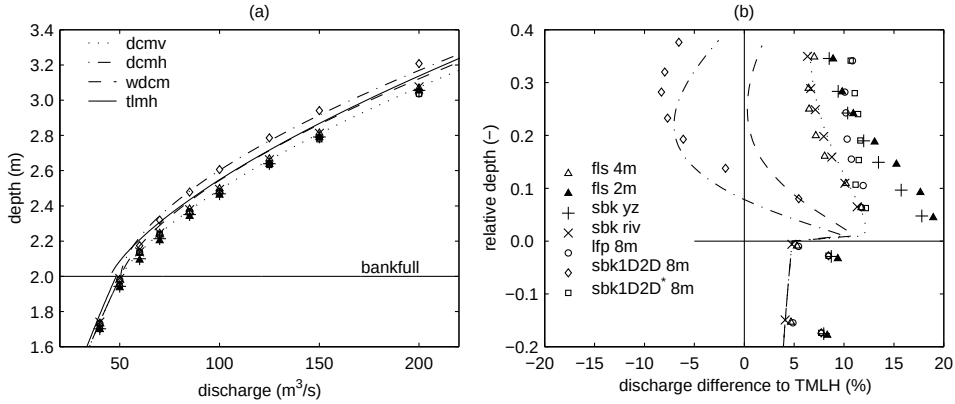


Figure 5.8: Straight channel with smooth horizontal floodplains (*s1*). (a) difference in predicted stage b) percentage difference compared to discharges predicted using the *tmlh* method against relative depth

to a larger overestimation. This is due to the simple concept used in coupling the 1D and 2D domains. The resolution is such that there are floodplain domain cells overlying the main channel, which are not explicitly coupled to the main channel. As a consequence conveyance in these cells is in effect accounted for both in the $1D$ and $2D$ domains. For the *fls* code with the finer $2m$ resolution results show even greater over-prediction of main channel discharges. The finer resolution means a better representation of the actual main channel geometry, but the use of the non-conservative approach results in an underestimation of the wetted perimeter comparable to the *sbk-yz* model and subsequent over-prediction of discharge.

Results from the *sbk1d2d* codes show very different behaviour to the other codes, with underestimation of discharge being greater even than for the *hdcm* method. Careful analysis of the model show this underestimation to be due to the accounting of roughness at the interface between the main channel and the floodplain. This interface follows the same principle as the *hdcm* with a horizontal division between main channel and floodplain at the bankfull depth. However, the roughness factor taken into account at the interface for overbank flows can be used to implicitly model momentum loss at the interface. Normally this roughness factor would be the same as that applied on the floodplain, and particularly for the case of rough floodplains this leads to significant under-prediction of discharge (see figure 5.9b). To resolve this under-prediction an additional run was done with this code where a roughness factor different to the floodplain roughness was applied to cells overlying the main channel that form the horizontal division between main channel and floodplain. A roughness factor of $0.005sm^{-1/3}$ was selected, where this value was calculated to give approximately the same total main channel flow for the main channel plus overlying cells as would the *vdcm* for low relative depths. Results from this run, denoted as *sbk1d2d** in figure 5.8 indeed follow those of the *vdcm* for low relative depths, but tend again to overestimation of discharge at higher relative depths.

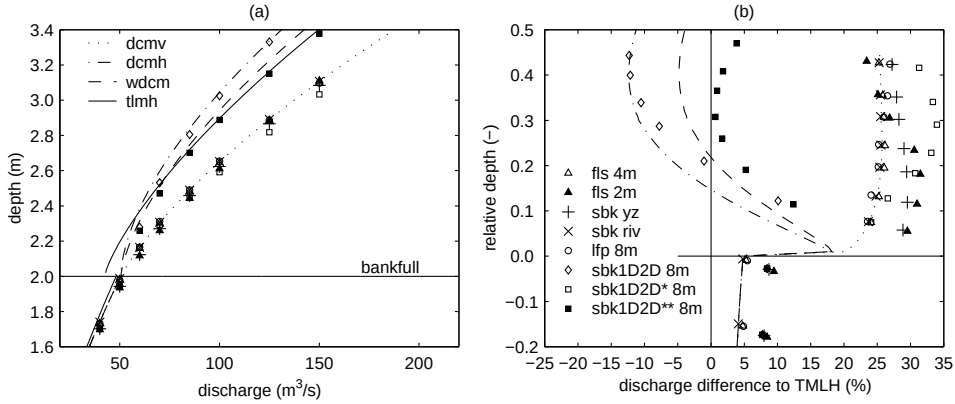


Figure 5.9: Straight channel with rough horizontal floodplains (*s2*). (a) difference in predicted stage b) percentage difference compared to discharges predicted using the *tmlh* method against relative depth

In principle the roughness factor applied to these cells should tend to the main channel roughness at higher relative depths as the main channel below the horizontal division becomes less significant. This would result in a depth dependent correction, making model parameterisation more complicated, which should be avoided. A third run was done for the channel configuration with rough floodplains, with the main channel roughness value applied at the interface. The results, denoted as *sbk1d2d*** in figure 5.9, show good comparison with discharges and levels predicted using the *tmlh* methods, except for low overbank flows, where *tmlh* is known to under-predict conveyance.

In comparing results for smooth and rough floodplains in figures 5.8 and 5.9 it is clear that the variation between different codes and methods increases as flow is concentrated in the main channel as floodplain roughness increases. The depth averaged velocities reflect this, with differences between codes being significant in the main channel area only. In channel configuration *s3* with inclined floodplains flow is concentrated even more in the main channel area, and table 5.2 shows that differences in stages calculated at the selected discharge conditions between codes become even more pronounced. The tendency of most codes to over-estimate the discharges when compared to *tmlh* is the same as in the horizontal floodplain configurations, but more pronounced. This is reflected even more strongly in the configuration with rough floodplains (*s4*). With concentration of flow in the main channel, results for the *sbk1d2d** run showed that high velocities in the cells overlying the main channel. These are attributed to the low roughness specified at the interface between inbank and overbank main channel, resulting in serious overprediction of discharge. Those for the *sbk1d2d*** run on the other hand showed better comparison to the *tmlh* and *wdcm* methods.

Table 5.2: Comparison of calculated stages for straight channel configuration with inclined floodplains (*s3*)

	tmlh	*fls*	*sbk-yz*	*sbk-riv*	*lfp*	*sbk1d2d***
Discharge				Stage		
m^3/s	m	m	m	m	m	m
40	1.79	1.73	1.70	1.74	1.73	1.70
50	2.04	1.98	1.94	1.99	1.98	1.95
60	2.26	2.19	2.15	2.19	2.19	2.30
70	2.42	2.36	2.32	2.36	2.35	2.57
85	2.63	2.57	2.54	2.58	2.55	2.81
100	2.80	2.75	2.72	2.75	2.71	2.99
125	3.03	2.98	2.96	2.99	2.94	3.21
150	3.23	3.17	3.16	3.18	3.11	3.38
200	3.51	3.47	3.46	3.47	3.40	3.66

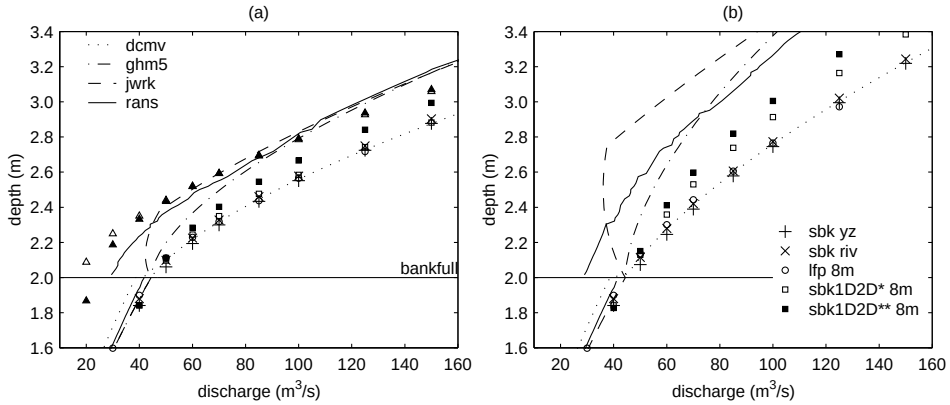


Figure 5.10: Predicted staged for different discharges for meandering channel with horizontal floodplains (*m1* & *m2*).

5.5.2 Meandering channel configurations

Figure 5.10 shows the stages calculated for the different discharge conditions in the meandering channel configuration with horizontal floodplains (*m1* & *m2*). Stage-discharge curves derived using the *vdcm*, *ghm5*, *jwrk*, and *rans* methods are also shown, with considerable differences between the methods. The over-estimation of discharges by the *vdcm* method when compared to those from the *rans* method are in the order of 30%, as reported also by *Greenhill and Sellin* (1993) for experimental results. The *rans* method is considered most accurate, but the figure shows minor fluctuation resulting from numerical problems in evaluation.

As expected, the *sbk-riv*, *sbk-yz*, and *lfp* follow the *vdcm* closely. Results for *fls* codes show severe underestimation of main channel discharge, and while stages at overbank flows calculated here give reasonable comparison to those predicted using

the *rans* method, this is due to the over-estimation of floodplain flow compensating the under-estimation of main channel flow. The $2m$ resolution model shows a slight improvement, though even then errors in main channel discharge prediction are significant. This effect has been shown in other applications of raster inundation models (*Beffa and Connell* 2001) and as a results the code is considered unsuitable for modelling compound channel flows for meandering planforms.

Results from *sbk1d2d* using the smooth roughness correction for cells overlying the main channel (*sbk1d2d**) do not show the over prediction of stage seen for the straight channel, but rather an under-prediction, with a tendency towards discharges predicted using the *rans* method. The reason for this is that the meandering channel does not allow the high velocities to establish in the cells overlying the main channel as seen for the straight channel configuration (see figure 5.7). For the run with the main channel roughness set at the horizontal floodplain / main channel interface ((*sbk1d2d***) results are improved slightly, but differences with the *rans* method are not insignificant. Comparable results are found for meandering channels with inclined floodplains. As with the inclined floodplains in the straight channels, the relative differences in discharges calculated are again greater than for the horizontal floodplains.

5.5.3 Influence of grid resolution

In all the results presented, only those for the lower resolution digital elevation model are shown. From running the codes at both high and low resolutions, it became clear that with the exception of the *fls* code where the main channel is also described using a regular grid, the differences between the two resolutions are negligible. This is not surprising as the main channel plays the most important role in flow conveyance and except for the *fls* model the resolution of the digital elevation model has no influence on main channel modelling. Results using the higher resolution models have not been included in the figures for the sake of readability.

5.6 Discussion

Application of the model codes to the straight channel configuration show that with the exception of the *sbk1d2d* code, these more or less comply with stage-discharge relationships derived using the traditional divided channel method (*vdcm*). This method is widely accepted to over-predict discharges as it does not take into account momentum loss through the turbulent interaction between main channel and floodplain (*Sellin* 1964; *Ackers* 1992; *Lambert and Myers* 1998). These model codes reflect this over-prediction, and although the *sbk-riv* code adheres to discharges derived using *vdcm* most closely, the differences with discharge-prediction methods that do take the turbulent interaction into account such as the *tlmh* method (*Lambert and Sellin* 1996a) are such that none of the codes can be said to be superior. In practical application of the codes, this additional momentum loss needs to be taken into account through main channel and floodplain roughness would need to be calibrated. This confirms the suggestion that these roughness factors then represent more than just bed friction (*Ackers* 1992; *Ervine et al.* 2000).

The *sbk1d2d* code shows the best resemblance to discharges predicted using the *tmlh* method, but this resemblance is sensitive to the use of a roughness factor at the horizontal interface between main channel and floodplain. This additional roughness factor can be taken independently from the main channel and floodplain roughness and considered an independent calibration parameter as a form of turbulent closure. From the depth averaged velocity profiles across the channel it is clear that although this additional parameter contributes to a good simulation of bulk flow conditions, the velocity profile in the main channel differs significantly from the true velocity profile, represented most closely by the *tmlh* method. If the roughness factor at the interface is chosen too low a high velocity filament seems to establish in the cells overlying the floodplain, this clearly being somewhat non-physical. On the other hand, using this additional parameter as a sort of explicit treatment of the momentum loss not accounted for could be considered more elegant than simply incorporating the losses in bed roughness factors. For simulations with rough floodplains, which would be the most likely in real river applications, taking the roughness factor at the interface the same as the main channel roughness seems acceptable without adding to complexity in model parameterisation and associated difficulties in identification using the limited data typically available. The effect of the factor is most apparent for low relative depths when turbulent interaction is the greatest, and as relative depths increase and the channel starts to act more as a single channel (*Ackers* 1992) the factor at the interface should tend to the main channel roughness. Using the main channel roughness at the interface seems a reasonable choice in practical applications.

In meandering channels the *fls* code, which describes both main channel and floodplain using a regular raster, is seen to be unsuitable. The limited resolution of the main channel results in severe underestimation of main channel flow. To account for this problem *Beffa and Connell* (2001) apply a correction factor to roughness values for diagonal flow vectors in raster cells to reduce these errors, but still find significant errors when a limited number of cells are defined across the channel width. This can be resolved by using a very fine grid, but this would eventually make application at the reach scale computationally impossible. In the other three codes applied, the main channel is resolved using a 1D approach, thus avoiding the problem of grid resolution. The full 1D approaches again conform well to the *vdcm*, but the differences between this and experimental results may be in the order of 30%. For meandering channels, momentum losses are increased further due to the complex flow characteristics such as crossing flows (*Lambert and Sellin* 1996b; *Ervine et al.* 2000), and neither the 1D codes nor the simple *lfp* code include this interaction, thus resulting in significant over-prediction of discharge. Again application to a real river would require calibration of roughness parameters to account for this additional momentum loss.

As in the straight channel the *sbk1d2d* code takes some account of additional momentum loss through the non-zero shear interface between main channel and floodplain. Using the main channel roughness factor at this interface compares better than any of the other codes to the empirical method proposed by *Greenhill and Sellin* (1993) who also apply a non-zero horizontal shear interface. Results show the method to reasonably represent experimental results, although for the

horizontal floodplain discharges are still over-estimated. Using a roughness factor at the interface to implicitly deal with turbulent momentum exchange does, however, make application more conceptual and less physically based as the code itself would suggest.

Differences between codes again increase as flow is concentrated to the main channel either due to high floodplain roughness and/or lateral floodplain inclination. If these codes are calibrated to real data it is clear that the roughness values found in a model calibrated using one code cannot be transferred to another code as the roughness values contain not only the lumped effect of turbulent momentum not considered in the model, but also differences in methods used to describe flow in the main channel. This again could be considered as moving away from the physical basis the code suggests to a more conceptual modelling.

From the results in both the straight and meandering channels it is clear that not taking turbulent momentum interaction into account leads to overestimation of discharges. It would then seem logical to conclude that all the codes of the type described here are not suitable for reach scale flood extent prediction and more complex 2D codes that do take this interaction into account should be used. *Wilson et al.* (2002) compare such a code and show that stage discharge relationships are indeed adequately described for both straight and meandering channels. They do note, however, that results are sensitive to the turbulence closure model used and how this is parameterised, showing that even with such a complex code conceptualisation of the momentum losses is required. They also find that depth averaged velocities across the channels compare poorly to the experimental values. These complex codes thus have the same problem as the codes investigated here, and roughness values will still need calibration to properly capture actual flow processes. Application of these complex codes to the reach scale also have the problem that the generation of the mesh used in the model is in itself a complex task, and significant computational resources in running are required. As a consequence simpler approaches where integration with GIS is much more straightforward as is the case in the codes used here are certainly viable.

The geometry of real rivers and floodplains is obviously much more complex than in the reaches used here (*Knight and Shiono* 1996; *Lambert and Sellin* 1996b; *Ervine et al.* 2000; *Babaeyan-Koopaei et al.* 2002), typically with floodplains of varying roughness and inclination as well as meandering main channels. Roughness values in models will need to be calibrated to account for all momentum losses not explicitly described. Although it is clear the *fls* model is less suited to this problem, for the other codes used here none can be seen to be superior, with roughness values for each code needing to be established through calibration using the limited available data. This underwrites the conclusions of *Horritt and Bates* (2002) who compare 1D and 2D codes in predicting flood extent against verification data and find that all codes used have similar problems in roughness identifiability and therefore that neither is of superior reliability.

5.7 Conclusions

Four model codes available for modelling inundation extent at the river reach scale have been applied to a hypothetical compound channel. The codes used vary between a 1D hydrodynamic code (SOBEK, a 2D raster based hydrodynamic code DELFT-FLS and two codes that use a hybrid approach where the main channel is modelled as a 1D structure and the floodplain using a coupled 2D approach (SOBEK1D2D and LISFLOOD-FP respectively). The first of these two uses the full shallow water equations in both domains, with a shared water level link between the two domains. A horizontal division at the bankfull in the main channel splits the domains, with all flow below the division being 1D main channel flow and flow above the division being 2D floodplain flow. The second of the hybrid codes uses a much more simple approach. Main channel flow is resolved using a simple 1D diffusive wave formulation, while floodplain flow is resolved using the quasi-2D cell inundation approach first described by *Cunge* (1975). These codes are applied to different configurations of hypothetical channel, with combinations of a straight or meandering main channel, horizontal or inclined floodplains, and smooth or rough floodplains.

Stage-discharge curves derived using these codes were compared to those derived using theoretical and empirical discharge prediction methods. The most traditional of these is the vertical divided channel method (*vdcm*), which although widely used is acknowledged to over-predict discharges in channels to the order of $5 - 10\%$ in straight compound channels and $\approx 30\%$ for meandering channels (*Lambert and Myers* 1998; *Greenhill and Sellin* 1993). This is due to the method ignoring turbulent momentum exchange and crossing flows. Other discharge prediction methods take some account of these and show better comparison to experimental results. Comparison of the codes used here show that these follow the *vdcm* method closely for a straight channel configuration, with variations stemming primarily from differences in how main channel flow is resolved. As a consequence variation between the codes increases as flow is concentrated in the main channel either due to either rough or laterally inclined floodplains. The exception to this is the SOBEK1D2D code where through application of a roughness factor at the horizontal floodplain—main channel interface a conceptual way of dealing with the additional momentum losses due to secondary currents is introduced. The same conclusions can be extended to the meandering channel configuration, except that the raster based FLS code is found unsuitable for modelling compound channel flow as the raster resolution required to properly simulate main channel flow make application at a reach scale computationally impossible.

In all cases it is clear that not accounting for turbulent momentum interaction results in over-prediction of discharge capacity. Codes of the type selected here are, however, widely applied in inundation extent modelling in river reaches (for an overview see *Bates and de Roo* (2000)). To calibrate these to the often limited data, roughness values are selected such that these lump the effects of not only momentum loss due to bed friction, but also due to the complex secondary flows not included in the model. Even in codes where either a conceptual or more physical concept is used to describe the momentum loss (respectively the SOBEK1D2D code and codes

using turbulent closure models, e.g TELEMAC as applied by *Wilson et al.* (2002)) calibration of roughness factors is still required to implicitly include all momentum loss not explicitly addressed. As a result roughness factors in calibrated reach scale inundation models should be considered as lumped (conceptual) momentum dissipation factors, and not having the pure physical meaning the model equations would suggest. *Lambert and Sellin* (1996b) note that application of empirical discharge prediction methods for estimating discharges in meandering channels should be done only with caution and a good understanding of the complex flow characteristics in such a channel. This is equally valid in application of hydraulic models to inundation extent modelling.

Acknowledgements

Chris Whitlow (Eden Vale modelling services) is thanked for his support in applying the Conveyance Estimation System. Paul Bates and Neil Hunter (both from Bristol University) are thanked for their invaluable support in applying the LISFLOOD-FP code.

6

Predictive reliability in flood extent modelling

Abstract

In this chapter a comparison is made of 1D, 2D and integrated 1D-2D hydraulic models in predicting stage and flood extent for a 17km reach of the River Saar in Germany. The models are shown to perform comparably when calibrated against limited available data for three low to medium size flood events. When validated against a larger event than those used in calibration, the 2D model is shown to be unreliable. Extrapolation with the 1D and particularly the integrated 1D-2D model is more reliable, though results are still considerably uncertain. The difference stems from how the models deal with main channel and floodplain flow and turbulent momentum interchange between the two domains. The importance of using spatial calibration data for testing models giving spatial predictions is shown. Even simple binary (eye-witness) observations on the presence or absence of flooding in establishing a reliable model structure to predict flood extent can be of great value.

based on M.Werner, "Predictive reliability in flood extent modelling approaches", Submitted for publication in *Hydrology and Earth System Sciences*

6.1 Introduction

A key element of flood risk analysis is quantification of flood hazard through estimation of the extent of flooding for design events of selected return periods. To derive flood extent maps for larger return periods, often of a larger magnitude than recorded events, a variety of approaches can be applied. These models are mostly based on the sound physical basis of the shallow water equations, but to adequately represent the flow characteristics in the reach under consideration, some form of calibration is required. In calibrating these models, however, two challenges are faced. First, there is typically very little spatial data available on the extent of flooding, with the only data available often being from reach scale gauges at intermediate distances of $10 - 30km$ (*Bates and de Roo* 2000). At best, there may be one or two flood extent maps from recent events (*Aronica et al.* 2002; *Horritt and Bates* 2002; *Romanowicz and Beven* 2003) or in rare occasions distributed observations of flood levels in the floodplain (*Aronica et al.* 1998a). Additional eye-witness accounts of flood extent or expert knowledge may equally be used (as shown in *Franks et al.* (1998) for a distributed hydrological model). The second challenge is that design events are mostly larger than the observed events available for calibration, thus requiring extrapolation. Extrapolation should always be treated carefully. This is most apparent in data driven modelling, but holds also in application of conceptual and physical models. An example of the danger in extrapolation of a conceptual model is given in *Uhlenbrook et al.* (1999).

A simple approach in establishing extent of flooding involves estimating a planar water level surface using observed water levels at gauges. The digital elevation model of the reach is then subtracted from this planar surface and areas with a depth greater than zero retained (*Priestnall et al.* 2000). The extreme simplicity of the approach is, however, reflected in its bad performance (*Horritt and Bates* 2001a), and application to larger than observed events requires reliable extrapolation of rating curves at the gauges used, which in itself poses a problem. More commonly some form of hydrodynamic modelling is used, including 1D hydrodynamic modelling and subsequent spatial interpolation (*Marche et al.* 1990; *Péron et al.* 1996; *Horritt and Bates* 2001a; *Werner* 2001; *Tate et al.* 2002), cell inundation based 2D modelling (*Cunge* 1975; *Bladé et al.* 1994; *Bates and de Roo* 2000), 2D hydrodynamic modelling (*Paquier and Farissier* 1996; *Bates et al.* 1998; *Beffa and Connell* 2001) and more recently integrated 1D-2D codes (*Verwey* 2001; *Frank et al.* 2001).

In this chapter three of these modelling concepts are applied in predicting extent of inundation on a $17km$ reach of the River Saar in Germany. Floodplain and main channel roughness coefficients in the models are conditioned using several medium to large flood events within the generalised likelihood uncertainty estimation (GLUE, see *Beven and Binley* (1992)) framework, and resulting posterior parameter distributions are subsequently applied in predictive mode to estimate extent of inundation during the large December 1993 event.

6.2 Study site and available data

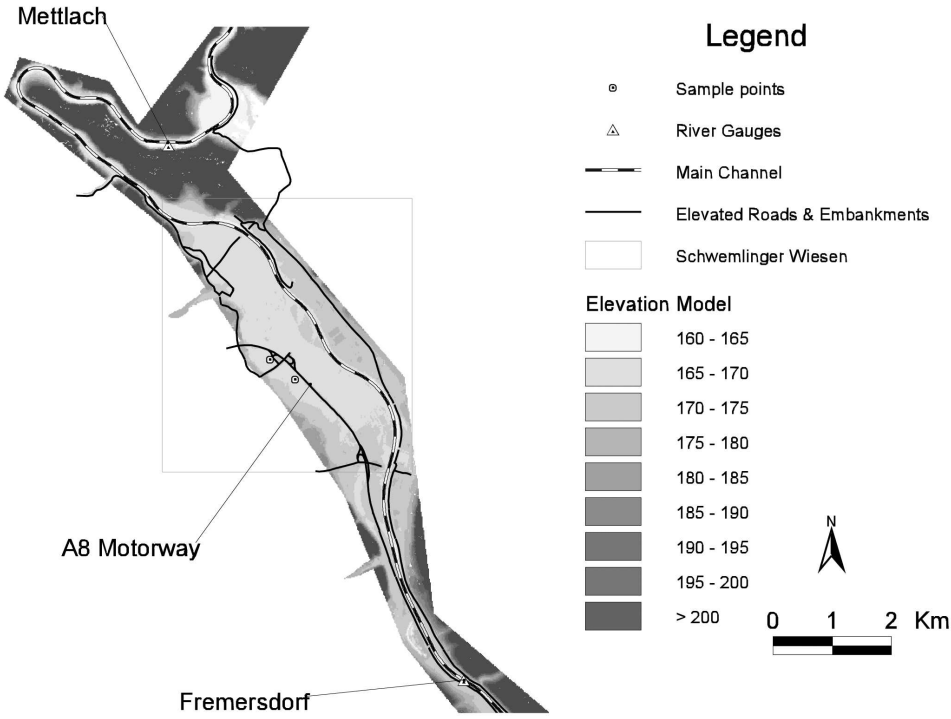


Figure 6.1: River Saar between the Fremersdorf and Mettlach gauging station. Flow is from South to North.

The Schwemlinger Wiesen floodplain is a relatively wide floodplain on the Saar River, a tributary of the Mosel River, which is a tributary of the Rhine. The floodplain is located just upstream of the weir at Mettlach and downstream of the gauging station at Fremersdorf, an important flow gauge in the German part of the Saar (figure 6.1). The reach under consideration contains three characteristic sections. In the section directly downstream of the Fremersdorf gauging station flow is constrained in the main channel with the floodplain constricted by a motorway on one side and a main road on the other. The middle section is the Schwemlinger Wiesen floodplain with a width of up to about $1km$. Extensive inundation occurs on the floodplain during high flood events, with the extent of flooding again mostly constrained by the motorway and other embankments. The last section is a narrow non-alluvial gorge, with in it an almost 180^o river bend known as the Saarschleife. Here, the Saar cuts through the Rhenish slate mountains, and the section is characterised by a narrow main channel with very steep valley sides. The bed slope in this section is also relatively steep, and the weir at Mettlach is used to maintain navigability. Head difference over the weir can be up to $14m$, and as

a consequence downstream levels do not affect flow over the weir even at very high discharges, making the weir site ideal as a downstream boundary to a model. The crest of the weir is set to maintain the upstream level at the weir at $167.5m$ for low to moderate flows. In order to reduce upstream flood stages this is lowered to 165.5 for high flows. To increase navigability further, the main channel in the entire reach has been enlarged (*WSV* 1987), and as a consequence significant out of bank flow occurs only for the largest events. For lower flows, backwater effects from the Mettlach weir prevail. Surveyed cross sections of the entire reach are available at $100m$ intervals, as well as a laser altimetry derived floodplain elevation model with a resolution of on average one observation per $2.5m \times 2.5m$.

Table 6.1: Peak discharge and level at Fremersdorf.

		Event 1	Event 2	Event 3	Event 4
Start Date		08-01-1993	13-12-1993	20-01-1995	15-03-1995
Q_{peak}	m^3/s	589	1271	941	640
H_{peak}	$m + NN$	170.53	172.91	171.48	170.28

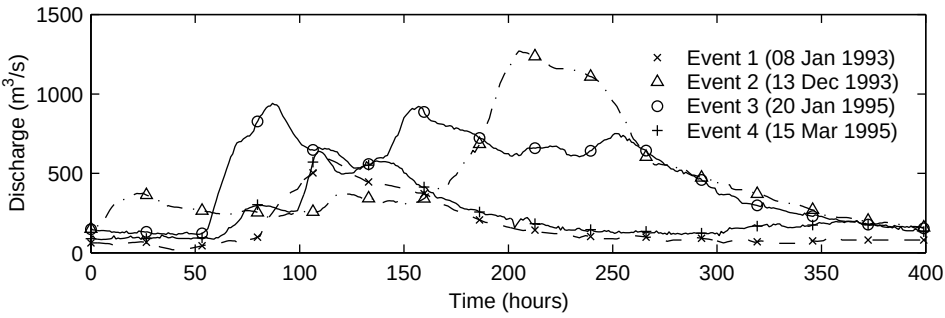


Figure 6.2: Flood hydrographs at the Fremersdorf gauging station.

Four flood events recorded at the gauging station at Fremersdorf are shown in Figure 6.2 and Table 6.1. The first and fourth of these events are of the order of the average annual flood. The January 1995 event, while being the second largest in the lower Rhine basin on record, has an estimated return period of only about 10 years at Fremersdorf. The December 1993 event is the largest in recent history in the Saar basin with an estimated return period at Fremersdorf of just under 100 years (*Krahe et al.* 2000).

6.3 Approach

Three of the codes described in chapter 3 were selected for modelling the extent of inundation in Schwemlinger Wiesen floodplain:

- The 1D hydrodynamic model code - SOBEK-RIVER, abbreviated to *sbk*.

- The 2D raster hydrodynamic code - DELFT-FLS, abbreviated to *fls*.
- The integrated 1D-2D hydrodynamic code - SOBEK-OVERLAND FLOW, abbreviated to *s2d*.

Maximum flood extent is derived for the 1D code by sampling maximum stages at calculation points in the main channel, and projecting these on the 2D plane as described in Appendix B.

6.3.1 Model parameterisation and calibration

To establish predictive uncertainties of each of the model concepts the generalised likelihood uncertainty estimation approach (GLUE) was adopted (*Beven and Binley* 1992). This is described fully in chapter 4. It rejects the calibration paradigm of one single optimal parameter set, considering rather an ensemble of possible parameter sets. This ensemble is constructed through sampling of constituent parameter prior distributions, and for each ensemble member the model is run and results compared against observations. Based on this comparison the acceptability of each parameter set is established in terms of a likelihood measure, expressing the comparative likelihood of that parameter set and model structure giving a good description of system behaviour. The procedure is set in a Bayesian framework (*Romanowicz and Beven* 2003), where likelihoods derived using a given calibration data set can be updated with those of subsequent data sets (*Freer et al.* 1996):

$$L(\theta_i \mid Y) = \frac{L_1(Y \mid \theta_i) L_0(\theta_i)}{\sum_{j=1}^{N} L_1(Y \mid \theta_j) L_0(\theta_j)} \tag{6.1}$$

$L_0(\theta_i)$ is the prior likelihood measure for parameter set θ_i, $L_1(Y \mid \theta_i)$ is the likelihood measure derived by comparing model output using parameter set θ_i to observations Y using a selected objective function, $L_1(\theta_i \mid Y)$ is the posterior likelihood of parameter set θ_i given observation Y, and N is the number of parameter sets sampled. Optionally a behavioural threshold can be applied to divide runs with acceptable performance from those with unacceptable performance (*Beven and Binley* 1992). Parameter sets that perform below the threshold are given a likelihood value of zero, and remaining likelihood values re-scaled.

6.4 Application

The three codes selected were applied to the reach between Fremersdorf and Mettlach. All three make use of the digital elevation model, based on the laser altimetry data available. The resolution of this data is so high that particularly in the *fls* and *s2d* models this would result in very impractical run times due to the size of the computational grid, without necessarily adding to model accuracy. The elevation data was therefore first aggregated to reduce the computational burden. Aggregating DEM's can have significant impact on flood extent prediction depending on how line elements are considered. Figure 6.3 compares elevations along the top of a dyke for a reach of the Meuse River in the Netherlands (see also chapter 8). The

original elevation model was available at a resolution of $2m$ and was aggregated to $50m$ through either taking the mean value of the smaller cells falling within each large cell, the maximum value, or through enforcing values in the larger grid using surveyed heights. Levels in grid cells running along the top of the dyke using the last two methods compare well against the surveyed levels, while those obtained through simple averaging result in serious gaps in the dyke. This would have significant influence on the predicted flood extent. Levels in the $2m$ grid show some difference compared to the surveyed points due to accuracy of the grid on the one hand, and deviation of the from the dyke crest line along which elevations were sampled on the other.

Lacking surveyed elevations for the top of the embankment in the reach considered here, aggregation was done in two steps. In the first step, an elevation model with a resolution of $10m \times 10m$ was established through averaging of laser altimetry points within each grid cell and taking the maximum for grid cells crossed by line elements (e.g. the motorway embankment). In the second step, an elevation model with a resolution of $20m \times 20m$ was established. Two models with a resolution of $20m \times 20m$ were derived. In the first of these, no account was taken of important line elements, and the averaging rule was used for all cells. In the second, line elements were again explicitly accounted for using the maximising rule for cells crossed.

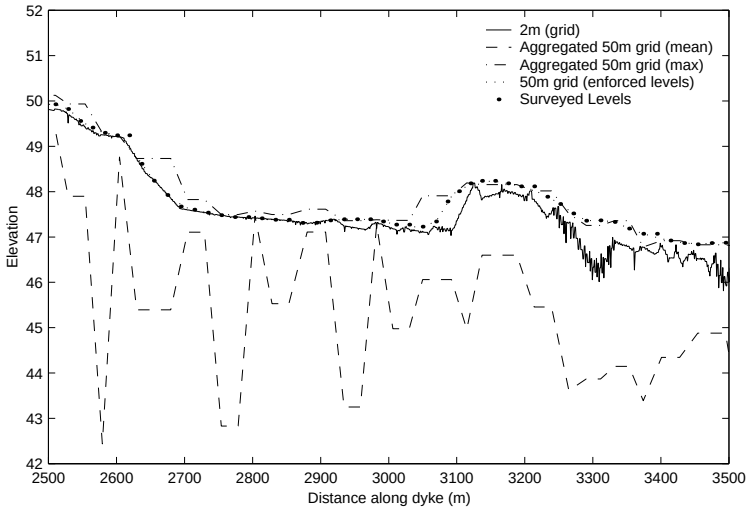


Figure 6.3: Comparisons of DEM levels along the line of a dyke sampled in grids aggregated from the original $2m$ resolution.

For developing the 1D model, the surveyed cross sections were found not to extend fully across the floodplain. These were completed using sampled elevations from the digital elevation model, and combined with the observed cross sections in the main channel (*Werner et al.* 2000). The observed discharge at the Fremersdorf gauging station was used at the upstream boundary of the model, while upstream

water levels observed at the Mettlach weir are defined by the operational strategy used to control the weir. Extent of inundation is established by projecting the 1D results on the available digital elevation model.

Models using the *fls* code were established using the $20m$ resolution elevation data, with cross section data in the main channel interpolated to complement floodplain elevation data. Of the three sections in the reach considered, flow in the first and third reach is predominantly in-bank. To minimise the effect of overestimation of stage in these sections due to the orientation of the main channel with respect to the relatively coarse grid (*Beffa and Connell* 2001), the extent of the 2D model was reduced considerably to cover only the second section. This section is the Schwemlinger Wiesen floodplain itself, where flood extent is of interest. The reduction of the 2D model extent served also to reduce the computational effort. To relate this reduced model to the boundaries at Fremersdorf and Mettlach, the head loss in these sections was determined using a simple steady state approximation. This uses the average main channel geometry in the reach, the downstream level at Mettlach and the (variable) main channel roughness as inputs (*French* 1986, p.229).

In the *s2d* model the 1D domain was applied to the full reach as in the *sbk* model and the 2D domain applied only for the second section of the Schwemlinger Wiesen as in the *fls* model. Cross sections in the 1D first and third sections were defined to cover both floodplain and main channel. Those in the second section were defined to cover only the main channel as floodplain flow is accounted for in the 2D domain. The elevation model along the main channel, being the interface between the 1D and 2D domains, was set to the bankfull level. Figure 6.4 schematically shows the setup of 1D and 2D domains for each of the three codes.

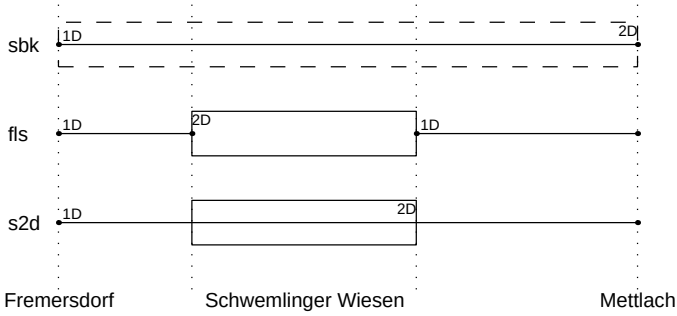


Figure 6.4: Schematic overview of three model structures showing 1D and 2D domains. The dotted box for the *sbk* model indicates that the 2D domain is not included in the model but is obtained through projection of the 1D results. The solid line indicates the extent where the 1D solution was used, while the solid box indicates where the 2D solution was used.

In each of the three modelling codes Manning's-n roughness values were defined for the main channel and floodplain, with the main channel roughness value also being applied to the non-zero shear interface in the *s2d* model. Although the morphology of the last section is different than that of the first two, where the river

Table 6.2: Prior parameter ranges for main channel and floodplain roughness.

Parameter	Range
Main Channel Roughness (n_{mc})	0.02 - 0.06
Floodplain Roughness (n_{fp})	0.02 - 0.20

runs in an alluvial bed, further disaggregation of roughness was not considered. This would limit the identifiability of parameters further, given that a low roughness in the first two sections could then compensate a high roughness in the third and vice versa. The prior ranges from which parameter sets were sampled are indicated in table 6.2, with ranges selected on the basis of tables in literature (*Chow* 1959) and similar studies (*Horritt and Bates* 2001a). From these parameter prior distributions, Monte Carlo sampling was applied to construct parameter sets. The sample size for *sbk* model with its relatively short run-times was set at 1000, while for the *fls* and *s2d* models only 100 parameter sets were used due to computational constraints in using these models. These were, however, sampled using a Latin-Hypercube sampling strategy (*McKay et al.* 1979; *Yu et al.* 2001) to ensure a good spread of samples in the parameter space. Comparison of runs using the *sbk* model using Latin Hypercube sampling from the uniform prior distribution with the full random sample of 1000 showed that parameters of posterior distributions stabilised between 50 and 100 runs, comparing well to results from *Yu et al.* (2001).

For each parameter set sampled, the model was run and resulting levels at Fremersdorf compared. To establish likelihood values within the context of the GLUE analysis using Equation 6.1, a suitable objective function was required. The objective function for comparing level results at Fremersdorf is selected on the basis that the maximum extent of flooding is related to the maximum level at Fremersdorf.

$$L_i = exp(-\frac{|\hat{h}_i^{max} - h^{max}|}{T}) \tag{6.2}$$

where L_i is the likelihood measure for parameter set i, $\hat{h}_i^{max}$ is the calculated maximum level at Fremersdorf using parameter set i, and h^{max} the observed maximum as given in Table 6.1. T is a scaling constant that acts similarly to the behavioural threshold used traditionally in GLUE analysis. The function can vary between zero for very poor models and one for models of zero error. Due to the exponential form of the selected function, T plays an important role in relative likelihoods between model runs. Its role is comparable to the behavioural threshold used in other applications of the GLUE procedure, reflecting the relative belief in the model (see chapter 4). Selecting the value to be close to zero has the effect of a very peaked response surface as only models with zero or near zero error will obtain relatively large likelihood values. Generally though larger values of T should be used, and for the model runs here this scaling factor is selected at $0.20m$, in the order of accuracy of the laser altimetry derived elevation model (*Marks and Bates* 2000). Although somewhat arbitrary, the value is considered to serve the purpose of demonstration.

The advantage of the exponential form of the likelihood function is that up-

dating of likelihoods from different data sets implies additive combination (*Lamb et al.* 1998). Parameter sets giving very poor performance for one data set but giving reasonable performance in another are not rejected outright as when using multiplication (Equation 6.3).

$$L(\Theta_i|Y_{1,\ldots,n}) = \frac{1}{C} exp\left[-\left(\frac{|\hat{h}^{max,1} - h^{max}|}{T} + ... + \frac{|\hat{h}^{max,n} - h^{max}|}{T}\right)\right] \quad (6.3)$$

where C is a constant to normalise likelihood values, and $L(\Theta_i|Y_{1,\ldots,n})$ is the likelihood value of parameter set Θ_i constrained on datasets $Y_{1,\ldots,n}$.

Although no spatial data for the extent of flooding is available, the knowledge that the motorway was not overtopped in any of these events is used to constrain likelihood values further. A binary selection of parameter sets is made on the basis of an indication of flooding behind the motorway (sample points in Figure 6.1). Parameter sets indicating flooding behind the motorway were assigned a zero likelihood and discarded, while those not indicating flooding were retained.Equation 6.2 is modified slightly by multiplying with the Dirac delta operator, P. The value of P is 0 for runs indicating flooding at either sample location behind the motorway and 1 for all other runs.

$$L = P \times exp(-\frac{|\hat{h}^{max} - h^{max}|}{T}) \quad (6.4)$$

After application of P likelihood values are re-normalised. Likelihoods for parameter sets can be used in obtaining prediction quantiles for the maximum water levels using the equation:

$$P(\hat{h}^{max} < h) = \sum_{i}^{N} L\left[(\Theta_i)|(\hat{h}^{max} < h)\right] \quad (6.5)$$

where N is the number of parameter sets. In predictive mode, quantiles can be determined for an event by using likelihood values constrained using data from other events only, as opposed to after updating using the likelihood values with the data of the event itself. To compare predictive uncertainties of the different modelling concepts, the runs described in Table 6.3 are carried out with the sampled parameter sets and models. The table indicates the event used in each run, the model used, whether the uniform priors are used or parameter likelihoods constrained using a previous run or runs, and, whether the likelihood values are updated using the information in the event used. Each run for the *sbk* model applied all 1000 sampled parameter sets while each *s2d* and *fls* run used the 100 sampled parameter sets. The table indicates where prior likelihood values from a previous run were used or where the uniform prior was used. The last three runs for the extreme December 1993 event were used to compare the value in updating parameter likelihoods with different sets of calibration data. In run e only the information in that event were used in determining parameter likelihoods, in run$f$ likelihoods determined using all events were combined. In predictive mode in run g, likelihood values were determined using all but the December 1993 event.

Table 6.3: Overview of runs and priors used in updating likelihoods.

Run Name	Event	Prior likelihood	Models	Comment
run a	Event 1	[-]	*sbk*	posterior likelihoods updated
run b	Event 4	run a	*sbk*	posterior likelihoods updated
run c	Event 3	run b	*sbk*	posterior likelihoods updated
run d	Event 3	[-]	*sbk,fls,s2d*	posterior likelihoods updated
run e	Event 2	[-]	*sbk,fls,s2d*	posterior likelihoods updated
run f	Event 2	run d	*sbk,fls,s2d*	posterior likelihoods updated
run g	Event 2	run d	*sbk,fls,s2d*	Predictive mode

6.5 Results and discussion

6.5.1 Impact of elevation model quality

The three elevation models derived using the laser altimetry data were run with the *sbk* model to evaluate the quality of the aggregated elevation data. Figure 6.5(a) shows the selected quantiles for predicted maximum level at Fremersdorf for *run e* using the $10m \times 10m$ elevation model (*dem10*), the $20m \times 20m$ elevation model where no account of line elements is taken (*dem20*) and the $20m \times 20m$ elevation model where line elements are explicitly included (*dem20**). Conditioning on the level at Fremersdorf only using equation 6.2 for determining likelihoods shows little difference between the elevation models. Application of equation 6.4 significantly changes this as most model runs giving a reasonable estimate of the maximum level at Fremersdorf are now rejected due to flooding behind the motorway when using the *dem20* elevation model. This confirms the model structure using this elevation model is unsuitable for estimating flood extent in this reach. Figure 6.5(b) shows the substantial difference in the extent of flooding for pixels inundated with a likelihood of 95% between the two elevation models, with the area behind the motorway being completely inundated when applying the flawed elevation model. While it is obvious a line element such as a motorway should be explicitly considered in the elevation data, smaller, or particularly thinner features such as flood walls may not be well represented in the elevation data, yet have a significant impact on inundation extent. For reliable evaluation of model structure for spatial prediction such as flood extent it is thus paramount that even simple binary observations are included. For all further runs, the coarser $20m \times 20m$ elevation model (*dem20**) with line elements included was used.

6.5.2 Effect of updating likelihood values using multiple data sets

The value of updating posterior likelihood values using multiple flood events was explored using runs *a*-*d* (Table 6.3) with the 1D *sbk* model. Figure 6.6 shows the cumulative likelihood distributions for main channel and floodplain roughness for successive updates from each of the events 1,4 and 3 (runs *a* to *c*), as well as if only Event 3 is used in updating likelihoods (run *d*). The difference between using all

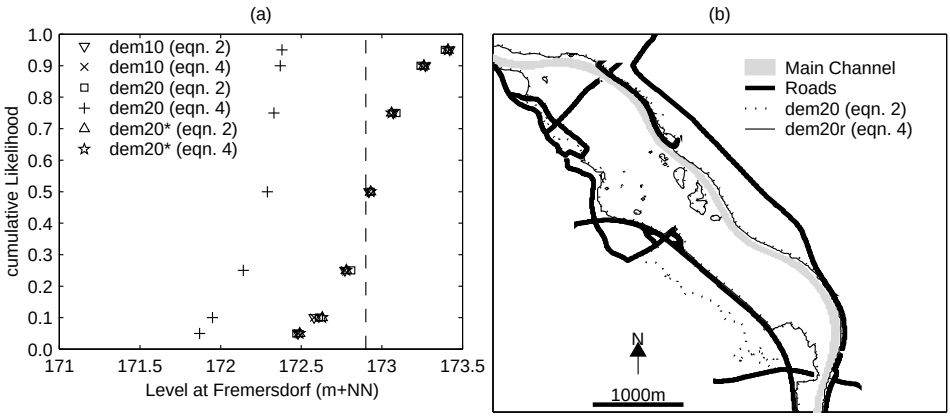


Figure 6.5: Cumulative likelihood for peak level predictions at Fremersdorf, (a) results for *sbk* model using DEM's of differing quality and resolution, (b) 95% flooded area percentile.

three events in updating likelihood values and using only the larger event 3 is very small. The reason for this is that identifying main channel roughness for Events 1 and 4 is relatively difficult as these are small flood events with little out of bank flow. Flow conditions in the reach are then dominated by backwater effects from the weir at Mettlach. For higher flow conditions, main channel roughness plays a more important role and is subsequently more identifiable. Floodplain roughness is insensitive in all events, as found in many similar reaches, where the floodplain plays an important role in storage and less so in conveyance (*Horritt and Bates* 2002; *Aronica et al.* 2002). Given the limited information content in constraining main channel roughness values, Events 1 and 4 were not applied in the *fls* and *s2d*, with predictive uncertainties of the different modelling concepts established using Events 2 and 3 only.

6.5.3 Comparison of predictive reliability of modelling concepts

Figure 6.7(a) and (b) depict selected quantiles for the three different modelling concepts as conditioned on the Events 3 and 2 respectively, using uniform prior likelihood distributions for parameter sets. The 50% quantile matches the observed value very well in both cases, which is not surprising as Equation 6.4 used to establish likelihood values has a tendency to penalise runs where the maximum predicted level deviates from that observed. Other quantiles show comparable performance, with only the *s2d* model having a slightly wider uncertainty envelope for *run d*. *Run e* renders similar results, suggesting the three modelling concepts are equally reliable. Combining the likelihood values for the two events in *run f*, however, shows that both the *sbk* and *fls* models are tending to under-predict the maximum level at Fremersdorf, while the *s2d* model shows good performance with the uncertainty envelope constrained when compared to that of *run e*. The under-prediction is strengthened in predictive mode with parameter likelihood values conditioned

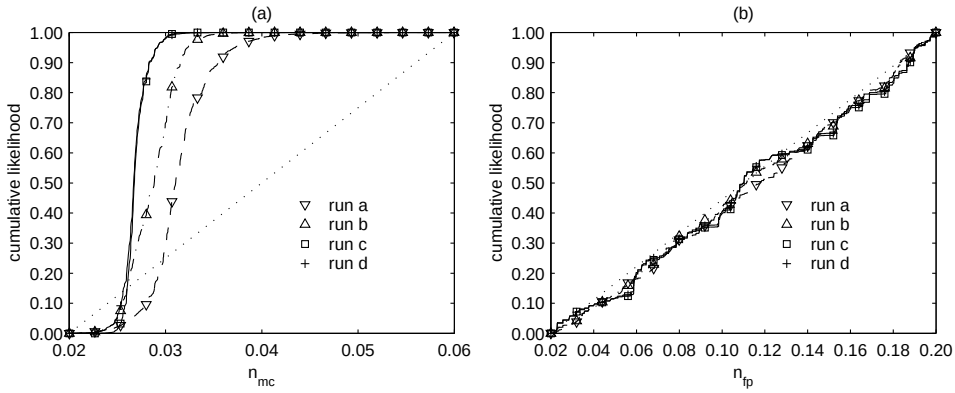


Figure 6.6: Cumulative likelihood distributions for (a) main channel and (b) floodplain roughness using the *sbk* model conditioned on different events.

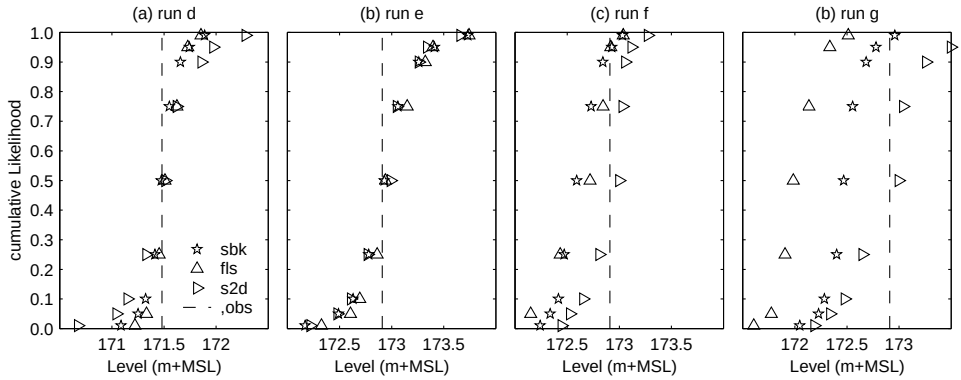


Figure 6.7: Quantiles for peak level predictions using different model concepts.

on the Event 3 only. Particularly under-prediction by the *fls* model is significant, confirming that this model is unsuitable for resolving flow where flow is dominated in the main channel described by only a few computational cells (*Beffa and Connell* 2001).

The well constrained nature of the main channel roughness in the 1D *sbk* model (figure 6.8(a)) would support the selection of the roughness value giving the best performance as an optimal calibration. However, it can be clearly seen that on independently calibrating using Event 2 (*run e*) rather than Event 3 (*run d*), this optimum shifts to a slightly higher roughness. This supports results from *Gupta et al.* (1998) and *Romanowicz and Beven* (2003), in that the optimum is non-stationary when evaluated on alternative measures or datasets. Despite the relatively low number of runs for the *s2d* model, likely main channel roughness values remain relatively constant between the three runs (figure 6.8(b)). Given that the models are most sensitive to main channel roughness values this explains the stability of

the predicted level using the *s2d* model, even in predictive mode. This stability is attributed to the structure of the model. Although not explicitly considered as a turbulence closure model, the non-zero shear at the interface between the 1D and 2D domains, allows for momentum exchange due to interaction between flow in the main channel and floodplain, thus giving a better description of the non-linear stage-discharge relationship. The shift in optimal roughness value for the pure 1D approach (figure 6.8(a)) is intuitively correct as the roughness values in a 1D model are the lumped effect of bed roughness, momentum interchange between main channel and floodplain and crossing flows (*Knight and Shiono* 1996). Out of bank flow is only limited in Event 3 and more significant in Event 2, with momentum losses through the main channel-floodplain interaction thus being higher.

To account for this effect a stage dependent main channel roughness parameterisation could be introduced (such as the discharge adjustment factor proposed in *Ackers* (1992)). Although this would potentially improve the reliability of the 1D model it would result in additional parameters, and further exacerbate the identification problem. Moreover, for the reach in question, main channel roughness is less sensitive at low flows (figure 6.6) due to the backwater effect from the Mettlach weir, leaving very little data to reliably estimate parameters of a stage dependent main channel roughness value. For higher events the impact of momentum interchange theoretically becomes less as the floodplain and main channel start to act as a single channel (*Ackers* 1992), and the optimum for the 1D model would be expected to again shift to lower roughness values.

Similar results for applicability of 1D modelling from *Ali and Goodwin* (2002) show that for the case they studied single channel behaviour was attained at a depth of in the order of twice the bankfull depth. This factor is, however, dependent on channel and floodplain geometry and relative roughness values making identification in a natural channel very difficult. Extrapolation in predictive mode for high magnitude design events of some empirical relationship derived on limited data then becomes very uncertain.

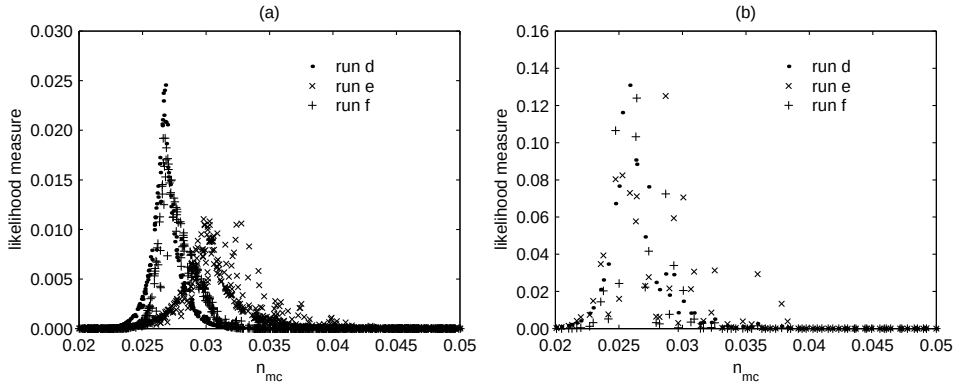


Figure 6.8: Dotty plots for main channel roughness for *run d*, *e*, and *f* using the (a) *sbk* model and (b) *s2d* model.

6.6 Conclusions

This chapter presents results of a comparison between the predictive reliability of three different approaches to reach scale flood extent estimation. In setting up these models, it has been shown that even for the most widely applied 1D hydrodynamic approach, the establishment of a suitable representation of floodplain topography is of prime importance. Particularly representation of line elements in the floodplain that can constrain the extent of flooding, even for larger events, is crucial. Despite this, models using low quality elevation data perform equally well as models using high quality elevation data when calibrated only against bulk flow data from river gauges. As the required model output is the spatially represented flood extent, use of spatial observations in establishing model suitability is paramount. Even simple (eye witness) observations, such as presence or lack of flooding behind embankments can prove invaluable in identifying flaws in the elevation model. Applying these in calibrating flood extent models rather than relying only on gauge data, could greatly improve reliability of flood extent modelling.

Three codes for modelling flood extent were selected here; a 1D hydrodynamic code with subsequent projection of water levels to the 2D domain through interpolation, a 2D raster hydrodynamic code, and an integrated 1D-2D code. Given the availability of a suitable digital elevation model, the three codes are shown to equally reliably predict flood extent for the events against which the codes are calibrated. Setting the calibration within the GLUE uncertainty framework, however, shows that extrapolation of models calibrated using medium and low events only can result in unreliable results. When validating the 2D model against maximum stages for the December 1993 event in the River Saar at Fremersdorf, these are severely underestimated if main channel and floodplain roughness parameters were constrained using the January 1995 event only. Even for the integrated 1D-2D approach the 90% confidence range for the maximum level at the Fremersdorf gauging station in the 1993 event increases from $58cm$ when predicted using roughness values constrained on both the 1995 and 1993 events to $115cm$ when these are constrained on the 1995 event alone. The December event is used here as a proxy to a design event, as these are often of a magnitude higher than events available for calibration, and this range would no doubt increase for design events of higher magnitude.

The differences between the codes comes primarily from how these resolve floodplain and main channel flow and the interaction between these two domains. Despite its easy integration with available GIS data formats, the 2D raster based hydrodynamic model is unsuitable for the type of river reach considered here as it is unable to properly capture the dominant main channel flow without resorting to a grid resolution that would result in an untractable computational problem. For the 1D code, the simplicity with which the main channel - floodplain interaction is described results in an over-estimation of conveyance for low over-bank flow. Roughness parameters applied are used in the model not only to describe momentum loss as a result of bed friction, but include a lumped representation of losses due to momentum interchange between main channel and floodplain through secondary currents and crossing flows. Although depth dependent roughness relationships can

be introduced such as described by *Ackers* (1992), identifying coefficients of this relationship can be difficult in a real river given the lack of data. Useful stage data in determining the relationship may be limited further because the flow regime in the river is influenced by backwater effects from structures in low and medium flood events. The ability of the integrated 1D-2D code to reliably extrapolate in this case is due to its conceptual consideration of the momentum exchange between floodplain and main channel. This allows for better representation of the actual stage-discharge curve, and more reliable extrapolation to larger events.

The results show that extrapolation to design events must be considered carefully. This applies not only in data driven or conceptual models (*Uhlenbrook et al.* 1999), but also to models where the basic equations are physically-based. Lack of calibration data, particularly for design events, combined with the conceptual approach with which complex flow dynamics such as turbulent momentum interchange are resolved, result in parameters being uncertain and difficult to identify. Given the three models compared here, the most reliable in extrapolating to design events greater than those available for calibration would be the integrated 1D-2D code, but even then predictive uncertainties remain substantial.

Acknowledgements

Peter Krahe of the Bundesanstalt für Gewässerkunde (BfG) in Koblenz, Germany is kindly thanked for permission to use the data for the River Saar. Part of this work was carried out within the context of the EUROTAS project funded by the EC (ENV4-CT97-0535).

7

Spatially distributed observations in constraining inundation modelling uncertainties

Abstract

Performance of two modelling approaches for predicting floodplain inundation is tested using observed flood extent and 26 distributed floodplain level observations for the 1997 flood event in the town of Usti nad Orlici in the Czech Republic. Although the 1D hydrodynamic model and the integrated 1D-2D model are shown to perform comparably against the flood extent data, the latter shows better performance against the distributed level observations. Comparable performance in predicting the extent of inundation is found to be primarily as a result of the urban reach, with flood extent constrained by road and railway embankments. Uncertainty in the elevation model used in both approaches is shown to have little effect on the reliability in predicting flood extent, with a greater impact on the ability in predicting the distributed level observations. These results show that reliability of flood inundation modelling in urban reaches, where flood risk assessment is of more interest than in more rural reaches, can be improved greatly if distributed observations of levels in the floodplain are used in constraining model uncertainties.

based on Werner, Blazkova and Petr "Spatially distributed observations in constraining inundation modelling uncertainties", Accepted for publication in *Hydrological Processes*

7.1 Introduction

Prediction of the spatial inundation extent of a flood event is of importance for detailed flood risk analysis and extensive work has been dedicated to method development. Current methods used to predict 2D maps of inundation extent at the river reach scale include the use of 1D codes where the output is projected in the 2D domain using spatial interpolation techniques (*Marche et al.* 1990; *Péron et al.* 1996; *Tate et al.* 2002) and 2D approaches ranging from simple quasi-2D cell inundation codes (*Cunge* 1975; *Romanowicz et al.* 1996), simple raster based inundation codes (*Bechteler et al.* 1994; *Bates and de Roo* 2000; *Horritt and Bates* 2001a; *Aronica et al.* 2002) and full two-dimensional finite element codes (*Paquier and Farissier* 1996; *Bates et al.* 1998; *Aronica et al.* 1998a; *McCowan and Collins* 1999). More recently hybrid 1D-2D full hydrodynamic codes have been described, where main river flow in the 1D domain is coupled to floodplain flow in the 2D domain (*Frank et al.* 2001; *Verwey* 2001). 1D codes have the drawback that these only represent flow between sections and not across the section, leading to various authors deeming these inferior to 2D codes (*Connell et al.* 2001; *McCowan and Collins* 1999). Although this is true from the point of view of representation of hydraulic detail on the floodplain, calibration and verification of inundation modelling suffers widely from a lack of spatial observation data and calibration and verification against this data is rare. Comparison of predictive performance of 1D and 2D codes against the limited verification data has proved that these can be equally reliable (*Horritt and Bates* 2002).

It is clear that calibration and verification of models is a prerequisite for reliable model application The difficulty faced with reach scale inundation modelling is that if data is available, it is typically only level and discharge data from river gauges (*Bates and de Roo* 2000). Despite this data being very useful in predicting bulk flow conditions at the reach scale, it may be of more limited use for assessing performance of the spatial inundation extent predicted by models. The value of conditioning distributed model predictions on distributed data has been widely demonstrated in distributed hydrological modelling (*Lamb et al.* 1998; *Franks et al.* 1998; *Feyen et al.* 2001; *Grayson et al.* 2002; *Blazkova et al.* 2002a,b) and in flood inundation modelling (*Aronica et al.* 1998a; *Horritt and Bates* 2001b; *Romanowicz and Beven* 2003). Spatial data used in flood inundation modelling to constrain roughness parameters in the models is mostly the observed flood extent, with observations derived from geo-referenced aerial photographs of the flood event (*Aronica et al.* 2002) or from remote sensing techniques such as satellite borne synthetic aperture radar (SAR) imagery (*Brackendridge et al.* 1998; *Horritt and Bates* 2002). Availability of these images is obviously dependent on overpass of satellite or aircraft with appropriate instrumentation, and, as in the case of SAR images, significant processing is required (*Horritt* 1999). Supplemental data of flood levels and/or depths in the floodplain are very rare, but can provide detailed spatial information on model predictions (*Aronica et al.* 1998a).

The ability of 2D modelling to provide 2D hydraulic detail may be misleading. This hydraulic detail is in part dependent on the accuracy of the topographical data. Ideally high resolution topographical data obtained from, for example, airborne

LiDAR surveys (*Marks and Bates* 2000) is used for floodplain topography, but this data is certainly not always available. *Marks and Bates* (2000) quote the accuracy of elevation maps based on LiDAR data of being at best $\pm 10cm$, while for elevation models based on digitised contour maps and spot elevations the vertical accuracy deteriorates to at best $\pm 50cm$. *Aronica et al.* (1998b) show the results of a 2D inundation model to be equally sensitive to topographical as to parametric uncertainty, although in *IRMA* (2002) topographic uncertainty is shown to be of much less significance. It appears that the difference in the two conclusions is due to the first being an application where floodplain flow is more dominant, while in the second main channel flow is dominant with the floodplain contributing primarily to storage.

In this chapter both the 1D and hybrid 1D-2D code discussed in chapter 3 are applied to simulation of the 1997 flood event in the Czech town of Usti nad Orlici. Sensitivity of floodplain and roughness parameters are investigated through Monte Carlo simulation within the generalised likelihood uncertainty estimation GLUE framework (*Beven and Binley* 1992), using both the observed flood extent map and distributed observations of flood levels in the floodplain. Parameter response surfaces of each of the model concepts are compared when constraining on flood map data only, the distributed level data or both. The topographical data available for the reach is of limited quality and the effect of topographic uncertainty on parameter response surfaces is explored.

7.2 Study site and available data

Usti nad Orlici is a small town in the central Czech Republic lying on the Ticha Orlice river at its confluence with the smaller Trebovka river. The Ticha Orlice joins the Divoka Orlice to form the main Orlice river, a tributary of the Elbe river. The river valley at the site of the town is relatively narrow, with the town straddling the valley floor at the confluence and a clear presence of infrastructure links such as railway lines and main roads (figure 7.1, flow is from East to West). The reach of the Ticha Orlice considered contains no less than twelve bridges, the most important of which are the road and railway bridges just upstream of the confluence with the Trebovka. There are also four weirs in the reach. The first three of these are now disused fixed crest weirs, with two of these derelict and being bypassed at low flows. The most downstream weir is still operationally used for maintaining head at an industrial intake.

The town suffered severe flooding during July 1997 with most of the town and downstream hamlet of Kerhartice being inundated. Gauging stations located at Libchavy on the Ticha Orlice and Hylvaty on the Trebovka, both just upstream of Usti nad Orlici recorded the hydrographs shown in figure 7.2. An aerial photograph of the estimated maximum flood extent was taken during the event and a total of 41 observations of the maximum flood level were made, primarily on the corners of houses along the main roads (figure 7.1).

Forty surveyed cross sections of the Ticha Orlice within the model extent shown in figure 7.1 were available, as well as the dimensions of bridges and weirs in the

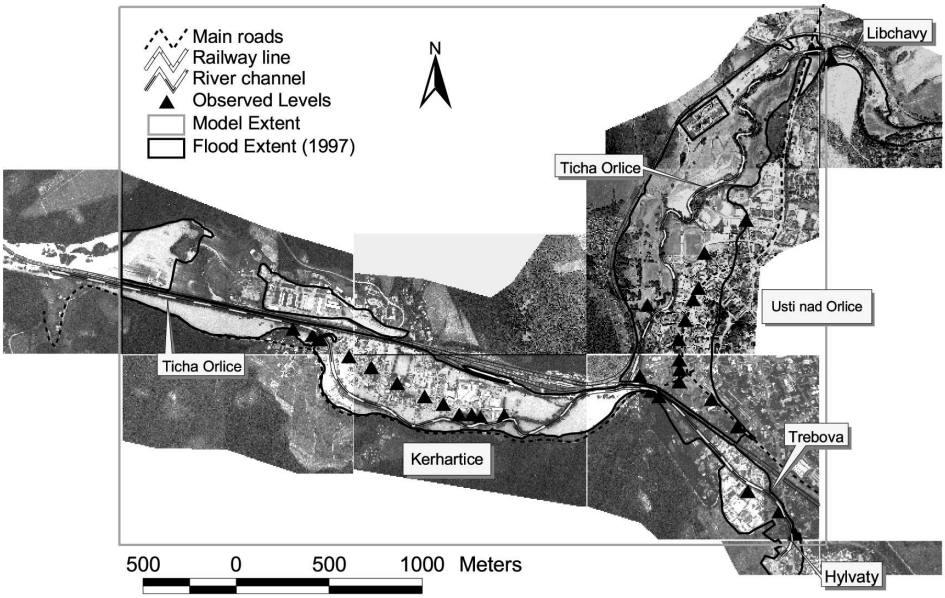


Figure 7.1: Aerial photo of the town of Usti nad Orlici showing the extent of flooding during the 1997 event (photo courtesy of the Elbe River Authority, Hradec Králové, Czech Republic)

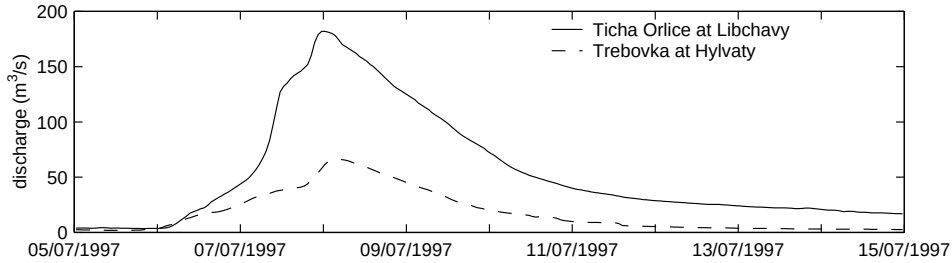


Figure 7.2: Observed hydrographs of the 1997 event.

reach. No data was available for the Trebovka, and cross sections were estimated using the channel top width obtained from 1:5000 scale topographic maps. Although the Trebovka is thus included in the models applied, the flood extent and level observations along the reach were not used for evaluation of model performance due to this lack of data.

Topographical data of the floodplain was also limited. Four sources of surveyed elevation data were available:

- 60 spot level observations.
- Over 5000 line elements with constant elevation with an average length of 25m.

These lines give good representation of roads, embankments, river banks etc.

- 850 point elevations from the cross section surveys on the floodplain.
- Additional elevation data obtained through digitising contours from 1:5000 scale topographical maps. Contour intervals in these maps are generally at $2m$, although in flatter sections intermediate $1m$ contours are also given.

Of the elevation data sources the digitised contours are the least accurate, estimated at half the contour interval. Availability of the other three data sources was the most limited along the steeper valley sides while coverage was good within the town. The combined elevation data was used to generate a triangulated irregular network (TIN) of the topography. This was then resampled to a regular grid digital elevation model (DEM) with a resolution of 10m. Special attention was given in resampling to representation of important line elements such as roads, railway lines and embankments.

7.3 Approach

Two of the codes described in chapter 3 are selected for modelling the extent of inundation in the reach;

- 1D hydrodynamic model code - SOBEK-RIVER, abbreviated to *sbk*,
- Integrated 1D-2D hydrodynamic code - SOBEK-OVERLAND FLOW, abbreviated to *s2d*

7.3.1 SOBEK-1D model

The one dimensional hydrodynamic code used is the SOBEK code using the staggered scheme. Output from the model are in the form of levels at each cross section calculation point along the main channel. To obtain a flood extent map, the longitudinal profile of maximum levels is projected to a 2D plane. Under the assumption of constant water levels along each cross section, water levels at the cross section are allocated to geo-referenced cross section elevation points. These are then interpolated using an inverse distance interpolation approach with orthogonal point selection to ensure a continuous surface. Once the water level surface is derived, this is crossed with the DEM of the floodplain and only depths greater than zero are retained. To ensure low lying areas (e.g. behind embankments) are not mistakenly considered flooded, all inundated cells without a contiguous connection to the main channel are removed from the final flood extent map. For a full description of the approach see *Werner* (2001) and Appendix B. Application of the code and subsequent interpolation is referred to as *sbk1D*.

7.3.2 SOBEK-1D2D model

The second model code applied in this chapter is the hybrid one-dimensional/two-dimensional SOBEK-1D2D code described in chapter 3. An advantage of using the

one-dimensional approach in the main channel, is that while most 2D hydrodynamic codes allow only for a poor representation of structures such as bridges and weirs in the reach under consideration, these can be explicitly incorporated in the main channel domain. Often application of full 2D codes avoid this problem through demonstration in rural reaches without such structures. As floodplain flows are resolved in 2D the maximum extent of inundation for the event can be immediately derived from model results. Application of the model is referred to here as *sbk1D2D*.

7.3.3 GLUE methodology

To explore the effect available data has on constraining parameters, the Generalised Likelihood Uncertainty Estimation methodology (*Beven and Binley* 1992) discussed in chapter 4 was applied. This is a Monte-Carlo based technique allowing explicit exploration of the value of data in constraining parameter uncertainties (*Freer et al.* 1996). An ensemble of parameter sets is sampled from prior distributions of the constituent parameters and the model run with each set. The acceptability of each run is assessed by comparing the predicted with the observed values using a chosen likelihood measure (*Aronica et al.* 2002). The likelihood measure is obtained using a selected objective function, and likelihood measures derived using different data sets and objective functions can be easily combined through application of Bayes theorem (*Lamb et al.* 1998; *Franks et al.* 1998),

$$L(\theta_i \mid Y) = \frac{L_1(Y \mid \theta_i) L_0(\theta_i)}{\sum_{j=1}^{N} L_1(Y \mid \theta_j) L_0(\theta_j)} \tag{7.1}$$

where $L_0(\theta_i)$ is the prior likelihood measure for parameter set θ_i, $L_1(Y \mid \theta_i)$ is the likelihood measure derived by comparing model output using parameter set θ to observations Y using a selected objective function, $L_1(\theta_i \mid Y)$ is the posterior likelihood of parameter set θ_i given observations Y, and N is the number of parameter sets. Optionally a behavioural threshold can be applied to divide runs with acceptable performance from those with unacceptable performance (*Beven and Binley* 1992). Parameter sets that perform below the threshold in the selected objective function are then given a likelihood of zero and likelihood values for the remaining sets are re-scaled.

To establish likelihood measures in assessing performance of flood extent maps predicted by the model against the observed flood extent map, an objective function is selected that deals with binary classification data. *Aronica et al.* (2002) use three different statistics to compare modelled to observed flood extent maps, the second of which they find to be superior. Referred to as $F^{<2>}$ the statistic is used also by *Bates and de Roo* (2000) and *Horritt and Bates* (2001b), and this measure is used here for comparing modelled and observed flood extent:

$$F^{<2>} = \frac{A^{obs} \bigcap A^{mod}}{A^{obs} \bigcup A^{mod}} \tag{7.2}$$

With A^{obs} being the observed area of inundation and A^{mod} the modelled area of inundation. In effect the statistic determines the ratio between the number of grid

cells classified correctly as being either dry or wet and the number of cells classified incorrectly. Equation 7.2 can then be reformulated as

$$F^{<2>} = \frac{\sum_{i=1}^{n} P_i^{D1M1}}{\sum_{i=1}^{n} P_i^{D1M1} + \sum_{i=1}^{n} P_i^{D1M0} + \sum_{i=1}^{n} P_i^{D0M1}} \tag{7.3}$$

where P_i^{D1M1} obtains a value of 1 for cells classified as inundated both in observed and modelled data, P_i^{D0M1} obtains a value of 1 for cells observed as dry but predicted to be wet, and P_i^{D1M0} obtains a value of 1 cells observed as wet but classified as dry.

Comparison of observed to modelled levels for the distributed floodplain level observations is more straightforward as these data represent continuous properties, and the mean square error (MSE) can be used as a good indication of model performance. Likelihood measures are derived from the MSE by scaling with the squared mean depth of the distributed observation points and subtracting from unity, the resulting scaled MSE measure is referred to as $sMSE$,

$$sMSE = 1 - \frac{\sum_j (\hat{h}_j - h_j)^2}{\bar{d}^2} \tag{7.4}$$

where $\hat{h}_j$ is the calculated level at observation point j, $\bar{d}$ is the mean depth of the observations points considered, with the depth $d_j = h_j - z_j$ where z_j is the level of the elevation model in the cell observation point j falls in. Although the observed points should all have a positive depth, errors in the elevation model may lead to a "negative" depth being determined. These points were excluded in determining the average depth in the denominator of equation 7.4.

Because the floodplain observation points are distributed over the floodplain, low roughness parameterisations will result in not all points being predicted as inundated. A binary classification similar to that in comparing flood extent predictions is introduced to account for this by weighting the $sMSE$ measure with the ratio of observation points predicted as inundated to the total number of observation points used. This measure is referred to as $wMSE$,

$$wMSE = \frac{\sum_j R^{M1}}{M} \times sMSE \tag{7.5}$$

where R^{M1} obtains a value of 1 for observation points predicted as inundated in the model and M the total number of observation points considered. Contrary to the binary comparison of flood extent data, no account needs to be taken of points predicted wet but observed dry, as all observations represent wet points.

The value of updating likelihood weights using additional data is evaluated through the Shannon Entropy measure H (*Beven and Binley* 1992; *Franks et al.* 1998), where a lower entropy value indicates more structure and therefore less uncertainty.

$$H = -\sum_i L(\theta_i) log_2 L(\theta_i) \tag{7.6}$$

where i is the model realisation index. As the value is a discrete summation, the number of realisations must be taken into account when comparing entropy values between simulations, making such comparison difficult. The entropy value is used here to compare the value of calibration data sets in lowering entropy values for simulations with the same number of model realisations.

7.3.4 Effect of topographical uncertainty

To explore the effect of topographical uncertainty the elevation data itself would need to be considered as a stochastic variable as are the model parameters. To fully investigate this effect, a set of elevation models would need to be randomly generated and each parameter sets selected in the GLUE analysis re-run with each elevation model. *Aronica et al.* (1998b) applied 363 different random topographical fields in investigating the impact of topographic uncertainty, but applied only one parameter set to each of the topographic fields. A different approach is taken here, primarily out of computational constraints. First the magnitude and spatial correlation of errors in the elevation model is estimated using a split sample of the available elevation data. Based on this estimate fifty random topographic fields are generated. Five parameter sets are then selected for each of the two models, where three of those selected give poor, average and good performance on the $F^{<2>}$ measure and the other being the parameter sets with the best performance for the $F^{<2>}$ and $wMSE$ measures respectively. These five parameter sets are run with each of the fifty topographical fields and the performance is compared to that using the original deterministic topographic field. The number of random topographical fields generated was selected such that the range of performance for the selected parameter sets stabilised. Despite this, the sample size of topographic fields is too small to give a precise description of the impact, but is considered sufficient to give an impression of the impact of topographic uncertainty on parameter response surfaces for the reach studied.

7.4 Application and results

7.4.1 Model validation against flood extent and point observations

Using the two model codes and available data, two models of the reach were developed. These models are identical between the main channel banks where the same cross section information was applied. The floodplain in the *sbk1d2d* model was described using the digital elevation model, while in the *sbk1D* model the full cross sections defined floodplain topography. Where the available cross section data was not sufficient to extend across the floodplain additional points are sampled from the elevation model. All twelve structures and four weirs in the reach were explicitly modelled using the available geometric data.

Prior ranges for roughness parameters in the floodplain and main channel given in table 7.1 were loosely based on those given in *Chow* (1959). The main channel was considered a clean winding minor stream with some pools and shoals. Although this is generally the case for the reach in question, a site visit showed that the

Table 7.1: Prior parameter ranges.

Parameter		Range
Floodplain Roughness	n_{fp}	0.02 - 0.30
Main Channel Roughness	n_{mc}	0.02 - 0.10

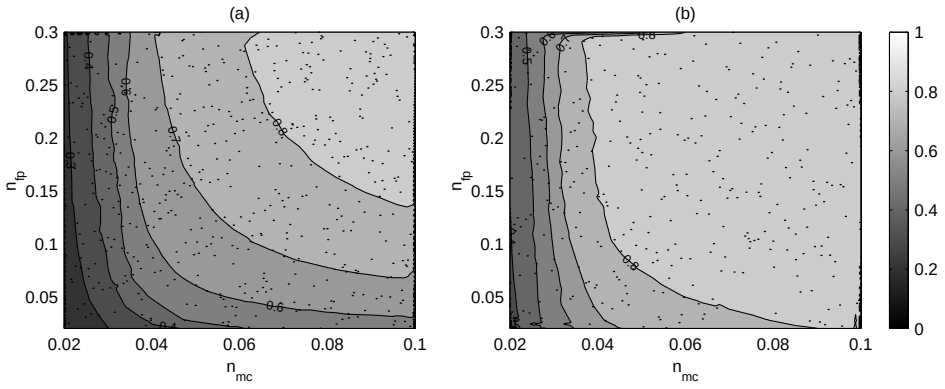


Figure 7.3: Contour lines for the $F^{<2>}$ performance measure. (a) *sbk1d* (b) *sbk1d2d*

main channel was littered in some sections with rubble, thus explaining a higher maximum than would normally be selected for a reach of this type. The tables supplied do not give an estimation of roughness for an urbanised floodplain as is the case here, and the maximum of the range selected for floodplain roughness was set to a value well above that applicable to a heavily wooded floodplain with brush (see table 7.1).

From these prior parameter ranges 500 parameter sets were randomly generated for application in the *sbk1d* model using Latin-Hypercube sampling from uniformly distributed priors to ensure a good spread of samples (*McKay et al.* 1979). For the *sbk1D2D* model the sample size was reduced to 325 out of computational considerations. For each parameter set the applicable model was run and model performance established through the $F^{<2>}$ and $wMSE$ performance measures. Due to the limited availability of cross section data on the Trebovka tributary a mask was used to exclude comparison of flood extent for the tributary. This mask was similarly applied to ignore comparison downstream of the narrow section below Kerhartice (see figure 7.1) as this is considered too close to the model boundary to allow independent comparison. Performance measures using the distributed floodplain points were similarly limited to those points not masked, resulting in 26 of the 43 distributed floodplain points being used.

Figure 7.3 shows contour lines interpolated from the $F^{<2>}$ performance measure for all parameter sets. Clearly parameter sets showing better performance for the *sbk1D* model have higher roughness than those in the *sbk1D2D* model, where even for low roughness parameter sets a reasonable performance is achieved. Comparing the optimal performance of the two codes shows these to be 0.861 and 0.840

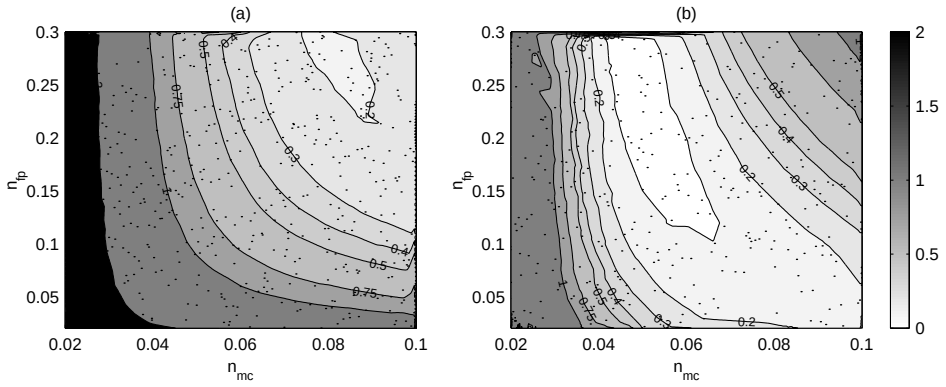


Figure 7.4: Contour lines for the MSE performance measure. (a) *sbk1d* (b) *sbk1d2d*

respectively, albeit in very different parts of the parameter space. Figure 7.4 shows a similar pattern for the MSE performance measure of the 26 floodplain points. Again the regions of good performance are in higher areas of the parameter space for the *sbk1D* model than for the *sbk1D2D* model. The latter does, however, show a better optimal performance with the minimum (optimal) MSE values of $0.191m$ and $0.048m$ respectively. Contour plots for the $wMSE$ measure are similar, although the performance for low roughness parameter sets tends to reduce more drastically as less and less points are correctly predicted as inundated.

Likelihood values derived using both the $F^{<2>}$ and $wMSE$ measures are given as dotty plots in figures 7.5 and 7.6. These plots represent projections of the parameter surfaces in figures 7.3 and 7.4 onto single parameter axes. Although these reveal little about parameter interactions (*Blazkova et al.* 2002a), they do show the spread of fit and resulting likelihood value across the parameter range. Particularly for the $F^{<2>}$ measure it is clear that the fit increases with roughness value for the *sbk1D* model. For the *sbk1D2D* model the fit for this measure increases to a given level, to remain almost constant from there with increasing roughness. Floodplain roughness is shown equally to give comparable performance across the domain, with again a tendency to increasing performance with roughness for the *sbk1D* model. Likelihood values for main channel roughness derived using the $wMSE$ show a clearer optimum within the selected parameter range, suggesting greater value in constraining parameter uncertainties using the distributed level observations.

This conclusion is reinforced through the Shannon Entropy values given in table 7.2. The total uncertainty in the uniform prior is reduced only slightly when constraining on flood extent maps ($F^{<2>}$ measure). A larger reduction of uncertainty is achieved with the distributed observation points, but combining the two measures does not reduce the uncertainty significantly more than when using only the distributed points. Likelihood values were re-calculated for both measures while applying a behavioural threshold of $F^{<2>} > 0.80$ and $wMSE$ where the MSE is less than $0.25m$. The table clearly shows the limited effect of using the flood

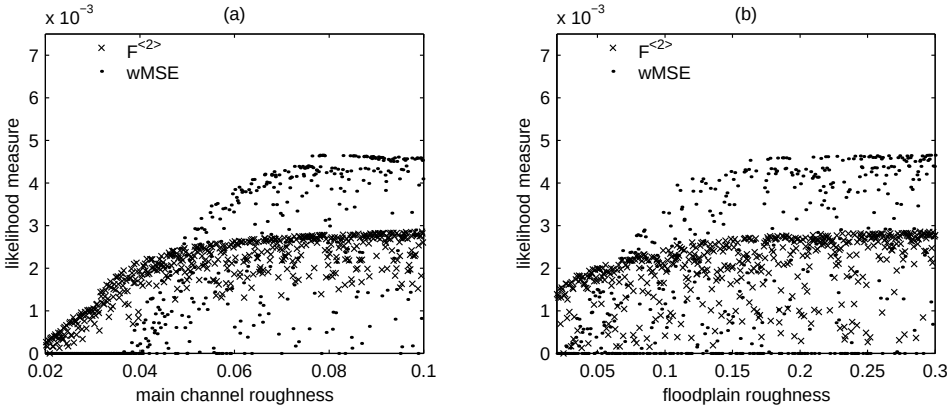


Figure 7.5: Dotty plots for likelihoods derived using the *sbk1D* model.

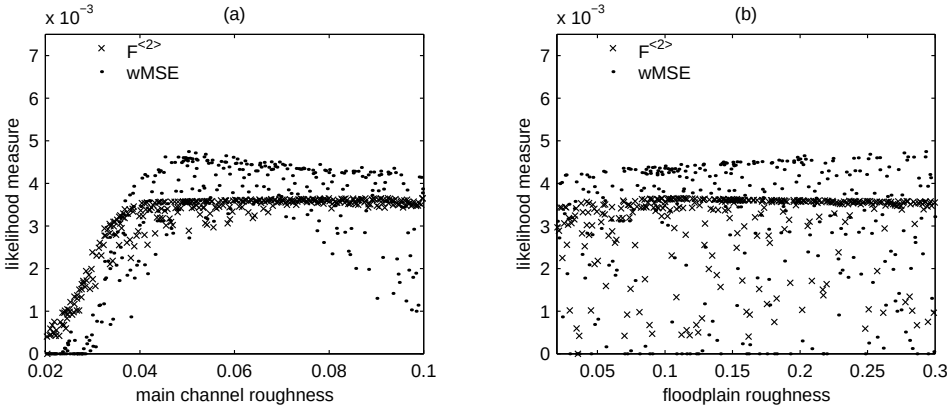


Figure 7.6: Dotty plots for likelihoods derived using the *sbk1D2D* model.

extent map to constrain uncertainties when compared to using the distributed level observations. This is confirmed in the upper and lower 90% uncertainty bounds for the calculated inundated area (observed area is $1.60 \times 10^6 m^2$) and depth at an example observation point (point 11), located on the left bank of the river on the main street through Usti nad Orlici with an observed depth of $1.51m$ (see figure 7.1). Differences in magnitude between H for different sets is due primarily to the different numbers of parameter sets retained (*Franks et al.* 1998). The cumulative likelihood distributions of flooded area at observation point 11 (figure 7.7) confirm using both the observations points and the inundation map in constraining parameters sets ($F^{<2>}$ and $wMSE$) has very little added value when compared to using the observation points alone ($wMSE$).

Using the likelihood values associated with each predicted flood extent map, an inundation likelihood map is derived through (*Aronica et al.* 2002)

Table 7.2: Shannon entropy values and 90% uncertainty bounds for calculated area and depth at observation point 11.

	sbk1d	*sbk1d2d*	*sbk1d2d*			
	H	H	Area		Depth (point 11)	
	[-]	[-]	$10^6 m^2$		m	
			lower	upper	lower	upper
Prior	8.97	8.34				
$F^{<2>}$	8.85	8.26	1.02	1.83	0.64	2.28
$wMSE$	8.23	8.04	1.31	1.80	0.98	2.14
$F^{<2>}$ and $wMSE$	8.16	8.02	1.32	1.80	0.99	2.14
$F^{<2>}$ (> 0.80)	6.83	7.75	1.46	1.83	1.12	2.31
$wMSE$ ($< 0.25m$)	6.64	7.29	1.43	1.72	1.09	1.81
$F^{<2>}$ (> 0.80) and $wMSE$ ($< 0.25m$)	6.64	7.20	1.46	1.72	1.12	1.81

$$p_i^{flood} = \frac{\sum_j f_{ij} L_j}{\sum_j L_j} \tag{7.7}$$

where p_i is the likelihood pixel i is inundated, L_j is the likelihood measure for parameter set used in run j and f_{ij} obtains the value 1 if pixel i is flooded in run j and 0 if it is dry. Figure 7.8 shows the resulting inundation likelihood map calculated with the combined $F^{<2>}$ and $wMSE$ measures using the *sbk1D2D* model. Dark grey indicates areas having a large likelihood of being inundated.

7.4.2 Assessments of impacts of uncertainty in digital elevation model

To establish the accuracy of the elevation model, it was assumed that elevation data from surveyed cross section points on the floodplain and the 60 spot elevations have a much higher accuracy than the digitised contours. Cadastral line elements along the railway lines and main roads are also considered of high accuracy, with elevation data in the flatter areas between being more uncertain. To estimate the accuracy of the elevation model, particularly on the flatter valley floor where the impact on hydraulic flow is considered most profound, a second elevation model was established in which the cross section and spot elevations points were omitted. The difference between elevations at these omitted points in the two DEM's was used as a measure of the overall uncertainty.

Elevation differences at the sampled points were found to have a mean of $0.007m$ and standard deviation of $0.33m$, indicating a negligible bias between the two sources of information. The spatial correlation of the residuals is explored through fitting a variogram (*Burrough and McDonnel* 1998), with the exponential variogram model found to be most suitable (see figure 7.9), where the sill is reached in a distance of in the order of $100m$. This indicates that beyond this range there is little correlation in residuals.

Fifty random maps were generated through unconditional gaussian simulation

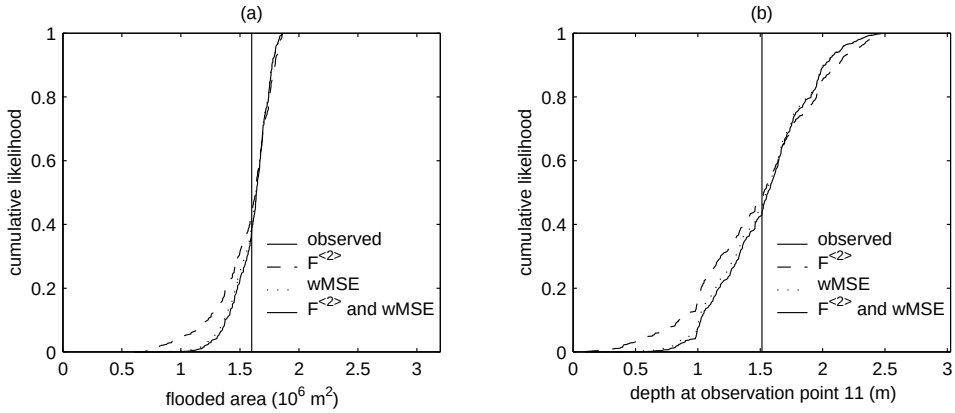


Figure 7.7: Cumulative likelihood distributions for model prediction of flooded area (a) and depth at point 11 (b) using the *sbk1d2d* model

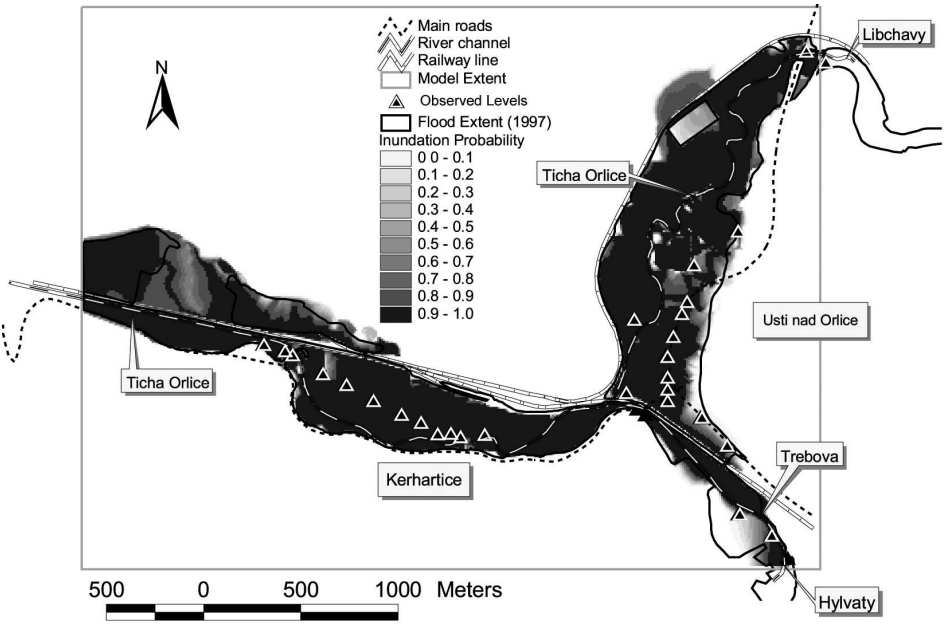


Figure 7.8: Inundation likelihood map.

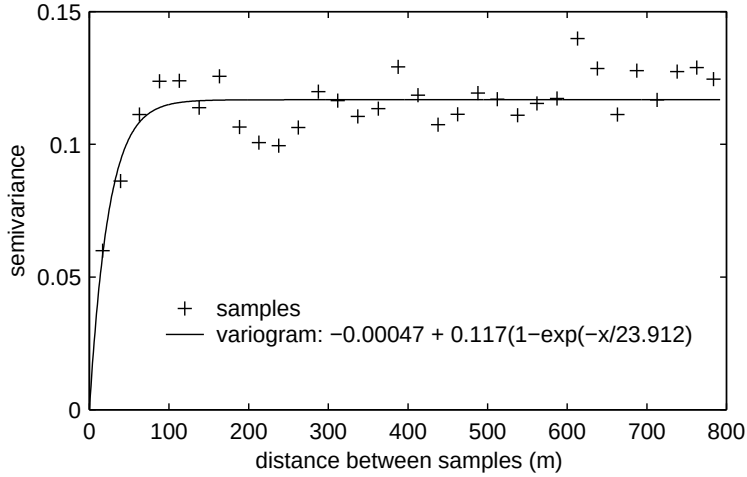


Figure 7.9: Variogram of sampled residuals between elevation models.

using this exponential variogram. Because the elevation data of the railway line and the main roads, available from the cadastral surveys is considered to be of higher accuracy, the elevations along these line elements were not varied in these maps, and the exact values superimposed on the random maps. The bankfull level, being the interface between the 1D and 2D models was also kept constant to avoid modelling anomalies. Although error in the bank level may have significant impact on flood extent in some cases, given the overbank depth seen in the reach considered, keeping this interface constant was considered not to influence flood extent greatly. These elevation models were then run with the selected five parameter sets for the *sbk1d* and the selected five parameter sets for the *sbk1d2d* models, and resulting $F^{<2>}$ and $wMSE$ performance measures calculated. Figure 7.9 shows the impact of including the elevation error on the performance measures. The performance of the unperturbed elevation model is indicated using a marker, while the full range found in the fifty simulations with the random elevation models for each of the parameter sets is shown using the line and whiskers.

7.5 Discussion

7.5.1 Comparison of model approach

Both models used here show comparable levels of performance in predicting the extent of flood due to the 1997 event. This confirms the results of *Horritt and Bates* (2002), showing that despite the fact the 1D approach does not explicitly resolve the hydraulic detail of complex floodplain flow (*Connell et al.* 2001; *McCowan and Collins* 1999) it is comparably reliable in predicting bulk flow conditions such as extent of flooding for this type of reach. Performance of the models with respect to predicting inundation levels distributed in the floodplain and evaluated using

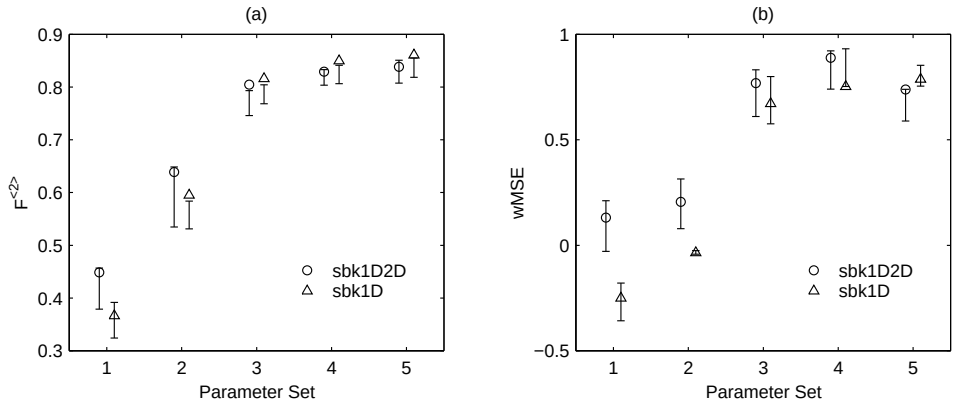


Figure 7.10: Impact of elevation model uncertainty on model performance.

the $wMSE$ measure, however, show better performance of the *sbk1d2d* code. This would suggest that resolving floodplain flow using the detail of the 2D model does indeed provide more reliable predictions than when interpolated from the 1D results.

The ranges of floodplain and main channel roughness for which model performance is reasonable is, however, very different between the two approaches. In the 1D *sbk1D* model in particular, the roughness factors used must be considered a bulk roughness factor, implicitly including all momentum losses due to turbulent interaction between the main channel and floodplain and crossing flows from floodplain to main channel (*Knight and Shiono* 1996). Roughness factors giving good performance are therefore high when compared to the ranges of values applicable to rivers of this type as suggested by *Chow* (1959). Although turbulent momentum interaction is also not explicitly considered in the *sbk1d2d* model through for example application of the more standard turbulence closure models (*Wilson et al.* 2002), the non-zero shear horizontal interface between the 2D floodplain flow domain and the 1D main channel flow domain effectively acts as an implicit turbulent closure model. As a result posterior ranges of particularly main channel roughness conform more to the intuitive range that would be selected based on literature.

7.5.2 Utility of available data in constraining uncertainties

Parameter response surfaces of the $F^{<2>}$ clearly show that while the flood extent map data has value in constraining roughness values, the shape of the response surface indicates an increasing tendency to good performance for parameter sets with high main channel and floodplain roughness. This bias to rougher parameter sets is also shown for a 1D model applied by *Horritt and Bates* (2002) on a reach of the River Severn. Similar parameter response surfaces from other reaches (*Horritt and Bates* 2001a; *Aronica et al.* 1998a, 2002) showed a different pattern, with performance again reducing for sets with higher roughness. It would seem the utility of the flood extent map data depends largely on the type of reach being considered. Contrary to most other reaches studied in literature, the reach modelled

here is of an urban setting, with the flood extent map being constrained by road and railway embankments and steep valley sides. On the basis of these constraints, the sensitivity of calculated flood extent to roughness values would be expected to be low. The inundation probability map (Figure 7.8) indeed clearly shows how little discrimination this allows between the flood extent predicted across a range of parameter sets. Variation between the predicted area from different parameter sets is apparent only for the lower roughness parameter sets where these constraints on the extent have not been reached. These, however, have low performance and would be considered unsuitable, particularly if some form of behavioural threshold is applied. This leads to a bias towards rougher parameter sets (fig. 7.5 and fig. 7.6), resulting in models over-predicting inundation depths having equally good performance as models giving more accurate predictions. Although not available for this reach, greater utility could perhaps be found from flood events of less extreme magnitude where the sensitivity of the inundated area to variation in roughness is greater than in the extreme event used here, but extrapolation to more extreme events would then need to be considered very carefully given the non-linearity of the inundated area - discharge relationship. Effective roughness values found in calibrating to lower magnitude events are likely to perform well in different parts of the roughness ranges as the balance of floodplain storage and conveyance changes (*Romanowicz and Beven* 2003), thus adding to the complexity of predicting high events through extrapolation of a model calibrated to low events.

The response surface of the $wMSE$ measure does not show these drawbacks, and there is a clear reduction of model performance as the predicted inundation depth at the distributed floodplain points is higher as main channel and floodplain roughness increase. Comparison of the reduction of uncertainty in terms of Shannon's entropy index H (table 7.2) show that using these data alone is of near-equal utility as using both this data and the flood extent data. This is reflected in the parameter response surfaces of the two measures (fig. 7.3 and 7.4), showing that parameter sets giving good performance for the $wMSE$ measure all lie in an area of equally good performance in terms of the $F^{<2>}$ measure. Although the number of points used is relatively low when compared to the flood extent map, the observed levels are much more effective in constraining parameter ranges. Unfortunately availability of such distributed floodplain observations from real flood events is perhaps even less than that of inundation extent maps. Although there are some examples of the use of observed floodplain levels (e.g. *Aronica et al.* 1998a), to date little use of this type of data has been made, even from smaller samples such as flood marks often recorded on buildings. *Puech and Raclot* (2002) propose an interesting technique of estimating inundation depths from flood extent maps using LiDAR elevation data and areal photographs and this would greatly improve the utility of flood extent maps. Distributed flood depths thus obtained could further establish 2D modelling approaches as superior, although the uncertainty of the elevation data would need to be carefully considered (*Marks and Bates* 2000).

In the models used here, a single roughness value was used for the floodplain, and as a result a good fit can not be expected for all of the observation points. Potentially this could be resolved by considering distributed roughness values on the basis of for example floodplain land-use. For the reach considered here, little

detailed information was available on floodplain land-use except where this was urban or non-urban. Increasing floodplain heterogeneity would also lead to a higher dimensional calibration problem, and may therefore ultimately result in higher predictive uncertainties (*Romanowicz and Beven* 2003).

7.5.3 Uncertainties in elevation model data

The impact of uncertainty in elevation model data on the $F^{<2>}$ measure is relatively small as shown in the ranges in figure 7.10, with this impact reducing as model performance improves. Inspection of the resulting flood maps reveals that differences stem primarily from the inundated area being somewhat more patchy in areas of low inundation depth, while the outline of the flood extent remains more or less constant, again constrained by the road and railway embankments. This also explains the impact being higher for low roughness parameter sets (1 and 2) and low for the better performing sets where the average inundation depth is higher. For the $wMSE$ measure the effects are not significantly different for different parameter sets, but still variation in performance due to the perturbed elevation models is relatively small compared to differences in performance due to variation in roughness. These results reflect the small impact on performance in flood extent prediction shown by *IRMA* (2002), with the latter study showing an even more negligible effect. This could, however, be due to errors in the elevation model not being taken as spatially correlated, therefore rapidly averaging out as more and more independent grid cells are considered. *Aronica et al.* (1998b) found the effect of elevation model uncertainty to be much more significant, but this would seem to result from the floodplain in their case being more important in conveying flow than is the case here, where the floodplain contributes largely to storage. This is reflected in the relative insensitivity to floodplain roughness, and also demonstrated for flood events in river reaches similar to that studied here (*Bates and de Roo* 2000; *Horritt and Bates* 2002).

7.6 Conclusions

The ability of two methods for predicting floodplain inundation in an urban reach of the Orlice river in the Czech republic have been tested. The first method considers hydraulic modelling of level and flow in the river and floodplain using a 1D hydrodynamic modelling code, while the second uses the same 1D representation of flow in the main channel, but uses a coupled 2D raster based inundation model for modelling floodplain flow. Prior ranges of main channel and floodplain roughness are selected from literature, and the generalised likelihood uncertainty estimation method (GLUE) is used for resolving posterior parameter distributions and predictive reliability of both methods. Model performance is evaluated using either comparison of the predicted and observed flood extent maps or comparison of model level predictions against 26 distributed observations of maximum flood levels on the urban floodplain. While both models give comparable performance in predicting the flood extent, the integrated 1D-2D approach is shown to be slightly

superior to the 1D approach in predicting the distributed levels. This is not surprising as the 2D approach resolves floodplain flow with more hydraulic detail than is achieved in the interpolated flood extent map derived from the 1D results. Comparison of the utility of the two types of data used in constraining uncertainties shows the flood extent data is of comparatively little use. This could have been expected as the reach considered is primarily urban, with the extent of flooding constrained primarily through road and railway infrastructure, thus giving little discrimination between model runs with different roughness values. Using only the flood extent map data can, however, introduce a bias to parameter sets with high main channel and floodplain roughness, resulting in over-prediction of inundation depths and possibly over-prediction of resulting flood damage. Distributed floodplain level data, even if available for only a limited number of points, would be of great use in improving predictive reliability of floodplain inundation models.

The impact of uncertainty in the elevation model used is shown to be relatively small on the performance in predicting the extent of flood when compared to uncertainty due to uncertain roughness parameters. This insensitivity is again due to the constraints on the extent of flooding posed by road and railway embankments. Impacts on the performance of the models in predicting levels at the distributed floodplain observation points is much greater. Improving accuracy of digital elevation model data could therefore potentially contribute in improving reliability of flood inundation models, particularly where reliable estimates of inundation depth are required, This does required floodplain flow be appropriately modelled in 2D.

The results show that the distributed level information is much more efficient in constraining uncertainties in roughness parameters than flood extent data, thus providing a higher predictive reliability. This holds particularly for urban reaches as is the case studied here. The importance of evaluating flood risk in urban reaches is obviously much greater than it is in more rural reaches, and the importance of collecting this data during flood events, and its subsequent use in calibrating flood inundation models would therefore seem apparent.

Acknowledgements

This work has been done in co-operation with the FRIEND project (UNSECO). The Czech Hydrometeorlogical Institute (CHMI) is thanked for kindly providing the hydrological data used. Keith Beven and two anonymous reviewers are thanked for making the text more consistent and readable.

8

Identifiability of distributed land use data in flood extent estimation

Abstract

In this chapter the potential for identifying roughness values for distributed land use types using a comprehensive calibration dataset is explored. The dataset used from the 1995 flood event in the River Meuse, includes gauged levels, flood extent maps and distributed floodplain level observations. A model for the reach studied established using an integrated 1D-2D hydrodynamic code, with main channel flow modelled in 1D and floodplain flow modelled in the 2D domain. Detailed information on floodplain land-use types are aggregated to form one, two or five classes of floodplain roughness. Sensitivity analysis of model performance against the calibration data shows that as the number of floodplain classes increase, sensitivity to these roughness values decreases, given allocation of prior roughness values on the basis of constituent land-use types and associated roughness values found from literature. Evaluating the identifiability of the roughness in these classes using the Generalised Likelihood Uncertainty Estimation (GLUE) method confirms this insensitivity. As a consequence, application of complex formulae to establish roughness values for changed floodplain land use would seem inappropriate, and evaluation of such changes within a probabilistic framework is suggested.

based on Werner, Bates and Hunter, "Identifiability of distributed land use data in flood extent estimation", Submitted for publication in *Journal of Hydrology*

8.1 Introduction

Anthropogenic influences on lowland rivers with extensive floodplains such as the river Rhine, have in the last centuries resulted in major changes in the riverine landscape, including constriction of floodplains by construction of embankments, discharge regulation, river normalisation, building of groynes, and dredging (*Hesselink* 2002). Although some of these changes have improved discharge capacity, the constriction of floodplains has, in particular, resulted in higher flood stages. Sedimentation on the constricted floodplain leads to still higher flood stages (*Asselman and van Wijngaarden* 2002), and projected changes in river regime as a consequence of enhanced climate change are foreseen to raise levels even further (*Middelkoop et al.* 2001). Traditionally, the engineering response to these higher flood stages has been to strengthen and raise embankments, but more recently public acceptance of these engineering measures has diminished (*Wijbenga et al.* 1994), and the focus is shifting to flood control as an integrated part of river restoration (*Pedroli and Dijkman* 1998). In this context a much broader range of measures are considered, attempting to combine sustainable measures such as nature development and floodplain lowering (*Duel et al.* 2002). Given the importance of safety, proposed measures need to be evaluated on the impact on flood risk, and various decision support systems have been developed to support this type of evaluation (*Silva and van de Langemheen* 1997; *Counsell et al.* 2000). In these, impacts may be assessed through some form of hydrodynamic modelling, requiring that measures are expressed in terms of changes in model structure and parameterisation. While translating measures affecting floodplain topography is relatively straightforward, translating measures that affect floodplain vegetation and therefore roughness is much less apparent.

Much empirical work has been undertaken in researching roughness characteristics of floodplain land use types. Research work has included laboratory experiments using stiff rods to represent vegetation (*Sellin et al.* 1993; *Nepf* 1999) or aluminium strips (*Sellin et al.* 2003), as well as actual vegetation such as submerged grass (*Wilson and Horritt* 2002), various types of aquatic vegetation (*Stephan and Gutknecht* 2002), and even coniferous trees (*Kouwen and Fathi-Moghadam* 2000). Based on such experimental work, analytical and numerical relationships have been derived to estimate roughness values for application in modelling based on the vegetation present on the floodplain (*Kutija and Hong* 1996; *Klopstra et al.* 1997). Simpler methods for evaluating floodplain roughness values are tables of roughness coefficients for different roughness types (*Chow* 1959) or through matching physical characteristics to photographs to establish a compound roughness coefficient (*Acrement and Schneider* 1989). For a complete overview of methods in estimating floodplain roughness see *Sellin et al.* (2003).

Establishing an effective roughness coefficient at a reach scale using all these methods requires some knowledge of the vegetation present on the floodplain, and therefore depends on the availability of spatial data with sufficient detail, and potentially vegetation data of higher accuracy will result in more accurate roughness estimation. Recent work has shown the use airborne scanning laser altimetry for establishing reach-scale distributed roughness coefficients (*Asselman et al.* 2002;

Mason et al. 2003; *Cobby et al.* 2003), but more traditional surveys of floodplain land use may be equally suitable. Estimating the change in roughness due to change in floodplain vegetation then follows the same principle as estimating the roughness for the unchanged situation.

Applying this procedure in evaluating the impact on flood levels due to land use change, however, relies on the validity of a reductionist approach in hydrodynamic modelling as it assumes that the bulk roughness of the reach is the sum of roughness due to distributed vegetation, and this assumption is at best doubtful (*Beven* 2000). Even for finite-element 2D hydrodynamic models, considered as the most complex model practicably applicable to dynamic reach scale flood stage prediction, comparison to laboratory experiments show these have shortcomings (*Wilson et al.* 2002), and as a result some calibration and validation of models will always be required before these can be reliably used in prediction (*Sellin et al.* 2003). The result of the calibration is, however, that the roughness factors no longer represent roughness due to vegetation only, but are bulk representations of momentum losses not explicitly modelled. This holds particularly for 1D modelling where turbulent momentum interchange is not explicitly accounted for (*Ackers* 1992), but applies equally to 2D modelling where turbulent closure models are used (*Wilson et al.* 2002).

The inverse problem tackled in calibration shows that floodplain roughness parameters are difficult to identify given the data typically available at the reach scale (*Khatibi et al.* 1997), with roughness values across a wide range giving equivalent, or near equivalent calibration results (*Aronica et al.* 1998a; *Horritt and Bates* 2001a; *Aronica et al.* 2002). This chapter addresses the problem of identifiability of distributed roughness values. Given a highly detailed data set available from the 1995 flood event for a $30km$ of the Meuse river in the Netherlands, as well as a detailed map of floodplain land-use, the utility of the calibration data in constraining uncertain roughness is investigated. Twenty types of land-use are distinguished in the original land use data, and these are aggregated to three levels, (a) a single floodplain land use class, (b) two floodplain land use classes, and (c) five floodplain land use classes. For each of these aggregated classes the sensitivity of model calibration to heterogeneity in roughness specification is investigated. Finally the utility of the different types of calibration data in constraining prior roughness distributions is explored.

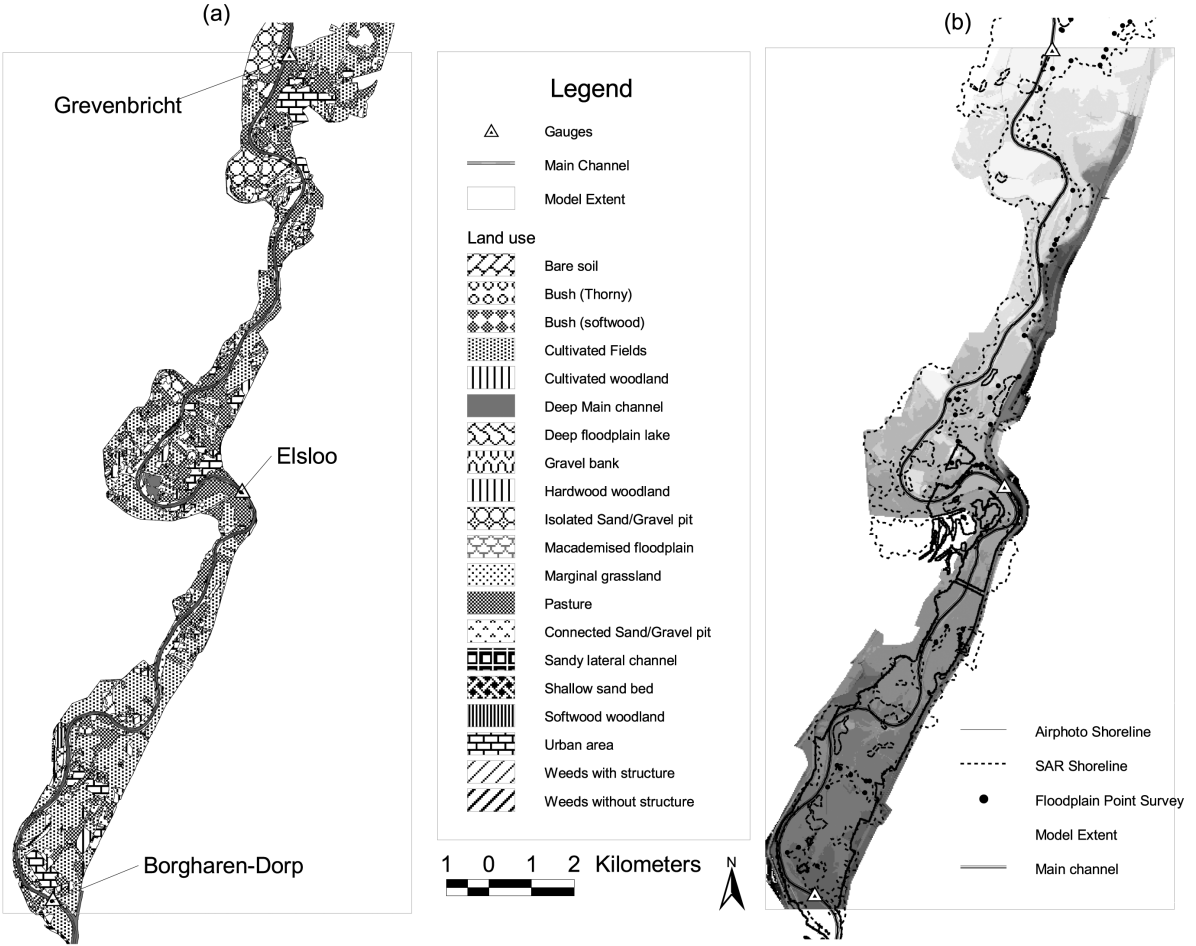


Figure 8.1: Meuse river between Borgharen-Dorp and Grevenbricht.

8.2 Study site and available data

The reach of the River Meuse considered in this study is just downstream (North) of the town of Maastricht in the Netherlands, covering about $30km$ between the gauging stations of Borgharen-Dorp and Grevenbricht, with the gauging station at Elsloo internal to the modelling domain (see figure 8.1a). This reach consists of a meandering channel with an approximate width of $100m$, and a floodplain of up to $3km$ in width, constrained by the high embankments of the Juliana canal to the east and the main river dyke running along the Belgian-Dutch border to the west. Land use in the reach is primarily agricultural with some 65% of the area being fields and pastures. An overview of land use in the reach in Table 8.1 (only land-use types $\gtrapprox 1$ % of area are given) shows that the floodplain also contains a number of urban settlements. The range of roughness values are given as estimated from the tables provided in *Chow* (1959) and *French* (1986). Despite the dominance of pasture, the significant areas of urban area, woodland, and weeds would be expected to add to roughness characteristics.

Table 8.1: Land-use, roughness values and aggregated classes.

Land-use Type	Area	Mannings-n $m^{1/3}s^{-1}$		Single class	Two classes	Five classes
	(%)	Min.	Max.	(id's)	(id's)	(id's)
Isolated Sand/Gravel pit	4.69%			mc	mc	mc
Main channel	6.27%	0.025	0.06	mc	mc	mc
Urban area	8.52%			fp	fp2	fp4
Weeds without structure	1.75%	0.035	0.08	fp	fp1	fp3
Weeds with structure	4.01%	0.035	0.08	fp	fp1	fp3
Cultivated Fields	34.63%	0.025	0.05	fp	fp1	fp3
Pasture	24.53%	0.025	0.05	fp	fp1	fp1
Marginal grassland	5.10%	0.025	0.05	fp	fp1	fp1
Bare soil	1.58%	0.02	0.04	fp	fp1	fp1
Hardwood woodland	2.45%	0.08	0.2	fp	fp2	fp5
Cultivated woodland	3.97%	0.08	0.2	fp	fp2	fp5

During the January 1995 flood event the floodplain in the reach suffered extensive inundation. An exceptionally complete dataset was collected by the Dutch Water Authorities during this event, making four types of calibration data available, as summarised in Table 8.2. Figure 8.2a shows the levels recorded at the three gauges, with the peak at Borgharen-Dorp being recorded at $45.71m$ on the morning of the 31^{st} of January. The peak flow was rated as $2746m^3/s$, estimated as having a return period of 63 years. The event showed the same triple peak seen in many adjacent basins and was quite prolonged when compared to other events in the Meuse such as the slightly larger December 1993 flood event (*Wind et al.* 1999). Although the two surveys of flood extent, one from a low altitude airborne survey on 27

January, and one from the ERS-1 satellite overpass on 30 January at 10:33, were some 70 hours apart, due to the elongated event the hydraulic conditions in the different samples are likely to be very similar, with the discharge at Borgharen-Dorp estimated at $2645m^3/s$ and $2631m^3/s$ respectively. Figure 8.1b, however, shows the shorelines indicating flood extent from these two sources, and considerable classification differences can be seen. The estimated spatial accuracy of the digitised air photo was in the order of $25m$ (*Hunter et al.* 2003). The flood extent shoreline from the satellite borne Synthetic Aperture Radar (SAR) image was processed using the snake algorithm described in *Horritt* (1999), with a spatial accuracy estimated at 1 pixel in the image ($\sim 12.5m$). However, due to back-scattering of the radar energy from the wind roughened water surface as well as from particular land-use types, some areas are misclassified in the SAR image, and the air photo is considered as more accurate (*Hunter et al.* 2003). Both images show inundation beyond the main river embankment to the west of Elsloo. This is believed to result from saturated areas due to excess rainfall and not from overtopping of the embankment and was not used in model evaluation.

The final set of data available were from a detailed ground survey of maximum flood levels distributed in the (mainly eastern) floodplain. These point data were considered to be of great value in giving a detailed view on hydraulic variability in the floodplain. 34 points were available in the model extent from Borgharen-Dorp and Grevenbricht, and the surveyed levels at these points are considered to be of good accuracy.

Cross section data were available at approximately $500m$ intervals, as well as a detailed digital elevation model of the floodplain for the reach. The digital data included surveyed heights of major embankments such as dykes and roads in the area.

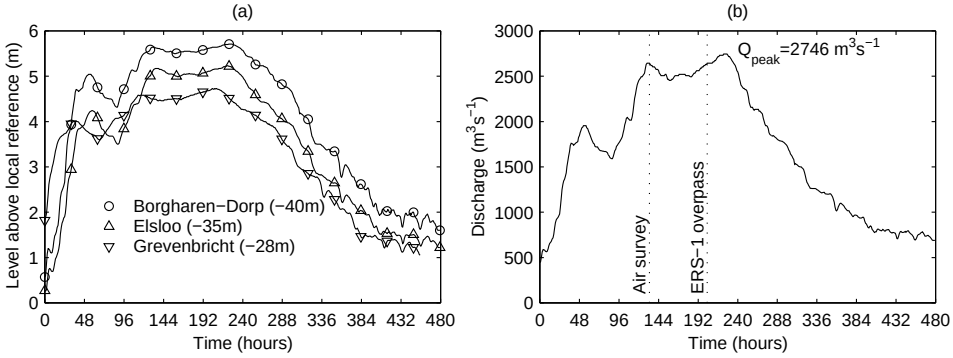


Figure 8.2: (a) Gauged levels at Borgharen-Dorp, Elsloo and Grevenbricht. Levels are given to local reference to increase readability. (b) Discharges derived for the Borgharen-Dorp gauge. The time of overpass for the air survey and ERS-1 satellite are indicated.

Table 8.2: Summary of observed data sources.

Data Type	Time	Description
Gauges	Hourly	Gauged levels at Borgharen-Dorp, Elsloo and Grevenbricht
	Hourly	Discharge at Borgharen-Dorp (derived through stage-discharge transformation
Vector	27-01-1995	Air photo survey. Image mosaic converted to shoreline by Dutch Water Authorities.
	30-01-1995 (10:33)	ERS-1 SAR image converted into a shoreline using statistical active contour model (*Horritt* 1999)
Point	Maximum level	Ground survey of maximum water levels on the floodplain. 34 points within the model extent were used.

8.3 Approach

8.3.1 Model description

The hybrid 1D-2D hydrodynamic code, SOBEK-1D2D, described in full in chapter 3 was applied in modelling the reach. Model boundaries were set at Borgharen-Dorp and Grevenbricht, using discharges observed at Borgharen-Dorp as the upstream boundary, and recorded water levels at Grevenbricht as the downstream boundary. With these boundary conditions defined, unknown water levels and discharge at the upstream and downstream boundary are solved through the model equations. Although the discharges at the upstream boundary have been derived through the rating curve for Borgharen-Dorp, the levels determined by the model are considered independent as the rating curve was not established through a model with a given set of downstream roughness values. Cross sections for application in the 1D main channel were derived as level-width tables giving an average geometry for river sections some $550m$ in length (see *Werner et al.* (2000) for details). Digital terrain models with grid resolutions of $25m$, $50m$, and $100m$ were aggregated from high resolution laser altimetry data. It was found that performance of models with the $100m$ grid deteriorated significantly when compared to the $25m$ grid, while this was much less so for the $50m$ grid. This same result was found for this reach by *Bates and de Roo* (2000), and the $50m$ resolution was used throughout. In aggregating the data, special attention was given to the various line elements in the floodplain, particularly the high embankments to the east and west. Point level data at regular intervals from survey data were available for the tops of these embankments (roads and dykes), and as these were considered to be of a higher accuracy than the laser altimetry data, the levels along the embankment lines were enforced in the grid.

Table 8.3: Range of Mannings-n roughness values (in $m^{1/3}s^{-1}$) for each aggregate land-use class. Bracketed values indicate "optimal" parameter values. Percent area of each class is indicated in italics.

Class	Single Class	Two Classes	Five Classes
Main Channel	0.016 - 0.040 (0.022) *12 %*	0.016 - 0.040 (0.022) *12 %*	0.016 - 0.040 (0.022) *12 %*
Floodplain 1	0.020 - 0.200 (0.040) *88 %*	0.020 - 0.080 (0.029) *72 %*	0.025 - 0.050 (0.030) *32 %*
Floodplain 2	-	0.050 - 0.200 (0.140) *16 %*	0.020 - 0.050 (0.030) *34 %*
Floodplain 3	-	-	0.035 - 0.080 (0.040) *6 %*
Floodplain 4	-	-	0.050 - 0.200 (0.100) *9 %*
Floodplain 5	-	-	0.050 - 0.200 (0.100) *7 %*
Number Runs	150	250	500

Roughness in the $2D$ floodplain domain can be applied to the same resolution as the digital terrain model itself, thus allowing easy change between different levels of floodplain roughness heterogeneity. Three levels of dis-aggregation were considered in using the distributed land use data (see Figure 8.1). In the first level, a single, uniform floodplain roughness was considered. For the second level the floodplain roughness was considered in two main groups, (i) high roughness stiff land-use types (urban and woodlands) (ii) and lower roughness flexible land-use types (cultivated fields, pastures, grasslands, and weeds). In the final level of dis-aggregation the main land-use types in the reach were considered individually. The last three columns in table 8.1 indicate how the land-use types were aggregated. Prior ranges of Mannings-n roughness were selected for each aggregate class based on the constituent land-use types as given in *Chow* (1959) and table 8.3, with some relaxation on the limits of the main channel roughness as good model performance was found at values tending towards the suggested minimum.

8.3.2 Evaluating model performance

The four datasets available for evaluating model performance are of two distinct types. The flood extent map data from the air survey and SAR image are essentially spatially distributed binary classification data (*Aronica et al.* 2002). Comparison of modelled flood extent data against the observed flood extent is achieved by comparing the area correctly classified as wet or dry against the area incorrectly classified. Here the $F^{<2>}$ statistic previously used by *Aronica et al.* (2002) is used:

$$F^{<2>} = \frac{A^{obs} \bigcap A^{mod}}{A^{obs} \bigcup A^{mod}} \tag{8.1}$$

where A^{obs} is the observed area of inundation and A^{mod} the modelled area of inundation. In effect the statistic determines the ratio between the number of grid

cells classified correctly as being either dry or wet and the number of cells classified incorrectly. Equation 8.1 can then be reformulated as

$$F^{<2>} = \frac{\sum_{i=1}^{n} P_i^{D1M1}}{\sum_{i=1}^{n} P_i^{D1M1} + \sum_{i=1}^{n} P_i^{D1M0} + \sum_{i=1}^{n} P_i^{D0M1}} \tag{8.2}$$

where P_i^{D1M1} obtains a value of 1 for cells classified as inundated both in observed and modelled data, P_i^{D0M1} obtains a value of 1 for cells observed as dry but predicted to be wet, and P_i^{D1M0} obtains a value of 1 cells observed as wet but classified as dry. Following *Hunter et al.* (2003) the measure is amended to additionally penalise over-prediction of the flood extent:

$$F^{<2>} = \frac{\sum_{i=1}^{n} P_i^{D1M1} - \sum_{i=1}^{n} P_i^{D0M1}}{\sum_{i=1}^{n} P_i^{D1M1} + \sum_{i=1}^{n} P_i^{D1M0} + \sum_{i=1}^{n} P_i^{D0M1}} \tag{8.3}$$

Comparison of flood extent with the air photo was restricted to the reach for which it is available (Borgharen-Dorp to Elsloo), while for the SAR image comparison was limited to upstream of the narrow floodplain section directly between Grevenbricht and Elsloo to minimise the effects of the imposed downstream boundary levels on the results.

Attenuation in the reach during the 1995 event is limited due to the elongated nature of the hydrograph, and differences in calculated levels at these gauges between model runs is primarily in the form of a negative or positive bias. Errors in the time series are therefore highly correlated in time, making some of the more widely used objective functions such as the Nash-Sutcliffe model efficiency unsuitable as these assume errors are normally distributed with zero mean and constant variance (*Beven and Freer* 2001). To account for autocorrelation of errors and possible changing variance the Heteroscedastic Maximum Likelihood Estimator (HMLE) measure (*Sorooshian and Dracup* 1980; *Gupta et al.* 1998) was used in comparing observed and calculated levels at gauges;

$$HMLE = \frac{\frac{1}{n}\sum_{t=1}^{n} w_t(\hat{h}_t(\theta, Y) - h_t)^2}{\left[\prod_{t=1}^{n} w_t\right]^{1/n}} \tag{8.4}$$

where h_t is the observed level at time t and $\hat{h}_t(\theta, Y)$ the calculated level given parameters θ and data Y. The weights w_t assigned to time t are computed as $w_t = h_t^{2(\lambda-1)}$, where λ is an unknown transformation factor to stabilise the variance. λ is estimated iteratively for each observed and calculated series compared (see *Sorooshian et al.* (1993) for a complete description of the procedure used here). The HMLE measure was derived primarily for comparing computed against observed discharge series, and the more or less constant bias of the level series with reference to the absolute datum was found to make the estimation procedure of λ instable. To increase stability both observed and calculated levels were first transformed to a local datum at each gauge. This transformation was found to have negligible effect on the resulting HMLE values.

The distributed floodplain observation points are compared using the Mean Absolute Error measure:

$$MAE = \frac{\sum_{k=1}^{m} |\hat{h}_k(\theta, Y) - h_k|}{n} \tag{8.5}$$

where $\hat{h}_k(\theta, Y)$ is the calculated level at point k, h_k is the observed level and m the number of points used. Similar to model comparison using the SAR image, points directly upstream of Grevenbricht were not included in the comparison as these were again considered too close to the downstream boundary, resulting in a total of 31 points being used in the comparison. For lower roughness parameter sets, model results did not predict flooding at all of these points. Where this occurred the level of the DEM cell in which the point falls is used in the comparison. Although this imposes an upper bound on the MAE measure, it implicitly allows for discrepancies between the DEM and the actual terrain (*Hunter et al.* 2003).

8.3.3 Sensitivity analysis

Sensitivity analysis is a widely used tool in modelling to determine how the variation in model performance can be apportioned to different parameters (*Crosetto et al.* 2000). Here a univariate sensitivity analysis was applied, where response of model performance due to variation in parameter values was determined for parameters individually, and interaction between parameters was ignored.

For each of the three levels of floodplain roughness aggregation, an "optimal" set of parameters was selected such that good performance in terms of the selected objective functions was found. Where different objective functions gave good results in different parts of the parameter space, the parameter set was selected with a preference of good performance in comparing levels predicted at the gauges, as the gauged levels are considered of higher reliability than the two flood extent observations. The values of these "optimal" parameter sets are given in brackets in table 8.3. In the subsequent sensitivity analysis one parameter was varied across its range in 10 to 15 increments, while the remaining parameters were kept at the "optimal" values. For each variation, the model was run and resulting performance against the four types of calibration data evaluated.

8.3.4 Uncertainty analysis

To elaborate on the sensitivity analysis where the influence of individual parameters on model performance was explored, an uncertainty analysis was undertaken. The uncertainty analysis is set within the context of the generalised likelihood uncertainty estimation method (GLUE, see *Beven and Binley* (1992) and chapter 4). This helps establish the effect uncertainty in individual parameters has on uncertainty of model predictions, while considering interaction between parameters. It also provides useful information on the value of the different types of calibration data in constraining these uncertainties (*Freer et al.* 1996). In this Monte-Carlo based technique an ensemble of parameter sets is sampled from prior distributions of the constituent parameters and the model is run with each set. The acceptability of each run is assessed by comparing the predicted with the observed values using a chosen likelihood measure (*Aronica et al.* 2002), where the likelihood measure

is obtained here using one or more of the selected objective functions. Likelihood measures derived using different objective functions can be easily combined analogous to combining likelihood values from different data sets through application of Bayesian updating (*Lamb et al.* 1998; *Franks et al.* 1998),

$$L(\theta_i \mid Y) = \frac{L_1(Y \mid \theta_i) L_0(\theta_i)}{\sum_{j=1}^{N} L_1(Y \mid \theta_j) L_0(\theta_j)} \tag{8.6}$$

where $L_0(\theta_i)$ is the prior likelihood measure for parameter set θ_i, $L_1(Y \mid \theta_i)$ is the likelihood measure derived by comparing model output using parameter set θ to observations Y using a selected objective function, $L_1(\theta_i \mid Y)$ is the posterior likelihood of parameter set θ_i given observations Y, and N is the number of parameter sets. Optionally, a behavioural threshold can be applied to divide runs with acceptable performance from those with unacceptable performance (*Beven and Binley* 1992). Parameter sets that perform below the threshold in the selected objective function are then given a likelihood of zero and likelihood values for the remaining sets are re-scaled.

8.4 Results

8.4.1 Sensitivity Analysis

Figure 8.3 shows the values of the $HMLE$, MAE, and $F^{<2>}$ measures for sensitivity tests for the main channel and a single floodplain roughness class (see Table 8.3 for parameter ranges and default parameters). Comparison of observed to calculated levels at the gauges of Borgharen-Dorp and Elsloo using the $HMLE$ measure shows clear sensitivity to both main channel and floodplain roughness. Values for the gauge at Elsloo are more sensitive to main channel roughness than Borgharen-Dorp, while for floodplain roughness this is reversed. This different response is due to the location of each of the gauges. Elsloo is upstream of a large bend in the river with the floodplain narrowing, making main channel flow more dominant, while Borgharen-Dorp is upstream of a relatively wide floodplain, with floodplain flow gaining in importance. The sensitivity of the distributed floodplain observations (MAE measure) again shows a very similar pattern. The best simulations from all three gauge level comparisons are in the same region of the roughness ranges. This range tends to the minimum of the selected prior roughness values. Although this would suggest this minimum roughness has been selected at too high a value, a lower value for floodplain roughness was not selected as this was considered physically unrealistic when compared against tables of suitable roughness values found in literature.

A similar pattern is shown in the response of the binary flood map comparison expressed by the $F^{<2>}$ measure. Even at low roughness values, the floodplain is filled completely, with flood extent bounded by the steep walls of the flood defence dykes to the west and the canal to the east. This is particularly so for the reach upstream of Elsloo, and as the air photo covers only this reach the $F^{<2>}$ measure remains fairly constant with increasing roughness. For comparison with the SAR

image performance improves with increasing roughness to show an optimum in the same region as the comparisons for the level data. Both measures start to decline, however, with a further increase in roughness. This decline is easily explained when the individual flood maps are studied. These show that as the levels increase, dykes in some sections start to overtop, and as the $F^{<2>}$ measure introduced in equation 8.3 penalises for over-prediction, this causes the measure to drop. This decline is somewhat erratic for the SAR image because of the patchy nature of the SAR shoreline towards the downstream end of the reach (Figure 8.1) As dyke thresholds overtop, some of these patches are predicted as being inundated, therefore increasing performance. A further increase leads again to over-prediction and a drop in performance.

Increasing the dis-aggregation of roughness values to two classes gave a very similar response for sensitivity to main channel roughness and is not shown here. Sensitivity to the first floodplain roughness class (dominant pastures and fields) is lower when compared to the single floodplain class, but zooming in on Figure 8.3b using the same floodplain roughness range as in Figure 8.4a reveals the response to be very similar. Sensitivity to the second roughness class (Figure 8.4b) is absent, with performance for all measures being the same for all roughness values. A further dis-aggregation to five floodplain roughness classes results in negligible sensitivity in any of the roughness classes within the ranges specified for each class (Figure 8.5).

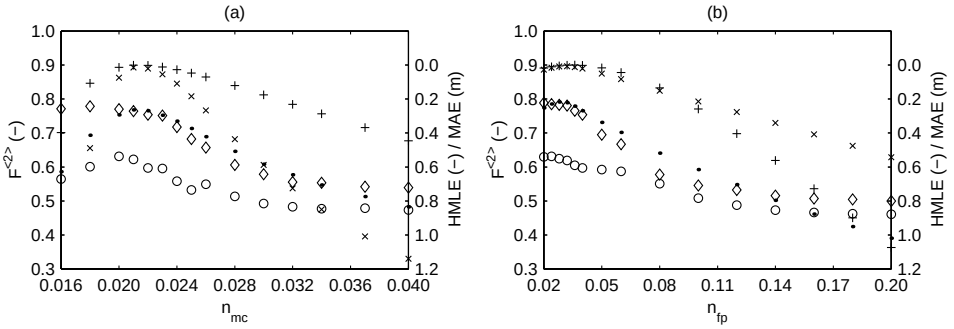


Figure 8.3: Sensitivity analysis for single floodplain roughness class (a) Main channel roughness (b) Floodplain roughness. + and × are the $HMLE$ values for Borgharen-Dorp and Elsloo respectively, • are the MAE results for the distributed floodplain points, ○ and ◇ are the $F^{<2>}$ results for comparison with the SAR image and the Air survey respectively.

8.4.2 GLUE Analysis

In the GLUE analysis parameter sets were sampled from the prior distributions. The sample sizes were set to 100 runs for models using a single floodplain roughness class, 250 runs for models using two floodplain roughness classes, and 500 runs for models with five floodplain roughness classes. For each of the parameter sets sampled, likelihood values were established using all four of the available calibration data types. This was through successive application of equation 8.5, with the

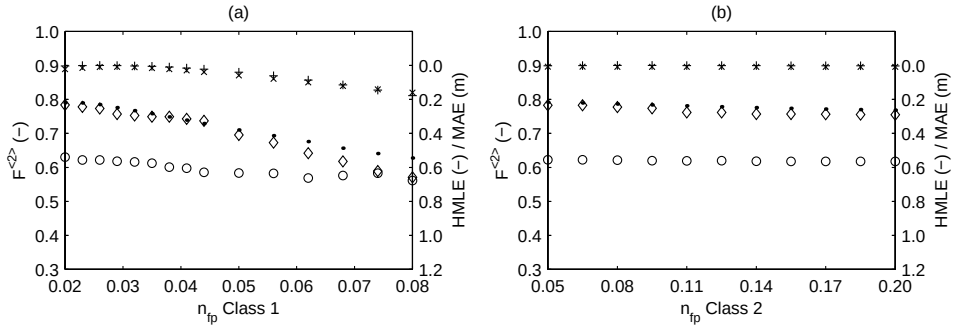


Figure 8.4: Sensitivity analysis for two floodplain roughness classes. See Figure 8.3 for legend.

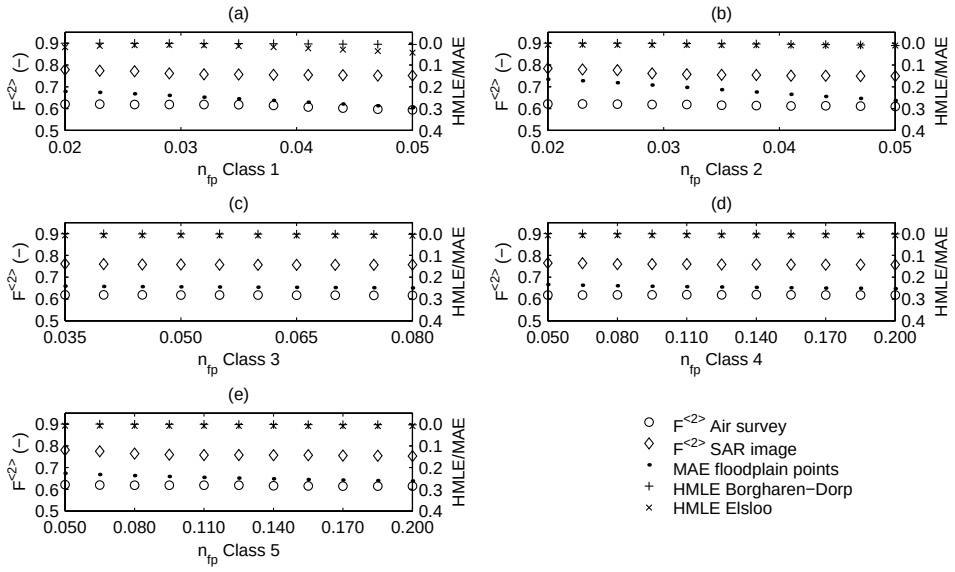


Figure 8.5: Sensitivity analysis for five floodplain roughness classes. See Figure 8.3 for legend.

sequence being (i) comparison of levels at gauges, (ii) comparison of flood extent to airphoto, (iii) comparison of flood extent to SAR image, and finally (iv) comparison of levels at distributed floodplain points. Resulting likelihood values for each parameter set are given in dotty plots in Figures 8.6 to 8.8. These plots show the likelihood value of each individual parameter set in the (multi-dimensional) parameter response surfaces as projected onto a single parameter axes, and although these reveal little explicit detail of parameter interaction (*Blazkova et al.* 2002a), they do show the spread of fit and resulting likelihood value across the parameter range. The vertical spread of likelihood values can also be used to infer parameter interaction, as is clearly seen in Figures 8.6 and 8.7. The main channel roughness shows high likelihood values in the same region as would be expected from the sensitivity analysis. However, some runs with the same main channel roughness show low likelihoods indicating significant interaction with the floodplain roughness. For very low main channel roughnesses this interaction is smaller, which is intuitively correct as flow would be more in-bank for these low roughness values.

As the number of floodplain roughness classes increase, the interaction between main channel roughness and floodplain roughness seems to be less (Figure 8.7 and Figure 8.8). With the increase in floodplain roughness classes, good model fits can be seen across the prior parameter ranges, reflecting the decrease in sensitivity of model performance to these parameters. Figures 8.9 to 8.11 show that for a single floodplain roughness class the marginal posterior distribution is well constrained when compared to the uniform prior (horizontal line) for both main channel and floodplain roughness. This holds equally for the main channel roughness with two floodplain roughness classes, but the posterior distribution of the first roughness class is constrained only slightly, while for the second class no improvement on the prior is made. With five floodplain roughness classes some improvement on the prior range is shown only for the first floodplain roughness class, confirming the results of the sensitivity analysis.

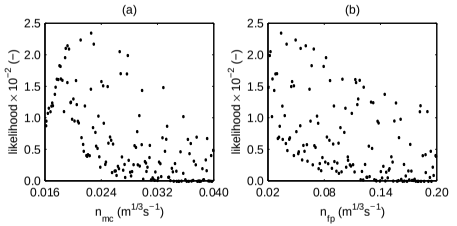


Figure 8.6: Dotty plots for single floodplain roughness class. (a) main channel (b) floodplain.

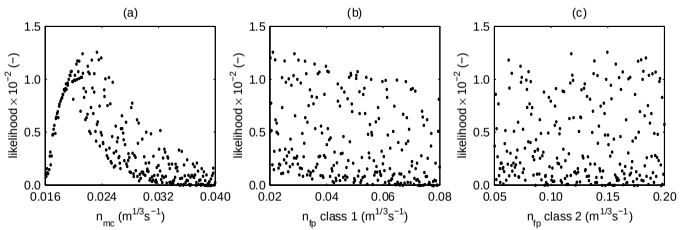


Figure 8.7: Dotty plots for two floodplain roughness classes. (a) main channel, (b-c) floodplain.

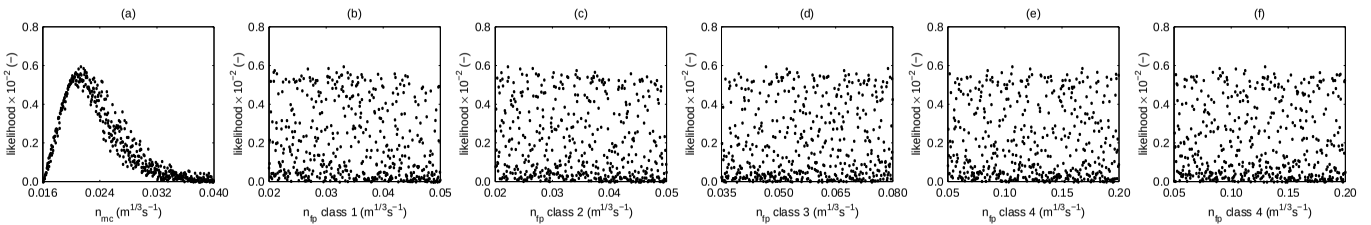


Figure 8.8: Dotty plots for five floodplain roughness classes. (a) main channel, (b-f) floodplain.

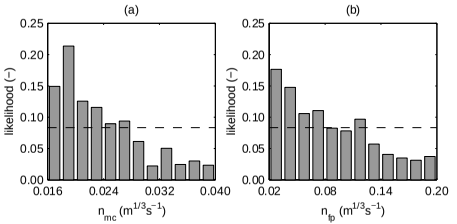


Figure 8.9: Posterior parameter distributions for single floodplain roughness class. (a) main channel (b) floodplain.

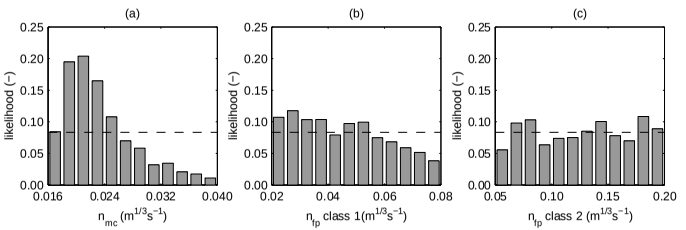


Figure 8.10: Posterior parameter distributions for two floodplain roughness classes. (a) main channel, (b-c) floodplain.

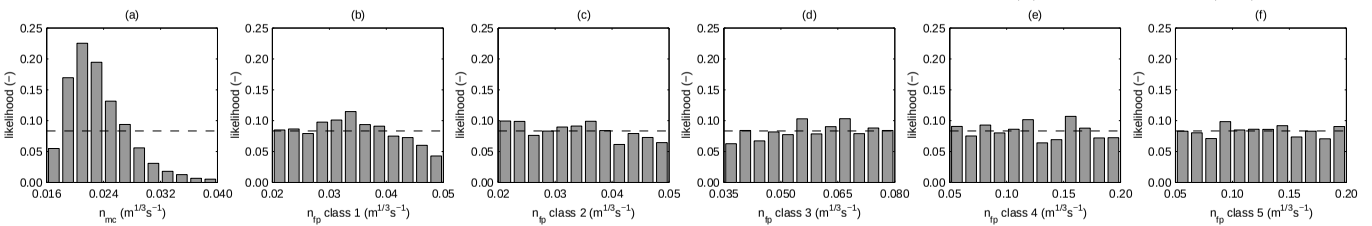


Figure 8.11: Posterior parameter distributions for five floodplain roughness classes. (a) main channel, (b-f) floodplain.

To explore the consequence of introducing a behavioural threshold on posterior roughness distributions (*Beven and Binley* 1992), the top performing 20% runs for each level of roughness aggregation are selected and the remaining 80% discarded. Although this threshold is arbitrary, and would more appropriately be defined on the basis of explicit criteria in view of the model's application, the selection serves the purpose of illustration. Figure 8.12 shows the full range of values for each parameter in the preserved parameter sets, when compared to the prior range. This again shows that the ranges are constrained considerably for the main channel and perhaps the first floodplain roughness class. This holds for the first roughness with two floodplain roughness classes, while for the remaining floodplain roughness classes, parameter sets with values almost across the full prior range are retained.

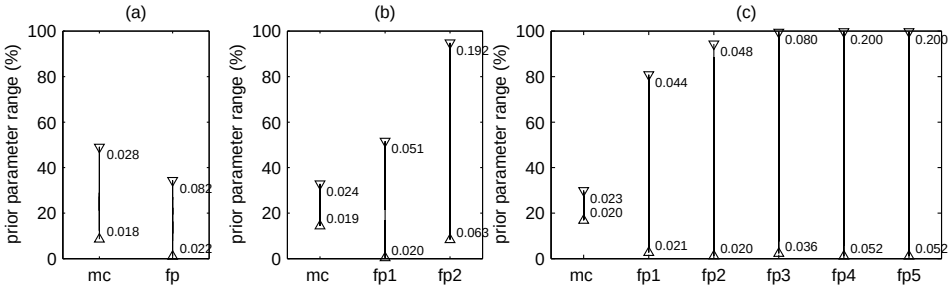


Figure 8.12: Constrained parameter ranges after applying threshold (a) single, (b) two, and (c) three floodplain roughness class(es).

8.5 Discussion

8.5.1 Impact of floodplain roughness aggregation on model performance

For the four different types of observations used in constraining roughness distributions in both main channel and floodplain, comparison of the best performing parameter set of those sampled shows, that for none of these a clear improvement in performance is achieved with increasing floodplain roughness dis-aggregation. This would suggest for the model used to simulate the given event in this reach, even the comprehensive data-set available here still does not provide sufficient detail on the distributed nature of floodplain flow, and can only be used as a descriptor of bulk flow at the reach scale.

To evaluate the value of updating likelihood weights using each of the available data sets the Shannon Entropy measure H (*Beven and Binley* 1992; *Franks et al.* 1998) was calculated, where a lower entropy value indicates more structure and therefore less uncertainty.

$$H = -\sum_{i} L(\theta_i) log_2 L(\theta_i) \tag{8.7}$$

where i is the model realisation index. As noted in chapter 7 the value is a discrete summation, with the number of realisations to be taken into account when comparing entropy values between simulations, making such comparison difficult. The entropy value is again used to compare the value of calibration data sets in lowering entropy values for simulations with the same number of model realisations. Table 8.4 shows the resulting values of H, and although the absolute changes are modest, relative changes show the value of the gauge data and the distributed floodplain points to be greatest. The relative reduction of entropy using all the data is 90.7%, 92.2% and 92.5% for a single, two and five floodplain roughness classes respectively, but the differences are too small to suggest an increase of total overall uncertainty with increasingly complex parameterisation.

Table 8.4: Shannon-Entropy measure.

likelihoods after updating using data type	single class (150 runs) H	two classes (250 runs) H	five classes (500 runs) H
Uniform prior	7.229	7.966	8.966
Gauges	6.936	7.722	8.709
SAR Image	6.860	7.646	8.633
Air survey	6.787	7.574	8.570
Floodplain points	6.556	7.346	8.294

Reduction of the Shannon's entropy index for comparison of the flood maps is found to be very sensitive to how the binary comparison is evaluated. The values in table 8.4 have been derived using the formulation as in Equation 8.3, where over-prediction of flood extent is penalised (*Hunter et al.* 2003). If the original formulation of *Aronica et al.* (2002) is used (equation 8.2) then discrimination between runs is much less pronounced and as a consequence reduction in Shannon's entropy is minimal. Amending the $F^{<2>}$ measure to additionally penalise under-prediction by adding P_i^{D1M0} to the numerator of equation 8.3 results in runs where the area behind the dykes is inundated being assigned higher likelihood, while for low roughness parameter sets where sections of the floodplain between the dykes remain dry obtain low likelihood values. As a consequence, good performing parameter sets for this measure shift to the rougher part of the friction parameter space, resulting in Shannon's Entropy value increasing rather than decreasing on updating likelihoods using the floodmaps after the gauge data. This confirms that optima for different objective functions may result in different parameter optima (*Gupta et al.* 1998), and illustrates the impact of selecting even small variations in objective function on calibration results.

8.5.2 Identifiability of distributed floodplain roughness

Both the sensitivity analysis and the results of the GLUE method show the identifiability of distributed floodplain roughness to be relatively low. In a number of other studies, where a single floodplain roughness is used, low sensitivity to floodplain roughness values has been shown (*Romanowicz et al.* 1996; *Horritt and Bates* 2001a), but this is not a conclusion universally applicable. More significant sensitivity to floodplain roughness for a similar reach has been shown (*Horritt* 2000), as well as in more two-dimensional polder type inundation events (*Aronica et al.* 2002; *Hesselink et al.* 2003). Floodplain friction sensitivity would be expected to be linearly proportional to the area inundated and non-linearly proportional to the velocity ($c_D \simeq v^2$), therefore having a strong relationship with how dominant floodplain flow is for the reach. The complex topography of natural floodplains will, therefore, have a dominant effect on the contribution of the floodplain to conveyance of flow as opposed to a storage element with impact only on flood wave attenuation. This topography also strongly influences sensitivity to different likelihood measures, as seen in the case here where the embankments strongly influence flood extent, with resulting sensitivity to comparison of flood extent maps being low. Besides the characteristics of the reach, however, the model code used also has an influence on the sensitivity. Cell-inundation type codes show lower sensitivity than finite element codes (*Horritt and Bates* 2001a). Indeed a model of the same reach of the Meuse river with a cell inundation code shows very low sensitivity to floodplain roughness (*Hunter et al.* 2003).

For the code used here, sensitivity to floodplain roughness for the single floodplain class is very apparent, but this sensitivity is dominated by the selection of the prior roughness range. This has been selected to be quite wide to reflect the full range of the constituent land use types. However, the posterior range of roughness values showing good results complies more or less with the prior that would be selected had only dominant land use type been considered. Establishing a more precise roughness value even for these dominant land-use types than the suggested range given in tables from literature is, however, shown to be difficult. The correlation between roughness values of each roughness class and resulting parameter set likelihood values is given in table 8.5. As would be expected the main channel roughness parameter shows good correlation with the likelihood values for all cases. Although low, some correlation is found for the dominant land use types at higher levels of heterogeneity, but what is surprising is the low influence of the roughness class in which the urban areas are incorporated (last class for both two and five floodplain roughness classes). Some 9% of the reach is urban, and although these are slightly elevated when compared to the surrounding floodplain, the position with respect to the flow direction (see figure 8.1) would be expected to influence results more, but the results imply the influence to be too little to have distinctive influence on the bulk roughness characteristics of the whole reach.

The dotty plots in figures 8.6 to 8.8 show that the effective main channel roughness becomes increasingly well defined as the number of floodplain roughness classes increase. This is in contrast to the apparent identifiability of the floodplain roughness values with the increase in heterogeneity, which at five floodplain roughness

classes show almost similar performance across the full range of prior roughness values. Although this effect is counter-intuitive, it may be explained by looking closely at the ranges of the roughness classes in relation to how dominant the particular class is in determining bulk roughness values at the reach scale. In the case of only one roughness value in the floodplain the prior range is chosen to be relatively wide. The constrained distribution shows a tendency to the lower roughness values, being in the range that would have been selected for the dominant land use types. The spread in the main channel roughness can be explained by effective main channel roughness values compensating for badly selected floodplain roughness values, and still giving reasonable performance. In the case of five floodplain roughness classes the ranges of roughness values for the dominant land use classes are much smaller. Within these ranges there is too little information content in the calibration data to constrain the values further than the prior range, but there is little room left for compensating ill chosen roughness values on the floodplain with channel parameters, therefore leaving the effective main channel roughness values better defined.

Table 8.5: Correlation between parameter values and likelihoods.

Parameter	single class	Two classes	Five classes
n_{mc}	0.660	0.720	0.724
n_{fp} class 1	0.537	0.297	0.140
n_{fp} class 2		0.058	0.109
n_{fp} class 3			0.077
n_{fp} class 4			0.032
n_{fp} class 5			0.011

The cell-inundation code used by *Hunter et al.* (2003) for the same reach also shows posterior main channel roughness values to be higher than those found here, while resulting model performance is comparable. In that code, however, no account is taken of turbulent momentum exchange between main channel and floodplain. The code used here also does not take this explicitly into account, but the non-zero shear interface between main channel and floodplain acts as a proxy turbulence model. The comparable performance confirms that calibrated roughness factors describe not only momentum loss due to resistance of flow to vegetation, but also incorporate all other turbulent momentum losses not explicitly described. As such, roughness factors cannot be seen as being independent of the layout and sinuosity of floodplain and main channel, the position of land-use types with respect to floodplain flow, and the resolution with which the complex topography is represented. Although the model used here solves the full shallow water equations, assumptions made in modelling the turbulent interaction between floodplain and main channel impact the relative roughness sensitivities, and the results found would need to confirmed through application of a full 2D depth averaged code with explicit accounting of turbulence. A comparison of depth averaged velocities across the floodplain in such

a code to laboratory observations by *Wilson et al.* (2002), however, shows this may be poor even in such complex codes, and calibrated roughness factors remain bulk representations of momentum dissipation.

8.6 Conclusions

This chapter shows that despite a very comprehensive calibration dataset being available, the utility of this data in constraining distributed floodplain roughness parameters is relatively low. Although the sensitivity to floodplain roughness is shown to be reasonable when only a single floodplain roughness class is used, the constrained range of values giving good model performance is found to be in the order of the range of roughness values for the dominant land-use type as given in tables from literature (cf. *Chow* 1959). Applying the values from literature to distributed land use types is not found to increase model performance, nor does the calibration data constrain the suggested ranges. A positive view of this result would be that to calibrate models for floodplain inundation such as used here attention need only be given to the main channel roughness values, while those on the floodplain can be set somewhere in the suggested range. Evaluating the effect of floodplain land-use change could then follow the same procedure, while keeping the main channel roughness to the value calibrated. The interaction between main channel and floodplain as seen in the reach studied here, however, suggests that independent treatment is flawed.

The problem of this limited ability to identify more precise distributed roughness values stems from these roughness values being more than simply the effect of floodplain vegetation on flow, but the bulk effect of turbulent momentum interaction between main channel and floodplain, discrepancies in elevation data, crossing flows, and all other momentum losses not explicitly accounted for in the model code. The relative contribution of these and vegetation roughness to the bulk roughness values is unfortunately not clear, nor is the combination linear. To compound the problem, effective roughness values for the individual floodplain land use type may be influenced by backwater effects from adjacent, rougher land use types. The calibrated values of main channel roughness are, moreover, not independent of the roughness values in the floodplain. The balance of these contributions may also shift if one contributor is changed, and as such evaluating the effect of land-use change by simply amending the roughness due to vegetation is not as straightforward as it would seem. In this light the utility of complex formulations of roughness with parameterised vegetation characteristics (cf. *Klopstra et al.* 1997) would seem limited, and estimations using the well established tables would suffice.

The low sensitivity to roughness values for land use types other than the dominant land use would suggest that changing these will have little impact on the bulk roughness characteristics of the reach, given the uncertainty in the value of the roughness for the dominant land use type. Changing the dominant land use type would on the other hand lead to a change in bulk roughness characteristics, but this change may not be due to change in roughness of the individual land use type alone. It would rather reflect a change in the balance of roughness values

across different land use types, resulting in a different pattern of floodplain storage, conveyance and backwater effects.

To substantiate the results found for the reach studied here with the selected model code, these conclusions will need to be assessed with a full 2D model code including explicit turbulence modelling, despite the added computational burden this will bring. The results do suggest that evaluation in a probabilistic setting would help, but the problem of independence of roughness values for distributed land use types would need to be tackled before these can be independently changed.

Acknowledgements

The authors wish to thank the Dutch Ministry of Public Works and Water Resources; Directie Limburg and the Institute for Inland Water Management and Waste Water Treatment (RIZA), for providing both the hydrological and topographic data, as well as the air photo. Ad de Roo of the Institute of Environment and Sustainability, European Union Joint Research Centre (Ispra, Italy) is thanked for giving kind permission to use the SAR Image.

9

Summary and Conclusions

9.1 Introduction

In this thesis, the integration of hydrological models and geographical information systems (GIS) is approached on the basis of performance. While performance is often seen as describing only the computational efficiency with which a solution can be found, a broader view on performance is taken here. Three aspects are considered; (i) the computational efficiency, (ii) the flexibility of application, and, (iii) the reliability of the integrated model.

The second aspect is determined by the level of integration of the model with GIS, as GIS is fast becoming the dominant tool for storing, analyzing and manipulating spatial data used in modelling. To allow integration with GIS, three main concepts are distinguished; (i) the loosely coupled approach where the model and GIS database remain disparate, with data exchanged between the two using files, (ii) the tightly coupled approach where the data structure is shared by the model and the GIS but with the two systems remaining separate, and (iii) the tightly coupled approach where the model is embedded within the GIS. Flexibility increases with these levels of integration, but in order to achieve the highest level in the embedded approach, assumptions will need to be made on how spatial and temporal variability are described. Similarly, these assumptions relate to the aspect of computational speed as this is determined largely by the numerical approach taken. Both the first and second aspect are therefore closely related to the selected model concept.

The third aspect of performance considers how reliably the model can be applied in making predictions with the model. Reliability is seen synonymously with predictive uncertainty, as large predictive uncertainties imply low reliability. Predictive model uncertainties result from a number of uncertain sources, including uncertainties in spatial data used to establish the model structure, uncertainties in boundary conditions, and uncertainties in model parameterisation. The influence of uncertainties in model parameterisation and structure on performance are the focus in this thesis.

Performance is addressed for the field of flood extent modelling at the river reach scale only. This is by nature spatial, and integration with GIS is therefore not only obvious, it additionally allows flood extent estimation to be easily integrated within the broader scope of spatial flood risk assessment. A variety of different hydrodynamic codes is available for flood extent estimation, and these may be integrated with GIS using either the loosely coupled principle or through the tightly coupled shared data model, but preclude embedding in GIS due to the requirement

of implicit time integration. A simpler cell-inundation code is also discussed, that allows full embedding with GIS as a consequence of assumptions made on the properties of flow. Each of the selected codes can be applied equally in deriving flood extent.

9.2 Summary of research results

9.2.1 Hydraulic assessment of codes for predicting flood extent

To establish reliability of codes suitable for modelling flood extent at the river reach scale, four selected codes were compared against methods used to estimate discharge in compound channels derived from experimental results. The codes include; (i) a one–dimensional hydrodynamic code; (ii) a two dimensional hydrodynamic code using a structured grid for representing floodplain and main channel topography; (iii) a hybrid hydrodynamic code describing channel flow in one dimension and overbank flow in two dimensions, and (iv) a similarly hybrid code, but using a much simpler description of main channel flow given by the diffusive wave approximation and floodplain flow given by the cell inundation method.

For straight planform channels, the most widely used method for estimating conveyance is the vertical divided channel method. This is, however, acknowledged to over-predict discharges in the order of $5-10\%$. This over prediction is due mainly to turbulent momentum interchange between the individual sections not being considered, and methods where this is taken into account show better comparison to experimental results.

In all codes except the hybrid hydrodynamic code, cross section conveyance is similarly described in a number of sections, and the total discharge is given as the sum of the individual sections. The codes are shown to over predict discharge in the same order as the vertical divided channel method, or higher still where the numerical solution follows the non-conservative momentum equation. In the hybrid code, the division between the main channel and floodplain flow domains is not assumed to be shear free. This gives a somewhat conceptual approach to describing additional momentum exchange, and overbank discharges compare better to those found using experimentally derived relationships.

For channels using the meandering planform, over-prediction using the traditional divided channel methods may be as high as 30%, as additional momentum exchange due to crossing flows is not explicitly accounted for. The one-dimensional and simple cell inundation codes again reproduced this degree of over-prediction, whereas the hybrid code reduced over-prediction due to the non zero shear interface. In the code describing the main channel using a structured grid, main channel conveyance was severely underestimated, proving this code to be unsuitable in reaches where channel flow dominates conveyance.

In applying any of the codes to real river reaches, roughness values would be calibrated such that conveyance is adequately described. The implication of not explicitly accounting for turbulent momentum interaction and crossing flows is that these calibrated roughness values no longer represent energy loss due only to bed friction, but are compound values of all contributing processes. For smooth, straight

channels these additional losses are limited. Bed roughness is then dominant, but increases as turbulent momentum exchange and crossing flows increase through rougher floodplains, floodplain inclination and channel sinuosity. The compound nature of calibrated roughness values, even when turbulence is explicitly modelled, means reliable application of hydrodynamic models is not possible without sufficient calibration and verification.

9.2.2 Predictive uncertainties in flood extent models

Flood extent estimation often requires models to be applied to design events greater in magnitude than those recorded and used in model calibration. Three of the selected codes were calibrated using data from a series of low flood events and compared in validation against data from a high flood event. Results indicate that while the codes compare equally in calibration, maximum stages may for some codes be severely under-predicted in extrapolation.

The three codes were applied in modelling flood extent for a $17km$ reach of the Saar River in Germany. This reach contains a wide floodplain frequently subject to flooding, with a motorway running through it acting as a constraint on the flood extent. River gauges are located at the upstream and downstream end of the reach, providing the only observed data sources for model calibration. As a result of the limited data, models using each of the three codes are shown to allow reasonable calibration, given a suitable elevation model. Calibration of roughness values for the main channel and floodplain in the reach was set in the context of the generalised likelihood uncertainty estimation method (GLUE), a probabilistic method that allows the value of data in constraining parameter uncertainties to be explicitly explored. Datasets for four flood events were used. Two of these are relatively small events in the order of $500 - 600m^3/s$, with limited overbank flow. A third is a medium sized event of about $950m^s$ with an estimated return period of ten years. The last event, from December 1993, is the largest on record at the gauge, peaking at $1271m^3/s$.

When all four events were used in calibration, the 50-percentile peak level for the December 1993 event at the upstream gauges in both the one-dimensional and full two dimensional model was found to be only $0.2 - 0.4m$ under the observed peak, while in the hybrid model this was just $0.05m$ over the observed peak. For all three models, the 90 % uncertainty bound was in the range of $0.90m$. This changed significantly when the December 1993 event was not used in constraining parameter distributions, and the models were applied to that event in pure predictive mode. As would be expected, the code using a structured grid to model both main channel and floodplain flow was shown to be inadequate, under-predicting the observed peak by about $1m$. In the one-dimensional model the peak was again under-predicted, now by about $0.40m$, while the hybrid code was found the most reliable, with a $0.05m$ over-prediction. The 90 % uncertainty bound, however, increased to the order of $1.15m$. Posterior parameter ranges in the hybrid model were quite stable, being located in the same area of the parameter space for different events.

These results clearly indicate the care that needs to be taken in extrapolating model predictions beyond the range of events used in calibration. Such extrapo-

lation is, however, commonplace in flood risk assessment, where flood envelopes often need to be determined for events with return periods well beyond the range of events observed. Uncertainties in the flood extent and levels due to uncertain parameters and differing model structures are shown to be considerable, and may be in the same order as uncertainties in establishing the design discharge itself.

9.2.3 Utility of spatially distributed observations

To establish how spatially distributed observations can be used in constraining predictive uncertainties, the value of distributed level observations was compared against the value of observed flood extent data. The distributed level data proved to be much more informative, with the observed flood extent being of relatively little value as flood extent is constrained by road and railway embankments in the floodplain.

For a short, urban, reach of the Orlice river in the Czech Republic, two sources of spatial observation data on the extent of flooding are available from the July 1997 flood event. These include the extent of flooding, as well as 26 level observations, giving an indication of the distributed flood depths in the floodplain. The reach is urban in nature and the floodplain is characterised by infrastructure such as railways and roads, often on elevated embankments. The reach was modelled using both the full one dimensional hydrodynamic code, and the hybrid one-dimensional/two-dimensional code. The GLUE method was again applied to allow the value of the different sets of calibration data to be made explicit. Both codes were shown to be equally reliable in predicting the extent of flooding, but the hybrid model gave better prediction of the distributed flood depths. Posterior roughness values for the hybrid code were, moreover, in the part of the parameter space that would be expected for the type of reach, while those in the one-dimensional code were in regions of higher roughness.

The error in the elevation data used in the reach is estimated to a standard deviation in the order of $0.35m$. The influence of these uncertainties in predicting flood extent were, however, shown to be small. For the distributed flood depth predictions from the hybrid model, the impact of these uncertainties were found to be larger than in the one-dimensional model. This would suggest that availability of high resolution elevation models is only of added value where floodplain flow is modelled in two dimensions, and distributed depth observations are available. Lacking these distributed data, reliability of the one dimensional and hybrid models would have been found comparable on the basis of calibrating using the flood extent data alone.

When the value of the two data sources in constraining roughness distribution are considered, it is clear that the flood extent data have a lower information content than the distributed depth observations. Although this could have been expected as the extent of flooding is constrained mainly by infrastructure embankments and the steep valley sides, such constraints will often be found in urban or semi-urban reaches, with reaches of this type being the most relevant in flood risk assessment. These results show that reliability in flood extent prediction could be improved if observations during events were concentrated on gathering distributed levels and

depths on the floodplain, rather than establishing maximum flood extent maps. Footage from extensive media coverage of flood events in urbanised areas could even be used in post event analysis for establishing such distributed level observations.

9.2.4 Utility of distributed roughness data

In both previous applications, roughness values were defined uniformly across the floodplain. A distributed definition of roughness could potentially contribute to the reliability for flood prediction, and sensitivity to defining roughness values at different levels of heterogeneity was investigated. It was found that as the heterogeneity increased, identifiability of roughness values decreased. With these values becoming less certain, evaluating the effect of floodplain land use change through simply amending roughness on the basis of the changed land use would seem unreliable.

The hybrid one-dimensional/two-dimensional code was applied to a $30km$ reach of the Meuse River, just downstream of the town of Maastricht in the Netherlands. A comprehensive calibration data set is available for the January 1995 flood event, including levels at three gauges in the reach (with one gauge internal to the model domain), one observation of flood extent taken from a satellite image, one observation of flood extent taken from an aerial photograph, and a large number of flood level observations distributed in the floodplain. A detailed GIS database of floodplain land use is available for the reach, allowing definition of distributed roughness values in the two dimensional floodplain model. These highly distributed data were aggregated to three levels; in the first level a uniform floodplain roughness value was considered the entire floodplain; in the second two floodplain roughness values were considered on the basis of land use being classified either as flexible or non-flexible; and in the third five floodplain roughness values were considered for the five main land use types in the reach.

The identifiability of floodplain roughness for each of the classes defined was established through a uni-modal sensitivity analysis, as well as an uncertainty analysis using the GLUE approach. Both showed the sensitivity of floodplain roughness values decreases as the heterogeneity of roughness definition increases. For five different values of distributed floodplain roughness values, parameter distributions were not constrained at all when compared to the prior distributions. This limited ability to identify distributed roughness values is attributed to calibrated roughness values representing bulk roughness values at the model scale rather than at the scale at which the distributed floodplain vegetation data is available.

These results have consequences on reliability of methods assessing impact on flood levels due to change in floodplain land-use. As calibrated values for distributed floodplain roughness are not independent of model structure, changing these due to changes in individual land use types may result in spurious results and a different approach needs to be taken. Changes in roughness would need to be evaluated probabilistically, with the complex interaction between parameters and model structure taken into account. The flood extent data is shown to have a lower information content than the observed gauge levels, and much lower than the distributed floodplain level observations. This reiterates the value of spatially distributed observations in giving reliable spatial predictions of flood extent and

depth.

9.3 Uncertainty in flood extent modelling

Application of the different codes described in estimating flood extent at the reach scale shows that while these allow practical prediction of flood extent, none can be reliably applied without calibration of roughness values for main channel and floodplain. Despite the sound physical basis of the shallow water equations the codes are based on, roughness values are difficult to identify, even where comprehensive calibration datasets are available. The difficulty in identifying unique parameter sets leads to uncertainty as to the roughness values to be used in prediction. This uncertainty is propagated into model prediction, and is therefore detrimental to model reliability.

Roughness values established through calibration are shown to represent "effective" roughness values, including not only boundary friction, but also other contributors to energy loss such as crossing flows and momentum exchange. In most codes applied for reach scale flood extent modelling, these are not explicitly accounted for, with all momentum exchange taken into account by the "effective" roughness parameter values. Where momentum exchange is taken into account, this cannot be done independently of the roughness parameters, with division between the two unclear. With calibrated roughness values being "effective" at the reach scale, and integrating all contributions to energy loss, sensitivity to the use of distributed roughness parameter values inferred through detailed GIS data on floodplain land use is low. The same holds for uncertainty in elevation data used in the model. As long as the elevation model is not fundamentally flawed (particularly in the representation of line elements), uncertainties in deriving "effective" roughness parameters and model structure dominate model reliability.

Considering calibrated roughness values as "effective" parameters, has parallels in the concept of "effective" parameters suggested in distributed hydrological runoff modelling. It can be argued that given that the roughness values implicitly describe all processes contributing to energy loss, these values are more conceptual than physical. The physical basis of hydrodynamic flood extent models is then not as sound as it may seem, and contains some degree of conceptual modelling.

The practical consequence of these uncertainties is that deterministic predictions made with these models on flood extent at the reach scale may be unreliable, particularly when the models are applied in extrapolation to design events larger than those used in model calibration. Equally the realisation that roughness values are less physical and more conceptual makes application of roughness values found for one reach to other, similar, reaches very difficult. To do so other contributors to effective roughness values than for example land use or bed material will need to be taken into account. Differences in model structure will, moreover, also influence the effective parameters. To evaluate the reliability of these model predictions, a more probabilistic approach is recommended. This will not only make the value of the available calibration data explicit, it will also help establish a suitable selection of model complexity.

In assessing impacts of floodplain land-use change, this probabilistic setting is equally recommended. As the roughness values are to be considered as "effective" values, changing roughness values for individual land-use types is difficult. Further research would certainly seem necessary to establish a reliable approach in assessing the impact of land-use change, while taking account of these interactions. Ideally this research could be undertaken in a reach with a detailed set of calibration data before and after a significant change in land-use, but such datasets are unlikely to be available, leaving the approach to take in how to assess impacts reliably unclear. One approach may be to undertake extensive experimental work using physical scale models, though even then the complexity of floodplain flow observed in the field will be difficult to model.

9.4 Performance of the integrated GIS-model

The four codes applied span a full range of performance described in terms of computational speed and flexibility of integration with GIS. From the point of view of reliability, it would seem that the hybrid code outperforms the other codes, but its ranking in terms of computational speed is worst, with flexibility at a medium level. The one-dimensional code outpaces the others with respect to computational speed. Where no spatially distributed level data for calibration is available, reliability is comparable to the hybrid code, and the highest performance could then be vested in the one-dimensional approach, despite its low level of integration. Although applicable for flood extent modelling, the code allowing full embedding with GIS is shown to require significant assumptions on numerically resolving the highly dynamic system. As embedding in GIS requires these assumptions to be made due to the limited power of GIS in solving non-linear numerical problems, the gain in performance through full embedding in GIS would therefore seem marginal.

On the basis of the work reported in this thesis, the conclusions on performance in integrating hydrological models with GIS include:

- Performance of integrating hydrological models with GIS should be evaluated from a broader perspective than computational speed and technical flexibility of using the integrated system, and should include reliability in application of the integrated model concept.

- Where spatial data is available to constrain uncertainties, models giving complex dynamic representation of the spatial process may prove most reliable, and thus perform best. Where this data is lacking, simpler distributed or lumped models may be of comparable reliability, but due to either higher computational efficiency, or greater integration with GIS, have an overall higher performance.

- Integration of models for highly dynamic systems with GIS poses significant limitations on numerical solution techniques that can be applied. This can have consequences on both the application domain and therefore on model

reliability. With model concepts sharing GIS databases but allowing independent numerical evaluation, these restrictions do not apply, and reliability is more robust.

Despite the additional burden in data exchange and management using either the loosely coupled or the tightly coupled approach with only a shared database, full embedding of dynamic models in GIS should only be pursued where the integration does not adversely affect the ability of the model to reliably represent the dynamics. The problems posed in integrating models where databases can be shared with GIS will also gradually reduce as open standards on data exchange become available, allowing focus of research in modelling to shift from the technical aspects of communication to the use of data in constraining predictive uncertainties.

10

Samenvatting

10.1 Inleiding

Integratie van Geografische Informatiesystemen (GIS) en numerieke hydrologische modellen is een logische stap gezien de behoefte aan ruimtelijke gegevens bij het hydrologisch modelleren, en de wijze waarin GIS zich heeft ontwikkeld als het medium voor de opslag, analyse en bewerking van ruimtelijke gegevens. Om modellen met GIS te integreren zijn er in hoofdlijn drie concepten; (i) een losse koppeling waarbij de gegevens in het GIS en het hydrologisch model onafhankelijk blijven, met een uitwisseling van gegevens door bestanden; (ii) een geïntegreerde koppeling waarbij de gegevens weliswaar in een gemeenschappelijke database worden opgeslagen, maar het GIS en het model onafhankelijk blijven; en, (iii) een koppeling waarbij het hydrologische model volledig in het GIS wordt geïntegreerd.

Bij de integratie van GIS en numerieke hydrologische modellen is het van belang de prestaties van het ge ïntegreerde systeem te beschouwen. Vaak worden deze prestaties beschouwd als alleen de rekensnelheid, en hoewel dit een belangrijk aspect is, wordt in dit proefschrift een bredere definitie van prestaties gehanteerd. Als indicatoren voor de algehele prestaties wordt naast genoemde rekensnelheid ook de flexibiliteit van het geïntegreerde systeem beschouwd, evenals de betrouwbaarheid waarmee het geïntegreerde systeem ingezet kan worden om modelvoorspellingen te maken.

De flexibiliteit van toepassing van het geïntegreerde systeem wordt in belangrijke mate bepaald door de wijze waarop het hydrologische model en het GIS worden gekoppeld. De flexibiliteit neemt toe bij een meer geïntegreerde koppeling. Om deze meer geïntegreerde koppeling te bereiken, moeten echter aannamen worden gedaan over de manier waarop ruimtelijke en temporele variabiliteit in het model worden beschreven. Deze aannamen zullen een grote invloed hebben op de rekensnelheid van het geïntegreerd systeem - waardoor deze keuze voor model structuur een grote invloed heeft op de eerste twee indicatoren.

De derde indicator is de betrouwbaarheid van het geïntegreerde modelsysteem voor het maken van modelvoorspellingen. Betrouwbaarheid wordt in dit proefschrift synoniem genomen aan de onzekerheid in de voorspelling, aangezien een voorspelling met grote onzekerheden een lage betrouwbaarheid heeft. De onzekerheid in de voorspelling wordt door een aantal factoren beïnvloed, onder andere de model structuur, onzekerheden in de randvoorwaarden, en onzekerheden in de modelparameters. Centraal in dit proefschrift staat de invloed van de model structuur en de modelparameters op de onzekerheden in de voorspelling en daarmee op

de betrouwbaarheid van het geïntegreerd systeem.

Hydrologische modellering beslaat een zeer breed scala aan processen. In dit proefschrift wordt slechts het numeriek modelleren van overstromingen vanuit rivieren beschouwd. Dit is van nature een ruimtelijk georiënteerde vraag, en de integratie met GIS is daarmee niet alleen een natuurlijke; deze vergemakkelijkt in grote mate het meenemen van resultaten van het modelleren in het gehele proces van ruimtelijke overstromingsrisicoanalyse. Om overstromingen te modelleren worden een aantal numerieke hydrodynamische modellen beschouwd. Deze kunnen zowel volgens de losse koppeling als volgens de geïntegreerde koppeling met het GIS geïntegreerd worden. Bij de geïntegreerde koppeling is het voor een volledig hydrodynamisch model alleen mogelijk te werken met de gemeenschappelijke database, hoewel de twee systemen onafhankelijk zullen blijven doordat de impliciete tijdintegratie die nodig is niet in het GIS beschikbaar is. Een eenvoudiger model die deze volledige integratie wel toestaat en waarbij een aantal aannamen worden gedaan ten aanzien van de stroming, wordt eveneens beschouwd. De gekozen modellen kunnen allen in de praktijk worden ingezet voor het berekenen van de ruimtelijke grenzen van overstromingen.

10.2 Samenvatting van de onderzoeksresultaten

10.2.1 Hydraulische evaluatie van overstromingsmodellen

Vier numerieke modellen zijn in dit proefschrift beschouwd: een 1D hydrodynamisch model; een 2D hydrodynamisch model op basis van een regelmatig rekenrooster; een hybride 1D-2D hydrodynamisch model waar de hoofdgeul in 1D gemodelleerd wordt en de uiterwaard in 2D; en een eveneens hybride model maar met sterk vereenvoudigde stromingvergelijkingen.

De door deze modellen berekende waterstands-afvoer relaties zijn vergeleken met een aantal theoretische en empirische relaties. De meest eenvoudige van deze theoretische relaties is die waarbij de hoofdgeul en de uiterwaard worden verdeeld in vakken met een hypothetische verticale scheiding. De wrijving op deze scheiding wordt verwaarloosd. Voor rivieren met een rechte planvorm is het bekend uit vergelijking met experimentele resultaten dat deze relatie de afvoer bij gegeven waterstand ca. 5 tot 10% overschat, met name door de verwaarlozing van de turbulente momentumuitwisseling tussen de verschillende vakken. Met uitzondering van het hybride hydrodynamische model laten alle hier gebruikte modellen een vergelijkbare overschatting zien, in sommige gevallen nog versterkt indien er in de hoofdgeul van de niet-conservatieve vorm wordt uitgegaan van de momentum vergelijking. Het hybride hydrodynamische model laat een veel betere vergelijking zien met experimentele resultaten. Dit komt doorat er in dit model een horizontale scheiding tussen hoofdgeul en uiterwaard wordt aangenomen ter hoogte van de bovenkant van de hoofdgeul. Aangezien deze scheiding niet als wrijvingsvrij wordt genomen, treedt er een vergroot verlies van momentum op die de het verwaarlozen van de turbulente momentumuitwisseling compenseert.

Voor meanderende rivieren is de overschatting van de theoretische relaties nog veel groter en kan in de orde van 30% liggen. Dit wordt veroorzaakt door een

versterkt momentumverlies als gevolg van het complexe stromingsbeeld. Ook hier laten het 1D model en het vereenvoudigd hybride model een vergelijkbare overschatting van de afvoer zien. Het hybride hydrodynamische model geeft wederom een veel kleinere overschatting. Voor het volledig 2D model op basis van een regelmatig rekenrooster is er een zeer sterke onderschatting van de afvoer. Dit wordt veroorzaakt door de relatief grove beschrijving van de hoofdgeul in het rechthoekig rooster, terwijl deze in werkelijkheid het overgrote deel van de afvoer voert.

Voor alle modellen geldt dat deze toegepast kunnen worden voor het modelleren van echte rivieren. Bij dit modelleren worden de ruwheden zodanig gekalibreerd dat de waterstands-afvoer relatie voldoende nauwkeurig de waargenomen relatie benaderd. Het gevolg van het verwaarlozen van turbulente momentumverliezen is echter dat deze verliezen dan impliciet worden meegenomen in de gekalibreerde ruwheidwaarden. Deze ruwheden zijn dan zeker niet alleen te beschouwen als het gevolg van wand- en bodemwrijving, maar moeten gezien worden als een samengestelde waarde die alle momentumverliezen moeten verklaren. Voor gladde, rechte rivieren zijn de additionele verliezen relatief beperkt, maar deze nemen toe bij toename van de uiterwaardruwheid, helling van de uiterwaard en bochtigheid van de hoofdgeul. Doordat de ruwheden een samengestelde waarde zijn, is een betrouwbare toepassing van deze modellen zonder voldoende kalibratie en verificatie daarmee niet mogelijk, zelfs in de complexere modellen waar de turbulentie expliciet wordt meegenomen.

10.2.2 Betrouwbaarheid van modelvoorspellingen

De modellen voor het bepalen van overstromingsgrenzen worden veelal ingezet bij het maken van voorspellingen voor ontwerphoogwaters die groter zijn dan de historische hoogwaters die gebruikt worden bij modelkalibratie. Drie geselecteerde modellen zijn gekalibreerd met gegevens van een aantal middelgrote hoogwaters en geverifieerd voor een groot hoogwater. De resultaten laten zien dat ondanks vergelijkbare resultaten in kalibratie een aantal van de modellen bij extrapolatie een significante onderschatting geven van de maximale waterhoogte.

De drie modellen zijn toegepast op een gedeelte van de Saar Rivier in Duitsland. Dit stuk van 17 km lang bevat een relatief brede uiterwaard die vaak wordt overstroomd. De uiterwaard wordt doorsneden door een snelweg, die tevens de overstromingsgrens bepaald. Meetgegevens zijn slechts beschikbaar van twee meetstations, één aan de boven- en één aan de benedenzijde van het gekozen stuk rivier. Alle drie modellen kunnen eenvoudig gekalibreerd worden als gevolg van de relatief geringe beschikbaarheid van gegevens (mits er een goed hoogtemodel van de uiterwaard bestaat waarin de snelweg expliciet wordt meegenomen). Om de onzekerheden in kaart te brengen, wordt de schatting van de ruwheidwaarden gedaan in het kader van de "generalised likelihood uncertainty estimation" methode (GLUE). Dit is een probabilistische methode waarmee expliciet de waarde van kalibratie data bij het verminderen van onzekerheden in modelparameters aangetoond kan worden.

Gegevens van vier hoogwaters waren beschikbaar. Twee van deze waren relatief klein, met een piekafvoer in de orde van $500 - 600 m^3/s$, met beperkte overstroming van de uiterwaarden. Een derde hoogwater had een piekafvoer van $950 m^3/s$ met

een geschatte herhalingstijd van tien jaar. Het vierde hoogwater van December 1993 was het hoogst gemeten, met een piekafvoer van $1271 m^3/s$. Indien alle vier hoogwaters ingezet werden bij de kalibratie, bleek het gemiddelde voor de hoogste waterstand voor het hoogwater van December 1993 bij het bovenstrooms gelegen meetstation ca. $0.2m$ tot $0.4m$ onder het waargenomen maximum bij zowel het 1D als het volledig 2D model. Voor het hybride 1D-2D model werd een lichte overschatting van $0.05m$ gevonden. In alle gevallen was de 90% onzekerheidsband in de orde van $0.90m$. Dit beeld veranderde significant als de gegevens voor het December 1993 hoogwater niet werden ingezet in kalibratie, en alleen ter verificatie werden gebruikt. Zoals verwacht bleek het volledig 2D raster gebaseerd model ongeschikt, met een onderschatting van het maximum van ongeveer $1m$. In het 1D model werd het maximum eveneens onderschat (ca. $0.4m$), terwijl het hybride model het meest betrouwbaar bleek, met dezelfde overschatting als voorheen. De 90% betrouwbaarheidsband nam echter toe tot ca. $1.15m$. Ook de *a posteriori* parameter verdelingen van het hybride model bleken relatief stabiel, met de beste parameters in hetzelfde deel van de parameterruimte. Deze resultaten tonen duidelijk het gevaar van extrapolatie aan voor hoogwaters groter dan die in kalibratie zijn gebruikt. Dergelijke extrapolatie is echter aan de orde van de dag voor risicoanalyse, waar de grenzen van overstroming bepaald moeten worden voor hoogwaters met veel hogere herhalingstijden dan de waargenomen hoogwaters. De onzekerheden in de berekende grenzen en waterstanden als gevolg van de parameteronzekerheden en verschillen in modelstructuur kunnen daarbij groot zijn, even groot zelfs als de onzekerheden in het bepalen van de ontwerpafvoer bij hoge herhalingstijden.

10.2.3 Waarde van ruimtelijke gegevens

Om te bepalen hoe ruimtelijke gegevens gebruikt kunnen worden in het verminderen van de onzekerheid in modelvoorspellingen is de waarde van gedistribueerde waterstandsmetingen vergeleken met die van lucht- en satellietbeelden van de ruimtelijke grenzen van overstroming. Het bleek dat de gedistribueerde waterstandsmetingen de meeste informatie bevatten. De waargenomen grenzen bleken van weinig waarde, doordat deze grenzen met name bepaald werden door aanwezige infrastructuur (wegen, spoorwegen, etc.).

Voor een kort stuk van de Orlice Rivier in Tsjechië waren voor het hoogwater van juli 1997 zowel de waargenomen grenzen van overstroming als de waterstand in de uiterwaard op een 26-tal locaties beschikbaar. Het stukje rivier stroomt door de stad Usti nad Orlici, en daardoor worden de uiterwaarden doorkruist met infrastructuur zoals wegen en spoorlijnen, vaak op verhoogde zandlichamen.

Twee numerieke modellen werden opgesteld, waarbij gebruik werd gemaakt van zowel het 1D model als het hybride 1D-2D model. De probabilistische GLUE methode werd eveneens toegepast om de waarde van de verschillende kalibratiegegevens te bepalen. Het bleek dat beide modellen vergelijkbare onzekerheden gaven in het voorspellen van de grenzen van overstroming. Het hybride model gaf echter een betere voorspelling voor de hoogte van de gedistribueerde waterstanden in de uiterwaard. Bovendien bleken de a posteriori parameter verdelingen voor het hybride model in dat deel van de parameterruimte te liggen waar men deze zou verwachten

op basis van de karakteristieken van de rivier, terwijl die van het 1D model in een veel hoger deel van de parameterruimte lagen.

De nauwkeurigheid van het hoogtemodel dat is gebruikt in de modellen is geschat op ca. $0.35m$. Het bleek echter dat de invloed van dit onzekere hoogtemodel betrekkelijk gering was. Het effect van de onzekerheid in het hoogtemodel was evenwel sterker in het hybride model dan in het 1D model. Een conclusie zou dan kunnen zijn dat de beschikbaarheid van hoge resolutie, nauwkeurige hoogtemodellen alleen een positieve bijdrage in de betrouwbaarheid geven als de uiterwaardstroming in 2D gemodelleerd wordt, en er bovendien een aantal gedistribueerde waterstandsmetingen in de uiterwaard beschikbaar zijn. Zonder deze gedistribueerde waterstandsmetingen en door alleen gebruik te maken van de waarnemingen van de grenzen van overstroming zou de objectieve betrouwbaarheid van het 1D en het hybride model dezelfde zijn. Indien de twee gegevensbronnen vergeleken worden, is het duidelijk dat de informatieve waarde van de grenzen van overstroming beduidend lager is dan de gedistribueerde waterstandsmetingen. Ondanks dat men dit van tevoren zou verwachten gezien het stedelijke karakter van de uiterwaard, zullen dergelijke begrenzingen vaak voorkomen in vergelijkbare uiterwaarden. Bovendien zijn dergelijke stedelijke uiterwaarden het meest interessant bij overstromingsrisicoanalyse. De resultaten tonen aan dat de betrouwbaarheid van overstromingsmodellen behoorlijk verbeterd kan worden indien er bij overstromingen aandacht wordt besteed aan het verzamelen van waterstands- en dieptemetingen op de uiterwaard, en minder aan het maken van overstromingskaarten. Een handige bron hierbij zou de vaak uitgebreide mediabeelden kunnen zijn, gezien de aandacht die gegeven wordt aan overstromingen in stedelijke gebieden.

10.2.4 Waarde van gedistribueerde ruwheden

In de twee vorige toepassingen is de uiterwaardruwheid uniform over de gehele uiterwaard genomen. Potentieel zou een gedistribueerde uiterwaardruwheid kunnen bijdragen aan de betrouwbaarheid van overstromingsberekeningen. De gevoeligheid van de betrouwbaarheid naar de heterogeniteit van definitie van uiterwaardruwheid is bekeken. Het bleek dat naarmate deze heterogeniteit toenam, de identificeerbaarheid van die uiterwaardruwheid juist afnam. Doordat deze ruwheidwaarden slecht bepaald zijn, moeten resultaten van studies naar effecten van landgebruikverandering door het aanpassen van de ruwheden op basis van het veranderd landgebruik in twijfel genomen worden.

Een hybride 1D-2D hydrodynamisch model is opgesteld voor een stuk van $30km$ van de Maas benedenstrooms van Maastricht. Voor het hoogwater van januari 1995 is in dit stuk een uitzonderlijk uitgebreide set aan kalibratiegegevens beschikbaar, inclusief waterstanden bij drie meetstations (met één intern aan het modeldomein), een opname van de overstromingsgrenzen vanuit een satelliet, een opname van de overstromingsgrenzen op een luchtfoto, en een groot aantal waterstandsmetingen in de uiterwaard. Een gedetailleerde GIS database is eveneens beschikbaar over het landgebruik in de uiterwaard, en deze is gebruikt voor de definitie van gedistribueerde ruwheidwaarden in het 2D domein. Deze zeer gedetailleerde data zijn vóór toepassing in het model in drie categorieën geaggregeerd: een enkele ruwheid-

klasse in de gehele uiterwaard; twee ruwheidklassen onderverdeeld in flexibele typen landgebruik en niet-flexibele typen landgebruik; en vijf ruwheidklassen op basis van de vijf belangrijkste typen landgebruik.

De identificeerbaarheid van de ruwheden in elke klasse werd bekeken zowel door een gevoeligheidsanalyse als wederom met de probabilistische GLUE methode. Voor beide gold dat de gevoeligheid van de ruwheidwaarden afnam bij een toename in heterogeniteit van de definitie van ruwheden. Daar waar vijf ruwheidklassen gedefinieerd waren, was er slechts een verwaarloosbaar verschil tussen de *a-priori* en *a posteriori* parameter verdelingen. De matige identificeerbaarheid van de ruwheidwaarden wordt toegeschreven aan het feit dat de ruwheden samengestelde ruwheden voorstellen op de modelschaal, en niet ruwheden op de schaal waarin het gedistribueerde landgebruik beschikbaar is.

Deze resultaten hebben consequenties voor de betrouwbaarheid van de gangbare methodieken ter bepaling van landgebruikverandering bij hoogwater. Aangezien de gekalibreerde ruwheidwaarden niet onafhankelijk zijn van de model structuur, kan het individueel veranderen van ruwheden als gevolg van verandering van individuele typen landgebruik misleidende resultaten geven. De veranderingen zouden probabilistisch benaderd moeten worden, waarbij de complexe afhankelijkheden tussen de verschillende ruwheden en de modelstructuur meegenomen moeten worden. Evenals in de vorige studie wordt ook hier aangetoond dat de informatieve waarde van de waarnemingen van overstromingsgrenzen veel lager is dan die in de gedistribueerde waterstandsmetingen. Dit benadrukt het belang van deze gegevens voor het betrouwbaar voorspellen van overstromingsgrenzen en -dieptes.

10.3 Onzekerheden in overstromingsmodellering

Toepassing van de verschillende modellen zoals hier beschreven in het voorspellen van overstromingsgrenzen laat zien dat ondanks dat met alle modellen in de praktijk een voorspelling gemaakt kan worden, het voor geen van de modellen geldt dat dit betrouwbaar gedaan kan worden zonder expliciete kalibratie van de ruwheidwaarden. Ondanks de gedegen fysische basis waarop de modellen berusten, zijn de onzekerheden in gekalibreerde ruwheidwaarden groot, zelfs daar waar uitgebreide sets kalibratiegegevens beschikbaar zijn. Deze onzekerheden werken door in de modelvoorspellingen, en verminderen daarmee de betrouwbaarheid van die modelvoorspellingen.

Gekalibreerde ruwheidwaarden moeten worden beschouwd als “effectieve” ruwheidwaarden, en niet alleen als gevolg van de wand- en bodemwrijving. Deze samengestelde ruwheidwaarden bevatten alle bijdragen aan energieverlies, inclusief momentum uitwisseling en het gevolg van complexe stromingspatronen bij meanderende rivieren. In de meeste modellen die in de praktijk worden toegepast voor overstromingsmodellering worden deze bijdragen niet expliciet meegenomen, en zelfs in modellen waar dit tot op zekere hoogte wel het geval is, is er een sterke afhankelijkheid tussen het turbulentiemodel en de gekalibreerde ruwheidwaarden. Doordat de ruwheidwaarden bovendien “effectieve” ruwheidwaarden voorstellen op de schaal van het model, alsmede doordat de gevoeligheid bij een gedetailleerde het-

erogene definitie van uiterwaardruwheid laag is, is de waarde van zeer gedetailleerde GIS data over het landgebruik in de uiterwaard betrekkelijk laag. Ditzelfde geldt voor de onzekerheden in het gebruikte hoogtemodel en, tenzij deze niet fundamenteel verkeerd is (met name in de weergave van lijnelementen), zullen de onzekerheden in de ruwheid en modelstructuur bepalend zijn voor de betrouwbaarheid van het model.

Het beschouwen van ruwheidwaarden als "effectieve" parameters in overstromingsmodellering is te vergelijken met het concept van "effectieve" parameters in gedistribueerd neerslag-afvoermodellering. Ook hier kan geconcludeerd worden dat de parameters daarmee meer een conceptuele beschrijving geven dan een fysisch gebaseerde. Daarmee lijkt deze vorm van hydrodynamisch modellering meer op conceptueel modelleren en minder fysisch dan vaak wordt aangenomen. Het gevolg van deze onzekerheden in overstromingsmodellering betekent in de praktijk dat voorspellingen onbetrouwbaar kunnen zijn, met name die waar het model wordt toegepast voor ontwerphoogwaters die groter zijn dan de waargenomen hoogwaters gebruikt in kalibratie. Een ander gevolg van de aanvaarding dat de gekalibreerde ruwheidwaarden meer conceptueel dan fysisch zijn, is dat het toepassen van gekalibreerde waarden in een ander (onbemeten) modelgebied minder eenvoudig is. Om dit te doen moeten alle bijdragen aan de "effectieve" ruwheidwaarden worden meegenomen, en niet alleen het bodemmateriaal en het landgebruik. Bovendien kan de gekozen modelstructuur invloed hebben op de "effectieve" ruwheidwaarden. Om de betrouwbaarheid te evalueren van voorspellingen die met deze onzekere ruwheidwaarden zijn gemaakt, wordt een probabilistische aanpak aangeraden. Een dergelijke aanpak toont bovendien expliciet de waarde van de beschikbare gegevens, en ondersteunt ook bij de keuze van een model met geschikte complexiteit.

Ook bij het evalueren van de effecten van landgebruikveranderingen wordt deze probabilistische aanpak sterk aangeraden. Doordat de ruwheidwaarden als "effectief" beschouwd moeten worden kunnen deze niet eenvoudig onafhankelijk veranderd worden als gevolg van landgebruikverandering. Verder onderzoek is dan ook nodig naar hoe alle afhankelijkheden expliciet meegenomen kunnen worden. Idealiter zou dit gedaan moeten worden daar waar er een zeer volledige set gegevens beschikbaar is van vóór en ná een significante verandering in landgebruik, maar aangezien de kans dat een dergelijke set gegevens inderdaad beschikbaar is zeer gering is, is de aanpak waarmee deze afhankelijkheden betrouwbaar in kaart gebracht moeten worden nog niet duidelijk. Een mogelijkheid zou een uitgebreide fysische experimentele opstelling zijn, maar ook daar zal de complexiteit van stroming in de echte uiterwaard slechts gedeeltelijk benaderd kunnen worden.

10.4 Prestaties van het geïntegreerde systeem

De vier in dit proefschrift beschouwde modellen beslaan de volledige reeks van genoemde prestatie indicators zoals rekensnelheid en flexibiliteit van integratie met GIS.Vergeleken op basis van betrouwbaarheid geeft het hybride 1D-2D model de beste prestaties, maar deze is qua rekensnelheid het langzaamst, met een middelmatig integratie niveau . Het 1D model is uiteraard het snelst, en indien er geen

ruimtelijke gegevens zijn voor de kalibratie is de betrouwbaarheid vergelijkbaar met die van de andere modellen, ondanks dat de integratie met GIS het minst is. Ook al kan het volledig met GIS geïntegreerd model worden toegepast voor overstromingsberekeningen, moeten significante aannamen worden gedaan ten aanzien van de dynamische stroming. Deze moeten gedaan worden om integratie met GIS mogelijk te maken, gezien de beperkingen van GIS in het impliciet oplossen van niet lineaire numerieke systemen. De winst in prestaties door de volledige integratie met GIS lijkt daardoor van ondergeschikt belang.

Ten aanzien van de integratie van GIS met hydrologische modellen worden op basis van de bevindingen in dit proefschrift de volgende conclusies gemaakt:

- Prestaties van een geïntegreerd GIS-model systeem moeten vanuit een breder perspectief worden beschouwd dan de rekensnelheid en de technische flexibiliteit alleen. De betrouwbaarheid van het geïntegreerde systeem bij de toepassing moet eveneens worden beschouwd.

- Indien er ruimtelijke gegevens zijn om onzekerheden te verminderen, kunnen modellen die het complexe dynamisch proces beschrijven relatief betrouwbaar zijn, en daarmee de beste prestaties leveren. Indien deze gegevens niet beschikbaar zijn, kunnen eenvoudigere modellen een vergelijkbare betrouwbaarheid hebben, maar door de hogere mate van integratie met GIS en/of de hogere rekensnelheid betere algehele prestaties leveren.

- Integratie van modellen voor hoogdynamische systemen met GIS kan vergaande beperkingen op de numerieke oplossingstrategie leggen. Dit kan van grote invloed zijn op het mogelijke toepassingsgebied en daardoor de betrouwbaarheid. Daar waar het model de database met het GIS deelt maar niet volledig wordt geïntegreerd is de betrouwbaarheid robuuster.

De strategie van zowel de losse koppeling als de gedeeltelijk geïntegreerde koppeling betekent een toename in de ad-hoc uitwisseling van gegevens en vermindering in de onderhoudbaarheid. Ondanks dit moet de volledige integratie alleen dan worden gekozen als daardoor de betrouwbaarheid waarmee het geïntegreerd model voorspellingen kan doen niet ondermijnd wordt door vereenvoudigingen gemaakt met als enig doel de volledige koppeling mogelijk te maken. Bovendien zullen technische problemen bij de uitwisseling van gegevens en het delen van gemeenschappelijke databases verdwijnen met het beschikbaar komen van open standaards in gegevensuitwisseling. Hierdoor kan bij onderzoek naar het gebruik van modellen de nadruk verschuiven van de technische aspecten van de integratie naar het gebruik van de ruimtelijke gegevens om onzekerheden in modelvoorspellingen te verminderen.

References

Aarts, L., and P. van der Veer, Neural network method for solving partial differential equations, *Neural Processing Letters*, *14*, 261–271, 2001.

Abbaspour, K., R. Schulin, and M. van Genuchten, Estimating unsaturated soil hydarulic parameters using ant colony optimisation, *Advances in Water Resources*, *24*, 827–841, 2001.

Abbott, M., J. Bathurst, J. Cunge, P. O'Connel, and J. Rasmussen, An introduction to the european hydrological sysem - systeme hydrologique europeen "SHE", 1: History and philosophy of a physically-based, distributed modelling system, *Journal of Hydrology*, *87*, 45–59, 1986.

Ackers, P., Hydraulic design of two-stage channels, *Proc. Instn Civ. Engrs Wat., Marit. & Energy*, *96*, 247–257, 1992.

Acrement, G., Jr, and V. Schneider, Guide for selecting manning's roughness coefficients for natural channel and floodplains, *Tech. Rep. WSP2339*, USGS, 1989.

Ali, S., and P. Goodwin, The predictive ability of 1-D models to simulate floodplain processes, in *Hydroinformatics 2002*, edited by R. Falconer, B. Bin, E. Harris, and C. Wilson, pp. 247–252, IWA publishing, 2002.

Andréassian, V., C. Perrin, C. Michel, I. Usart-Sanchez, and J. Lavabre, Impact of imperfect rainfall knowledge on the efficiency and the parameters of watershed models, *Journal of Hydrology*, *250*, 206–223, 2001.

Aronica, G., B. Hankin, and K. Beven, Uncertainty and equifinality in calibrating distributed roughness coefficients in a flood propagation model with limited data, *Advances in Water Resources*, *22*, 349–365, 1998a.

Aronica, G., B. Hankin, and K. Beven, Topographic sensitivity and parameter uncertainty of a 2D inundation model, in *Hydroinformatics '98*, edited by Babovic and Larsen, pp. 1083–1088, Balkema, Rotterdam, 1998b.

Aronica, G., T. Tucciarelli, and C. Nasello, 2D multilevel model for flood wave propagation in flood-affected areas, *Journal of Water Resources Planning and Managament*, *124*, 210–217, 1999.

Aronica, G., P. Bates, and M. Horritt, Assessing the uncertainty in distributed model predictions using observed binary pattern information within GLUE, *Hydrological Processes*, *16*, 2001–2016, 2002, dOI: 10.1002/hyp.398.

Asselman, N., and M. van Wijngaarden, Development and application of a 1D floodplain sedimentation model for the river rhine in the netherlands, *Journal of Hydrology*, *268*, 127–142, 2002.

Asselman, N., H. Middelkoop, M. R. M. Straatsma, E. Velzen, and P. Jesse, Assessment of the hydraulic roughness of river flood plains using laser altimetry, in *The Structure, Function and Management Implications of Fluvial Sedimentary Systems*, edited by F. Dyer, M. Thoms, and J. Olley, no. 276 in IAHS publication, pp. 381–388, Int.Comm. On Continental Erosion & Unesco, Alice Springs, 2002.

Babaeyan-Koopaei, K., D. Ervine, P. Carling, and Z. Cao, Velocity and turbulence measurements for two overbank flow events in river severn, *Journal of Hydraulic Engineering*, *128*, 891–900, 2002.

Bates, B. C., and E. P. Campbell, A markov chain monte carlo scheme for parameter esimation and inference in conceptual rainfall-runoff modelling, *Water Resources Research*, *37*, 937–947, 2001.

Bates, P., and A. de Roo, A simple raster-based model for flood inundation simulation, *Journal of Hydrology*, *236*, 54–77, 2000.

Bates, P., M. Anderson, D. Price, R. Hardy, and C. Smith, Analysis and development of hydraulic models for floodplain flows, in *Floodplain Processes*, chap. 7, pp. 215–254, John Wiley & Sons, 1996.

Bates, P., M. Stewart, G. Singers, C. Smith, J. Hervout, and R. Sellin, Internal and external validation of a two-dimensional finite element code for river flood simulations, *Proc. Instn Civ. Engrs Wat., Marit. & Energy*, *130*, 127–141, 1998.

Bechteler, W., S. Hartmann, and A. Otto, Coupling of 2D and 1D models and integration into geographic information systems GIS, in *River Flood Hydraulics*, edited by W. White and J. Watts, pp. 155–165, John Wiley & Sons Ltd, 1994.

Beffa, C., and R. Connell, Two-dimensional flood plain flow. i: Model description, *Journal of Hydrologic Engineering*, *6*, 397–405, 2001.

Beffa, C., and R. Faeh, Flood propagation on mobile beds under mountainous flow conditions, in *Proceedings of the Specialty Conference on Modelling of Flood Propagation over Intitially Dry Areas*, edited by P. Molinaro and L. Natale, pp. 327–341, ASCE, New York, NY, USA, Milan, Italy, 1994.

Bergougnoux, P., Editorial: A perspective on dynamic and multi-dimensional GIS in the 21st century, *Geoinformatica*, *4*, 343–348, 2000.

Beven, K., Changing ideas in hydrology. the case of physically based models, *J. Hydrology*, *105*, 157–172, 1989.

Beven, K., Prophecy, reality and uncertainty in distributed hydrological modelling, *Advances in Water Resources*, *16*, 41–51, 1993.

Beven, K., Linking parameters across scales: sub-grid parametrisations and scale dependent hydrological models, *Hydrological Processes*, *9*, 507–526, 1995.

Beven, K., Uniqueness of place and process reprentations in hydrological modelling, *Hydrology and Earth System Sciences*, *4*, 203–213, 2000.

Beven, K., On hypothesis testing in hydrology, *Hyrdological Processes*, *15*, 1655–1657, 2001a.

Beven, K., On landscape space to model space mapping, *Hyrdological Processes*, *15*, 323–324, 2001b.

Beven, K., On stochastic models and the single realization, *Hydrological Processes*, *15*, 895–896, 2001c, doi:10.1002/hyp.438.

Beven, K., Towards an alternative blueprint for a physically based digitally simulated hydrologic response modelling system, *Hydrological Processes*, *16*, 189–206, 2002, dOI: 10.1002/hyp.343.

Beven, K., and A. Binley, The future of distributed models: Model calibration and uncertainty prediction, *Hydrological Processes*, *6*, 279–298, 1992.

Beven, K., and P. Carling, Velocities, roughness and dispersion in the lowland river severn, in *Lowland Rivers: Geomorphological Perspectives*, edited by G. Petts and P. Carling, pp. 71–93, John Wiley & Sons, 1992.

Beven, K., and J. Freer, Equifinality, data assimilation, and uncertainty estimation in mechanistic modelling of complex environmental systems using the glue methodology, *Journal of Hydrology*, *249*, 11–29, 2001.

Beven, K., and P. Young, Comment on "bayesian recursive parameter estimation for hydrologicl models" by m. thiemann, m. trosset, h. gupta, and s. sorooshian, *Water Resources Research*, *39*, 1116, 2003, doi:10.1029/2001WR001183.

Bhowmik, N., Shear stress distribion and secondary currents in straight open channels, in *Gravel Bed Rivers*, edited by R. Hey, J. Bathurst, and C. Thorne, pp. 31–61, John Wiley & Sons Ltd., 1982.

Bladé, E., M. Gómez, and J. Dolz, Quasi-two dimensional modelling of flood routing in rivers and flood plains by means of storage cells, in *Proceedings of the Specialty Conference on Modelling of Flood Propagation over Intitially Dry Areas*, edited by P. Molinaro and L. Natale, pp. 156–170, ASCE, New York, NY, USA, Milan, Italy, 1994.

Blazkova, S., and K. Beven, Flood frequency estimation by continuous simulation for a catchment treated as ungauged (with uncertainty), *Water Resources Research*, *38*, 1139, 2002, doi:10.1029/2001WR000500.

Blazkova, S., K. Beven, and A. Kulasova, On constraining TOPMODEL hydrograph simulations using partial saturated area information, *Hydrological Processes*, *16*, 441–458, 2002a.

Blazkova, S., K. Beven, P. Tacheci, and A. Kulasova, Testing the distributed water table predictions of TOPMODEL (allowing for uncertainty in model calibration): The death of TOPMODEL?, *Water Resources Research*, *38*, 1257, 2002b, doi:10.1029/2001WR000912.

Blongewicz, M., The development of the integrated catchment modelling system, in *European Conference on Advances in Flood Research*, edited by A. Bronstert, C. Bismuth, and L. Menzel, pp. 67–72, Potsdam, Germany, 2000.

Boogaard, v. d. H., A.E.Mynett, and T. Heskes, Resampling techniques for the assessment of uncertainties in parameters and predictions of calibrated models, in *Proceedings of the 2000 Hydroinformatics conference*, Iowa Institute of Hydraulic Research, 2000.

Brackendridge, G., B. Tracy, and J. Knox, Orbital SAR remote sensing of a river flood wave, *Int. Journal of Remote Sensing*, *19*, 1439–1445, 1998.

Brimicombe, A., Flood risk assessment using spatial decision support system, *Simulation*, *59*, 379–380, 1992.

Bronstert, A., Capabilities and limitations of detailed hillslope hydrological modelling, *Hydrological Processes*, *13*, 21–48, 1999.

Burrough, P., Whither GIS (as systems and as science), *Computers, Environment and Urban Systems*, *24*, 1–3, 2000.

Burrough, P. A., and R. A. McDonnel, *Principles of Geographic Information Systems*, Oxford University Press, 1998.

Cameron, D., K. Beven, J. Tawn, S. Blazkova, and P. Naden, Flood frequency estimation by continuous simulation for a gauged upland catchment (with uncertainty), *Journal of Hydrology*, *219*, 169–187, 1999.

Cameron, D., P. Kneale, and L. See, An evaluation of a traditional and a neural net modelling approach to flood forecasting for an upland catchment, *Hydrological Processes*, *16*, 1033–1046, 2002, doi:10.1002/hyp.317.

Campbell, E. P., D. Fox, and B. Bates, A bayesian approach to parameter estimation and pooling in nonlinear flood event models, *Water Resources Research*, *35*, 211–220, 1999.

Carpenter, T., J. Sperfslage, K. Georgakakos, T. Sweeney, and D. Fread, National threshold runoff estimation utilizing GIS in support of operational flash flood warning systems, *Journal of Hydrology*, *224*, 21–44, 1999.

Chalise, S., S. Kansakar, G. Rees, K. Croker, and M. Zaidman, Management of water resources and low flow estimation for the Himalayan basins of Nepal, *Journal of Hydrology*, *282*, 23–35, 2003, doi:10.1016/S0022-1694(03)00250-6.

Chen, J., and J. Jiang, An event-based approach to spatio-temporal data modeling lin land subdivision systems, *Geoinformatica*, *4*, 387–402, 2000.

Chow, V., *Open Channel Hydraulics*, McGraw-Hill Book Company, New York, 1959.

Chow, V., D. Maidment, and L. Mays, *Applied Hydrology*, McGraw-Hill Book Company, New York, 1988.

Clark, M., Putting water in its place: a perspectibe on GIS in hydrology and water management, *Hydrological Processes*, *12*, 823–834, 1998.

Cobby, D., D. Mason, M. Horritt, and P. Bates, Two-dimensional hydraulic flood modelling using a finite-element mesh decomposed according to vegetation and topographic features derived from airborne scanning laser altimetry, *Hydrological Processes*, *17*, 1979–2000, 2003, doi: 10.1002/hyp.1201.

Connell, R., D. Painter, and C. Beffa, Two-dimensional flood plain flow. ii: Model application, *Journal of Hydrological Engineering*, *6*, 406–415, 2001.

Counsell, C., E. E. Gammal, and P. Samuels, Demonstration of a decision support system for assessing the impacts of engineering works and environmental change on flood risk - the thames catchment study, in *European Conference on Advances in Flood Research*, edited by A. Bronstert, C. Bismuth, and L. Menzel, pp. 87–98, Potsdam, Germany, 2000.

Crosetto, M., and S. Tarantola, Uncertainty and sensitivity analysis: tools for gis-based model implementation, *International Journal of Geographical Information Science*, *15*, 415–437, 2001.

Crosetto, M., S. Tarantola, and A. Saltelli, Sensitivity and uncertainty analysis in spatial modelling based on gis, *Agriculture, Ecosystems and Environment*, *81*, 71–79, 2000.

Cunge, J., Two dimensional modeling of floodplains, in *Unsteady Flow in Open Channels*, edited by K. Mahmood and V. Yevjevich, vol. II, chap. 17, pp. 705–762, Water Resources Publications, P.O.Box 303, Fort Collins, Co. USA, 1975.

Cunge, J., F. Holly Jr., and A. Verwey, *Practical Aspects of Computational Hydraulics*, Pitman Publishing Ltd., London, UK, 1980.

de Roo, A., Modelling runoff and sediment transport in catchments using GIS, *Hydrological Processes*, *12*, 905–922, 1998.

de Wit, M., Nutrient fluxes at the river basin scale. i: the PolFlow model, *Hydrological Processes*, *15*, 743–759, 2001, doi: 10.1002/hyp.175.

DEFRA, Reducing uncertainty in river flood conveyance, *Tech. rep.*, DEFRA/Environment Agency, Flood and Coastal Defence R & D programme, 2004, interim Report 2: Review of methods for estimating conveyance, Project W5A-057.

Dhondia, J., and G. Stelling, Application of one dimensional - two dimensional integrated hydraulic model for flood simulation and damage assessment, in *Hydroinformatics 2002*, edited by R. Falconer, B. Bin, E. Harris, and C. Wilson, pp. 265–276, IWA publishing, 2002.

Döll, P., and B. Lehner, Validation of a new global 30-min drainage direction map, *Journal of Hydrology*, *258*, 214–231, 2002.

Doull, G., and J. Bright, Flood hazard in palmerston north city, new zealand, in *Hydroinformatics 1996*, edited by Müller, pp. 33–40, Balkema, Rotterdam, 1996.

Duel, H., M. Baptist, G. Geerling, A. Smits, and J. van Alphen, Cyclic floodplain rejuvenation as a strategy for both flood protection and enhancement of the biodiversity of the river rhine, in *Proceedings of the conference on Environmental flows and ecohydraulics*, edited by K. et al., IAHR, Cape Town, 2002.

Dutta, D., S. Herath, and K. Musiake, A mathematical model for flood loss estimation, *Journal of Hydrology*, *277*, 24–49, 2003.

Ervine, D., K. Babaeyan-Koopaei, and R. Sellin, Two-dimensional solution for straight and meandering overbank flows, *Journal of Hydraulic Engineering*, *126*, 653–669, 2000.

ESRI, *ArcView Spatial Analyst*, Environmental Systems Research Institute, Inc, 1996.

Estrela, T., and L. Quintas, Use of a GIS in the modelling of flows on floodplains, in *River Flood Hydraulics*, edited by W. White and J. Watts, pp. 177–183, John Wiley & Sons Ltd, 1994.

Fedra, K., GIS and environmental modeling, in *Environmental Modeling with GIS*, Oxford University Press, Inc., 1993.

Feyen, L., K. Beven, F. D. Smedt, and J. Freer, Stochastic capture zone delineation within the generalized likelihood uncertainty estimation methodology: Conditioning on head observations, *Water Resources Research*, *37*, 625–638, 2001.

Frank, E., A. Ostan, M. Coccato, and G. Stelling, Use of an integrated one dimensional two dimensional hydraulic modelling approach for flood hazard and risk mapping, in *Proceedings of the 1st Conference on River Basin Management*, edited by R. Falconer and W. Blain, pp. 99–108, WITPress, Southampton, UK, 2001.

Franks, S., P. Gineste, K. Beven, and P. Merot, On constraining the predictions of a distributed model: The incorporation of fuzzy estimates of saturated areas into the calibration process, *Water Resources Research*, *34*, 787–797, 1998.

Freer, J., K. Beven, and B. Ambroise, Bayesian estimation of uncertainty in runoff prediction and the value of data: An application of the glue approach, *Water Resources Research*, *32*, 2161–2173, 1996.

French, R., *Open Channel Hydraulics*, McGraw-Hill Book Co., 1986.

Gan, T., E. M. Dlamini, and G. F. Biftu, Effects of model complexity and structure, data quality, and objective functions on hydrological modelling, *J. Hydrology*, *192*, 81–103, 1997.

Garbrecht, J., and G. Brown, Calculation of total conveyence in natural channels, *Journal of Hydraulic Engineering*, *117*, 788–798, 1991.

Gelb, A., *Applied optimal estimation*, M.I.T. Press, 1982.

Gelman, A., B. Carlin, H. Stern, and D. Rubin, *Bayesian Data Analysis*, Chapman and Hall, 1995.

Giammarco, P. D., E. Todini, D. Conseugra, F. Joerin, and F. Vitalini, Combining a 2D flood plain model with GIS for flood delineation and damage assessment, in *Proceedings of the Specialty Conference on Modelling of Flood Propagation over Intitially Dry Areas*, edited by P. Molinaro and L. Natale, pp. 171–285, ASCE, New York, NY, USA, Milan, Italy, 1994.

Gilard, O., and P. Givone, Flood risk management: new concepts for objective negotiations, in *Destructive Water: Water-Caused Natural Disasters, their abatement and control*, pp. 145–155, IAHS, 1997, iAHS Publication 239.

Goodchild, M., The state of GIS for environmental problem solving, in *Environmental Modeling with GIS*, Oxford University Press, Inc., 1993.

Gourbesville, P., Mike 11 GIS: Interest of GIS technology for conception of flood protection systems, in *Proceedings of the second International Conference on Hydroinfromatics*, edited by V. Babovic and L. Larsen, pp. 1365–1373, Balkema, Rotterdam, 1998.

Grayson, R., G. Blöschl, A. Western, and T. McMahon, Advances in the use of observed spatial patterns of catchment hydrological response, *Advances in Water Resources*, *25*, 1313–1334, 2002.

Green, I., and D. Stephenson, Criteria for comparison of single event models, *Hydrological Sciences Journal*, *31*, 395–411, 1986.

Greenhill, R., and R. Sellin, Development of a simple method to predict discharges in compound meandering channels, *Proc. Instn Civ. Engrs Wat., Marit. & Energy*, *101*, 37–44, 1993.

Gupta, H., S. Sorooshian, and P. Yapo, Toward improved calibration of hydrological models: Multiple and noncommensurable measures of information, *Water Resources Research*, *34*, 751–763, 1998.

Gurnell, A., and D. Montgomery (Eds.), *Hydrological applications of GIS*, Advances in Hydrological Processes, John Wiley & Sons., 1997.

Han, K., J. Lee, and J. Park, Flood inundation analysis resulting form levee break, *Journal of Hydraulic Research*, *36*, 747–759, 1998.

Harris, E., and D. Archer, Floodplain mapping of the river leam and river itchen, *Journal of the Chartered Insitution of Water and Environmental Management*, *13*, 280–285, 1999.

Hausmann, P., and M. Weber, Possible contributions of hydroinfromatics to risk analysis in insurance, in *Proceedings of the second International Conference on Hydroinfromatics*, edited by A. Müller, pp. 57–62, Balkema, Rotterdam, 1996.

Hervouet, J., TELEMAC modelling system: an overview, *Hydrological Processes*, *14*, 2209–2210, 2000.

Hervouet, J., and L. V. Haren, Recent advances in numerical methods for fluid flows, in *Floodplain Processes*, chap. 6, pp. 182–214, John Wiley & Sons, 1996.

Hesselink, A., History makes a river: Morphological changes and human interference in the river rhine, Ph.D. thesis, Faculty of Geographic Sciences, Utrecht University, 2002.

Hesselink, A., G. Stelling, J. Kwadijk, and H. Middelkoop, Inundation of a dutch river polder, sensitivity analysis of a physically based inundation model using historic data, *Water Resources Research*, *39*, 1234, 2003.

Hicks, F., Hydraulic flood routing with minimal channel data: Peace river, canada, *Canadian Journal of Civil Engineering*, *23*, 524–535, 1996.

Hock, R., Temperature index melt modelling in mountain areas, *Journal of Hydrology*, *282*, 104–115, 2003, doi:10.1016/S0022-1694(03)00257-9.

Hoersch, B., G. Braun, and U. Schmidt, Relation between landform and vegetation in alpine regions of wallis, switzerland. a multiscale remote sensing and GIS approach, *Computers, Environment and Urban Systems*, *26*, 113–139, 2002.

Holawe, F., and R. Dutter, Geostatistical study of precipitation series in austra: time and space, *Journal of Hydrology*, *219*, 70–82, 1999.

Horritt, M., A statistical active contour model for SAR image segmentation, *Image and Vision Computing*, *17*, 213–224, 1999.

Horritt, M., Calibration of a two-dimensional finite element flood flow model using satellite imagery, *Water Resources Research*, *36*, 3279–3291, 2000.

Horritt, M., and P. Bates, Prediciting floodplain inundation: raster-based modelling versus the finite-element approach, *Hydrologcial Processes*, *15*, 825–842, 2001a.

Horritt, M., and P. Bates, Effects of spatial resolution on a raster based model of flood flow, *Journal of Hydrology*, *253*, 239–249, 2001b.

Horritt, M., and P. Bates, Evaluation of 1D and 2D numerical models for predicting river flood inundation, *Journal of Hydrology*, *268*, 87–99, 2002.

Huang, B., and B. Jiang, Avtop: a full integration of TOPMODEL into GIS, *Water Resources Research*, *38*, 1257, 2002, doi:10.1029/2001WR000912.

Hunter, N. M., P. Bates, M. Horritt, A. de Roo, and M. Werner, Utility of different data types for calibrating flood inundation models within a GLUE framework, *Hydrology and Earth System Sciences*, 2003, submitted.

IRMA, FRHYMAP - flood risk scenarios and hydrological mapping, *Tech. rep.*, Final report of the IRMA-SPONGE Project, European Community, 2002.

Jakeman, A., and G. Hornberger, How much complexity is warranted in a rainfall-runoff model, *Water Resources Research*, *28*, 2637–2649, 1993.

James, C., and J. Wark, Conveyance estimation in meandering channels, *Tech. rep.*, HR Wallingford, 1992, report SR329.

Joerin, C., K. Beven, I. Iorgulescu, and A. Musy, Uncertainty in hydrograph seperations based on geochemical mixing models, *Journal of Hydrology*, *255*, 90–106, 2002.

Jones, J., T. Haluska, A. Williamson, and M. Erwin, Updating flood inundation maps efficiently, online, 1996, http://wwwdwatcm.wr.usgs.gov/reports/floodgis, last accessed 29 feb. 2004.

Jonge, T. d., M. Kok, and M. Hogeweg, Modelling floods and damage assesment using GIS, in *HydroGIS '96: Application of Geographic Information Systems in Hydrology and Water Resources Management*, edited by K. K and H. Nachtnebel, IAHS Publications no. 235, pp. 299–306, IAHS Publications, 1996.

Karssenberg, D., The value of environmental modelling languages for building distributed hydrological models, *Hydrological Processes*, *16*, 2751–2766, 2002, dOI: 10.1002/hyp.1068.

Khatibi, R., J. Williams, and P. Wormleaton, Identification problems of open-channel friction parameters, *Journal of Hydraulic Engineering*, *123*, 1078–1088, 1997.

Kisiel, C., Efficiency of parameter and state estimation methods in relation to models of lumped and distributed hydrological systems, in *United States-Japan bi-lateral seminar in hydrology, Honolulu*, pp. 246–278, 1971.

Kleměs, V., Editorial: Keeping techniques, methods, and models in perspective, *Journal of water resources planning and management*, *125*, 181–185, 1999.

Klis, v. d., H., Uncertainty analysis applied to numerical models of river bed morphology, Ph.D. thesis, Delft University of Technology, 2003.

Klopstra, D., H. Barneveld, J. J.M. van Noortwijk, and E. van Velzen, Analytical model for hydraulic roughness of submerged vegetation, in *Proceedings of the 27th IAHR Congress*, pp. 775–780, IAHR, San Francisco, USA, 1997.

Knight, D., and K. Shiono, River channel and floodplain hydraulics, in *Floodplain Processes*, chap. 5, pp. 139–181, John Wiley & Sons, 1996.

Kopp, S., Developing a hydrological extension for ArcView spatial analyst, ArcUser, 1998.

Kouwen, N., and M. Fathi-Moghadam, Friction factors for coniferous trees along rivers, *Journal of Hydraulic Engineering*, *126*, 732–740, 2000.

Kovar, K., and H. Nachtnebel (Eds.), *Application of Geographic Information Systems in Hydrology and Water Resources Management*, no. 235 in IAHS Publications, IAHS Press, 1996.

Krahe, P., N. Busch, K. Daamen, C. van Haselen adn M. Hils, and M. Werner, Assessment of flood risk for the river saar with respect to environmental changes - results of a case study within the EUROTAS project, in *European Conference on Advances in Flood Research*, edited by A. Bronstert, C. Bismuth, and L. Menzel, pp. 99–110, Potsdam, Germany, 2000.

Kuczera, G., Efficient subspace probabilistic parameter organization for catchment models, *Water Resources Research*, *33*, 177–185, 1997.

Kuczera, G., and E. Parent, Monte carlo assessment of parameter uncertainty in conceptual catchment models: The metropolis algortihm, *J. Hydrology*, *211*, 69–85, 1998.

Kutija, V., and H. Hong, A numerical model for assessing the additional resistance to flow induced by flexible vegetation, *Journal of Hydraulics Research*, *34*, 99–114, 1996.

Kwadijk, J., The impact of climate change on the discharge of the river rhine, Ph.D. thesis, Faculty of Geographic Sciences, Utrecht University, 1993.

Lacroix, M., L. Martz, G. Kite, and J. Garbrecht, Using digital terrain analysis modeling techniques for the parameterization of a hydrologic model, *Environmental Modelling and Software*, *17*, 127–136, 2002.

Lamb, R., K. Beven, and S. Myrabø, Use of spatially distributed water table observations to constrain uncertainty in a rainfall-runoff model, *Advances in Water Resources*, *22*, 305–317, 1998.

Lambert, M., and W. Myers, Estimating the discharge capacity in straight compound channels, *Proc. Instn Civ. Engrs Wat., Marit. & Energy*, *130*, 84–94, 1998.

Lambert, M., and R. Sellin, Discharge prediction in a straight compound channel using the mixing length concept, *Journal of Hydraulics Research*, *34*, 381–394, 1996a.

Lambert, M., and R. Sellin, Velocity distribution in a large-scale model of a doubly meandering river channel, *Proc. Instn Civ. Engrs Wat., Marit. & Energy*, *118*, 10–20, 1996b.

Lammersen, R., H. Engel, W. van de Langemheen, and H. Buiteveld, Impact of river training and retention measures on flood peaks along the rhine, *Journal of Hydrology*, *267*, 115–124, 2002.

Leavesley, G. H., S. L. Markstrom, P. J. Restrepo, and R. J. Viger, A modular approach to addressing model design, scale, and parameter estimation issues in distributed hydrological modelling, *Hydrological Processes*, *16*, 173–187, 2002, dOI: 10.1002/hyp.344.

Lees, M., Data-based mechanistic modelling and forecasting of hydrological systems, *Hydroinformatics*, *2*, 15–34, 2000.

Li, C., and R. Falconer, Depth integrated modelling of tide induced circulation in a square harbour, *Hydraulic Research*, *33*, 321–332, 1995.

Liong, S. Y., S. Khu, and W. Chan, Derivation of pareto front with genetic algorithm and neural networks, *J. Hydrol. Engrg*, *6*, 52–61, 2001.

Mackay, D., Introduction to monte carlo methods, in *Proceedings of an Erice summer school*, edited by M.Jordan, 1997, http://www.inference.phy.cam.ac.uk/mackay/erice.pdf.

Madsen, H., Parameter estimation in distributed hydrological catchment modelling using automatic caibration with multiple objectives, *Advances in Water Resources*, *26*, 205–216, 2003.

Marche, C., G. Lessard, and B. el Gharbi, Kriging technique for river flood representation, *Journal of Hydraulic Research*, *28*, 629–643, 1990.

Marks, K., and P. Bates, Integration of high-resolution topographic data with floodplain flow models, *Hydrological Processes*, *14*, 2109–2122, 2000.

Marquínez, J., J. Lastra, and P. Garciá, Estimation models for precipitation in mountainous regions: the use of GIS and multivariate analysis, *Journal of Hydrology*, *270*, 1–11, 2003.

Mason, D., D. M. Cobby, M. Horritt, and P. Bates, Floodplain friction parameterization in two-dimensional river flood models using vegetation heights from airborne scanning laser altimetry, *Hydrological Processes*, *17*, 1711–1732, 2003, doi:10.1002/hyp.1270.

McCowan, A., and N. Collins, The use of mike21 for full two-dimensional flood impact assessment, http://www.dhi.dk/softcon/papers/030/DHIflood.html, 1999.

McKay, M., R. Beckman, and W. Conover, A comparison of three methods for selecting values of input variables in the analysis of output from a computer code, *Technometrics*, *21*, 239–245, 1979.

Melching, C., An improved first order reliability approach for assessing uncertainties in hydrologic modeling, *Journal of Hydrology*, *132*, 157–177, 1992.

Melching, C., Reliability estimation, in *Computer Models of Watershed Hydrology*, edited by V. Singh, pp. 69–118, Water Resources Publications, New York, 1995.

Middelkoop, H., et al., Impact of climatic change on hydrological regimes and water resource management in the rhine basin, *Climatic Change*, *49*, 105–128, 2001.

Miles, S., and C. Ho, Applications and issues of GIS as a tool for civil engineering modeling, *Journal of computing in civil engineering*, *13*, 144–152, 1999.

Molinaro, P., A. D. Filippo, and F. Ferrari, Modelling of flood wave propagation over flat areas of complex topography in presence of different infrastructures, in *Proceedings of the Specialty Conference on Modelling of Flood Propagation over Intitially Dry Areas*, edited by P. Molinaro and L. Natale, pp. 209–228, ASCE, New York, NY, USA, Milan, Italy, 1994.

Nash, J., and V. Sutcliffe, River flow forecasting through conceptual models, part i: a discussion of principles, *J. Hydrology*, *10*, 282–290, 1970.

Nepf, H., Drag, turbulence, and diffusion in flow through emergent vegetation, *Water Resources Research*, *35*, 479–489, 1999.

Nickel, A., Hochwasser in talräumen, visualiserung und entscheidungshilfen, Ph.D. thesis, Institute of Water Resources Management, Hydrology and Agricultural Hydraulic Engineering, University of Hannover, 1998.

Owen, A., Latin hypercube sampling for very high-dimensional simulations, *ACM Transactions on Modeling and Computer Simulation*, *8*, 71–102, 1998.

Pang, M., and W. Shi, Development of a process-based model for dynamic interaction in spatio-temporal GIS, *Geoinformatica*, *6*, 323–344, 2002.

Paquier, A., and P. Farissier, Use of a 2D model for simulating the flooding of a plain, in *Hydroinformatics 1996*, edited by Müller, pp. 129–136, Balkema, Rotterdam, 1996.

Pauwels, V., R. Hoeben, N. Verhoest, and F. D. Troch, The importance of the spatial patterns of remotely sensed soil moisture in the improvement of discharge predictions for small-scale basins through data assimilation, *Journal of Hydrology*, *251*, 88–102, 2001.

Pebesma, E., *GSTAT User's manual*, Utrecht University, NL, 1998.

Pedroli, B., and J. Dijkman, River restoration in european lowland river systems, in *Restoration of degraded rivers: challenges, issues and experiences*, edited by D. Loucks, pp. 221–227, Kluwer Academic Publishers, 1998.

Penning-Rowsell, E., and S. Tunstall, Risks and resources: Defining and managing the floodplain, in *Floodplain Processes*, chap. 15, pp. 493–533, John Wiley & Sons, 1996.

Péron, S., O. Quiquempoix, and C. Coureau, CAZIMIR: Project for a representation of the results of 1D calculations of floods resulting from dam breaks on 2D maps, in *Hydroinformatics 1996*, edited by Müller, pp. 123–127, Balkema, Rotterdam, 1996.

Perrin, C., C. Michel, and V. Andréassian, Does a large number of parameters enhance model performance? comparitive assessment of common catchment model structures on 429 catchments, *J. Hydrology*, *242*, 275–301, 2001.

Peuquet, D., Space-time representation, in *Publications on Geodesy 47: Time in GIS: Issues in spatio-temporal modelling*, edited by L. Heres, pp. 3–12, Netherlands Geodetic Commission, Delft, The Netherlands, 2000.

Peuquet, D., Making space for time: Issues in space-time data representation, *Geoinformatica*, *5*, 11–32, 2001.

Priestnall, G., J. Jaafar, and A. Duncan, Extracting urban features from LiDAR digital surface models, *Computers, Environment and Urban Systems*, *24*, 65–78, 2000.

Puech, C., and D. Raclot, Using geographical information systems and aerial photographs to determine water levels during floods, *Hydrological Processes*, *16*, 1593–1602, 2002, dOI: 10.1002/hyp.1023.

Pullar, D., and D. Springer, Towards integrating GIS and catchment models, *Environmental Modelling and Software*, *15*, 451–459, 2000.

Reggiani, P., and J. Schellekens, Modelling of hydrological responses: the representative elementary watershed approach as an alternative blueprint for watershed modelling, *Hydrological Processes*, *17*, 3785–3789, 2003, doi:10.1002/hyp.5167.

Romanowicz, R., and K. Beven, Dynamic real-time prediction of flood inundation probabilities, *Hydrological Sciences Journal*, *43*, 181–196, 1998.

Romanowicz, R., and K. Beven, Estimation of flood inundation probabilities as conditioned on event inundation maps, *Water Resources Research*, *39*, 1073, 2003, doi:10.1029/2001WR001056,.

Romanowicz, R., K. Beven, and J. Tawn, Evaluation of predictive uncertainty in nonlinear hydrological models using a bayesian approach, in *Statistics for the Environment 2: Water Related Issues*, edited by V. Barnett and K. Turkman, chap. 17, pp. 297–317, John Wiley & Sons Ltd., 1994.

Romanowicz, R., K. Beven, and J. Tawn, Bayesian calibration of flood inundation models, in *Floodplain Processes*, chap. 15, pp. 493–533, John Wiley & Sons, 1996.

Savenije, H., Equifinality, a blessing in disguise?, *Hydrological Processes*, *15*, 2835–2838, 2001.

Schmugge, T., W. Kustas, J. Ritchie, T. Jackson, and A. Rango, Remote sensing in hydrology, *Advances in Water Resources*, *25*, 1367–1385, 2002.

Scholten, M., BASELINE a GIS oriented database and application for river modelling, in *Proceedings of the 2000 Hydroinformatics conference*, Iowa Institute of Hydraulic Research, 2000.

Schultz, G., Remote sensing and GIS from the perspecitve of hydrological systems and process dynamics, in *Application of Geographic Information Systems in Hydrology and Water Resources Management*, edited by K. Kovar and H. Nachtnebel, no. 235 in IAHS Publication, pp. 637–647, 1996.

Schumann, A., R. Funkeb, and G. Schultz, Application of a geographic information system for conceptual rainfall-runoff modeling, *Journal of Hydrology*, *240*, 45–61, 2000.

Seibert, J., Estimation of parameter uncertainty in the hbv model, *Nordic Hydrology*, *28*, 247–262, 1997.

Sellin, R., A laboratory investigation into the interaction between the flow in the channel of a river and that over its flood plain, *La Houille Blanche*, *19*, 793–801, 1964.

Sellin, R., D. Irvine, and B. Willets, Behaviour of meandering two-stage channels, *Proc. Instn Civ. Engrs Wat., Marit. & Energy*, *101*, 99–111, 1993.

Sellin, R., T. Bryant, and J. Loveless, An improved method for roughening floodplains on physical river models, *Journal of Hydraulics Research*, *41*, 3–14, 2003.

Sen, D., An algorithm for coupling 1D river flow and quasi 2D flood inundation flow, in *Hydroinformatics 2002*, edited by R. Falconer, B. Bin, E. Harris, and C. Wilson, pp. 103–108, IWA publishing, 2002.

Silva, W., and W. van de Langemheen, Landscape planning of the river rhine in the netherlands - integrated flood protection, in *RIBAMOD: River Basin Modelling, management and flood mitigation, proceedings of the first workshop*, pp. 355–357, European Community, EAR18019EN, 1997.

Singh, V., and M. Fiorentino (Eds.), *Geographical Information Systems in Hydrology*, no. 26 in Water Science and Technology, Kluwer Academic Publishers, 1996.

Sorooshian, S., and J. Dracup, Stochastic parameter estimation procedures for hydrological rainfall-runoff models: Correlated and heteroscedatic errors, *Water Resources Research*, *16*, 430–442, 1980.

Sorooshian, S., and H. Gupta, Calibration of hydrological models using multi-objectives and visualization techniques, *Tech. rep.*, Department of Hydrology and Water Resources, University of Arizona, 1998, final Report project EAR-9418147.

Sorooshian, S., and V. Gupta, Model calibration, in *Computer Models of Watershed Hydrology*, edited by V. Singh, pp. 23–68, Water Resources Publications, New York, 1995.

Sorooshian, S., and V. K. Gupta, Automatic calibration of conceptual rainfall-runoff models: The question of parameter observeability and uniqueness, *Water Resources Research*, *19*, 260–268, 1983.

Sorooshian, S., V. K. Gupta, and J. Fulton, Evaluation of maximum likelihood parameter estimation technique for conceptual rainfall-runoff models: Inluence of calibration data variability and length on model credibility, *Water Resources Research*, *19*, 251–259, 1983.

Sorooshian, S., Q. Duan, and V. Gupta, Calibration of rainfall-runoff models: Application of global optimization to the sacramento soil moisture accounting model, *Water Resources Research*, *29*, 1185–1194, 1993.

Spear, R. C., T. M. Grieb, and N. Shang, Parameter uncertainty and interaction in complex environmental models, *Water Resources Research*, *30*, 3159–3169, 1994.

Stelling, G., and S. Duinmeijer, A staggered conservative scheme for every froude number in rapidly varies shallow water flows, *Int. J. Numer. Meth. Fluids*, *43*, 1329–1354, 2003, doi:10.1002/fld.537.

Stelling, G., H. Kernkamp, and M. Laguzzi, Delft flooding system: A powerful tool for inundation assessment based on a positive flow simulation, in *Hydroinformatics '98*, edited by Babovic and Larsen, pp. 449–456, Balkema, 1998.

Stephan, U., and D. Gutknecht, Hydraulic resistance of submerged flexible vegetation, *Journal of Hydrology*, *269*, 27–43, 2002.

Sui, D., and R. Maggio, Integrating GIS with hydrological modelling: Practices, problems and prospects, *Computers, Environment and Urban Systems*, *23*, 33–51, 1999.

Syed, K., D. Goodrich, D. Myers, and S. Sorooshian, Spatial characteristics of thunderstorm rainfall fields and their relation to runoff, *Journal of Hydrology*, *271*, 1–21, 2003.

Tate, E., and D. Maidment, Floodplain mapping using HEC-RAS and ArcView GIS, *Tech. rep.*, Center for Research in Water Resources, The University of Texas at Austin, 1999.

Tate, E., D. Maidment, F. Olivera, and D. Anderson, Creating a terrain model for floodplain mapping, *Journal of Hydrologic Engineering*, *7*, 100–108, 2002.

Thiemann, M., M. Trosset, H. Gupta, and S. Sorooshian, Bayesian recursive parameter estimation for hydrologicl models, *Water Resources Research*, *37*, 2521–2535, 2001.

Tsanis, I., and M. Gad, A GIS precipitation method for analysis of storm kinematics, *Environmental Modelling & Software*, *16*, 273–281, 2001.

Uhlenbrook, S., J. Seibert, C. Leibendgut, and A. Rodhe, Prediction uncertainty of conceptual rainfall-runoff models caused by problems in identifying model parameters and structure, *Hydrological Sciences Journal*, *4*, 779–797, 1999.

Uran, O., and R. Janssen, Why are spatial decision support systems not used? some experiences from the netherlands, *Computers, Environment and Urban Systems*, *27*, 511–526, 2003.

van der Linden, S., and M. Woo, Application of hydrological models with increasing complexity to subartic catchments, *Journal of Hydrology*, *270*, 145–157, 2003.

van der Perk, M., Effect of model structure on the accuracy and uncertainty of results from water quality models, *Hydrological Processes*, *11*, 227–239, 1997.

van Deursen, W., Geographical information systems and dynamic models, Ph.D. thesis, Faculty of Geographic Sciences, Utrecht University, 1995.

van Deursen, W., and C. Wesseling, Integrating dynamic environmental models in GIS: the development of a prototype dynamic simulation langauge, in *Application of Geographic Information Systems in Hydrology and Water Resources Management*, edited by K. Kovar and H. Nachtnebel, no. 235 in IAHS Publication, pp. 71–77, 1996.

van Gelder, P., Statistical methods for the risk-based design of civil structures, Ph.D. thesis, Delft University of Technology, 2000.

van Oosterom, P., Time in cadastral maps, in *Publications on Geodesy 47: Time in GIS: Issues in spatio-temporal modelling*, edited by L. Heres, pp. 36–45, Netherlands Geodetic Commission, Delft, The Netherlands, 2000.

Verwey, A., Latest developments in floodplain modelleling - 1D/2D integration, in *Conference on Civil Engineering Hydraulics, Institution of Engineers, Australia, Hobart*, 2001.

Viney, N., M. Sivapalan, and D. Deeley, A conceptual model of nutrient mobilisation and transport applicable at large catchment scales, *Journal of Hydrology*, *240*, 23–44, 2000.

Vrugt, J., H. Gupta, L. Bastidad, W. Bouten, and S. Sorooshian, Effective and efficient algorithm for multiobjective optimization of hydrologic models, *Water Resources Research*, *39*, 1214, 2003a, doi:10.1029/2002WR001746.

Vrugt, J., H. Gupta, W. Bouten, and S. Sorooshian, A shuffled complex evolution metropolis algorithm for optimization and uncertainty assessment of hydrologic model parameters, *Water Resources Research*, *39*, 1201, 2003b, doi:10.1029/2002WR001642.

Weingartner, R., M. Barben, and M. Spreafico, Floods in mountain areas - an overview based on examples from Switzerland, *Journal of Hydrology*, *282*, 10–24, 2003, doi:10.1016/S0022-1694(03)00249-X.

Werner, M., Impact of grid size in GIS based flood extent mapping using a 1d flow model, *Physics and Chemistry of the Earth, Part B: Hydrology, Oceans and Atmosphere*, *26*, 517–522, 2001.

Werner, M., M. Ververs, C. van Haselen, K. Daamen, and M. Muerlebach, A comparison of methods for generating cross sections for flood modelling using detailed floodplain elevation models, in *European Conference on Advances in Flood Research*, edited by A. Bronstert, C. Bismuth, and L. Menzel, pp. 73–86, Potsdam, Germany, 2000.

Wijbenga, J., J. Lambeek, E. Mosselman, R. Nieuwkamer, and R. Passchier, River flood protection in the netherlands, in *River Flood Hydraulics*, edited by W. White and J. Watts, John Wiley & Sons Ltd, 1994.

Wilson, C., and M. Horritt, Measuring the flow resistance of submerged grass, *Hydrological Processes*, *16*, 2589–2598, 2002, dOI: 10.1002/hyp.1049.

Wilson, C., P. Bates, and J.-M. Hervouet, Comparison of turbulence models for stage-discharge rating curve prediction in reach-scale compound channel flows using two-dimensional finite element methods, *Journal of Hydrology*, *257*, 42–58, 2002, dOI: 10.1002/hyp.1049.

Wind, H., T. Nierop, C. de Blois, and J. de Kok, Analysis of flood damages from the 1993 and 1995 meuse floods, *Water Resources Research*, *35*, 3459–3465, 1999.

Wormleaton, P., J. Allen, and P. Hadjipanos, Discharge assessment in compound channel flow, *Journal of the Hydraulics Division, ASCE*, *108*, 975–994, 1982.

WSV, Ausbau der Saar - eine dokumentation, *Tech. rep.*, Wasser- und Schifffahrtsverwaltung des Bundes [WSV], Saarbrücken, Germany, 1987.

Yoshida, H., and A. Dittrich, 1D unsteady-state flow simulation of a section of the upper rhine, *Journal of Hydrology*, *269*, 79–88, 2002.

Young, P., A. Jakeman, and D. Post, Recent advances in the data-based modelling and analysis of hydrological systems, *Water Science Technology*, *36*, 99–116, 1997.

Yu, P.-S., T.-C. Yang, and S.-J. Chen, Comparison of uncertainty analysis methods for a distributed rainfall-runoff model, *Journal of Hydrology*, *244*, 43–59, 2001.

Zang, W., and G. Hunter, Temporal interpolation of spatially dynamic objects, *Geoinformatica*, *4*, 403–418, 2000.

A

Notation

A	cross section area	m^2
B	width	m
f	Darcy-Weisbach friction factor	m
g	gravitational constant	m/s^2
h	flow depth	m
i, j	grid point subscripts in x and y	$[-]$
Kc	Contraction coefficient	[-]
L	reach length	m
n	manning's roughness coefficient	$m^{-1/3}s$
Q	discharge	m^3/s
R	hydraulic radius	m
S	longitudinal slope	$[-]$
s	channel and floodplain side slope	$[-]$
V	mean velocity	m/s
u, v	x, y components of flow velocity	m/s
x, y	horizontal cartesian coordinates	m
z	vertical coordinate (bed level)	m
θ	parameter set	[-]
ζ	water level above reference plane	m
ρ	Water density (taken as $1000kg/m^3$)	kg/m^3
τ	Shear stress	N/m^2
Δt	Time step	s
$\Delta x, \Delta y$	size of grid cells in x and y	m

subscripts

mc	main channel
fp	floodplain
bf	bankfull
mb	meander belt
lat	lateral discharge
1-4	channel zone

B

Interpolation of 1D results

Abstract

Flood hazard in areas adjacent to rivers may be estimated by applying hydrological/hydraulic models to calculate parameters such as flood extent, depth and duration. Using a two-dimensional flow model based on the topography has the drawback that computational requirements are high, making this approach unattractive when applying in, for example, a decision support system. This appendix presents a simple GIS based method for assessing the extent and depth of flooding based on water levels calculated using a 1-dimensional flow model and an extended inverse distance interpolation method. Local depressions not directly connected to the river by a continuous water surface are easily removed. The method is demonstrated on a $9km^2$ floodplain area, where the effect of varying grid size on flood extent estimation and evaluation time is investigated. Possible points of improvement as well as future work to assess the accuracy are discussed.

B.1 Introduction

Estimating flood hazard in areas subject to flooding from rivers is the basis of many hydrological studies. Typically runoff hydrographs and associated stages are studied, and although these give quite relevant information on hydrological characteristics of the catchment, emphasis is on the peak discharges and possibly the duration during which a given critical discharge is exceeded etc. An estimate of the spatial dimension of the flood event is implicitly deduced from these stages. Flood risk assessment, where risk is considered a comparison between the hazard of a given area combined with the vulnerability of that area (*Gilard and Givone* 1997) calls for a better spatial understanding of the flood event.

Geographical Information Systems (GIS) form a powerful tool for this analysis, as GIS can not only be used to visualise the extent of flooding, but may also be applied to further analyse these maps to produce flood damage estimation maps and flood risk maps etc. (*Hausmann and Weber* 1996; *Clark* 1998). To estimate the extent of flooding associated with a given return period, however, the GIS must be combined with an applicable hydrological/hydraulic method for estimating stages. Many examples exist of the integration of 2-D flow models with GIS (*Stelling et al.*

"Impact of Grid Size in GIS Based Flood Extent Mapping using a 1D Flow model", in *Physics and Chemistry of the Earth, Part B: Hydrology, Oceans and Atmosphere*, 26(7-8), 517—522.

1998; *McCowan and Collins* 1999). Although this is reported to give the most satisfactory results (*McCowan and Collins* 1999) there are some drawbacks that make this approach less applicable in, for example, a decision support system environment, where emphasis is on rapid assessment of the impact of possible catchment and river engineering measures. Another disadvantage is that application of a 2-D model requires comprehensive and consistent data of the area under study which may not be readily available at the feasibility study stage, and also that due to computational demands the reaches studied are often limited in their areal extension. An alternative is to determine stages in the river using a 1-D flow model and subsequently interpolating these to create a flood map using GIS based techniques. Many authors give examples of coupling results of 1-D flow models with GIS. The methods described differ substantially, ranging from application of geostatistical interpolation routines (*Marche et al.* 1990) through neighbourhood analysis (*Jonge et al.* 1996) to methods that calculate the interception points of water levels in the cross section profile and subsequently map these interception points (*Tate and Maidment* 1999). GIS based interpolation routines have preference over the neighbourhood analysis method due to the slope in the water level profile, whereas mapping interception points has the disadvantage that between cross sections the information content is relatively low.

Applying interpolation routines, such as Inverse Distance Weighted Interpolation or Kriging, is relatively easy and is provided by most GIS packages. The interpolation methods result in a water level surface that after subtracting elevations from a digital elevation model (DEM) of the area yields a map of flood depths. One of the difficulties of this straightforward routine is that areas not directly connected to the main channel at the given stage (e.g. local depressions) are considered as flooded because the terrain elevation lies under the interpolated water level surface. The method introduced here for estimating flood extent maps using a simple Inverse Distance Weighted Interpolation easily avoids this problem by using an algorithm based on "cost distance mapping". The method itself is discussed in the next section. Subsequently the impact of varying grid size is investigated using an example floodplain. Finally merits of the method are discussed as well as some points of improvement and further research.

B.2 Inverse distance weighted interpolation

Inverse distance weighted (IDW) interpolation is a simple interpolation method where the water level at each unknown point is calculated as a weighted average of the levels at known locations. The known locations are typically irregularly spaced, whereas the interpolations are made for locations on a regular grid (*Burrough and McDonnel* 1998). The general formula for IDW is given in Equation B.1.

$$\hat{z}(x_j) = \frac{\sum_{i=1}^{n} z(x_i) \times d_{ij}^{-r}}{\sum_{i=1}^{n} d_{ij}^{-r}} \tag{B.1}$$

where x_j are the points where the water level is to be interpolated and x_i are the points where the water levels are known. The distance between each pair of unknown and known points is represented by d_{ij} raised to the power r. This method is known as an exact interpolator because the interpolated surface will pass exactly through the known data points. For a relatively smooth surface such as a water surface profile this should not pose a serious problem. A potential problem is that the resulting surface will show local patterns according to the density of points within a given search radius. Altering the search criteria with which points are selected may resolve this problem (*Burrough and McDonnel* 1998). In this case, with a high density of known points along the cross section lines and absence of points between cross section lines, the "known" points used in the interpolation are selected such that these lie equally distributed in the quadrants with respect to the point being calculated.

B.3 Estimating extent of flooding map

Two basic data requirements must be met to estimate an extent of flooding map. An elevation model of the area under consideration must be available, as well as a line indicating the centre of the main channel, i.e. the river delineation. Secondly, cross section lines must be available, showing on the map the lines along which cross-sections have been measured (or sampled from the digital elevation model). These cross section lines should ideally stretch across the full floodplain width. In compliance with 1D flow calculations, water levels are assumed constant along each cross section line. "Known" points are then distributed along the cross section line, and to each of these points the calculated level for that cross section is assigned. The inverse distance interpolation algorithm is subsequently applied to fit a water surface profile through these known points, with the exponent in Equation B.1 typically set to 1. The selection of "known" points in four quadrants is illustrated in Figure B.1, showing a short reach of river with the elevation model and a number of cross-section lines. For two of these cross sections the "Known points" are shown (as an illustration), as well as the quadrants used for selecting points when calculating the level at an unknown location or grid cell.

By subtracting the terrain elevation from the water level surface thus calculated, a "first guess" for the extent of flooding map is created through retaining all grid cells with a depth greater than zero and setting all other cells to missing values. This initial guess may still indicate flooding in local depressions not directly connected to the main channel. To remove these, a simple algorithm is applied to investigate if a cell with a water depth greater than zero is connected to the main channel by any possible route. The first step of the algorithm is to create a so-called friction map, where all values in the "first-guess" flood map that have a value greater than zero are assigned a unit friction. All cells with no value (indicating land above the water level surface) are assigned a large friction value. Using a cost distance algorithm (*ESRI* 1996), the accumulated cost to travel from the river axis to each cell

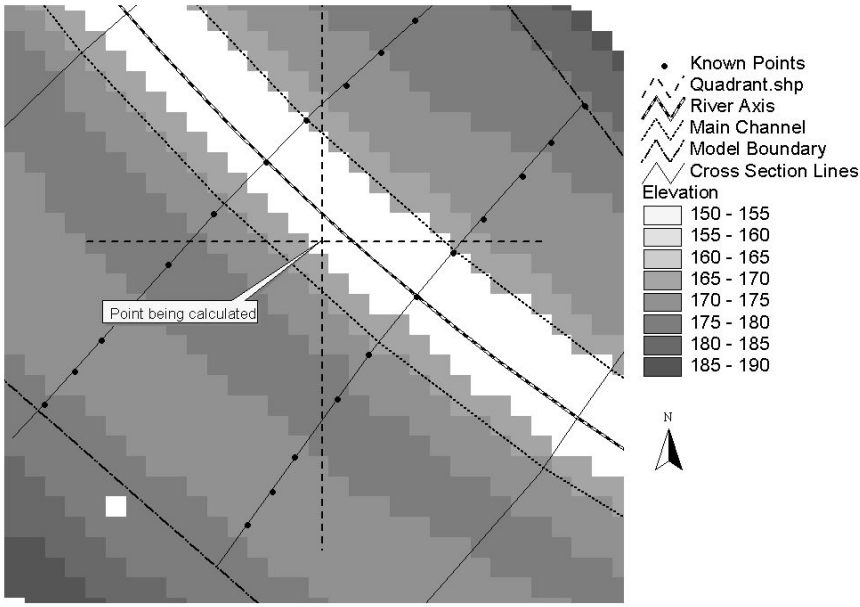


Figure B.1: Example of a quadrant used to select known points

in the grid is calculated, where cost of travelling through each individual cell along the route is determined by the friction assigned to that cell in the friction map. In the resulting map each cell in the grid is assigned the value of the "cheapest" route between itself and the river axis line. It is apparent that for cells without a direct connection to the river axis one or more cells of "dry-land" with a very high friction must be crossed, thus substantially raising the cost of travelling from the river axis to that cell. Once the cost of each cell in the grid is calculated, all cells with a cost value an order of magnitude larger than the Euclidean distance between that cell and the main channel may be considered as not being connected to the main channel. These are discarded from the "first-guess" flood map to produce a "final" extent of flood map.

B.4 Impact of grid size on accuracy

Hydraulic controls in the floodplain, such as embankments and elevated roads, have an obvious effect on the extent of flooding, and their correct representation in the digital elevation model has a profound impact on the accuracy of the extent of flood map calculated. If a coarse grid is applied, then these local elevations may be locally averaged out, thus allowing the cost distance algorithm to find a route "through". Using a very fine resolution grid, however, has the disadvantage that

calculation time again becomes excessive, thus eliminating this advantage of using a simple method. A balance must therefore be found between the available DEMś of different resolution and accuracy. To demonstrate the method and illustrate these effects, it is applied to a case study on a floodplain reach along the River Saar in Germany. Impacts of grid size on the estimation of the flood extent map as well on the evaluation time are investigated.

B.5 Test case: Schwemlinger Wiesen

The Schwemlinger Wiesen is a relatively wide floodplain adjacent to the Saar River, some 40 km upstream of the confluence of the Saar River with the Moselle, one of the major tributaries of the Rhine River. Fig. 2 shows the elevation of the floodplain (resolution 10x10 m2). Note the motorway (including an exit) that runs across the floodplain. The white patches where there is no elevation data available are floodplain lakes. Although the river flow model is available for the full length of the river an "area of interest" is used in this case to limit computation time (see Fig. 2, area of interest is approximately 9.4 km2). The routine for estimating flood extent maps is implemented as an ArcView GIS script (ArcView version 3.1 with the Spatial Analyst 1.1 extension), while the actual interpolation of the water level surface is carried out by GSTAT (*Pebesma* 1998)). This is a specially designed command line Geostatistical Interpolation Package, and is called from the ArcView Script. GSTAT is applied for interpolation rather than the available ArcView routines because of its superior selection options for points to be used in the inverse distance interpolation algorithm. The elevation model used was based on laser altimetry data for the River Saar and its floodplains. These data were available at a resolution of on average 1 point every $2.5 \times 2.5m^2$, and were aggregated to four different resolutions of the Digital Elevation Model (DEM), $25 \times 25m^2$, $10 \times 10m^2$, $5 \times 5m^2$ and $2.5 \times 2.5m^2$. The aggregation algorithm simply averaged elevation points within each grid cell. No further refinement was performed, and as a consequence it was seen that - particularly when choosing finer resolution grids - the number of cells with no data (i.e. none of the laser altimetry points fall in that cell) tended to increase. Refinement of the aggregation method could alleviate this problem.

For the generation of flood extent maps, two return period events were applied, the 1/50 year flood and the 1/200 year flood. Figures B.3 to B.6 show the steps used in calculating the flood map. In the initial flood extent map (Fig. B.3) the area behind the elevated motorway is shown as inundated. The cost distance map (Fig. B.5), however, shows that the cost to travel to this area is very large due to the cheapest path crossing this ridge of high friction (Fig. B.4). In the final flood map (Fig. B.6) this area is subsequently excluded. The friction assigned to the "dry land" cells in the order of the diagonal length of the area of interest proved sufficient. Table B.1 shows the flooded areas calculated for different grid sizes of varying depths. The slight differences between the areas calculated are accredited

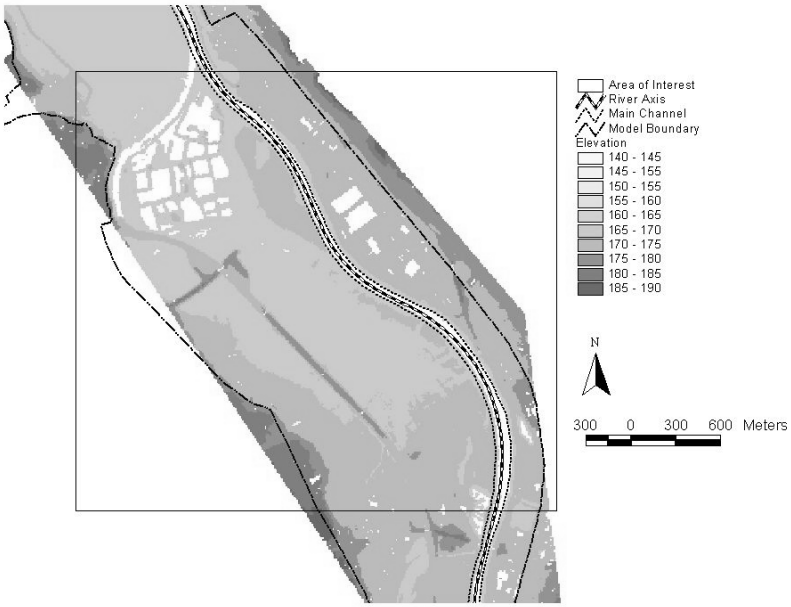


Figure B.2: Elevation model and layout of Schwemlinger Wiesen.

to edge effects and differing areas of cells with no value. Most apparent, however, is the difference between the inundated area determined using the $25 \times 25m^2$ grid size for the 200 year event when compared to the area calculated using the other grid sizes. This is illustrated in Figures B.7 and B.8 where the flood extent maps for the $5 \times 5m^2$ and $25 \times 25m^2$ grids are shown.

The figure shows that the area behind the motorway is partly flooded due to it now being "connected" to the river axis through a "low" point in the representation of the motorway in the DEM. The calculation time (as performed on a standard 400 MHz PC with 128 MB memory and Windows NT4.0) does reduce drastically when grid sizes are increased (Table B.1). In the example investigated the inundated areas do not vary significantly for all but the $25 \times 25m^2$ resolution grid, suggesting that in this case the optimal combination between resolution and accuracy, given the available DEMś, is the $10 \times 10m^2$ grid.

B.6 Conclusions and discussion

The method presented proves very applicable to estimate the extent of flooding based on water levels provided either as design level or calculated by a 1D flow model at cross section locations. Particularly the use of the friction grid to omit low areas not connected to the actual river from the flood map is useful. The eval-

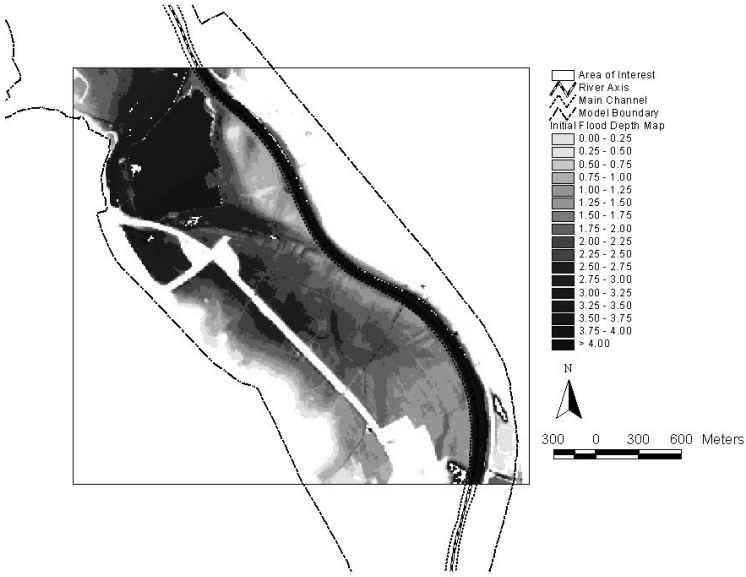


Figure B.3: Initial flood depth for 1/50 year event. Grid resolution is $10 \times 10m^2$.

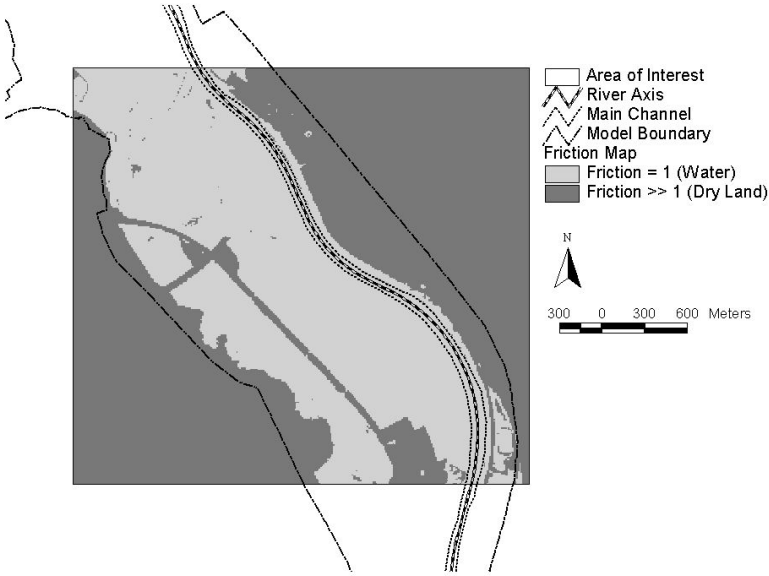


Figure B.4: Friction map for 1/50 year event. Grid resolution is $10 \times 10m^2$.

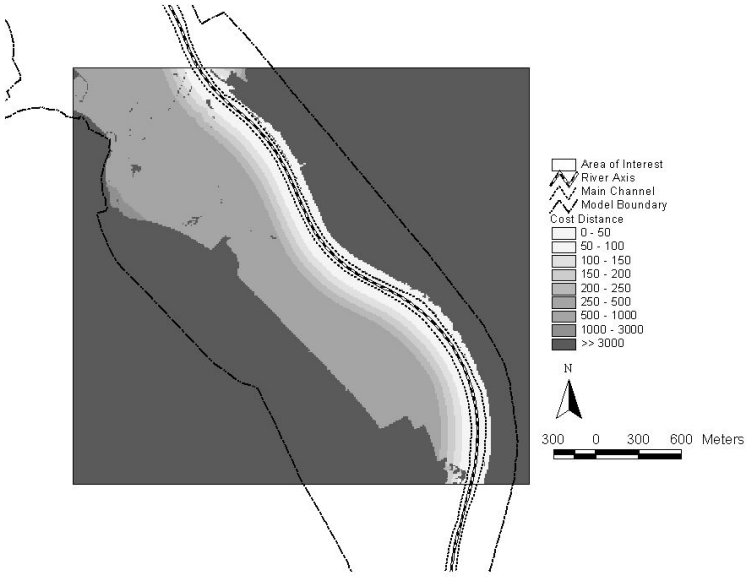


Figure B.5: Cost distance map for 1/50 year event. Grid resolution is $10 \times 10m^2$.

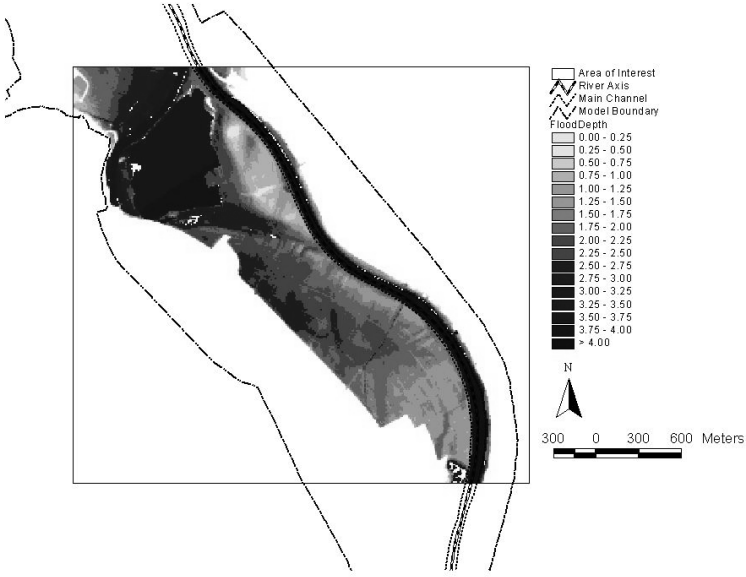


Figure B.6: Final flood depth map for 1/50 year event. Grid resolution is $10 \times 10m^2$.

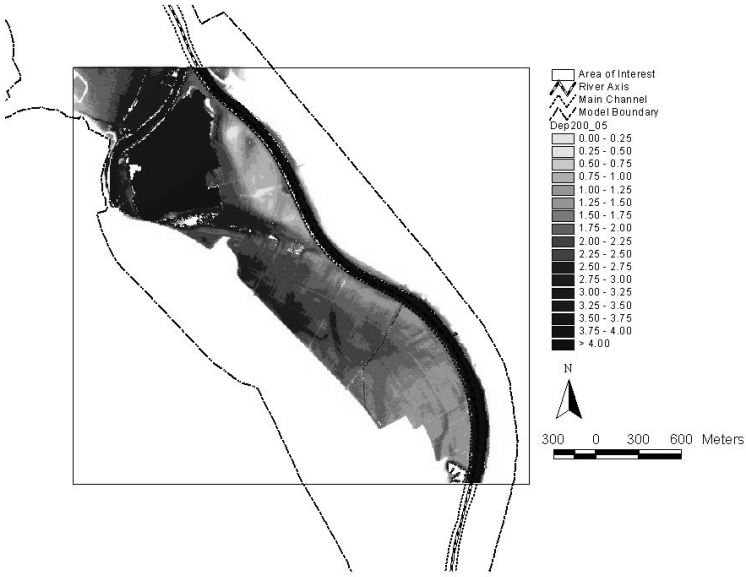


Figure B.7: Flood Extent map for the 200 year event using $5 \times 5m^2$ grid

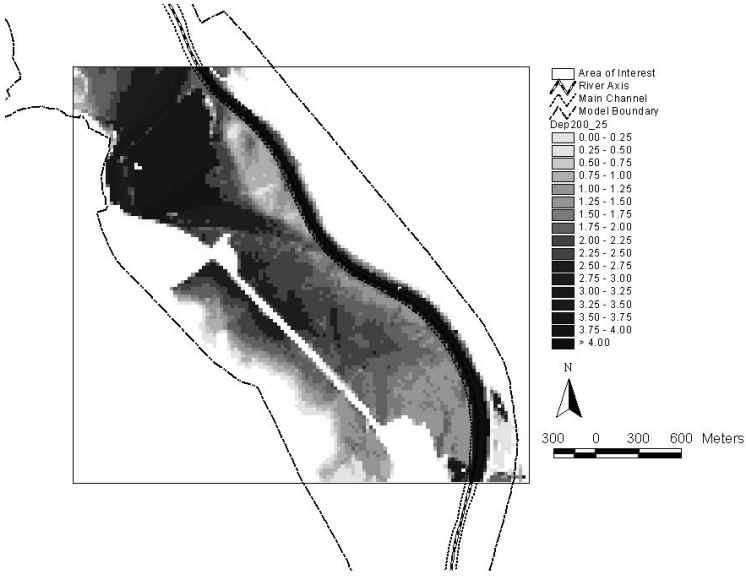


Figure B.8: Flood Extent map for the 200 year event using $25 \times 25m^2$ grid.

Table B.1: Flood Area and evaluation time for different grid sizes

Event	Grid Size	Flooded Area				Evaluation
		$d > 3m$	$d > 2m$	$d > 1m$	Total	Time
Year	m^2	$\times 10^5 m^2$	$\times 10^5 m^2$	$\times 10^5 m^2$	$\times 10^5 m^2$	Seconds
50	2.5×2.5	7.36	9.81	21.36	26.14	7095
	5×5	7.37	10.32	23.13	28.62	1575
	10×10	7.34	10.48	23.49	29.06	422
	25×25	7.34	10.56	23.57	29.43	81
200	5×5	8.57	18.23	27.98	29.32	-
	10×10	8.59	18.50	28.24	29.70	-
	25×25	8.57	20.41	33.30	37.08	-

uation time diminishes rapidly as grid sizes increase, but sufficient care must be taken to choose an appropriate grid size such that the effects of hydraulic controls on the extent of flooding are not omitted. Although the method proves to be useful for rapid evaluation of flood extent maps, further research will be directed at two improvements that will give a more realistic water level surface. The first aspect is that the impact of hydraulic controls on the flood extent is such that even for the smallest grid size used here significant errors may be made. Even at fine resolutions very narrow structures such as floodwalls may be "missed" by the areal survey and the resulting flood map would therefore contain significant error.

One possibility to account for such structures is to use Triangulated Irregular Networks (TIN) or nested grids to represent the elevation. The method would also be improved if a second inverse distance interpolation run is carried out where the distances used to weight the known points are not the Euclidean distances but rather the cost distances. This would have the advantage that the water level surface would not show a slope in, for example, a dead end river arm running adjacent to the main channel. An alternative method for detecting low lying areas not connected to the river axis by any possible route, and therefore not considered as flooded, is to determine contiguous groups of cells with the same value in the friction map. The contiguous group of cells intersecting with the river axis is retained, and the complement of this group is used to mask out those areas not connected to the river axis from the initial flood map, thus obtaining the final flood map. Extent of flooding maps obtained through these two methods have been found to be identical, and although this alternative method reduces the calculation times (by 2.5% in the case of the $10 \times 10m^2$ grid). The disadvantage is that the second interpolation considered above can not be used, as it requires the cost distances be calculated. A disadvantage of using the inverse distance interpolation algorithm is that the water surface profile shows unrealistic characteristics at the "known" points. This algorithm is an exact interpolator, where the resulting surface passes exactly through the known "points", with the value of the exponent r in the algorithm (see Equation B.1) having significant influence on how the surface passes through these points. In the case of r set to 1 the interpolation is linear, but edge effects along the cross section lines can be seen. For higher values of the exponent these edge effects are

smoothed, but the slope of the surface will then be unrealistic, where for exponent values of 2 or higher the water surface calculated tends to horizontal at known points. Other interpolation techniques may show to be more suitable for calculating a more realistic water surface, and current research is directed at investigating these alternatives. It is, however, considered that the emphasis lies in the estimation of an extent of flooding map and not an exact water surface profile. In the example investigated the differences in the flood levels calculated using values of the exponent r in Equation (1) between 1 and 2 did not exceed 0.01 m. Obviously the accuracy and applicability of method for determining extent of flooding maps relies on the accuracy and applicability of 1D flow model calculations for the reach considered. In the case of highly sinuous channels, particularly where the sinuosity of the main channel is greater than that of the floodplain, a 1D approach may not be suitable (*Knight and Shiono* 1996). A 2D approach or a semi-2D approach (parallel branches in the 1D model to represent floodplain and main channel) may need to be adopted in these cases. In any case the cross section lines used as the basis of the interpolation routine should be determined such that these are more or less perpendicular to the assumed flow direction in the main channel as well as the floodplain. As a consequence cross-section lines can not intersect when properly determined. Further research is directed at exploring the range of applicability of the method, as well as verification of the method against both real flood events and 2D flow model calculations.

Acknowledgements. This work has been carried out partly for the EUROTAS project funded by the EC (Contract No. ENV4-CT97-0535). The Bundesanstalt für Gewasserkunde in Koblenz, Germany is also thanked for kind permission to use the data.

C

Numerical methods

In this appendix the numerical solution procedure applied in the SOBEK hydrodynamic code used in the thesis is briefly described. The description is taken largely from *Hesselink et al.* (2003) and *Stelling and Duinmeijer* (2003), and is given only for the one dimensional solution, but this can easily be extended to two dimensions (see *Stelling and Duinmeijer* (2003)). The procedures are applied in one dimension in solving flow in the SOBEK one-dimensional code and in the main channel of the hybrid SOBEK-1D2D code, as in the two dimensional domain of the DELFT-FLS code and the SOBEK-1D2D code.

Using Chézy's formulation for friction, the shallow water equations for continuity and momentum in one-dimension are given as,

$$\frac{\partial \zeta}{\partial t} + \frac{\partial (uh)}{\partial x} = 0 \tag{C.1}$$

$$\frac{\partial u}{\partial t} + u\frac{\partial u}{\partial x} + g\frac{\partial \zeta}{\partial x} + g\frac{u|u|}{C^2 h} = 0 \tag{C.2}$$

where u is velocity, ζ is water level above the reference plane, C is the Chézy friction coefficient, and h is the total water depth ($h = \zeta + d$). With the bottom invariant in time, the continuity equation can be rewritten as,

$$\frac{\partial \zeta}{\partial t} + \frac{\partial (uh)}{\partial x} = 0 \tag{C.3}$$

with $F(h) = uh$, the continuity equation can be considered as a transport equation, allowing application of so-called positive schemes (*Hesselink et al.* 2003). A simple semi-discretisation of equation C.3 uses a staggered grid, with water levels at grid cell centre-points given by:

$$\frac{dh}{dt} + (uh(u))_{0x} = 0 \tag{C.4}$$

The momentum equation (equation C.2) describing the flux between two cells is given by:

$$\frac{du}{dt} + a(u,u) + g\zeta + g\frac{u|u|}{C^2 h(u)} = 0 \tag{C.5}$$

with $a(u,u)$ being an approximation of advection (see later). In the volume equation the flux difference u_{0x} is calculated at the water level point as,

$$u_{0x} = \frac{u_{i+1/2} - u_{i-1/2}}{\Delta x} \tag{C.6}$$

while the in the momentum equation the slope at the cell boundaries (at $i + 1/2$) is given as,

$$\zeta_{0x} = \frac{\zeta_{i+1} - \zeta i}{\Delta x} \tag{C.7}$$

The water depth at the cell boundary $(i + 1/2)$ is taken depending on the flow direction,

$$h_{i+1/2}(u) = \begin{cases} h_i, & u \geq 0 \\ h_{i+1}, & u < 0 \end{cases} \tag{C.8}$$

Time integration is based on the θ method, with a simple locally linearised form of this method given by,

$$\frac{h^{n+1} - h^n}{\Delta t} + (u^{n+\theta} h^n(u^n))_{0x} = 0, at(i) \tag{C.9}$$

$$\frac{u^{n+1} - u^n}{\Delta t} + a(u^n, u^n) + g\zeta_{0x}^{n+\theta} + g\frac{|u^n|u^{n+1}}{C^2 \bar{h}^x} = 0, at(i + 1/2) \tag{C.10}$$

where $u^{n+\theta} = \theta u^{n+1} + (1 - \theta)u^n$, $\bar{h}^x at(i + 1/2) = (h_i + h_{i+1})/2$, and $\zeta^{n+\theta} = \theta\zeta^{n+1} + (1 - \theta)\zeta^n$. If positive flow is assumed ($u_{i+1/2}^{n+\theta} \geq 0$ and $u_{i-1/2}^{n+\theta} \geq 0$), Equation C.9 can be re-written as;

$$h_i^{n+1} = \left(1 - \frac{\Delta t u_{i+1/2}^{n+\theta}}{\Delta x}\right) h_i^n + \frac{\Delta t u_{i-1/2}^{n+\theta}}{\Delta x} h_{i-1}^n \tag{C.11}$$

Strictly positive depths can be assured if:

$$\frac{\Delta t u^{n+\theta} i + 1/2}{\Delta x} < 1 \tag{C.12}$$

Conditions to assure strict positivity can be similarly derived for other flow conditions. Fulfilling these conditions through adaptive time stepping means that no additional wetting and drying procedure is required.

Dealing with advection (see equation C.5) requires special attention near local discontinuities such as discontinuities in bathymetry, hydraulic jumps, bores etc. To approximate advection, energy head and momentum conserving formulations can be considered. For rapidly varied flow, time variation and bottom friction can be ignored locally, and with $\frac{u^2}{2g} + \zeta$ being constant the energy head conserving formulation of equation C.2 is given by:

$$\frac{\partial u}{\partial t} + \frac{\partial}{\partial x}\left(\frac{1}{2}u^2 + g\zeta\right) + g\frac{u|u|}{C^2 h} = 0 \tag{C.13}$$

Similarly the momentum conserving formulation is given by:

$$\frac{\partial}{\partial t}(hu) + \frac{\partial}{\partial x}(hu^2) + gh\frac{\partial \zeta}{\partial x} + g\frac{u|u|}{C^2} = 0 \tag{C.14}$$

For gradually varied flow conditions these two formulations are equivalent, but at discontinuities where there is in general no unique solution of equations C.13 and C.14, conservation properties are needed to connect the equations at both sides of the discontinuity. This is achieved by consecutively applying the energy head conserving formulation in the contraction to establish an estimate of the energy loss, followed by the momentum conserving formulation in an abrupt expansion.

Two numerical approximations are used in the codes, the first energy conservative and the second momentum conservative. The energy conservative approximation is given by:

$$\frac{dh}{dt} + (uh(u))_{0x} = 0, at(i) \tag{C.15}$$

$$\frac{du}{dt} + \left(\frac{(u(\bar{u}^x))^2}{2}\right)_{0x} + g\zeta_{0x} + g\frac{|u|u}{C^2\bar{h}^x} = 0, at(i+1/2) \tag{C.16}$$

The expression for the advection approximation at $(i+1/2)$ reads

$$\left(\frac{(u(\bar{u}^x))^2}{2}\right)_{0x} = \frac{\left(u_{i+1}\left(\frac{u_{i+3/2}+u_{i+1/2}}{2}\right)\right)^2 - \left(u_i\left(\frac{u_{i+1/2}+u_{i-1/2}}{2}\right)\right)^2}{2\Delta x} \tag{C.17}$$

where:

$$u_i\left(\frac{u_{i+1/2}+u_{i-1/2}}{2}\right) = \begin{cases} u_{i-1/2}, & \frac{u_{i+1/2}+u_{i-1/2}}{2} \geq 0 \\ u_{i+1/2}, & \frac{u_{i+1/2}+u_{i-1/2}}{2} < 0 \end{cases} \tag{C.18}$$

Based on these definitions, the approximation of the advection for positive values of $u \forall i$ yields:

$$u\frac{\partial u}{\partial x} \approx \frac{\left(u_{i+1}\left(\frac{u_{i+3/2}+u_{i+1/2}}{2}\right)\right)^2 - \left(u_i\left(\frac{u_{i+1/2}+u_{i-1/2}}{2}\right)\right)^2}{2\Delta x} = \frac{u_{i+1/2}^2 - u_{i-1/2}^2}{2\Delta x} \tag{C.19}$$

For the momentum conservative approximation a similar approach is followed. With $q = uh$, the following identities are denoted:

$$u\frac{\partial u}{\partial x} = \frac{1}{h}\left(\frac{\partial (u^2 h)}{\partial x} - u\frac{\partial (uh)}{\partial x}\right) = \frac{1}{h}\left(\frac{\partial (uq)}{\partial x} - u\frac{\partial q}{\partial x}\right) \tag{C.20}$$

and using the continuity equation (C.1):

$$u\frac{\partial u}{\partial x} = \frac{1}{h}\left(\frac{\partial (uq)}{\partial x} + u\frac{\partial \zeta}{\partial t}\right) \tag{C.21}$$

The spatial discretisation for conservation of momentum is then given by:

$$\frac{dh}{dt} + (uh(u))_{0x} = 0, at(i) \tag{C.22}$$

$$\frac{du}{dt} + \frac{1}{\bar{h}^x}((\bar{q}^x u(\bar{q}^x))_{0x}) - u(\bar{q}^x)_{0x} + g\zeta_{0x} + g\frac{u|u|}{C^2\bar{h}^x} = 0, at(i+1/2) \tag{C.23}$$

where $q = uh$, $\bar{h}^x ati + 1/2 = \frac{h_i + h_{i+1}}{2}$, and $\bar{q}^x at(i+1/2) = \frac{q_{i-1/2} + q_{i+1/2}}{2}$. Averaging equation C.22 over the grid points i and $i+1$ gives:

$$u\frac{d\bar{h}^x}{dt} + u(\bar{q}^x)_{0x} = 0, at(i+1/2) \tag{C.24}$$

Multiplying equation C.23 by $\bar{h}^x$ and adding equation C.24 gives:

$$\frac{d(u\bar{h}^x)}{dt} = (\bar{q}^x u(\bar{q}^x))_{0x} + g\bar{h}^x)\zeta_{0x} + g\frac{u|u}{C^2} = 0, at(i+1/2) \tag{C.25}$$

This is consistent with the momentum conservative equation C.15. For positive flow directions $\forall i$ the advection approximation is given as

$$u\frac{\partial u}{\partial x} \approx \frac{u_{i+1/2}h_i + u_{i-1/2}h_{i-1}}{h_{i+1} + H_i} \cdot \left(\frac{u_{i+1/2} - u_{i-1/2}}{\Delta x}\right) \tag{C.26}$$

The differences between the energy conserving and the momentum conserving approximations are small for smooth conditions. These play a role only at discontinuities, where the energy conservative approximation is selected in contractions. At all other times the momentum conservative solution is applied. Temporal integration is achieved again by the θ method. With $\theta = 1/2$ non-linear equations are obtained. Local linearisation is, however, used to avoid using iterative solver.

Hesselink et al. (2003) note that the approach is only of first order consistency. Higher order approaches are available, but may require additional wetting and drying procedures and flux limiters. They show that for inundation type calculations the first order approximation is sufficiently accurate.

The method can be extended to two dimensions. For details see *Hesselink et al.* (2003) and *Stelling and Duinmeijer* (2003).

Acknowledgements

In writing this thesis, I am indebted to a large number of people who have contributed is some way to the writing of this thesis.

First, Peter van de Veer for initiating the research project together with Theo Bogaerts and Josef Cser. It is a pity that Peter could not see the research project through to the end. I would like to thank him for his faith in my completing the project, even though I slightly changed the original objectives. I am very grateful to Huub Savenije for picking up where Peter left off, and providing motivated and much needed support in completing the thesis. I am equally grateful to the members of the examination committee, particularly Keith Beven and Axel Bronstert, who have taken great time and energy in reviewing the thesis. Their helpful suggestions have improved the thesis considerably. Sarka Blazkova, Paul Bates and Neil Hunter are thanked for the excellent cooperation during our joint work.

I am particularly thankful for the encouragement from Martin Lambert, who in 1992 suggested the idea of undertaking a PhD, which I then laughed at. Both, he and Jaap Kwadijk provided me with much motivation and inspiration during the first years of the project. The encouragement from my colleagues at Delft Hydraulics has also been very important, and I am particularly grateful to Karel Heynert, Jos Dijkman, Henk van den Boogaard, Paul ten Brummelhuis (who is sadly missed), Ferdinand Diermanse, as well as many others who contributed in many ways. At the university, the support from Henk Boere and other colleagues is very much appreciated.

My thanks go also to the (extended) EdP group, in particular Po Wen Cheng for all the help in trying to explain Monte Carlo and statistics properly, though I am sure my understanding is still lacking; and Hans van Woudenberg for his excellent help and advice in producing the thesis. Last but certainly not least, I would like to thank Barbara for her endless patience and putting up with a computer-bound husband. Hopefully, I will now get to spend more time with her and our lovely children, Paul and Emily, who were born just before I started writing up, and can now already walk and talk.

Finally, to all those who I have not mentioned, but who have helped, contributed, encouraged or even discouraged. Maximum respect.

Micha Werner
Pijnacker, 2004

Curriculum Vitae

Micha Werner was born on 23^{rd} August 1969 in Nicosia, Cyprus. After completing secondary school in 1988, he pursued studies in civil engineering at the faculty of Civil Engineering at Delft University of Technology. He graduated "cum laude" in 1994, specialising in Irrigation Control Engineering, with a minor in Hydrology. During his studies, Micha Werner worked for nine months at the University of Bristol, assisting in research work on two-stage channel flow and various hydrological studies. He undertook most of the work for his MSc. thesis while in Loxton, Australia, studying the problems of on-demand delivery in open channel irrigation systems.

After graduating in 1994, and having completed his 12 month "state social service" at the university in Delft, Micha Werner joined Delft Hydraulics, where he has been working since in the Hydrology and Flood Management Group. His prime field of work is in the development of real time flood forecasting systems and decision support systems, both in the Netherlands and abroad. In 1999 he returned to the university in Delft to start his PhD work on a part time basis with the Civil Engineering Informatics group, focussing on the integration of hydrological models and geographical information systems. Since November 2003 Micha Werner is again employed full time at Delft Hydraulics.